

SCANNING ELECTRON MICROSCOPE APPLICATIONS
TO INTEGRATED CIRCUIT TESTING

A thesis submitted to the Faculty of Science of the
University of Edinburgh, for the degree of
Doctor of Philosophy

by

J M HANNAH, BSc



ABSTRACT

The Scanning Electron Microscope (SEM), with its large depth of focus and variety of modes of operation, is a valuable tool in work on semiconductor devices. A summary is given of applications already found in this field.

A consideration of the manufacture and testing of integrated circuits indicates the need for a method of voltage measurement on operating circuits which does not make use of mechanical probes. The use of the voltage contrast mechanism in the SEM is suggested as a solution to this problem. A survey of approaches to voltage contrast shows their various limitations and experimental work further identifies the basic nature of the difficulties.

An electron lens and energy analyser arrangement is designed to overcome these problems and experimental results are presented which demonstrate the great improvement in performance over previous approaches. An automated voltage measuring system using this lens and analyser is shown to give very good results for integrated circuit type specimens.

Efficient methods are developed for the calculation of potential distributions and electron trajectories in the lens and analyser. Computer aided analysis, design and simulation studies are carried out using these. An analysis of the operation of the system is presented and consideration is given to the design of the lens and analyser with a view to further improving performance. Simulation of the voltage measuring system for integrated circuit type specimens shows that limitations in performance of the experimental system are due to the characteristics of the type of analyser used. The considerable potential of the basic lens and analyser approach to voltage measurement on integrated circuits is demonstrated.

A number of applications are proposed for the voltage measuring system in integrated circuit testing and guidelines are given for further work in this area.

ACKNOWLEDGMENTS

The financial support of a Science Research Council research studentship during the period of this work is gratefully acknowledged.

I wish to thank Dr A R Dinnis for his helpful guidance and supervision during my time of study. Also Professor W E J Farvis for his interest in this work and provision of research facilities.

Thanks are due to Mr James Goodall for technical assistance and for expert instruction in the art of operating a scanning electron microscope. Thanks are also due to Miss Irene Black for her care and efficiency in typing the manuscript.

Finally, I would like to thank my wife Irene for her patience and encouragement during the preparation of this thesis.

CONTENTS

*Note: Pages containing figures are interleaved within the text and
are not numbered*

	<i>Page</i>
TITLE PAGE	<i>(i)</i>
ABSTRACT	<i>(ii)</i>
ACKNOWLEDGMENTS	<i>(iv)</i>
CONTENTS	<i>(v)</i>
LIST OF SYMBOLS AND ABBREVIATIONS	<i>(x)</i>
CHAPTER 1 INTRODUCTION TO THESIS	1
CHAPTER 2 THE SCANNING ELECTRON MICROSCOPE	4
2.1 The Instrument	4
2.1.1 History	4
2.1.2 Introduction	4
2.1.3 Comparisons	4
2.1.4 Construction	5
2.2 Electron Optics	6
2.2.1 Electron gun	6
2.2.2 Electron lenses	6
2.2.3 Scanning coils	8
2.3 Modes of Operation	9
2.4 Beam Specimen Interactions	11
2.4.1 Introduction	11
2.4.2 Qualitative connection of basic processes	11
2.4.3 Behaviour of primaries in the specimen ..	12
2.4.4 Electron backscattering	13

	<i>Page</i>
2.5	Secondary Electron Emission 14
2.6	Beam Induced Conductivity 17
2.7	Contrast Mechanisms in the SEM 17
2.7.1	Introduction 17
2.7.2	Emissive mode 18
2.7.3	Conductive mode 20
2.8	Effects on Specimen due to Observations in SEM 21
2.8.1	Introduction 21
2.8.2	Beam induced contamination 21
2.8.3	Irradiation effects 22
 CHAPTER 3	
	INTEGRATED CIRCUITS AND THE SCANNING ELECTRON MICROSCOPE 24
3.1	Introduction 24
3.2	Integrated Circuits 24
3.2.1	Introduction 24
3.2.2	Bipolar - manufacture 25
3.2.3	MOS - manufacture 26
3.2.4	Large scale integration 27
3.2.5	Processing yield 29
3.2.6	IC testing 29
3.2.7	IC reliability 30
3.3	Current Applications of the SEM to Integrated Circuits 32
3.3.1	Introduction 32
3.3.2	Electron beam fabrication 32
3.3.3	Basic device and materials studies 33
3.3.4	Routine testing 36
3.3.5	Failure analysis 38

	<i>Page</i>
3.4	Damage to Semiconductors 38
3.5	Voltage Measurement for IC Testing 40
3.6	Approaches to Voltage Contrast in the SEM 42
3.6.1	Using conventional collector system .. 42
3.6.2	Using modified collection system 46
3.6.3	Using Auger electrons 51
3.6.4	Approach adopted 52
CHAPTER 4	DEVELOPMENT OF A TECHNIQUE FOR VOLTAGE MEASUREMENT ON INTEGRATED CIRCUITS .. 54
4.1	General Approach 54
4.2	Evaluation of the use of an Energy Analyser 55
4.2.1	Construction of analyser 55
4.2.2	Operation 55
4.2.3	Experimental setups and results 56
4.2.4	Study of limitations 58
4.3	An Electron Lens and Energy Analyser System 60
4.3.1	Requirements 60
4.3.2	Design 61
4.3.3	Construction and installation 63
4.3.4	Experimental results 64
4.3.5	Discussion of results 70
4.4	An Automated Measuring System 72
4.4.1	Introduction 72
4.4.2	Requirements and design 72
4.4.3	Counter/display and high speed D/A converter 73
4.4.4	Amplitude control circuit 74
4.4.5	Peak detection circuit 75
4.4.6	Operation and performance 76

	<i>Page</i>
CHAPTER 5	METHODS FOR POTENTIAL DISTRIBUTION AND ELECTRON TRAJECTORY CALCULATIONS 79
5.1	Introduction 79
5.2	General Approach 79
5.3	Potential Distribution in Lens and Analyser 81
5.3.1	Methods of calculation 81
5.3.2	Computer program 83
5.4	Potential Distribution Near Specimen Surface 85
5.4.1	General approach 85
5.4.2	Theory 86
5.4.3	Computer programs 89
5.5	Calculation of Electron Trajectories .. 91
5.5.1	Theory - cartesian co-ordinates 91
5.5.2	Theory - cylindrical co-ordinates 93
5.5.3	Calculation of electric field 95
5.5.4	Simulation programs 97
5.6	Efficiency, Accuracy and Scope of Programs 100
5.6.1	Efficiency 100
5.6.2	Accuracy 101
5.6.3	Scope 101
CHAPTER 6	COMPUTER AIDED ANALYSIS DESIGN AND SIMULATION 103
6.1	Introduction 103
6.2	Characteristics of the Electron Lens and Energy Analyser 103
6.2.1	Electron lens characteristics 103
6.2.2	Energy analyser characteristics 105

	<i>Page</i>
6.3	Analysis of Operation of the System 107
6.3.1	Introduction 107
6.3.2	The region above the specimen surface .. 107
6.3.3	Electron lens 110
6.3.4	Energy analyser 111
6.4	Design Studies for Lens and Analyser .. 113
6.4.1	Electron lens design 113
6.4.2	Energy analyser design 115
6.5	Simulation of System 118
6.5.1	Introduction 118
6.5.2	General approach 118
6.5.3	Results from simulation of the experimental system 120
6.5.4	Results from simulation of a system with an "idealised" analyser 127
6.5.5	Consideration of limitations 128
<hr/>	
CHAPTER 7	CONCLUSIONS 131
	REFERENCES 137

LIST OF SYMBOLS AND ABBREVIATIONS

Al	Aluminium
BCD	Binary Coded Decimal
D	Electric flux density
DAC	Digital to Analogue Converter
Δt	Short time interval
e	Charge on electron
eV	Electron volt (Energy)
E	Electric field
EHT	Extra High Tension (high voltage)
ϵ	Permittivity
FET	Field Effect Transistor
Ge	Germanium
∇	Gradient operator
GaAs	Gallium Arsenide
Hg	Mercury
IC	Integrated Circuit
LSB	Least Significant Bit
LSI	Large Scale Integration
m	Mass of electron
MOS	Metal Oxide Semiconductor
MSI	Medium Scale Integration
NIXIE	Gas filled, numerical indicator tube
r	Distance of electron from axis
RAM	Random Access Memory
ROM	Read Only Memory

Si	Silicon
SiO ₂	Silicon Dioxide
SE	Secondary Emission
SEM	Scanning Electron Microscope
SEMM	Scanning Electron Mirror Microscope
σ	Secondary emission coefficient or yield
torr	1 mm mercury (1.3332×10^2 N/m ²)
TTL	Transistor Transistor Logic
<u>v</u>	Underlining indicates vector quantity

CHAPTER 1

INTRODUCTION

The Scanning Electron Microscope (SEM) is an instrument which has greatly aided the study of microscopic phenomena. It is a convenient and versatile tool which has found wide fields of application in science and engineering. In this thesis applications of the SEM to integrated circuit testing are considered and demonstrated.

In chapter 2 the principles of operation and the construction of a SEM are described. The various modes of operation of the instrument are explained and the physical processes basic to these are considered. The contrast mechanisms in the SEM and the effects of observation on the specimen are discussed.

Chapter 3 commences with a description of the manufacture and testing of integrated circuits. A summary of current applications of the SEM to integrated circuits is then given. This demonstrates the mainly qualitative nature of work published on routine testing and failure analysis of these devices. The ability to make voltage measurements on working integrated circuits is identified as a very desirable development in device testing and the use of the SEM is shown to offer an attractive approach. A survey of published work on approaches to voltage measurement in the SEM indicates the limitations of the various methods and the need for further research with a view to improving the performance obtainable. A particular type of approach is chosen for further study.

The first part of Chapter 4 is an evaluation of the use of an energy analyser for voltage measurement in the SEM. Experimental results are given for a simple type of energy analyser. These reveal the considerable limitations of such an arrangement. Analysis of the limitations of the simple system and a consideration of the requirements for voltage measurement lead to the design and construction of an electron lens and energy analyser arrangement. Experimental results are presented for an automated measuring system using this lens and analyser. These results show the considerable improvements in performance of this setup over other approaches and demonstrate its ability to fulfil the requirements of the desired measuring system. A description of the design and operation of the electronics of the measuring system is also given.

In Chapter 5 consideration is given to further study of the experimental voltage measuring system. Methods are developed for the calculation of potential distributions and electron trajectories in the lens and analyser. The complexity of the setup is shown to necessitate numerical methods of solution. Computer programs which adopt novel approaches to obtaining these solutions are described.

Chapter 6 describes work which utilises these methods of calculation. Determination of the characteristics of the lens and analyser is followed by a detailed explanation of the operation of the electron optics. Consideration is then given to the results of computer aided design studies carried out with a view to improving lens and analyser design. Results of computer simulations for integrated circuit type specimens are presented for both the experimental setup and one using an "idealised" energy analyser. These results show the particular type of energy analyser used to be the

limiting factor in the experimental system. They also demonstrate the capabilities of the electron lens and energy analyser approach to voltage measurement on integrated circuits.

The last chapter summarises the conclusions of this work. Applications of the voltage measuring system in the testing of integrated circuits are suggested. Possibilities for further work in this field are noted.

CHAPTER 2

THE SCANNING ELECTRON MICROSCOPE

2.1 THE INSTRUMENT

2.1.1 History

The first Scanning Electron Microscope was built by Von Ardenne¹ in 1938. This was a fairly crude scanning transmission instrument. Work at Cambridge began in 1948 under Oatley and this group made major contributions to the development of the first commercial SEM² which became available in 1965.

2.1.2 Introduction

As an introduction to the SEM can be found in many places³⁻⁷, only a brief outline is given here.

The basic operating principles are outlined in Figure 2.1.1. The instrument consists of an electron-optical column, a vacuum system and control and display electronics.

An electron gun produces a beam of electrons which is then focussed by a series of lenses to a narrow probe. This beam is then scanned over the specimen, in a manner similar to a television raster, by a set of scanning coils. The electrons emitted from the specimen due to the effects of the primary beam are collected. This signal is used to intensity modulate a cathode ray tube scanned in synchronism with the electron beam in the column so giving a 'picture' of the specimen surface.

2.1.3 Comparisons

The SEM has considerable advantages over the conventional light microscope. The main improvement is in the depth of focus which is at least 300 times better than that of a light microscope, for similar picture quality and with both adjusted for optimum performance.

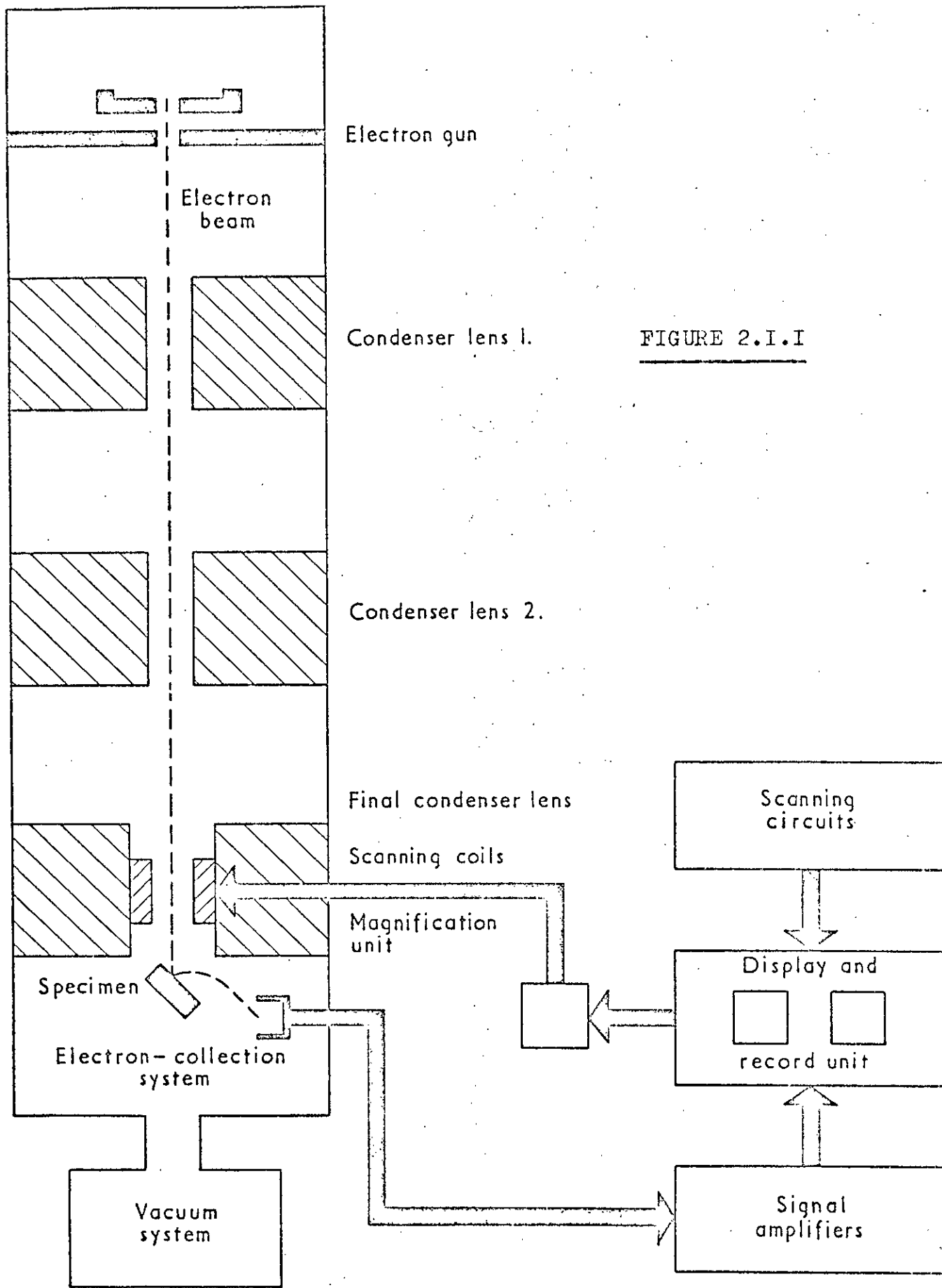


FIGURE 2.1.1

BLOCK SCHEMATIC DIAGRAM OF
BASIC OPERATING PRINCIPLES

The ultimate resolution is of course improved over the light microscope which is limited by diffraction effects.

The SEM also has advantages over the Transmission Electron Microscope in that it can be used to examine thick, rough specimens directly and electronic processing can easily be carried out on the signals it produces.

The SEM has found applications in almost every field of science⁸.

2.1.4 Construction

A sectional drawing of the electron-optical column of the SEM⁹ used in the present work is shown in Figure 2.1.2.

The triode electron gun at the top of the column has a tungsten hairpin filament cathode. Three prealigned electromagnetic lenses are fitted complete with replaceable apertures.

The distance between the lower surface of the final lens and the specimen is known as the *working distance* and is normally in the range 0-15 mm. Double deflection scanning coils, 8-pole stigmator and fine shift coils are mounted inside the bore of the final lens.

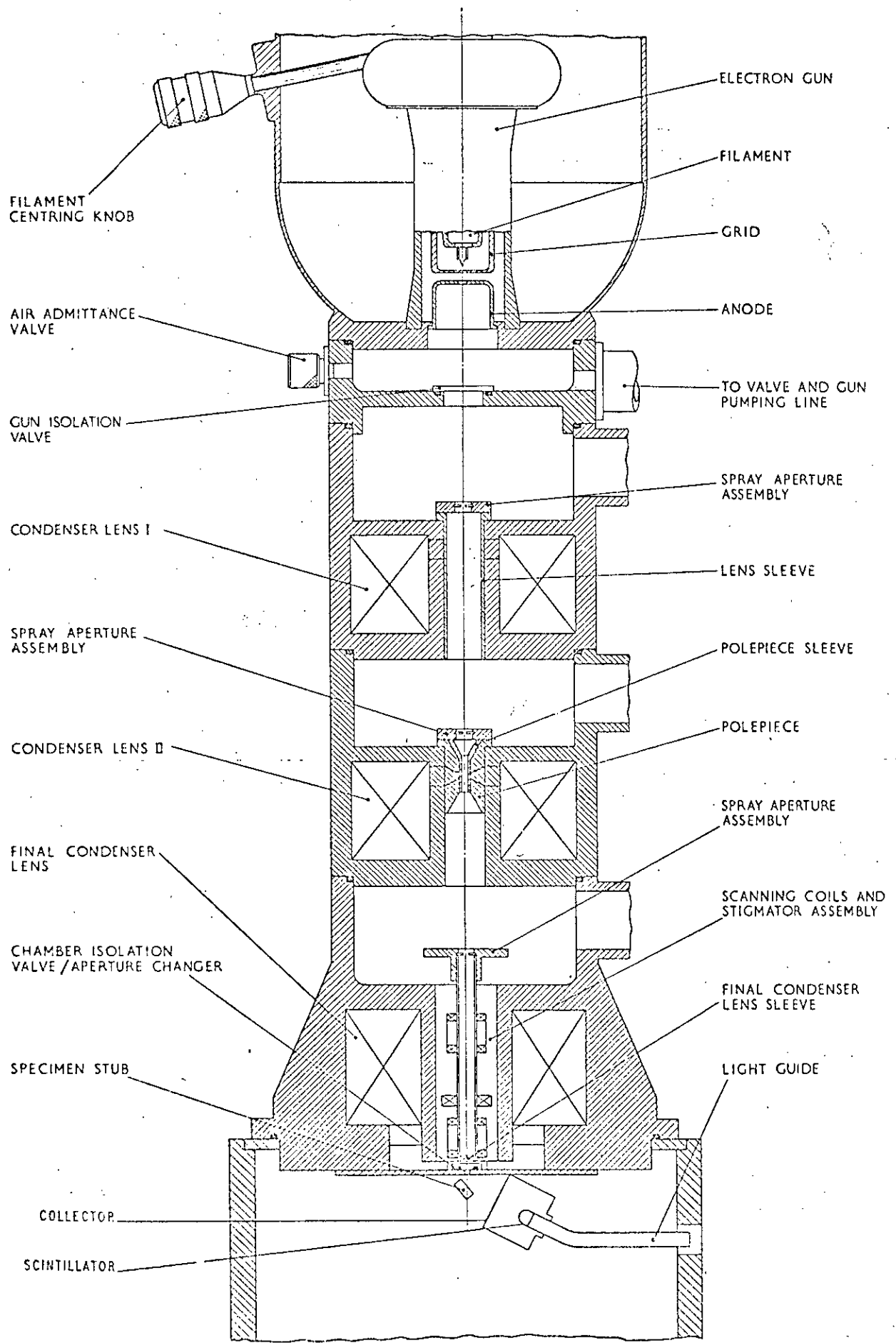
The electron collector is of the type first described by Everhart and Thornley¹⁰. This consists of a scintillator-photomultiplier combination. The photomultiplier is mounted outside the vacuum at the end of the light guide.

The vacuum system consists of a rotary pump and two oil diffusion pumps with the larger one used primarily for the specimen chamber and the other used for the column by means of the valving arrangements shown. The operating vacuum is better than 10^{-4} mm Hg (torr).

A large amount of electronic circuitry is associated with the operation of the microscope and this is housed in a separate console. All power supplies are housed in cabinets at a distance from the machine to minimise troublesome effects of stray magnetic fields.

FIGURE 2.1.2

Cross section of SEM electron-optical column



('STEREOSCAN IIA' Cambridge Instrument Company Ltd)

2.2 ELECTRON OPTICS

2.2.1 Electron Gun

The most common electron source used at present is the directly heated tungsten filament cathode which operates by thermionic emission. Other types of cathodes have been used such as Lanthanum Hexaboride¹¹ and Field Emission from a tungsten tip¹². These offer improvements over the tungsten hairpin but require better vacuum conditions. For a comparison see, Broers¹³.

The cathode is normally between 1 and 20 kV negative with respect to the anode (grounded). The gun produces an electron beam with a cross over just outside the grid region.

2.2.2 Electron Lenses

The function of the lenses is to demagnify the effective spot size of the beam from around 50 μm at the first cross over to 5-20 nm by the time the beam reaches the specimen. The lenses are normally electromagnetic lenses as these have several practical advantages over electrostatic lenses and also can give a slightly better performance as regards lens aberrations. The magnetic lenses used in the SEM are normally weak lenses; the focal length is long compared with the extent of the lens field.

The final diameter of the electron beam at the specimen surface is determined by the dimensions of the column and the focal lengths of the lenses. These focal lengths can be varied by adjusting the currents flowing through the coils in the lenses. In this way the beam can be focussed on the specimen surface. Lens currents have to be adjusted as the gun accelerating voltage is varied and as the specimen is moved around.

The lower limit of the beam spot size at the specimen is limited by the inherent aberrations of the lens system. Various types of aberration can occur in a lens system, only those important in the SEM will be mentioned here.

Chromatic aberration is due to the spread of velocities of the electrons in the beam. The electron velocities may vary due to changes in the gun EHT voltage and lens currents so that the power supplies for these must be very stable (<1 part in 10^5). If these are stable the residual chromatic aberration is due to the spread of the emission velocities of the thermionic electrons from the cathode.

Astigmatism is caused by the lenses not possessing perfect rotational symmetry about the axis. This type of aberration can be reduced by careful design and construction of the lenses and by keeping the lens bores and apertures clean. It can also be corrected to a great extent by means of coils built into the column (Figure 2.1.2). These can introduce a field adjusted manually to compensate for observed astigmatism in the operation of the SEM.

Spherical aberration arises because electrons moving on trajectories which are more inclined to the lens axis experience stronger fields and are more deflected. This is primarily a function of the strength and distribution of the focussing field in the lens.

There is also a fundamental limit due to *diffraction* which is a function of the wavelength of the electrons in the beam.

All these aberrations mean that instead of a point focus being produced at the specimen surface a *disc of least confusion* exists. The diameter of this is taken as the effective beam diameter.

This effective diameter is a complex function of the parameters mentioned but for low values of spherical and chromatic aberration the best value approaches 5 nm at 20 kV with a beam current of 10^{-12} A for a tungsten hairpin filament. (Broers¹³ also gives limits for other types of electron gun). Low beam currents can help to reduce the effective spot size but this conflicts with noise considerations for the final image.

2.2.3 Scanning Coils

Since there is an optimum working distance which gives the smallest spot diameter an increase in working distance is accompanied by a drop in performance. The increase in aberrations at lower lens excitation levels and therefore longer focal lengths is the reason why the scanning coils are normally placed above the final lens or in the lens housing (Figure 2.1.2). Two sets of coils are fitted to provide double deflection in both X and Y directions so that a greater overall deflection is obtained since the beam passes through the centre of the final aperture. Fine shift of the beam position is obtained by feeding the coils with a manually variable DC current to give a constant deflection field.

The same sweep current supply is used to feed both the deflecting coils in the display CRT and the column scanning coils ensuring synchronism between the rasters. The magnification of the instrument is varied by attenuating the current fed into the scanning coils so as to vary the size of the region on the specimen which is scanned by the beam. Since the display on the CRT is the same size at all times the attenuator can be calibrated to read the relative magnification.

2.3 MODES OF OPERATION

When a beam of electrons strikes a specimen a number of effects may be produced. Those important to the operation of the SEM are:

- a* Reflection of primary electrons
- b* Secondary electron emission
- c* Cathodoluminescence
- d* X-ray excitation
- e* Beam-induced conductivity
- f* Radiation damage

Effects *a* to *e* are all used in different modes of operation of the SEM. This is one of the advantages of the SEM since a great deal of information about a specimen can be obtained in one instrument.

Detectors are necessary for all these modes to convert the signal into an electrical one for display or processing.

For modes *a* and *b* use can be made of the same detector - normally that due to Everhart and Thornley¹⁰. As shown in Figure 2-1.2 this consists of a glass or perspex light pipe with plastic scintillator material on one end. The scintillator is coated with a thin aluminium layer held at +12 kV. A metal collector cage with a mesh front surrounds the scintillator and a voltage between -50 and +200 V is applied. Electrons entering the cage are attracted to the scintillator and hit it at high velocity causing light emission which produces an electrical signal by means of a photomultiplier at the end of the light pipe. This signal is amplified and used to intensity modulate the display CRT. When the collector cage is positive (wrt the specimen) the low energy secondary electrons (<50 eV) will form the major part of the signal and when it is negative these will be repelled, leaving the signal due to the higher energy reflected primaries.

In mode *c* use is made of the fact that certain materials emit light (fluoresce) when bombarded by electrons. This emitted light can be conveyed to a photomultiplier by means of a suitably placed light guide.

X-rays are normally detected by liquid nitrogen cooled semiconductor (Si or Ge) detectors placed as near the specimen as practicable. The signal can be displayed and used by a multichannel analyser. Crystal wavelength dispersive spectrometers are also used and have better wavelength resolution. This mode of use of the SEM can give useful information about the composition of the specimen.

Beam-induced conductivity can occur in specimens by the production of current carriers due to the action of the beam. If an electric field exists in the specimen (due to an externally applied voltage or is built-in due to a *pn* junction) a current, up to 10^3 times the beam current, will flow in the external circuit. This will vary as the beam scans the specimen surface giving a mode of operation mainly of interest for semiconductor specimens.

A current also flows from specimen to ground (anode potential) due to the charge carried by the electrons in the primary beam. The magnitude of this current will be the difference between the beam current and the total emission current from the specimen. If this *specimen current* is used to modulate the display CRT another 'picture' of the specimen is obtained.

It is convenient to use three terms to describe these modes of operation. If use is made of emitted electrons the SEM is said to be operating in the *emissive mode*. When any electric current produced by the beam is used the term is *conductive mode*. The term *luminescent mode* is adopted when use is made of light emitted from the specimen.

2.4 BEAM SPECIMEN INTERACTIONS

2.4.1 Introduction

In order to understand the operation of the SEM in the modes which have been mentioned it is necessary to consider the physical processes involved in the interaction of an electron beam with a specimen. The interactions between 1-30 keV electrons and the specimen are many and complex and no complete quantitative model has yet been proposed which adequately explains them all. Only those interactions which produce signals of use in the emissive and conductive modes of the SEM will be considered here.

2.4.2 Qualitative Connection of Basic Processes

The first interaction of primary electrons with the specimen is with the surface potential barrier. In the general case this can result in reflection of some of the primaries with the rest entering the solid. These will suffer both elastic collisions with atomic nuclei, whereby their direction of motion is more or less changed, and loss of energy through interaction with electrons. Those which suffer elastic collisions will in general be moving against the direction of the primary beam and may again undergo elastic collisions and loss of energy to electrons in the solid. Some of these redirected electrons will escape from the solid surface.

Thus there will be a distribution of excited crystal electrons which will interact with components of the solid such as electrons and phonons. These electrons will spread throughout the solid in a similar manner to the redirected primaries and some will reach the surface where a proportion will escape depending on their particular energy and direction of incidence. These are called emitted secondaries.

Some of these may be produced by excitons produced by the primaries rather than directly by primary electrons.

A general energy distribution curve for emitted electrons is given in Figure 2.4.1. This can be seen to have three more or less distinct sections. One group, 1, has the energy of the primary beam indicating that they must be considered to be elastically reflected primaries.

A second group, 2, can be defined as having energies between the primary energy and around 50 eV. The shape of this part of the curve would indicate that the electrons in this group are reflected to the surface only after having passed through a comparatively thick layer of the solid. These electrons are called rediffused primaries.

The third group (below 50 eV) exhibits a sharp maximum at a few electron volts. These electrons may be greater in number than the incident primaries. They are true secondary electrons emitted from the solid.

These divisions are of course not exact, since it is obvious that the division between true secondaries and rediffused primaries is very difficult to draw.

2.4.3 Behaviour of Primaries in the Specimen

Much of the work on the energy loss and scattering of primaries has been carried out on thin films by measuring the characteristics of transmitted and reflected electrons¹⁴⁻¹⁶.

Work in this field differentiates between cases when the number of scattering acts is such that the resultant angular distribution (of backscattered electrons) is Gaussian - *multiple scattering*, and when the number of scattering acts is greater - *diffusion* or less than this - *plural scattering*. The term *diffusion depth* has a number of definitions

but is basically the depth at which the electron motion becomes completely diffusive.

Experimental work has been carried out over the energy ranges used in the SEM in order to compare the results with the predictions of the different theoretical approaches to this problem. The assumptions which have to be made in developing any manageable theoretical approach normally mean that the results are only useful over a limited range of one of the parameters involved. No description of any of these approaches is given here since no *one* has emerged as clearly superior and since their various virtues have been adequately described elsewhere¹⁶.

2.4.4 Electron Backscattering

Experiments show that the backscattering coefficient (total flow of backscattered electrons per incident primary) varies with atomic number of the specimen and also with the energy of the incident electrons. In general the backscattering coefficient increases with atomic number of the target as might be expected. The variation with the incident energy is not very great. Kanter¹⁷ has reported that the angular distribution of the backscattered electrons can be approximated by a Lambert cosine distribution.

Simplified theoretical approaches have been developed by Everhart¹⁸ and Archard¹⁹. Everhart assumed *single scattering* and obtained fair agreement with experiment for elements with lower atomic numbers. Archard on the other hand assumed no energy loss until the onset of *diffusion* and obtained reasonable predictions for elements of large atomic number.

The deduction from this that these mechanisms predominate for extremes of the range of atomic numbers has been considered in comparison to experimental work by Coslett and Thomas²⁰. Their work on very thin films indicates that approximately 50% of backscattering from a solid target must be due to single scattering.

2.5 SECONDARY ELECTRON EMISSION

Secondary electrons are those emitted with energies less than say, 50 eV, as noted in section 2.4.2.

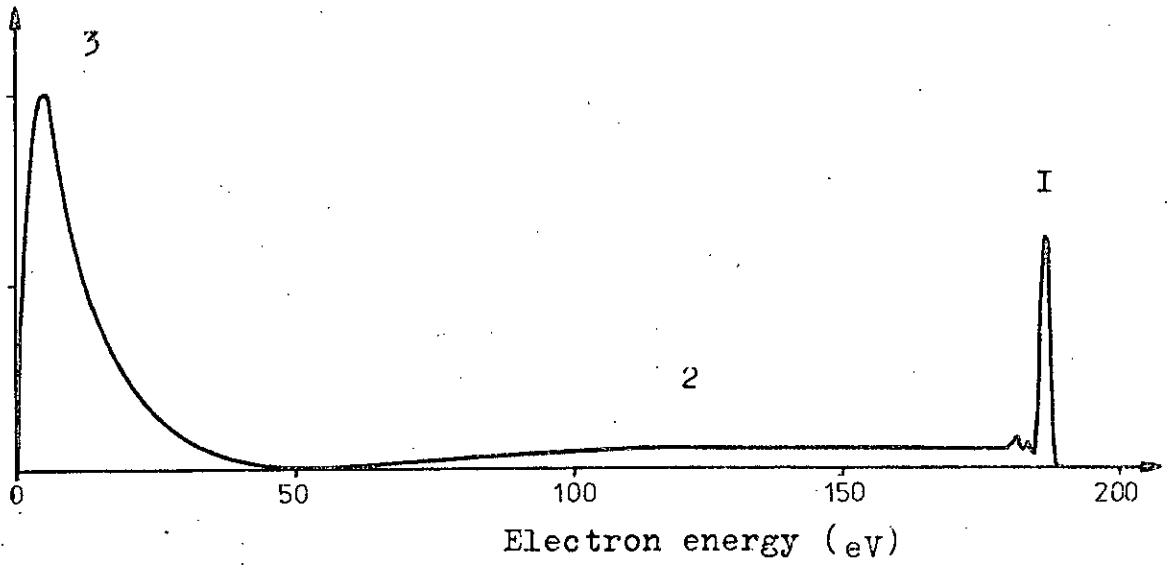
Much experimental work has been done on measuring the characteristics of secondary emission. Measurement is complicated by the need for surface cleanliness of the specimen since the majority of secondary electrons come from close to the surface. A parameter which is particularly difficult to measure is the absolute energy of the secondaries since the energy of these electrons is very low (most probable energy <10 eV).

Figure 2.5.1 shows the results of measurements made by Kollath²¹ of the *range* of energy spectra for 10 different metals. These curves are normalised with the vertical axis indicating, in arbitrary units, the number of electrons emitted, with a given energy. These energy distribution curves can be seen to have a marked maximum ranging between 1.3 and 2.5 eV. The energy distribution was observed to be independent of primary electron energy for values in the range 20 eV to 1 keV.

While the secondary emission energy distribution curves are generally of the shape already shown, slight subsidiary maxima can be seen for extremely clean metal surfaces and very good vacuum conditions. These occur at higher energy levels than "true" secondaries and are considered to be formed by *Auger* processes. In these processes primary electrons interact with deeper levels in the atomic structure than for "true" secondaries.

Semiconductors and insulators give energy distributions generally similar to those for metals but with the peak narrower and lower on the energy scale. Measurements on insulators are a special problem since the specimen will tend to build up an electric charge when bombarded by the electron beam.

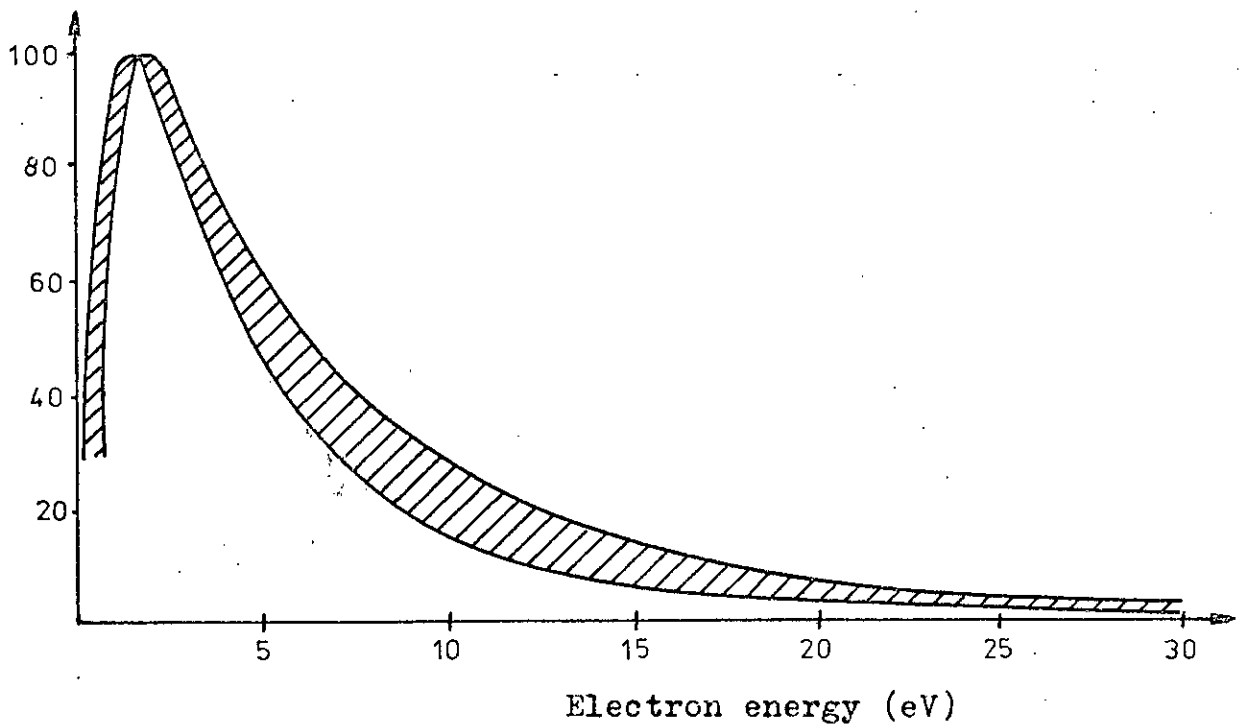
Number of electrons



General energy distribution curve for emitted electrons

FIGURE 2.4.I

Relative number of electrons



Range of energy spectra measured for 10 different metals

FIGURE 2.5.I

Qualitatively it appears²² that the maximum of the energy distribution curve is produced by the surface barrier. Despite the fact that the density of occupied energy levels in metals increases towards low energies, the surface barrier has such a strong influence on slow electrons (closely above vacuum energy level) that the decrease in the number of emitted electrons produces a maximum at a nearly constant distance above vacuum level. The position of the maximum is of course dependent on the energy angular distribution of the internal excited electrons as well as on the potential barrier. With a low potential barrier the maximum is generally expected at low energies. This is in fact borne out by the behaviour of alkali halides.

The energy angular distribution is of course required for a complete description of emitted secondaries. This is extremely difficult to measure accurately but Figure 2.5.2 shows results obtained by Jonker²³ (for Nickel). These show normalised yield radially for different energy secondaries and indicate the close relationship to the cosine law, the shape of the broken circle. The higher energy secondaries can be seen to follow the cosine law more closely (ie be circular) than do the lower energy electrons. The curves are independent of the crystal structure of the target and no fine structure was found in the distribution. The distribution was also found to be practically independent of the angle of incidence of the primary electrons.

The number of secondaries which leave the solid, produced by one primary is called the yield. This is an important parameter in secondary emission and has been measured for many materials under various experimental conditions. It is found that the yield or secondary emission coefficient depends on the material of the solid and also the energy of the incident electrons. The general shape of the yield curve ie secondary emission coefficient plotted against primary energy is shown in Figure 2.5.3. The yield increases with primary energy to a maximum and then falls off. The maximum yield for metals is around unity but the maximum varies with

energy for different metals. The maximum yield for insulators appears to be greater than this with the values obtained varying considerably between different samples. The measurements are of course complicated by the charging problem already mentioned.

Oblique incidence of the primary beam results in an increase of the yield with increasing angle of incidence from the normal to the specimen surface. This effect is only noticeable for primary energies considerably greater than that for maximum yield. The relation

$$\log_e \frac{\sigma_\theta}{\sigma_0} = K(1 - \cos\theta) \quad \dots 2.5.1$$

has been obtained (where $\frac{\sigma_\theta}{\sigma_0}$ is the ratio of the yields at angles θ to normal and normal incidence and K is a constant).

Because of their interactions with the electrons and phonons in the solid the secondaries released inside the solid have only a limited range. Experiments on thin films²⁴ indicate that the escape depth of secondaries from metals is of the order of a few nano-metres. The escape depth is the maximum depth from which created secondaries can reach and escape from the surface.

The time constant of secondary emission may be of interest in some applications. This has so far not been measured but it is deduced by indirect methods to be smaller than 10^{-11} sec.

Experimental evidence has been produced²⁴ that the number of secondaries produced within a volume element of a solid is proportional to the energy dissipated in that volume element by the primary electrons. Kanter²⁵ has shown results which indicate that about 40% of the total emitted secondaries are produced by backscattered electrons.

The theory of secondary emission and the development of a model of the complete process are very complex and further consideration here would be out of place. Excellent coverage is given to this elsewhere, particularly Hachenberg and Brauer²⁶.

2.6 BEAM INDUCED CONDUCTIVITY

Section 2.4 has indicated that the primary electrons create impact ionization in the specimen. This can be regarded as the creation of free carriers in the surface layer of the specimen. The number of these carriers can often be large compared with that required to give a significant change in surface conductivity in semiconductor specimens. Thus considerable modulation of the current flowing in a semiconductor specimen can occur when an electron beam impinges on the surface.

For thin insulators the penetration distance of the beam may be sufficient to reduce the effective resistance of the specimen in the region of impact of the primary beam, due to the conductivity induced by it. This may mean that thin insulating specimens do not build up much excess charge when bombarded with an electron beam. When the specimen is thicker or the beam induced conductivity is not so great, high potentials may exist across the thickness of the sample due to the *total* electron emission coefficient being less than unity.

2.7 CONTRAST MECHANISMS IN THE SEM

2.7.1 Introduction

The physical processes which have been described can all take place in the SEM. The factors that are now of interest are how these processes give rise to useful signals which can be displayed and observed. Only general indications can be given here since the variations of signals produced are as many as the specimens observed.

Contrast is a term used for the difference in intensity of the signal produced by a detector when the electron beam moves from point to point over the specimen. The mechanisms of contrast are different for each mode of operation of the SEM. The subject has been investigated often, with no great change of conclusions from the early workers in this field^{27,28}. A good review is that by Clarke²⁹.

2.7.2 Emissive Mode

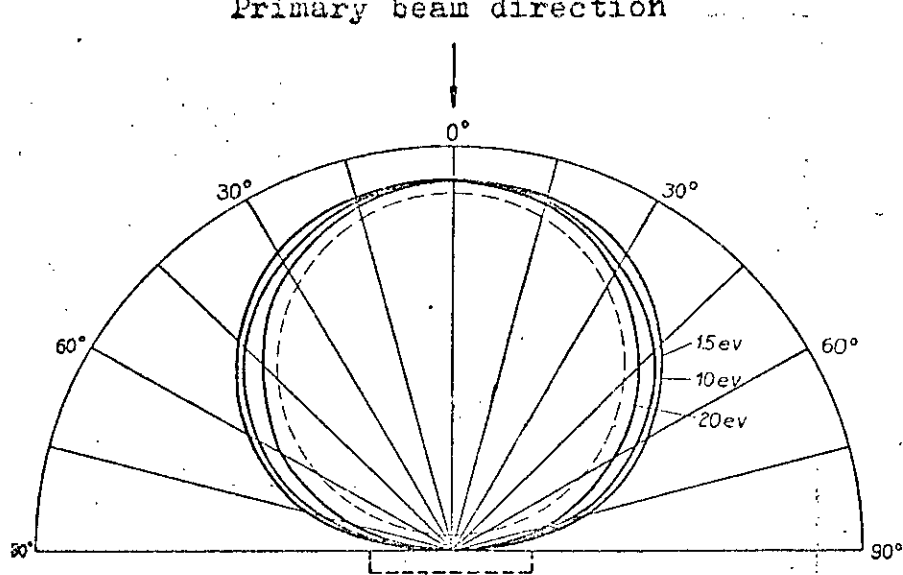
Assume the use of the Everhart-Thornley collector system (Figure 2.1.1). The number of secondary electrons which reach the collector will depend on a number of factors.

Firstly the number of secondaries emitted from the surface will depend on the angle of inclination of the surface to the primary beam (equn 2.5.1). If the surface is very rough the total secondary emission from points such as A and C in Figure 2.7.1, may be different. The total secondary emission from C will be greater than that at A due to the greater number of secondaries formed within the escape distance from the surface. The electrons with paths shown dotted may be shielded from the collector and may be collected by the specimen itself.

Electric and magnetic fields near the specimen surface and in the specimen chamber will affect the trajectories of the secondaries and may help or hinder their collection by the detector. A major component of the electric field will be produced by the voltage on the collector mesh. The inclination of the detector to the specimen will also affect the collected fraction.

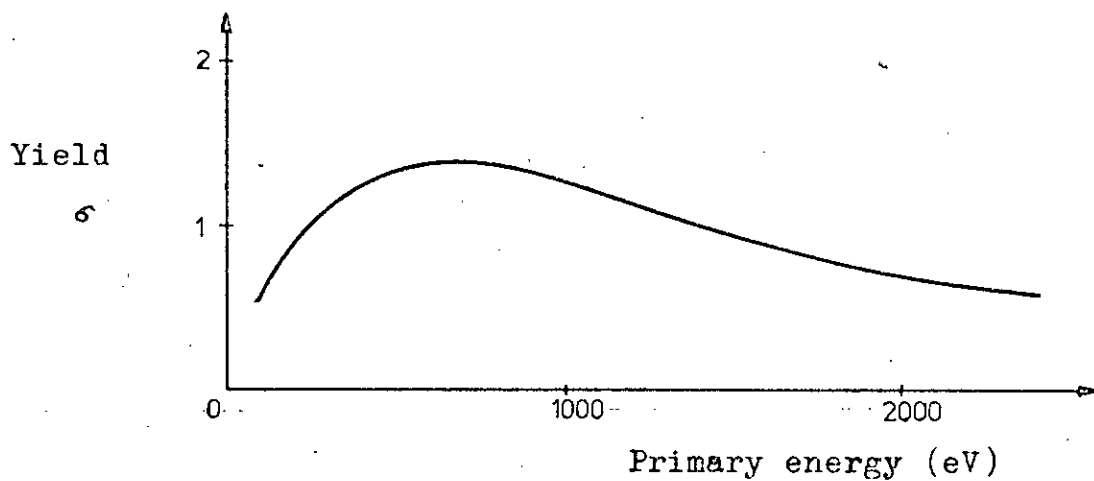
All these factors will result in a different signal at the photomultiplier output when the beam is at different points on the specimen.

In the case of backscattered electrons the factors will be similar but of differing magnitudes. The backscattered electrons have a much higher energy than secondaries and so tend to travel away from the specimen in straight lines. One of the consequences of this is that only a small fraction of the total backscattered electrons which are



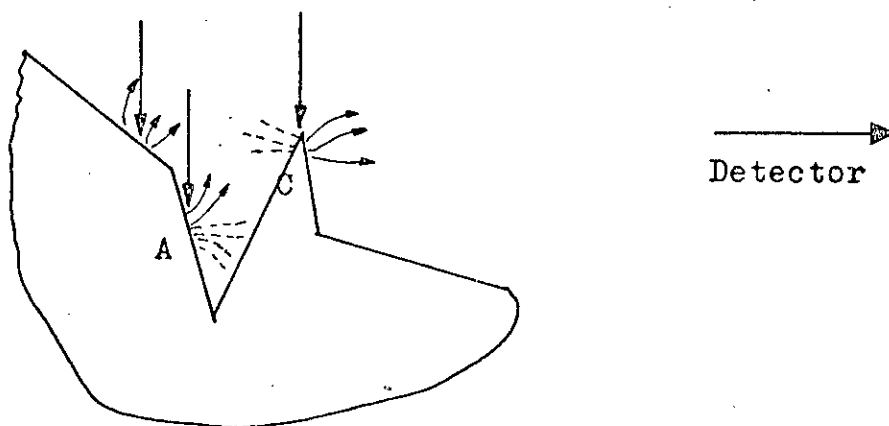
Measured energy angular distribution of emitted secondaries

FIGURE 2.5.2



General shape of yield curve

FIGURE 2.5.3



Emissive mode contrast mechanisms
(dotted paths indicate collection by specimen)

FIGURE 2.7.I

emitted within the solid angle subtended at the specimen by the collector will contribute to the signal. With the detector placed horizontally to the right in Figure 2.7.1 no high energy backscattered electrons from point A would reach it whereas some low energy secondary electrons might escape and be drawn towards and reach the collector. The angle of the specimen to the primary beam also affects the backscattered electrons. They will also be affected to a limited extent by local electric and magnetic fields. The backscattering coefficient varies with atomic number of the sample so that compositional contrast will be seen for certain relatively smooth specimens²⁸.

Thus in general it can be seen that the image produced by the two signals will be different with the secondaries producing a considerably bigger signal than the backscattered primaries.

A consideration of these contrast mechanisms shows that they will produce images which are similar in form to those which would be seen by looking at the object with the human eye along the incident beam direction, with illumination of the object from the direction of the detector. This is an extremely important feature of emissive mode images since it means they are fairly straightforward to interpret. A very different situation from the complicated shadow images of conventional transmission microscopy. To the user the SEM appears as just a very powerful light microscope.

An important factor in any consideration of contrast is the signal to noise ratio of the final signal since this limits the changes in contrast which can be observed. The two main noise sources are in the emission signal itself and in the detector system. The electron emission signal itself has inherent shot noise due to its physical nature. The detector system assumed has a noise level smaller than that of the signal. Everhart (see Ref 3) has evaluated an expression for the noise

performance which relates it to the current in the beam, the beam scan rate and the minimum detectable contrast desired. This indicates that the minimum contrast which can be detected decreases with increasing beam current and also as the scan rate is reduced. These conflict with low beam current to optimize spot size for best resolution and convenient sweep times. A compromise has to be reached.

2.7.3 Conductive Mode

The first effect, which is of great value in the semiconductor field, is charge collection. The theory of this is given in Thornton³.

The three mechanisms which occur in this case are the creation of hole electron pairs, the diffusion of carriers to junction (if any) and the charge collection process itself. A factor which affects these mechanisms can lead to contrast on the charge collection image. The number of hole electron pairs created will be affected by the electron backscattering and the secondary electron yield. Localised processes may affect the diffusion of carriers and carrier lifetime. These may consist of recombination centres, dislocations and traps as well as internal faults and micro-cracks.

The interpretation of contrast resulting from these effects is obviously complex and requires careful consideration of the factors involved. It is however a useful form of contrast particularly in the investigation of subsurface conditions.

For materials in which charge collection does not occur the specimen current mechanism can be exploited. Since the specimen current is the difference between the beam current and the total electron emission current the contrast mechanism in this case will be a combination of those described for the emissive mode. The contrast will in general be reversed from that in the emissive mode since regions of high total emission will give low specimen currents. The actual current is normally very low and requires a sensitive low noise current amplifier.

2.8 EFFECTS ON SPECIMEN DUE TO OBSERVATION IN SEM

2.8.1 Introduction

It is important to consider the ways in which a specimen is affected by observation in the SEM. A large number of different effects can occur but they are all mainly concerned with the interaction between the primary beam and the specimen surface. The term *surface* has two meanings here since there may be layers of contamination on the actual surface of the specimen. Those effects which might occur on certain types of specimen (eg biological) due to the vacuum in the SEM will not be considered here.

2.8.2 Beam Induced Contamination

Under normal laboratory conditions the surface of a solid will have contamination layers on it. These may consist of traces of chemicals left over from manufacture of the solid, cleaning agents, greases, absorbed water vapour etc. Even if the surface is "cleaned" prior to insertion in the SEM the very process of evacuating the specimen chamber will cause outgassing of component parts which will result in contamination on the surface.

A very great source of surface contamination in the conventional SEM is oil vapour which backstreams from the oil filled diffusion and rotary pumps used to evaporate the system. "O" ring seals and mechanical couplings also emit hydrocarbon vapours from grease used on them.

The effect of the electron beam on these contaminants is complex but in general it produces surface layers with undesirable properties. The thin surface layers (normally insulating) may build up potentials on them which interfere with collection of the emitted electrons. The beam seems to produce polymerisation of the hydrocarbons in the deposited oil and the results of this can be observed both in the SEM and the optical microscope. In most cases these effects are undesirable as they interfere with normal contrast mechanisms and complicate

interpretation.

The rate of formation of this contamination depends very much on particular conditions but some degradation can be observed in certain modes in less than one minute²⁹.

Fortunately this type of contamination can be considerably reduced if certain precautions are observed. Liquid nitrogen cooled baffles can reduce the backstreaming from a diffusion pump. A cold region (liquid nitrogen temperatures) near the specimen can considerably reduce the rate of formation of contamination³⁰. The greatest improvement can be obtained by eliminating the use of oil filled pumps. Various types of alternatives are possible such as *ion pumps*, *turbo-molecular pumps* and *cryopumps*. SEM's using these types of pumps have shown significantly reduced beam induced surface contamination problems³. The disadvantages of these types of ultra high vacuum systems are the long pump down time and requirement of baking the system to a high temperature to outgas the parts.

2.8.3 Irradiation Effects

The effects already described are also irradiation effects but the main concern here is with those changes produced by the beam in the actual surface region of the specimen.

The surface of a solid is in general less well ordered from a crystallographic point of view than the bulk material. It normally contains a higher density of surface states, which may act as fast or slow traps or recombination centres, than the bulk material. The density and type of these states may be important to the operation of specimens such as semiconductor devices.

The interaction between the electron beam and these surface states can take a number of forms all of which are complex and difficult to predict or even measure. It has already been noted that the primary electrons form regions of intense ionisation near the surface of

specimens. This may alter the degree of occupancy of local states and for certain materials this change may be semi-permanent although it can normally be annealed out at a high temperature.

Another effect is the creation of further defects by the action of the beam. These can interact with existing defects to form new stable defects.

The number of surface states is often important for semiconductor devices especially those employing surface effects for their operation eg MOS devices. These devices operate due to inversion layers, and beam induced charge in surface states can produce further troublesome inversion layers. The presence of bias voltages on these devices during observation can further complicate matters, often producing more permanent effects.

Whether or not these effects mentioned above produce difficult problems in SEM observation of specimens depends very much on the particular cases considered. Very long observation times can produce difficult problems for certain specimens but in general the effects on specimens due to SEM observation are not serious enough to limit the wide use of this instrument in every field of science.

CHAPTER 3

INTEGRATED CIRCUITS AND THE

SCANNING ELECTRON MICROSCOPE

3.1 INTRODUCTION

The scanning electron microscope has already been shown to be a versatile instrument providing a great amount of information about specimens examined in it. The field of semiconductor devices in general and microelectric integrated circuits in particular is one in which the SEM has many applications. In order to understand the requirements of this field of application it is necessary first to consider some basic points about the construction and manufacture of these devices.

3.2 INTEGRATED CIRCUITS

3.2.1 Introduction

An integrated circuit (IC) consists of a single-crystal chip of silicon containing both active and passive elements and their interconnections. These circuits are produced by the same type of processes used to form individual transistors and diodes. The main benefits from this technology are high reliability, small size and low cost as compared with the use of discrete components interconnected by conventional methods.

A term often used is monolithic integrated circuits since they are built into a single chip. The term hybrid is used when one or more components of the circuit are mounted on the surface of the basic chip.

Just as there are two main types of transistor, bipolar and unipolar, there are two main types of IC each using one of these transistor types. These are commonly known by the terms *bipolar* and *MOS* (metal oxide semiconductor) integrated circuits.

3.2.2 Bipolar - Manufacture

A very simple circuit is shown in Figure 3.2.1a and its construction cross section in bipolar monolithic form in Figure 3.2.1b.

The starting point in the manufacture of such a circuit is a polished slice of monocrystalline silicon which may be up to 75 mm in diameter.

There are four major process steps in bipolar IC production. These are epitaxial growth, isolation diffusion, base diffusion and aluminium metallisation. The diffusion processes act on areas which are defined by photolithographic etching of silicon dioxide areas formed during oxide growth.

The first step is *epitaxial growth* of a 25 μm thick layer of n-type ($\sim 0.03 \Omega\text{m}$ resistivity) silicon on the p-type substrate ($\sim 0.1 \Omega\text{m}$) by heating the slice to around 1200°C in an atmosphere of a suitable mixture of gases. After polishing and cleaning *oxide growth* takes place by forming a thin layer (0.5 μm) of SiO_2 over the entire slice by heating to 1000°C in an oxygen atmosphere.

A *photolithographic etching* process is used to open windows in the oxide layer. This consists of covering the surface with a layer of *photoresist* which is then exposed by light shone through a chromium *mask* of the desired pattern. The unexposed photoresist is etched away leaving areas of oxide which can also be etched.

Heating the slice to 1000°C in an atmosphere of gases with a p-type impurity produces the *isolation diffusion*. The p-type regions so formed leave isolated n-type islands separated by back-to-back

p-n junctions giving electrical isolation between circuit components.

Oxide growth takes place again, openings are made using another mask and the *base diffusion* carried out. This produces a p-type region with higher resistivity than the isolation regions. Resistors and diode anodes may be formed in this step.

Oxide growth and photolithographic etching precede the n-type *emitter diffusion* process when diode cathode regions are formed.

A final oxide growth forms the layer which has windows etched to allow contacts to be made via the thin (1 μm) aluminium layer which is formed over the surface. This aluminium is then masked and etched to give the *metallisation* interconnection pattern required. A passivation glass layer may be added for protection.

The areas formed in these processes are marked in Figure 3.2.1b with the relative impurity concentrations indicated.

The procedure described is only one particular approach to a bipolar process but all processes include the same basic steps and methods.

In practice a large number of identical circuits are manufactured simultaneously on a single wafer which is finally scribed and separated into individual chips. Each chip is then mounted onto a suitable header and wires are bonded to it using thermocompression or ultrasonic bonding.

The completed device is then encapsulated.

3.2.3 MOS - Manufacture

A section of a typical MOS device is shown in circuit form in Figure 3.2.2a and in monolithic IC construction in Fig 3.2.2b.

The manufacturing process is somewhat different from the bipolar one.

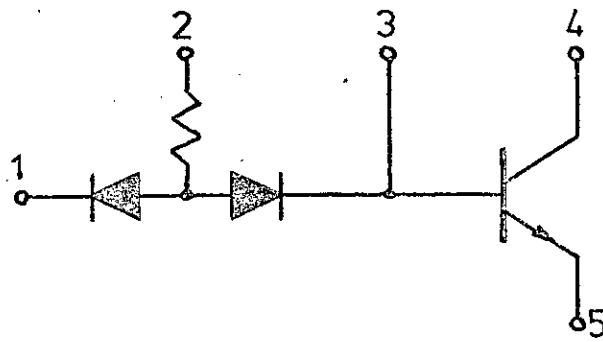


FIGURE 3.2.1a

Simple Circuit

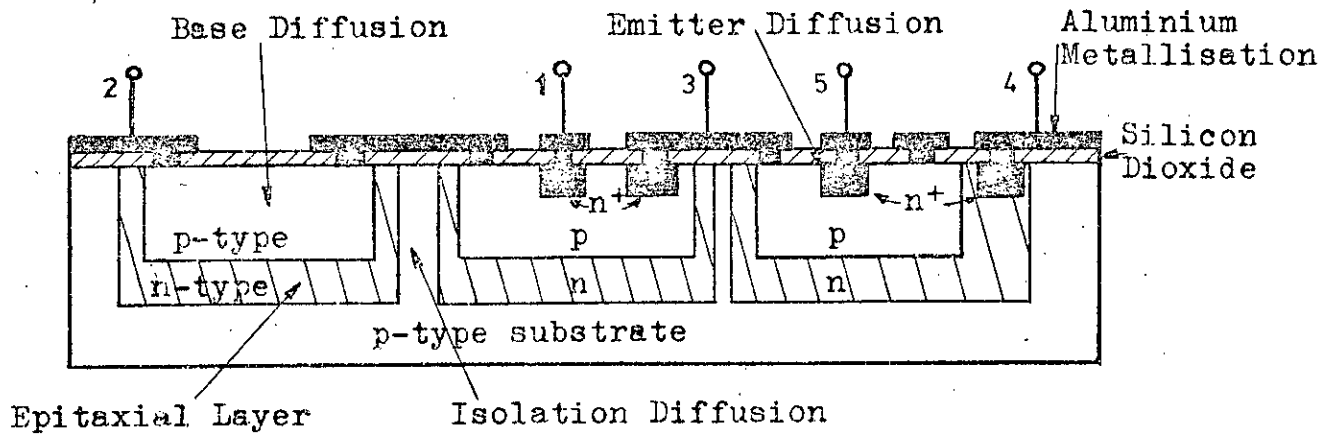


FIGURE 3.2.1b

Construction Cross Section In Bipolar Monolithic Form

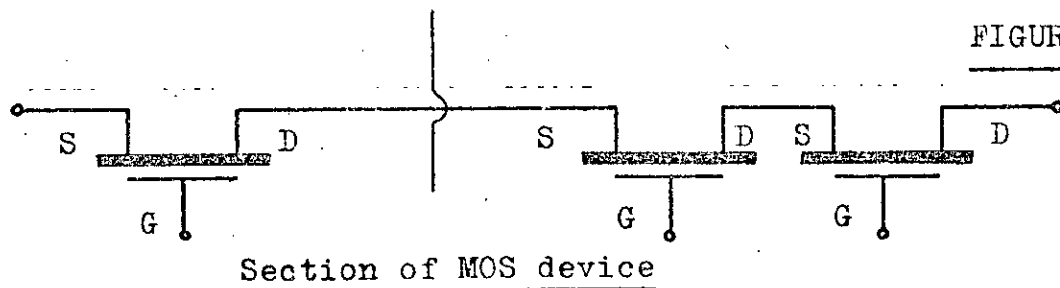


FIGURE 3.2.2a

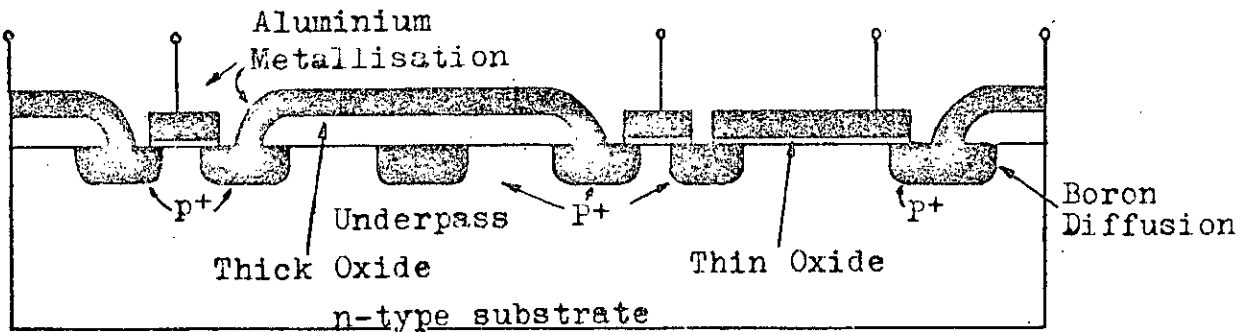


FIGURE 3.2.2b

Cross Section of P-Channel IC Realisation

The basic silicon slice undergoes a $0.6\ \mu\text{m}$ oxide growth. This is then photolithographically etched to define the areas where p-type diffusions are required for source drain and underpass regions. Boron (p-type) is deposited and diffused or driven in at a high temperature producing a layer about $2\ \mu\text{m}$ deep. Oxide growth to a total thickness of $1.5\ \mu\text{m}$ then takes place after which gate areas and contact hole regions are etched away. A thin (gate) oxide of about $0.12\ \mu\text{m}$ is grown over these areas and this is treated to remove undesirable effects such as charge centres.

A third photoresist stage defines the contact holes which are then opened by an acid etch. Finally an aluminium metallisation layer is formed and etched to the desired interconnected pattern as in the bipolar process. Again a passivation layer may be added for protection.

This process gives a thin oxide threshold voltage of $2.5\text{--}4.5\ \text{V}$. The purpose of the thick oxide marked in Figure 3.2.2b is to ensure that these areas do not act as parasitic MOS devices, by making their threshold high ($>40\ \text{V}$).

Again this description has been of a specific process. Others exist but use similar techniques. Further information on this and more detailed information on integrated circuit production can be found in textbooks on the subject.^{31,32}

3.2.4 Large Scale Integration

Since the introduction of integrated circuits there has been continual pressure to make them more and more complex. This arises for both technical and economic reasons.

Terms in current use are medium scale integration (MSI) and large scale integration (LSI). The distinctions are difficult to draw and are purely a matter of convention. At the present time, for example, two J-K flip flops on one chip would be regarded as a 'normal' IC, a complete 8 stage shift register on a single chip as MSI and a 256 bit ROM (read only memory) on one chip as LSI.

The descriptions already given show that the MOS process is simpler than the bipolar process. There are no isolation diffusions in the MOS process resulting in a significant reduction in chip area. The reduced number of diffusions in the MOS process (1 instead of 3) eases the problem of cumulative mechanical processing tolerances giving further economy of area. In fact a single MOS transistor may occupy only 5% of the total surface area required by a typical bipolar transistor.

A consideration of these facts shows that MOS technology is to be preferred for LSI, where it is desired to have as complex a circuit function (as many devices) as possible on one chip. Normally conventional bipolar techniques are used only up to MSI size.

The choice in individual situations depends very much on the operational requirements for the circuit since there are considerable voltage level and interfacing differences between bipolar and MOS devices. Conventional MOS is normally much slower than bipolar but the relative merits are varied as different processes come into production.

Current LSI complexity is considerable since complete, sophisticated calculator circuits are now available on one chip. In memory devices 2048 bit ROM's and RAM's (random access memories) are available with the number of functions per chip continuing to increase.

3.2.5 Processing Yield

Obviously to a manufacturer of integrated circuits the overall yield is important. The yield is defined as the number of saleable devices produced, compared to the number of circuits on a slice at the first stage of the process. For "normal" bipolar IC's the yield may be high (80%) whereas for MOS LSI the yield may be low (20%). IC processing is costly so that all factors resulting in a loss of yield must be controlled.

Reductions in yield may be due to imperfections in the initial silicon wafer, poor alignment of masks, poor etching, impure oxide growth, poor metallisation, handling damage or of course any combination of these and other factors³³. As might be expected the yield of large scale circuits is normally poorer than smaller circuits. Also although the MOS process appears simpler it is in fact more difficult to produce MOS devices due to the very high cleanliness required especially during formation of the gate oxide.

3.2.6 IC Testing

The silicon slices may be examined by an optical microscope at each stage in the process to observe the alignment of the various steps of the process. The final aluminium interconnection pattern may be observed to check for breaks and faults. Often however, the testing is restricted to the final circuits, as they are on the slice prior to scribing. This is done by probes being placed on the bonding pads of each circuit in turn and applying various DC and functional tests depending on the type of circuit. This is often carried out by a computer controlled tester which checks out each circuit, automatically moving on to the next. Faulty circuits are automatically marked by an ink blob. The speed of testing depends on the number of tests carried out on each circuit but can be extremely fast (several circuits per second). For LSI memory circuits testing is obviously quite a problem

since it takes a considerable time to exercise each function of the circuit. In some cases dynamic signal relationships are important in a circuit and it is difficult to check these. Normally these tests are go-no go according to a set standard.

The slices are now scribed and separated with the good chips being mounted to a header and bonded out. Some may be encapsulated in epoxy or plastic packages. The final circuits are now computer tested again when a number will fail due to damage produced in these processes.

The testing processes described vary from manufacturer to manufacturer and between device types and also for different final applications. Those described are the ones normally carried out on consumer devices. Devices for military and aerospace applications normally undergo more exacting test procedures. This introduces the involved subject of device reliability.

3.2.7 IC Reliability

The factors involved in the reliability of IC's are very complicated and are not completely understood so that it is only possible to consider those effects which have been found to be of practical importance.

All the factors which affect the yield of the process are important in this field since the dividing line between good and bad devices will depend on the tests applied.

Material imperfections, whether in the initial silicon or in the diffusion or oxide areas involved in the process, may affect device performance as temperature varies, or after a long period of operation. These are obviously very difficult to investigate since they may be variations in crystal structure, dopant profile etc. As will be shown later the SEM can give useful information in this field.

A major factor in device reliability has been found to be the quality of the aluminium interconnection layer. This is often narrow (10 μm wide) and thin (0.5 μm thick) so that even although it is only required to pass low currents the current density may be very high (10^{10} A/m²). This means that any imperfections, thinning, holes etc, may be potential causes of failure. Electromigration, (current induced mass transport) or thermal fusing may occur. The place of greatest difficulty is normally where the aluminium goes over an oxide step. The SEM has proved very useful in examining these metallisation areas.

Pinholes in the oxide (especially gate oxide) are also a cause of failure which may be observed with the SEM.

Poor bonding is also an important factor in reliability since mechanical or electrical weakness here can affect the shock resistance of the device. Chemical reactions between gold bonding wires and the aluminium bonding pads can be a source of difficulty. The SEM is useful in examining these bonding areas.

In consideration of these factors, devices for military applications normally go through mechanical shock tests, temperature and load cycling tests and perhaps radiation tests. These testing procedures obviously result in the final product being more expensive. While devices tested in this way are justifiably expected to be more reliable than "commercial" devices there is still a continual search for ways to improve the reliability of integrated circuits.

Testing is in fact an area in which there is a very great interest as devices become more complex so that reliability is of increasing importance.

A particular problem in integrated circuits is that unlike circuits made up of discrete components, the "component parts" of IC's cannot be tested "before assembly". Attempts to use mechanical probing methods on sections of the fabricated circuit prove difficult, particularly for LSI circuits. The area of checking the operating conditions of individual devices in a large IC is one in which the SEM could offer tremendous advantages over conventional methods. This will be dealt with at greater length in a later section.

3.3 CURRENT APPLICATIONS OF THE SEM TO INTEGRATED CIRCUITS

3.3.1 Introduction

It has already been noted that the SEM has a very useful role to play in the design and manufacture of integrated circuits.

Applications of the SEM in the semiconductor field were explored early in the history of the instrument. More recently it has become very much accepted as an important facility in the manufacturing plant of many large semiconductor device manufacturers.

There has been a considerable amount of information published on semiconductor applications, much of which is of at least a semi-quantitative nature.

Major applications areas are:

1. Fabrication of devices
2. Basic device and materials studies
3. Routine inspection
4. Failure analysis

3.3.2 Electron Beam Fabrication

It will already have been observed that the fabrication of ICs depends on the use of photolithographic techniques to define areas on the slice of silicon. This results in a fundamental limitation on

the smallest areas which can be defined using this technique. The limit is caused by diffraction effects on the light used to expose the photoresist. This makes it difficult to obtain the very small ($<1 \mu\text{m}$) devices which may be desirable in some applications.

Since the use of electron beams is potentially capable of giving smaller line widths a considerable amount of work has been carried out on this³⁴⁻³⁹. The SEM is particularly useful in this work since the beam position can be controlled by a computer³⁷ thus eliminating the requirement of making masks. The approach is to use the electron beam to expose photoresist which is then etched in the normal way. Conductors of width $0.5 \mu\text{m}$ have been produced in this way³⁸.

Use of the SEM offers other possibilities such as automatically positioning device electrodes³⁹ by using normal signal modes while carrying out the process of photoresist exposure.

The development of electron beam fabrication is continuing with linewidths of 200 nm with unity line to gap ratio being obtainable. These techniques will become of increasing importance as the complexity of devices increases, particularly in the areas of very high frequency and high switching speed circuits.

3.3.3 Basic Device and Materials Studies

Mention has already been made of the phenomenon known as electromigration. It is a factor which can be a failure mode in aluminization of IC's. Investigations of this effect have been carried out using the SEM in its emissive mode to examine the topography of the metal film surface⁴⁰⁻⁴³. The SEM provides detail which is not observable with an optical microscope as well as X-ray analysis of the metal film under test⁴². Studies have even been carried out

by taking motion pictures of the process of mass transfer, and eventual conductor destruction, in the SEM⁴³.

Some work has been done on using the SEM to investigate the characteristics of the semiconductor crystals from which devices are fabricated⁴⁴⁻⁴⁹. This has mainly been concerned with measuring the resistivity⁴⁵ of the materials, particularly the variation over the sample⁴⁶. This approach would be useful for small specimens where the four point probe method would be difficult, but so far has only been found applicable for fairly high resistivity materials. Measurements have been made in materials at points near p-n junctions to determine parameters such as minority carrier lifetimes and diffusion length.^{47,48}

A very important feature of the SEM is its ability to show clearly a p-n junction, as was first demonstrated by Oatley and Everhart in 1957⁴⁹. It was suggested that the contrast observed was due to the variation of collection efficiency of the detector as a function of the potential at the point of emission of the secondary electrons. This was called voltage contrast and has been widely used in semiconductor work. (This effect will be dealt with in greater detail in a later section).

A p-n junction also shows up clearly on a conductive mode micrograph. This is to be expected since the "built in" field in the junction will separate the hole electron pairs produced by the primary beam resulting in a current across the junction.

Using these contrast mechanisms, measurements have been made of the depletion layer width and its variation with applied bias, for planar diffused p-n junctions^{45,50}. By lapping the device surface and applying these methods measurements have been made of the junction profile and depth, which compare well with theoretical calculations⁵¹.

Since the electron beam penetrates the specimen, to a depth dependent on the material parameters and the energy of the beam, it is possible to "see" effects which are due to conditions under the actual surface. This is particularly useful in the conductive mode of operation since carriers produced by the beam below the surface will be affected by material characteristics and electric fields in the region in which they are created, thus leading to observable contrast. This gives information about the device which is not obtainable in any other way.

This means that junctions can be delineated under passivation layers (protective covering oxide over complete device) and estimates of junction depth obtained by noting contrast differences as the energy of the incident beam is varied, thus varying the depth of penetration⁵². In the case of MOS devices, the SEM in the conductive mode can show inversion layer formation under the gate electrode^{53,54} allowing the process of pinch-off to be observed⁵⁵.

The electron beam in the SEM can be used to initiate processes such as avalanching in a semiconductor⁵⁶ and by chopping the beam (ie turning it on and off rapidly) more information can be obtained about this process for specific devices⁵⁷. Variations of avalanche behaviour over the device are important in such areas as impatt diodes and secondary breakdown of transistors.

The range of devices investigated in the SEM is wide, including switching lateral transistors in IC's⁵⁸ silicon mesa diodes⁵⁹, epitaxial gallium arsenide varactor diodes⁶⁰, gallium arsenide Gunn diodes⁶¹ and silicon carbide light emitting devices⁶². These investigations yield information, about the behaviour of particular devices, which would be very difficult to obtain in any other way.

The use of the SEM in its different modes of operation is well represented in these examples given. In general the mode used will depend on the information it is desired to obtain and the type of device to be investigated. Since, in general, conductive and emissive micrographs of the same device carry different information⁶³, some of the work already mentioned has used the technique of combining the signals from the two main modes.

3.3.4 Routine Testing

This term is used to cover the tests carried out on a discrete device or integrated circuit, in the manufacturing process, after it has been fabricated. It includes tests carried out either on a 100% or a sampling basis.

As already mentioned, the quality of the metallisation layers on integrated circuits is an important factor in the reliability of these devices. The SEM offers the only really useful method of checking this quality.

SEM⁹ micrographs of integrated circuit metallisation are shown in Figures 3.3.1 and 3.3.2 to demonstrate the use of the SEM for this purpose. The SEM gives detail not readily observable in the optical microscope such as that shown in Figure 3.3.2. This metallisation over an oxide step has already been mentioned as a major problem. Even in the SEM it can be difficult to determine the cross section of the strip which remains electrically conductive, as in Figure 3.3.2. In very serious cases of bad step coverage it can be difficult to tell whether the layer is conductive or not. A means of electrical testing in the SEM would be useful for this application.

In recent years some customers have been requiring manufacturers to check the quality of metallisation on a sampling basis. This has been particularly true in the aerospace and military field and has

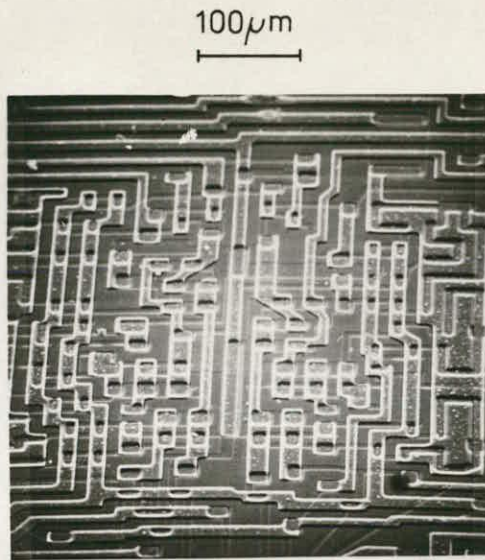


FIGURE 3.3.1

SEM MICROGRAPH GIVING GENERAL VIEW OF
INTEGRATED CIRCUIT METALLISATION



FIGURE 3.3.2

MICROGRAPH GIVING CLOSE UP VIEW OF
METALLISATION OVER OXIDE STEP

made it necessary for manufacturers to devise methods to carry out this examination⁶⁴. The use of the Scanning Electron Mirror Microscope (SEMM)⁶⁵⁻⁶⁷ has been proposed for 100% screening of metallisation for devices for military applications⁶⁷. (The SEMM operates with the specimen at or very close to the cathode voltage so that the incident electrons either do not reach the surface or hit it at a low velocity. The equipotentials above the surface act as a mirror to the incident electrons, thus forming contrast in the image produced by collecting the "reflected" electrons. This has advantages in terms of reduction of damage to the specimen as will be discussed later).

One difficulty in testing many production devices is the passivation "glass" protection layer used on some of these devices. It is possible to overcome this by virtue of the localised conductivity induced by the electron beam in this layer^{68,69}. This allows the use of the voltage contrast mechanism.

Work has been done on the possibility of operational testing of LSI arrays by stroboscopic scanning electron microscopy using the voltage contrast mechanism⁷⁰. In this approach the SEM is used in a manner similar to a sampling oscilloscope, by chopping the beam in synchronism with the waveform to be examined^{70,71}.

A comparison method of testing has often been suggested⁶⁷⁻⁷⁰, where the contrast signals obtained from a circuit under test would be compared with equivalent ones from a known "good" device, possibly using a computer. This would involve a complex system and has not yet been realised in practice.

Thus it can be seen that the SEM has so far not made major inroads into the realm of routine testing. This is mainly due to the qualitative nature of much of the work carried out in this

field, because of the difficulties of interpretation associated with some contrast effects.

3.3.5 Failure Analysis

This term is used here to mean the investigation of devices which have failed to pass electrical tests or failed in operation.

The use of the SEM for this purpose consists of applying the techniques already mentioned. Thus the presence of troublesome inversion layers^{68,72}, impurity inclusions, dislocation faults⁷³, faulty packaging materials and seals⁷⁴ and other failure mechanisms, can be investigated for devices which have proved faulty.

A review of work in this area has been given by Thornton, et al, 1969⁷⁵, with their specification for a SEM laboratory for this purpose (1969)⁷⁶.

Although the SEM is useful in this field the information it gives is mainly qualitative and can sometimes be difficult to interpret⁷². This is particularly true of use in the conductive mode. This means that to obtain the maximum information from a sample considerable experience in the use of the SEM is necessary.

This does not prevent the frequent use of the SEM to investigate faults in specific devices. In fact often this is the only way the desired information can be obtained. It would obviously be useful to have a technique capable of being used by any device engineer to investigate failed devices using the SEM, since the information obtained could be used to improve the fabrication process.

3.4 DAMAGE TO SEMICONDUCTORS

An important consideration in the application of the SEM to device testing is the effect which viewing in the SEM has on the performance of the device. The complexity of the effects produced

by electron beam irradiation of a specimen has already been mentioned. The exact effects on a structure such as a semiconductor device or integrated circuit are even more difficult to determine.

The electron beam may produce both charged states and surface states in the specimen. (See also Section 2.8) The changes produced in the number, type and occupancy of states both surface and bulk may temporarily or permanently affect the operation of the device. The effects are different for bipolar and MOS devices.

Experiments have been carried out on bipolar, planar transistors in the SEM^{77,78}. The results of these experiments showed that the current gain of these devices dropped markedly, quickly and then levelled off, with time, for a beam voltage of 16 kV and a beam current of 10^{-10} A. This effect could be reversed by heating (250°C) for a period of minutes in air. The explanation given is that the beam produces changes in the surface recombination velocity in the area of the base region accessible to emitter minority carriers. The effect is considered to be very localised.

Measurements on MOS transistors⁷⁸⁻⁸⁰ have indicated that the important effects in this case are the positive charge states created in the gate oxide and the surface states created near the Si-SiO₂ interface. The evidences for this are the observations that the shift of "threshold voltage" which takes place depends on the gate bias applied during irradiation and that subsequent bombardment with a -ve gate voltage removes the effect. This effect can also be annealed out by heating. These investigations used accelerating voltages in the range 5 to 40 kV.

The published measurements have not been dealt with in any great detail since they are dependent to some extent on the devices used. However the results fit into the pattern of electron beam

specimen interactions which have already been considered.

The practical implications for integrated circuit testing in the SEM are difficult to assess since little work has been done on this. Since the electron beam penetration depth depends on its energy, the results will depend on this as well as the thickness of metallisation, oxide layers etc. In general the use of low beam energies will reduce damage. In practical cases where the examination time is kept relatively short and reasonable metallisation thicknesses exist the damage produced will be unimportant^{38,68}.

The use of the SEMM has been proposed to completely eliminate problems due to these effects, including charge induced in the "glass" layer on passivated devices⁶⁷. This would be the case since the electrons in the incident beam will either not reach the surface or hit it at a very low velocity. The drawback of this approach is that the contrast mechanisms in the SEMM are more complicated than those of the SEM, especially in the case of rough specimens, as well as the reduced resolution which has so far been obtained with this instrument.

Another effect on the sample which can be produced in both the SEM and the SEMM is beam induced contamination due to hydrocarbons deposited on the specimen. This is a function of the vacuum in the specimen chamber and is not of great importance since it can be reduced by the use of cold traps and cold fingers and "clean" vacuum pumps (Section 2.8.2).

3.5 VOLTAGE MEASUREMENT FOR IC TESTING

The considerations given previously of IC manufacture, testing, reliability and failure studies have indicated the need for a method of voltage measurement in a "working" circuit. This would allow the testing and fault finding approaches used in discrete circuitry to

be adopted. Voltages "inside" the circuit could be measured to ensure that they were within the desired range and so regions of potential failure could be identified as well as actual fault areas. This would also fulfil the need, mentioned earlier, for information capable of being fed back to designers of new circuits and process engineers, about mask and fabrication weaknesses.

A possible specification for such a measuring system would be:

1. Very low circuit loading
2. Good frequency response
3. Measuring voltage range at least 30 volts
4. Accuracy around 5%
5. Linear response
6. Simple to use - direct readout
7. Automatic in operation - preferably capable of computer control

Since these requirements, as well as the need to test LSI circuits, rule out the use of conventional mechanical probing methods, an electron beam method seems the best solution. (Even where size problems do not preclude their use, mechanical probes are undesirable due to the high risk of surface damage and the difficulty of obtaining good electrical contact).

The use of the SEM gives an ideal solution to the first two requirements since the electron beam applies very low loading to the test circuit and by using the stroboscopic or sampling method it is possible to operate at gigahertz frequencies⁷¹.

It is obviously necessary to make use of the voltage contrast mechanism in the SEM to obtain the required information. Many different approaches to voltage contrast have been adopted and it is necessary to consider the basic factors involved as well as these different methods.

The success or otherwise of meeting the remaining requirements of the specification will be dependent on the characteristics of the measuring technique adopted.

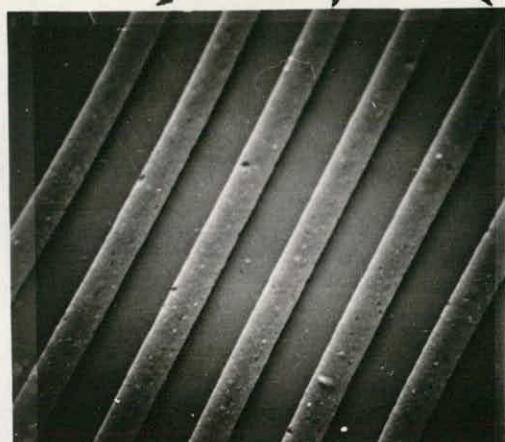
3.6 APPROACHES TO VOLTAGE CONTRAST IN THE SEM

3.6.1 Using Conventional Collector System

Early work on voltage contrast in the SEM was carried out by Everhart and reported in his Thesis in 1958 (See ref 82). Trajectory plots were carried out, for secondary electrons leaving the specimen surface, to show that the collection of electrons depended on the potential of the specimen. A slotted disk was placed over the collector to make the system more sensitive to potential variations on the specimen. This greatly reduced the collection efficiency and experiments showed that the relationship between video signal and specimen potential was very non-linear, with the shape dependent on the orientation of the aperture in the disk. It was suggested that transverse electric fields on the specimen surface (eg p-n junction) might produce contrast by affecting the electron trajectories. The use of a grid between the collector and specimen was reported, with similar results to the slotted disc. The use of a velocity-analyser for voltage detection was suggested.

It is possible to observe voltage contrast in the SEM using the normal Everhart-Thornley detector system.(eg Figures 3.6.1(a)-(c) show SEM⁹ photographs of voltage contrast for interdigitated Al fingers on SiO₂ on Si substrate. The voltages marked are for three of the strips with respect to the other three which are earthed.) The problems are that the contrast observed is very dependent on the position and angle of the specimen to the collector. It is very difficult, in general, to relate the contrast observed to the actual

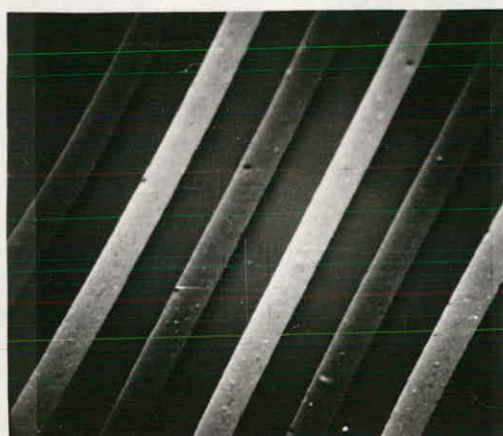
THESE STRIPS ALWAYS EARTHED



FIGURES 3.6.1(a)-(c)

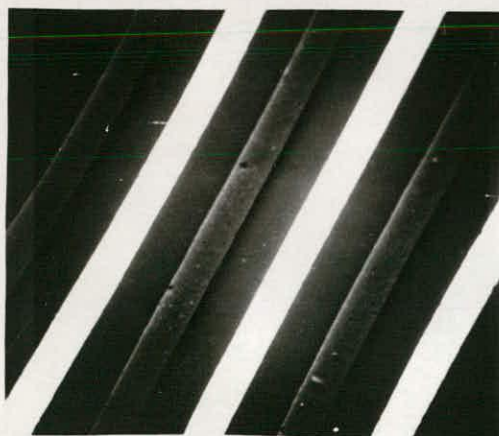
(a)

OV APPLIED TO OTHER
STRIPS



(b)

-10V APPLIED TO OTHER
STRIPS



(c)

-20V APPLIED TO OTHER
STRIPS

All: beam voltage 20kV
angle 40°

20µm

voltages on the specimen (eg negative voltages do not always make the picture brighter). There are many reasons for this, one of which is that the micrograph contains topographical contrast as well as contrast due to potentials on the specimen. (eg left hand edges of strips in Figures 3.6.1(a)-(c)). Thus although in many cases potential differences do show up clearly, very little quantitative information can be obtained and even qualitative interpretation can be difficult for a device such as an IC. (Figures 3.6.1(a)-(c) were the best that could be obtained for this sample and even for this 10 volts were required to give the contrast in (b)).

Various methods of separating the component of the output signal due to the potential on the specimen from the overall signal have been suggested.

A method of switching the potentials on the specimen on and off at a high frequency (200 kHz) and obtaining a difference signal from the video outputs corresponding to *bias* and *no bias* on the specimen, was used by Oatley⁸³. Assuming the contrast signal consists of the sum of components due to surface topography and potential, obtaining the difference signal should result in contrast due to potential alone.

Figure 3.6.2 shows a block diagram of an experimental setup built to test this approach. The results obtained were unsatisfactory for a number of reasons. One of these was the great difficulty in removing topographic contrast completely in a normal sweep (micrographs are no problem). This is a limitation of the switching frequency (three times higher than Oatley's ie 1.6 μ s period) since even in this short interval the topographic contrast signal will be different at each sampling point due to the motion of the beam over the surface.

Bandwidth and phase shift limitations in the standard photomultiplier head amplifier⁹ precluded increasing the switching frequency. This approach was dropped in favour of a simpler system.

The circuit adopted for this approach is given in Figure 3.6.3 and is similar to Thornton (Ref 3, p 327). The specimen potential is switched on and off on alternate line scans with the difference signal again expected to eliminate topographical contrast leaving only potential contrast. Figures 3.6.4(a) and (b) show typical results (linescans - no frame sweep) obtained by this method using the copper printed circuit board specimen shown in Figure 3.6.4(c). The right hand strip is kept at earth potential and the potential on the other strip is as shown. The upper trace in both figures is the response for both strips at earth potential.

A number of interesting points can be seen from Figures 3.6.4(a) and (b). Consider the *left* hand strip first. In Figure 3.6.4(a) the traces can be seen to be very similar but with a separation between them. In Figure 3.6.4(b) the separation is greater, as would be expected, but the shift is not linear with applied voltage, and the trace shapes are much less similar than in Figure 3.6.4(a). Considering the *right* hand strip, all the traces should be identical (on the assumptions made earlier). This is almost true for Figure 3.6.4(a), except near the gap, but markedly not true for Figure 3.6.4(b). Since this strip is always earthed, the shift must be due to the electric field near the surface of the specimen, this having the greatest effect near the gap. The error introduced by this effect can be very considerable.

A consideration of these results shows that an assumption that the signal is the *sum* of a component due to the topography and a component due to specimen potential is not valid (in this case at least). Some thought shows this to be consistent with Everhart's explanation of potential contrast. He suggested that the effect of the potential

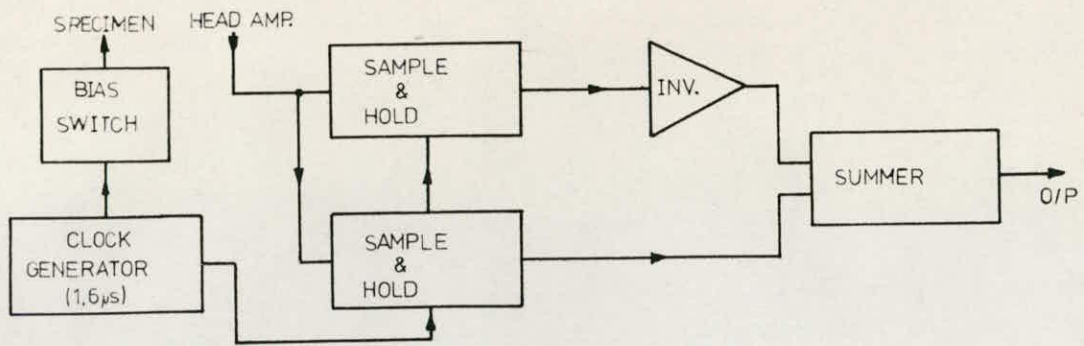


FIGURE 3.6.2 EXPERIMENTAL SETUP FOR BIAS SWITCHING APPROACH

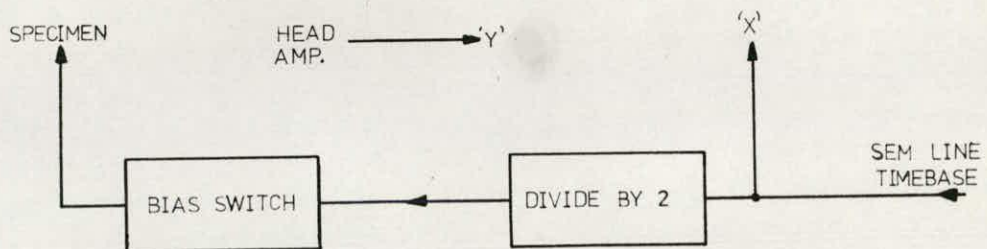
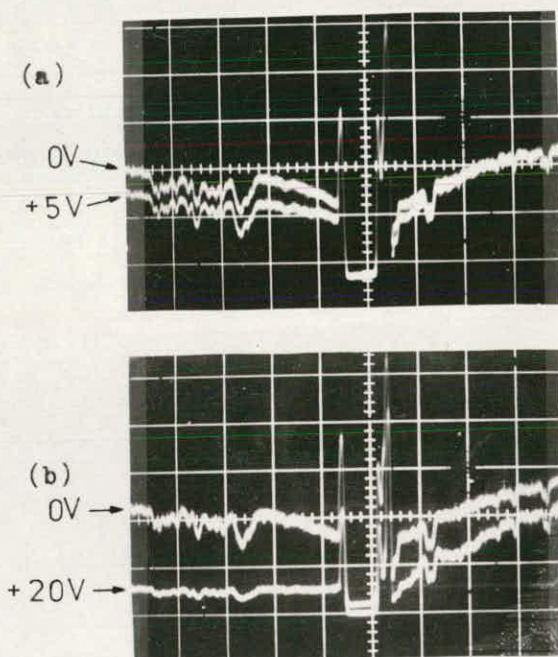


FIGURE 3.6.3 ALTERNATE LINE BIAS SWITCHING APPROACH



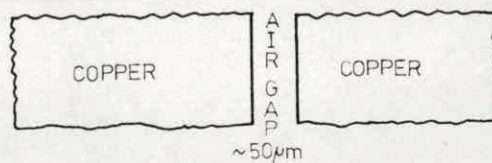
FIGURES 3.6.4(a)&(b)

RESULTING LINESCANS
(ALTERNATE LINE METHOD)

RIGHT HAND STRIP
ALWAYS EARTHED
LEFT HAND STRIP AT
POTENTIAL NOTED

(Beam swept across
specimen at right
angles to gap)

FIGURE 3.6.4(c)



PRINTED CIRCUIT BOARD
SPECIMEN USED

was to alter the electron trajectories so that more or fewer reached the collector. This would be expected to alter the *fraction* of emitted electrons which reach the collector. Thus for any point, with no potential applied we might have:

$$S_o = Kx F_t x E \quad \dots 3.6.1$$

where S_o is the collector output signal (volts), K is a conversion factor for the collector (volts/electron), F_t is a factor (fractional) due to the surface topography and E is the total number of secondary electrons emitted from that point. With a potential applied the situation is complex, but if the topographical factor (F_t) is assumed to have greatest effect on electrons very close to the surface, a reasonable approximation would be:

$$S_p = Kx F_t x F_p x E \quad \dots 3.6.2$$

where S_p is the collected signal and F_p is a factor (greater or less than unity) due to the applied potential. The difference signal would be:

$$S_d = S_o - S_p = K x F_t x E(1 - F_p) \quad \dots 3.6.3$$

This would mean that the difference signal will still be a function of the specimen topography. Figures 3.6.4(a) and (b) clearly show this behaviour in that the height of the topographical variations changes with the applied potential in the manner indicated by these equations. While giving good agreement in this case, the above approach is a simplified one, but it does serve to indicate that in the general case the relationship between topographical and potential contrast is too complex to allow simple separation of their effects.

Even if straightforward separation was always possible these experiments show that transverse electric fields are a problem.

Gaffney⁸⁴ has used a phase-lock amplifier and sinusoidal bias signals as an alternative approach to this problem. The particular specimen (a thin film resistor with no significant transverse field) and configuration used gave a linear response up to six volts applied. This technique has the limitation of requiring a periodic signal and will also be subject to the problems dealt with above.

From these considerations it can be seen that although the methods described do give some measure of improvement, some other type of approach is required to obtain quantitative information from the voltage contrast mechanism.

3.6.2 Using Modified Collection System

Driver⁸⁵ has used hemispherical meshes to form a type of spherically symmetrical detector in the SEM. This consisted of two meshes between the specimen and a large aperture form of the Everhart-Thornley collector system. The specimen was at the centre of the concentric hemispheres formed by the meshes. The first mesh was at 150 volts positive to earth potential, and the second was at a potential from 0 to 30 volts negative to the specimen. The meshes therefore acted as an energy filter only allowing electrons which had energies above a certain minimum, to pass through. The energy spectrum for these electrons was produced by means of 100kHz modulation of the specimen potential and a tuned amplifier-detector at the output of the photomultiplier. Results, for an npn silicon transistor, showed that the observed shift in the energy spectra did not give a very accurate measurement of the potential applied to the specimen.

Results were good for a point on the base region when it was 6 volts *negative* to the emitter, but a point on the emitter showed a 2 volt shift in the spectrum when -6 volts was applied to the base. In this specimen the emitter and base metallisation regions were approximately 50 μm apart. The author noted that the shape of the spectrum and the shift of the maximum was dependent on the position of the inner mesh relative to the specimen, the potential on the inner mesh, the relative positions of the meshes and the transverse fields on the specimen. It was also suggested that some problems were due to the lack of complete spherical symmetry, since the collector system will only collect some of the electrons passed by the energy filter. The signal to noise ratio was also worsened by an order of magnitude.

Gopinath et al^{86,87} have used a target cage and three grid, retarding field analyser with overall feedback loop as shown schematically in Fig 3.6.5. The feedback loop was used to keep the output (video) signal constant. The device was placed in the target cage and the voltages, on the different parts of the cage and the front grid of the retarding grid analyser, adjusted to attempt to obtain collection which was independent of the specimen local potential. This was checked by examining the displacement of the video signal - retarding voltage curve, with local potential, with the beam held on spot. The devices used in these experiments⁸⁷ were GaAs transverse Gunn diodes with a 10 μm contact gap. The electrode voltages were set up to give linear displacement of curves, for the beam held stationary on anode and cathode. The anode was grounded, *all* voltages were *negative* with respect to this and up to 10 volts was applied. The *minimum* linearized voltage distribution measured

was 2 volts and the *maximum* was 10 volts. The authors' gave their estimate of accuracy as 10%. The voltage contrast linescans produced were found to be noisy and the authors stated that the setting up of the system was difficult because of the degree of empiricism involved. Another problem mentioned was that electrons might not be normal to the analyser front grid, as would be desirable for proper energy analysis.

A consideration of this system shows that the feedback amplifier serves to vary the pass energy of the analyser so that a constant number of electrons pass through. Thus the amplifier output voltage will be related to the electron energies by the grid voltage - pass energy characteristic of the analyser. "Linearisation" of voltage contrast will thus be a complicated function of the target cage and grid voltage effects on the electron trajectories.

Flemming and Ward⁸⁸⁻⁹⁰ have used a variety of approaches the latest of which⁹⁰ is shown in Fig 3.6.6. This consisted of two meshes in a nylon holder placed over the specimen (an npn transistor) and the normal Everhart-Thornley collector system. The inner mesh was held at a high potential, 1000 volts positive, with respect to the specimen, which was near earth potential, as was the outer mesh. A feedback loop was used to vary the voltage on the specimen so that the photomultiplier output was kept constant at all times. An AC modulation technique with lock-in amplifier was used to separate the potential contrast from topographical. The high voltage on the first grid was used to reduce the effects of transverse fields on the specimen. The system had a 0.5 volt noise level at the output.

^{91,92}
Banbury and Nixon have used a cylindrical cage, above the specimen, with a grid in one wall and the normal Everhart-Thornley

collector system. A diagram of the type of arrangement is given in Fig 3.6.7. This was described as using a combination of a small retarding field due to a negatively biased disc facing the specimen, and a positively-biased collector set into the cylindrical wall of the detector configuration, to reduce the effect of transverse fields. The voltages on the electrodes were in the range ± 300 V. The voltage contrast characteristic, for an unspecified metallic test specimen, was found to be symmetrical, monotonic, but *not linear*, with its highest slope of 8% per volt at the voltage origin. The authors estimated the error for smooth evaporated conductors to be of the order of 0.5 volts, with a measurement range of ± 10 volts.

Yakowitz et al⁹³ has given a more quantitative description of this approach, as well as describing a modified version of this cylindrical detector. Results were given for a test specimen, consisting of 50 μm wide aluminium strips, separated by 60 μm , on an SiO_2 on Si substrate, using the type of detector already described (and shown in Fig 3.6.7). These showed that the video signal, versus specimen bias curves, were very dependent on the voltages on the various electrodes. They were taken over a range of ± 5 volts with the beam in the centre of a strip and were non-linear, in general, but linearity was obtained for one particular combination of electrode voltages for this particular specimen position. The modified version of the cylindrical detector is shown in Figure 3.6.8. Results for this detector showed that for carbon rod and copper specimens, the output current (pico-ammeter) versus specimen voltage curves were again *non linear* but with a slope which was generally greater than for other types of cylindrical detector (33% per volt). Trajectory calculations showed that the collected current must have been mostly due to secondary emission from the bottom plate of the detector.

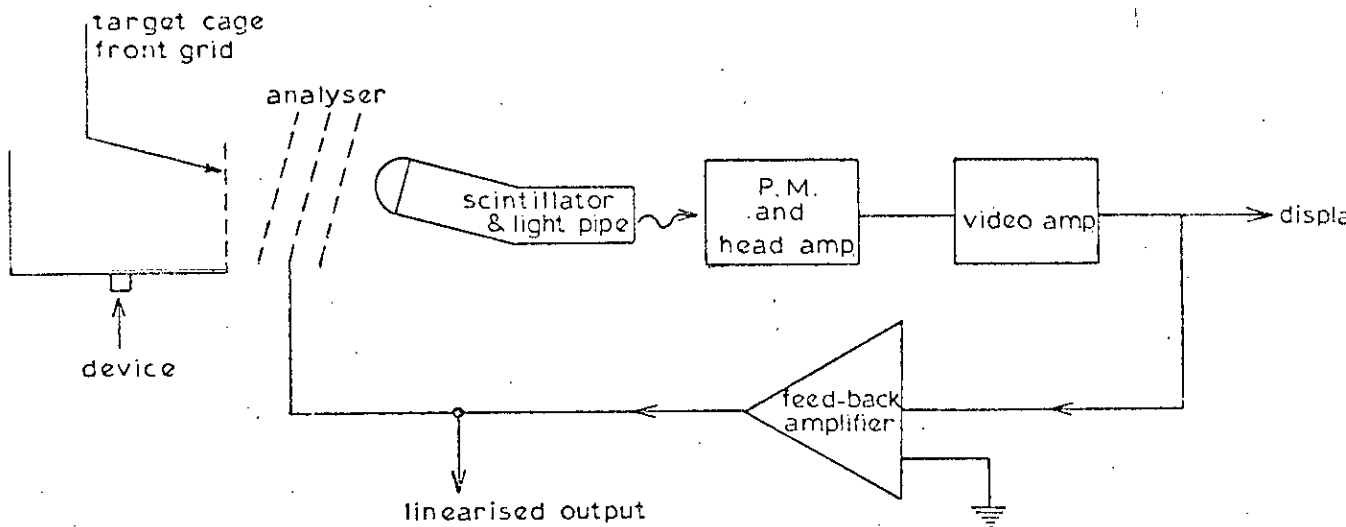


FIGURE 3.6.5 (Gopinath et al)

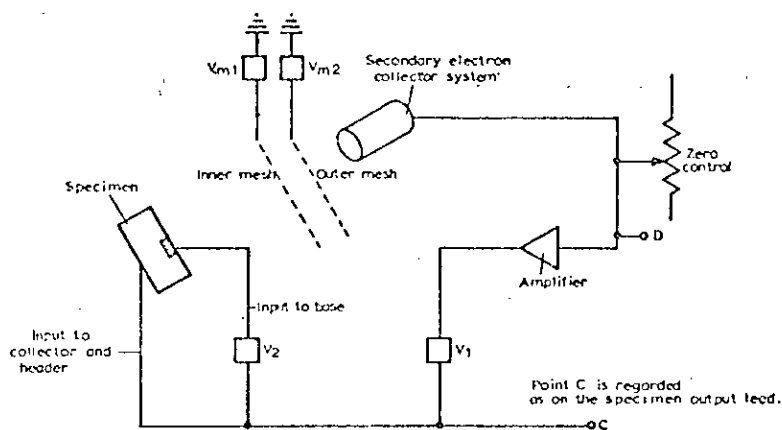


FIGURE 3.6.6 (Flemming & Ward)

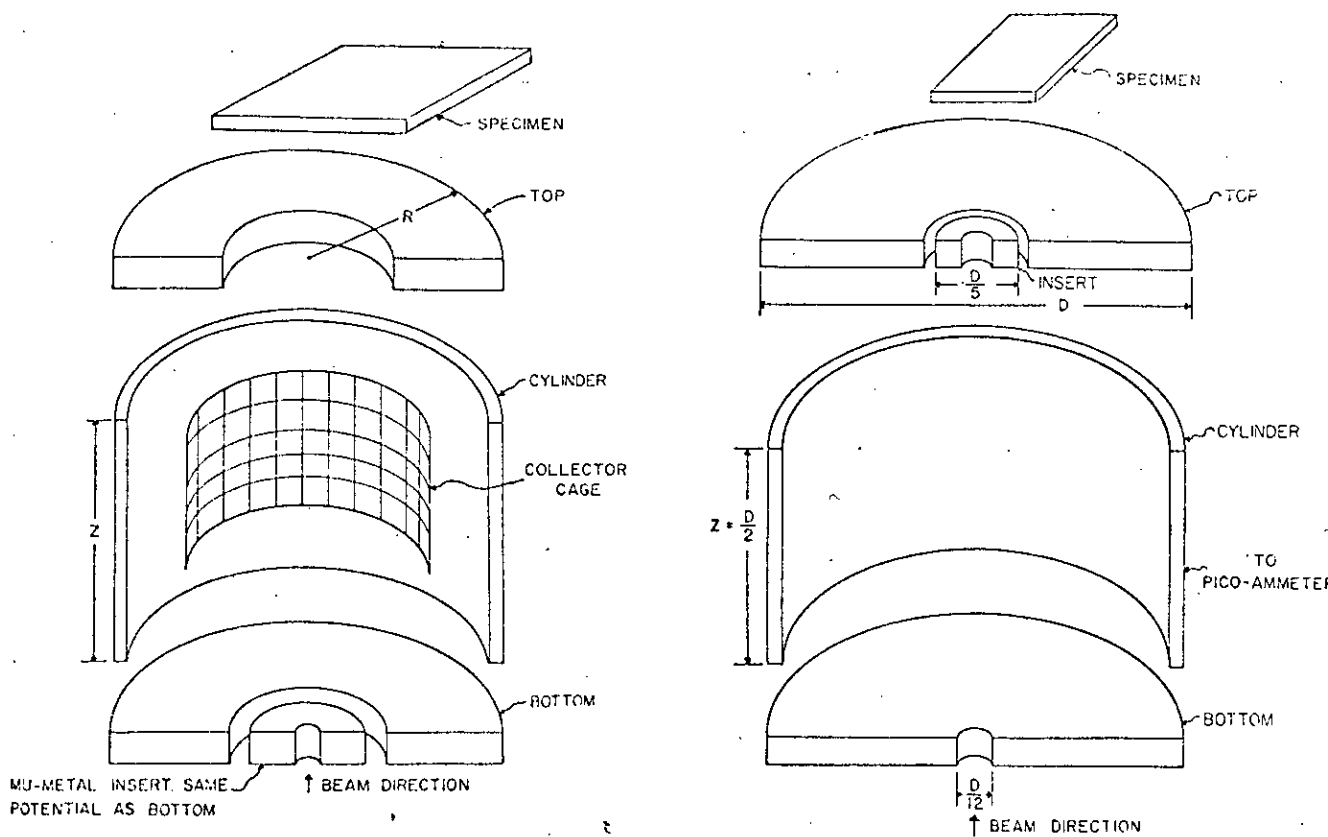


FIGURE 3.6.7 (Yakowitz et al)

FIGURE 3.6.8 (Yakowitz et al)

It was suggested that this detector would be more suitable for voltage contrast work than other types of cylindrical detector, but no quantitative estimates of performance were given.

Wells and Bremer⁹⁴⁻⁹⁶ have used two types of energy analyser, to measure potentials by locating the peak of the secondary emission curve. An 84 degree cylindrical mirror analyser was used first^{94,95} and then improved performance was obtained by using a 63 degree curved plate analyser⁹⁶. The later analyser had a higher transmission factor and produced less defocussing of the beam. This analyser had a collimator, at the exit end of which the normal scintillator was placed. The authors noted the effect of finite energy resolution on the curve shape and the various errors due to transverse fields, insulator charge up, magnetic fields and poor vacuum. Their estimate of accuracy with the improved analyser was ± 1 volt.

The voltages on the analyser were kept constant and the specimen voltage was varied to give the energy spectrum of the emitted electrons. Deflection plates at the entrance to the analyser could be used to increase the collected signal.

More information on this approach will be given later.

Ogilvie⁶⁶ has used the SEMM in a voltage contrast mode. The contrast in this case is produced by the equipotentials above the specimen surface, as the incident electrons are reflected in this region. The reflected electrons were collected by an array of detectors above the specimen. As yet no quantitative information on this technique is available. The contrast mechanisms would be expected to be more difficult to deal with than those for the conventional SEM.

3.6.3 Using Auger Electrons

An alternative approach to the use of low energy secondary electrons has been described by Macdonald^{97,98} and Waldrop et al⁹⁹. This consisted of using Auger electrons.

A summary of Auger electron spectroscopy has been given by Macdonald¹⁰⁰. Auger electrons are produced as a result of electronic transitions in an atom that occur after excitation of atomic levels by incident electrons. An element may have a number of Auger peaks in the distribution curve of its secondary electrons, and these may occur over a wide range of energies. The escape depth of these electrons is very small, 0.1 to 1 nm for 10 to 1000 eV electrons, the escape depth being dependent on the energy. This means that Auger electron emission is a surface effect so that very high vacuum standards are necessary (a minimum of 10^{-8} torr and a "clean" system). The Auger peaks are very small so that the energy distribution must be differentiated to enable them to be detected. The noise performance is such that, using a tungsten cathode in the SEM and a 10^{-8} A beam current, 6 minutes may be required to record a 200 by 200 point image for a 270 eV carbon peak, with a reasonable signal to noise ratio.

The approach to voltage measurement using these electrons⁹⁷⁻⁹⁹ was to measure the shift of the 270 eV carbon peak with applied potential. The detector used in these approaches was a coaxial cylindrical spectrometer with an energy resolution of less than 1%, an acceptance half angle of 6 degrees and a transmission energy of 1.6 eV, where V_a is the voltage applied to the analyser. A lock-in amplifier was used to obtain the derivative of the energy distribution⁹⁸. Using this particular setup results were given, for an FET sample over a range of 20 volts with the maximum transverse field estimated



at 6×10^5 V/m, showing linear shift with the gradient a function of the analyser characteristic. The use of a computer to control the beam position, analyser and peak detection operation has been reported⁹⁸. Results for an aluminium film on SiO_2 on Si with 12 volts applied to the Al showed a voltage resolution of ± 1 volt with a spatial resolution of $0.8 \mu\text{m}$. Qualitative results have also been given for a power transistor specimen⁹⁹.

This approach is claimed to have considerably less sensitivity to the effect of surface electric fields than the low energy secondaries methods, since the Auger electrons have a much higher energy and will be deflected less by these fields.

While this claim will certainly be true, the problems; vacuum, surface, noise etc of using Auger electrons are such that this method will be generally less useful than the methods for lower energy electrons. Since the electrons have a high energy, to obtain greater accuracy the analyser will require to have a very narrow passband, so making the already difficult noise problems even worse. This approach will also be very difficult to use for fast phenomena due to the long integration times required for adequate noise performance.

3.6.4 Approach Adopted

A consideration of these approaches in the light of the specifications mentioned already for a voltage measuring system (Section 3.5), shows that none meet the requirements in their existing form.

The approaches using electrical signal processing and the conventional collector system are clearly not suitable. The practical problems of using Auger electrons have already been dealt with and this would appear to be too difficult an approach to adopt.

Those approaches using feedback loops offer no special performance advantages since the feedback amplifiers serve mainly to avoid manual adjustment of voltages. The factors which determine the performance of these methods are the analyser and collector characteristics of the system.

The merits of the cylindrical detector systems are difficult to estimate but their performance does not seem very satisfactory, particularly the non-linearity of their response.

The most promising approach for the present application seems to be that of Wells and Bremer⁹⁶, since it appears to give reasonable results and has a straightforward mode of operation.

This approach was therefore chosen for further study with a view to applications for measuring voltages on integrated circuit type specimens.

CHAPTER 4

DEVELOPMENT OF A TECHNIQUE FOR VOLTAGE

MEASUREMENT ON INTEGRATED CIRCUITS

4.1 GENERAL APPROACH

The various approaches suggested for voltage contrast observation in the SEM, have already been discussed. The conclusion was drawn that the best method of approach would be the use of some type of energy analyser for the secondary electrons.

The basis of the approach investigated here is shown in Fig 4.1.1. The solid curve shows a typical secondary emission energy curve with peak at energy E_1 . The dotted curve is that which would be produced when a potential V is applied to the specimen. The whole curve shifts with the peak now at energy E_2 (with respect to initial zero of energy). Thus the potential V would now be given by $(E_2 - E_1)$. The use of an energy analyser for the secondary electrons would give the positions of the peaks of the curves and hence the required difference could be obtained.

Measuring the shift of the peak of the number of secondaries versus energy curve is necessary, since in practice the absolute energy of the electrons (ie wrt true zero) is very difficult to measure. Thus this approach measures changes in potential.

The simplest realisation of this approach is the direct use of an energy analyser on the secondary electrons emitted from the specimen surface. An energy analyser was constructed and experiments carried out, to investigate the possibilities of this approach.

4.2 EVALUATION OF THE USE OF AN ENERGY ANALYSER

4.2.1 Construction of Analyser

The energy analyser used in this work was similar to that described by Wells and Bremer⁹⁶.

A photograph of the analyser is shown in Fig 4.2.1 and a cross section of the analyser and its position in the SEM is given in Fig 4.2.2.

This analyser is of the cylindrical electrostatic type with a collimator, and was constructed of brass sheet as shown. Because of the construction of the SEM (Stereoscan 2) specimen stage, electron collector and light pipe, some modifications were introduced to give the arrangement shown in Fig 4.2.2. These consisted of alterations to mechanical parts of the specimen stage, and replacement of the bent perspex light pipe with a straight quartz light pipe, with a hemispherical end coated with scintillator material, using the method described by Hatzakis¹⁰¹. This new light pipe and scintillator arrangement proved excellent and was adopted for use in the SEM in its normal modes of operation.

4.2.2 Operation

This type of energy analyser has a bandpass characteristic. The width and position of the energy passband is a function of the design and construction of the analyser and the voltages applied to the various electrodes. Thus the position of the peak of the secondary electron emission curve could be determined by varying the voltage between the analyser plates until maximum output, from the photomultiplier, was obtained. Due to fringing fields and other effects this method would not be expected to give a linear shift in bandpass energy with voltage applied between the plates,

NUMBER OF
ELECTRONS
WITH ENERGY
'E'

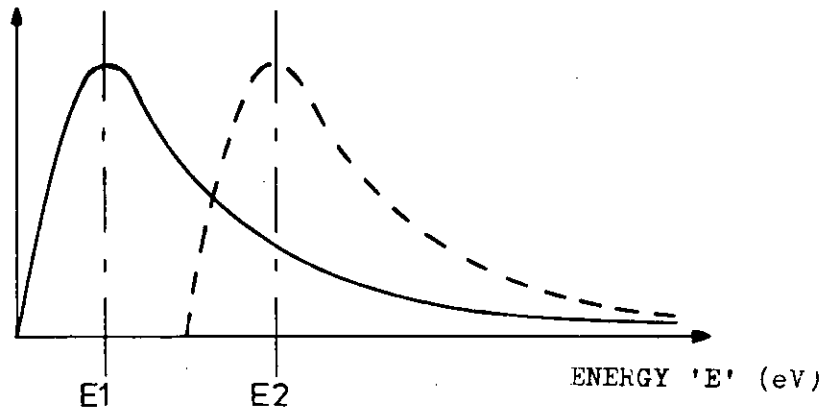


FIGURE 4.1.1 SHIFT IN CURVE PEAK METHOD OF POTENTIAL MEASUREMENT

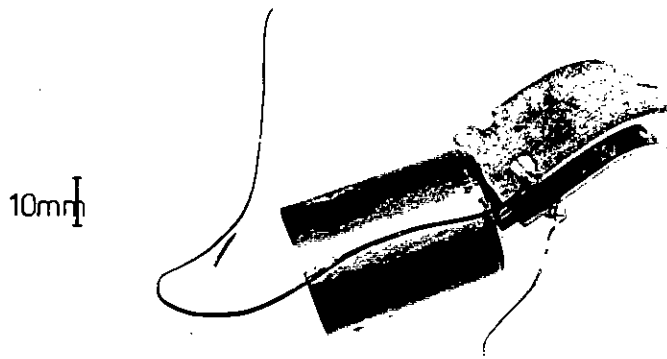


FIGURE 4.2.1
ENERGY ANALYSER AS
ORIGINALLY CONSTRUCTED

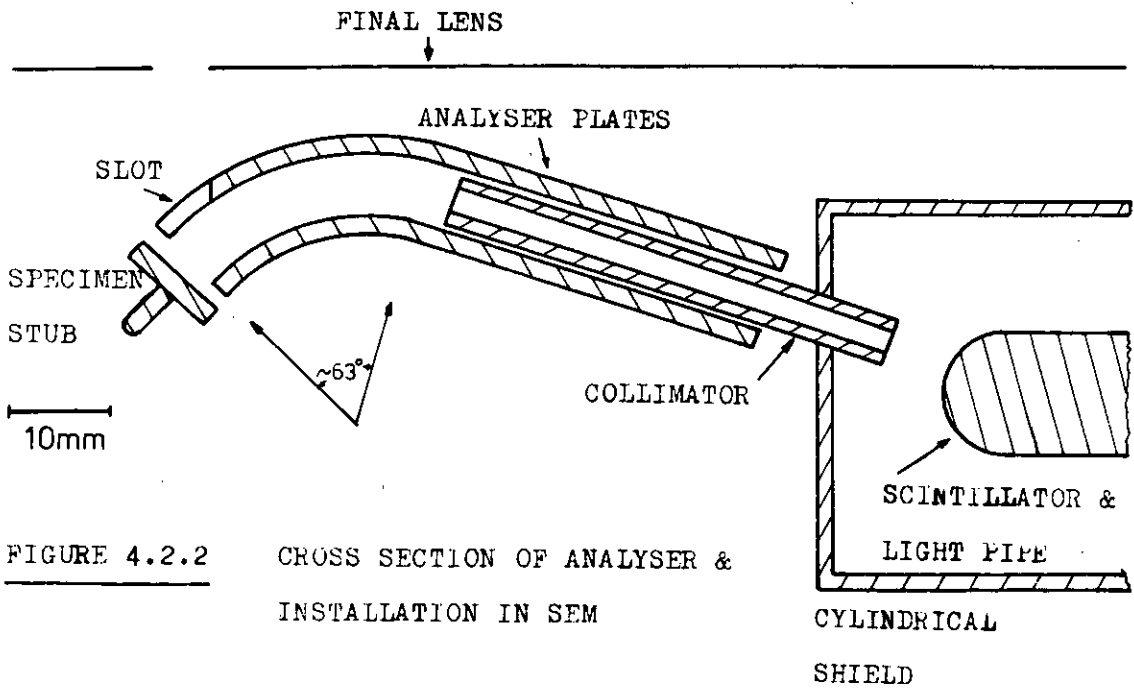


FIGURE 4.2.2 CROSS SECTION OF ANALYSER & INSTALLATION IN SEM

over an appreciable energy range. The measurement method adopted, overcame this difficulty, by keeping the voltages on the analyser fixed and applying a variable voltage between specimen and earth. The value of this voltage, for maximum output from the photomultiplier, was used as a measure of the position of the peak of the secondary emission energy curve. In this way the energy analyser always passes electrons in an energy band which remains constant with respect to earth potential.

4.2.3 Experimental Setups and Results

An experimental arrangement used to obtain initial results for this approach, is shown in Fig 4.2.3. This made use of the sweep output voltage from an oscilloscope to obtain the secondary emission curve and display it. Some results obtained with this setup, using a copper strip specimen are given in Figs 4.2.4(a)-(e). The sweep polarity is such that the oscilloscope traces display increasing secondary electron energy from left to right. The Y signal is the output from the SEM head amplifier (0.5 V/div) and the X scale is approximately 5 V/div, in all traces.

The sample used in these experiments was the same as that used for Figs 3.6.4(a) and (b) and a comparison of the results shows the very considerable improvement achieved by using the present system. Figures 4.2.4(a)-(c) show the good linearity of the curve shift versus applied voltage. The difference in initial (ie left hand) curve positions between Fig 4.2.4(a) and 4.2.4(b) illustrates the difficulty, mentioned earlier, of measuring *absolute* potentials, since the two points are at the same potential. The *shift* with applied voltage is still linear. The effect of transverse electric

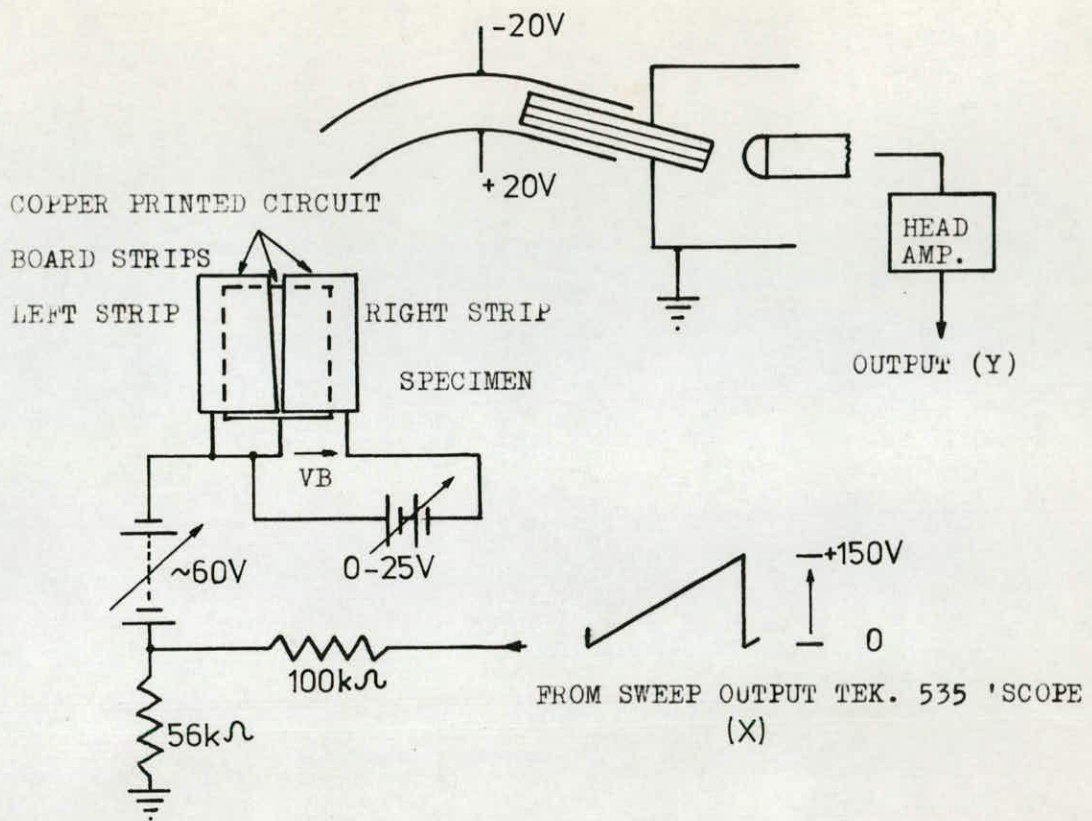


FIGURE 4.2.3 EXPERIMENTAL SETUP USED TO OBTAIN INITIAL RESULTS

Y - 0.5V/DIV. X - ~5V/DIV. → INCREASING ENERGY

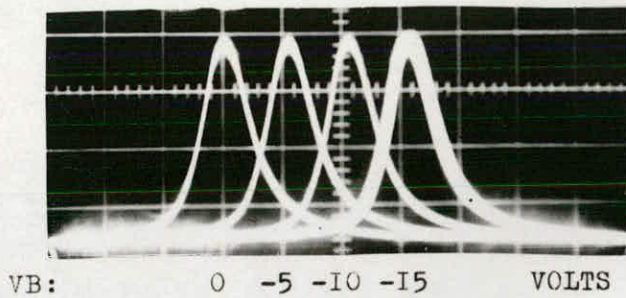


FIGURE 4.2.4(a)

BEAM ON RIGHT STRIP
AWAY FROM GAP

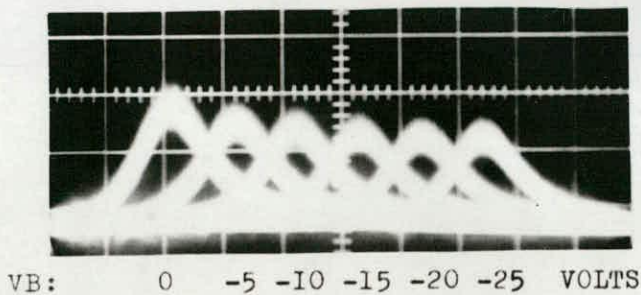


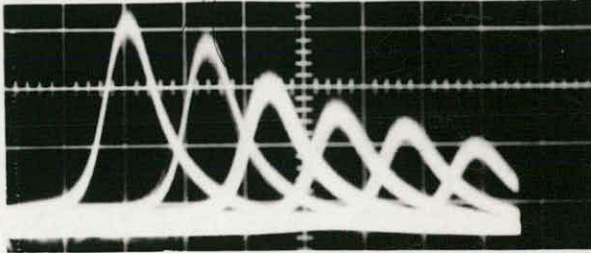
FIGURE 4.2.4(b)

BEAM ON RIGHT STRIP
SAME DISTANCE FROM
GAP AS IN (a) BUT
DIFFERENT POINT

Y - 0.5V/DIV.

X - ~5V/DIV.

→ INCREASING ENERGY

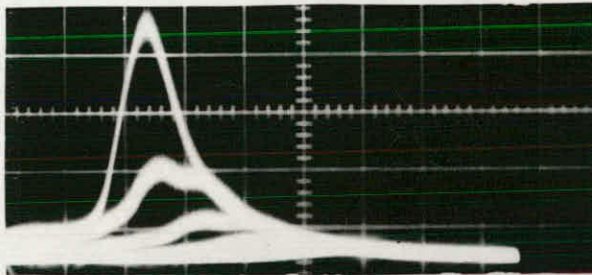


VB: 0 -5 -10 -15 -20 -25 VOLTS

FIGURE 4.2.4(c)

BEAM ON RIGHT STRIP

POINT NEAR GAP

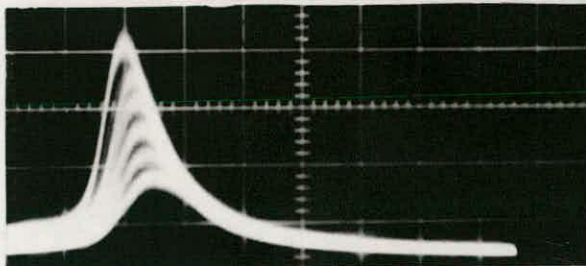


VB:(TOP TO BOTTOM) 0 -5 -10 -15 -20 -25 VOLTS

FIGURE 4.2.4(d)

BEAM ON LEFT STRIP

POINT NEAR GAP



VB:(TOP TO BOTTOM) 0 -5 -10 -15 -20 -25 VOLTS

FIGURE 4.2.4(e)

BEAM ON LEFT STRIP

POINT AWAY FROM GAP

fields is shown by Figs 4.2.4(c) and 4.2.4(d). In these photographs the height of the curve varies with applied potential, the shift in Figure 4.2.4(c) is not so linear as before and Figure 4.2.4(d) shows a shift even though the voltage on this strip (LH) does not vary. The fact that this shift is dependent on the distance from the gap is demonstrated by Figure 4.2.4(e) which shows less shift (error) for a point further away.

The curves in these photographs do not show the "classical" secondary emission curve shape exactly, due to the finite width of the energy analyser passband.

Although it gave a good guide to the results expected from this approach, this setup did not lend itself to accurate measurement of performance due to the errors introduced by the linearity of the sweep voltage and the visual estimation of curve shift.

A system (similar to Figure 4.2.5), which detected the peak of the secondary emission curve and gave a direct readout of its position, gave results for the copper strip specimen which showed errors of less than 0.2 volts and good linearity up to 20 volts (the highest value used).

The experimental setup of Figure 4.2.5 was used to investigate potentials on a BC108 npn planar transistor. The functions of the various parts of the system are self explanatory (full details will be given later when an improved system is described).

Figure 4.2.6 shows a view of the transistor used. The electron beam was positioned on the centre of the emitter bond (left hand).

Figures 4.2.7(a) and (b) show some results which were obtained. In Fig 4.2.7(a) the lower trace shows the voltage waveform V_1 applied to the emitter and base wrt the collector. The upper trace is the output voltage V_0 produced by the measuring circuit of Fig 4.2.5.

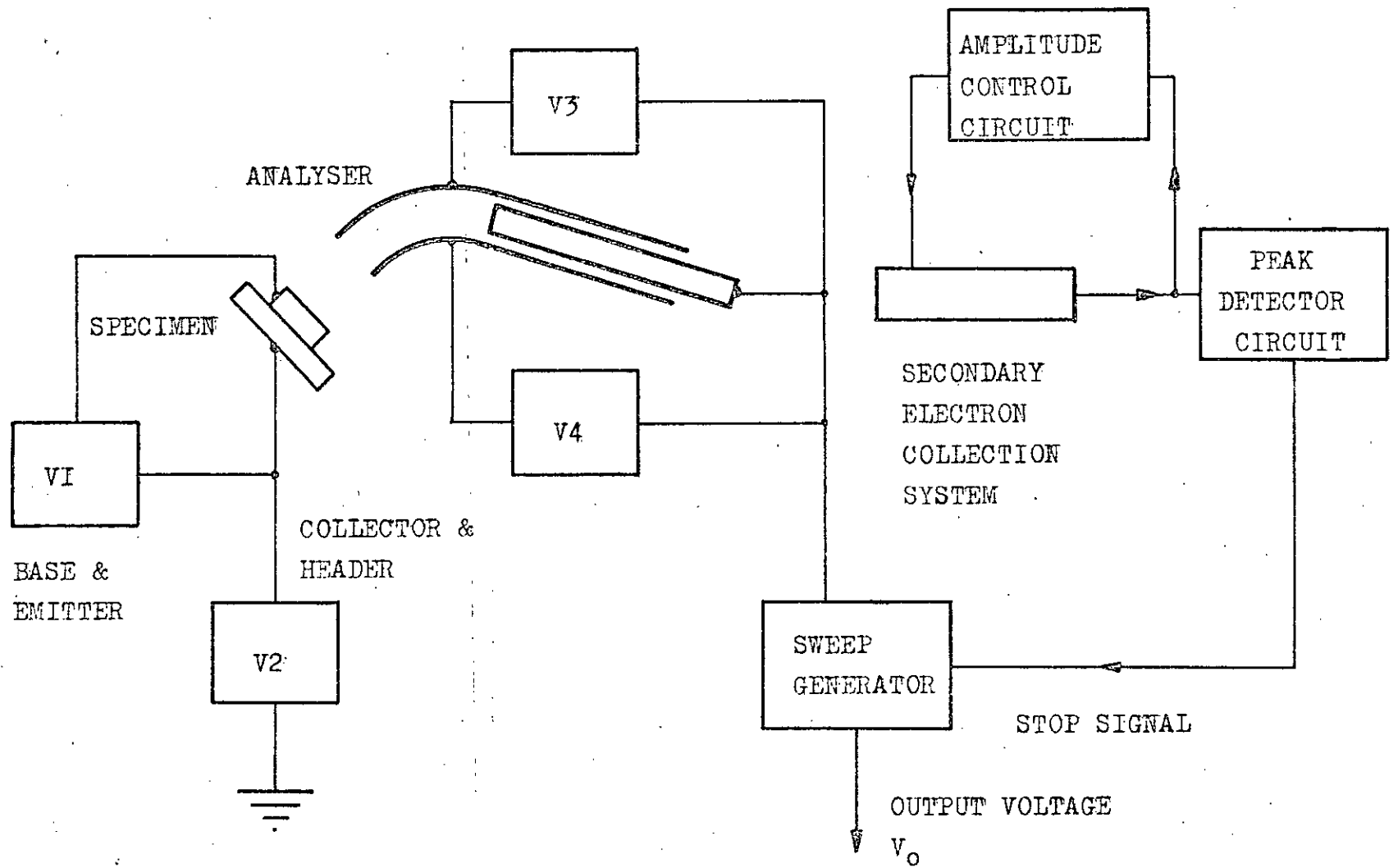


FIGURE 4.2.5

AUTOMATED VOLTAGE MEASURING SYSTEM

EMITTER

COLLECTOR



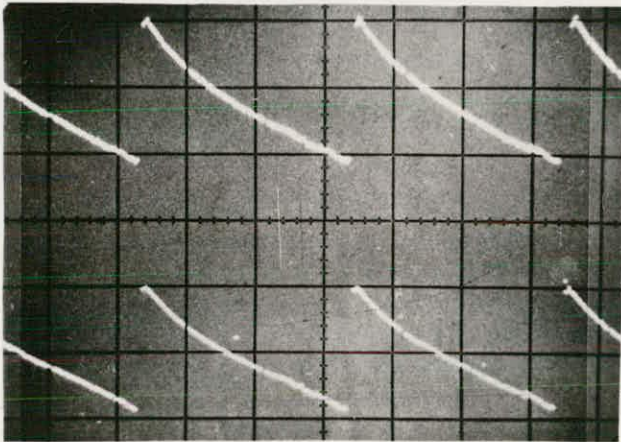
BASE

100 μ m

FIGURE 4.2.6

SPECIMEN -

BC108 TRANSISTOR

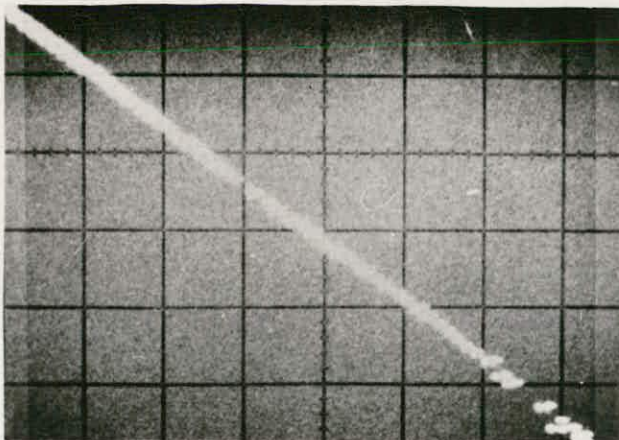


V_o \uparrow 2V/DIV. MEASURED
VOLTAGE

FIGURE 4.2.7(a)

V_i \uparrow 2V/DIV. APPLIED
VOLTAGE

\longrightarrow 2.5 S/DIV.



V_o 2V/DIV. MEASURED
VOLTAGE

FIGURE 4.2.7(b)

\longrightarrow V_i 1.5V/DIV.

These two waveforms are identical in shape with almost equal magnitudes. Fig 4.2.7(b) shows the linear relationship found to exist between V_0 and V_1 over the range 0 to -10 volts. Voltages greater than 10 volts were not applied to the device. The linear relationship was found to hold good within about 3% for different points on the surface and to be reproducible over a fairly lengthy period of time.

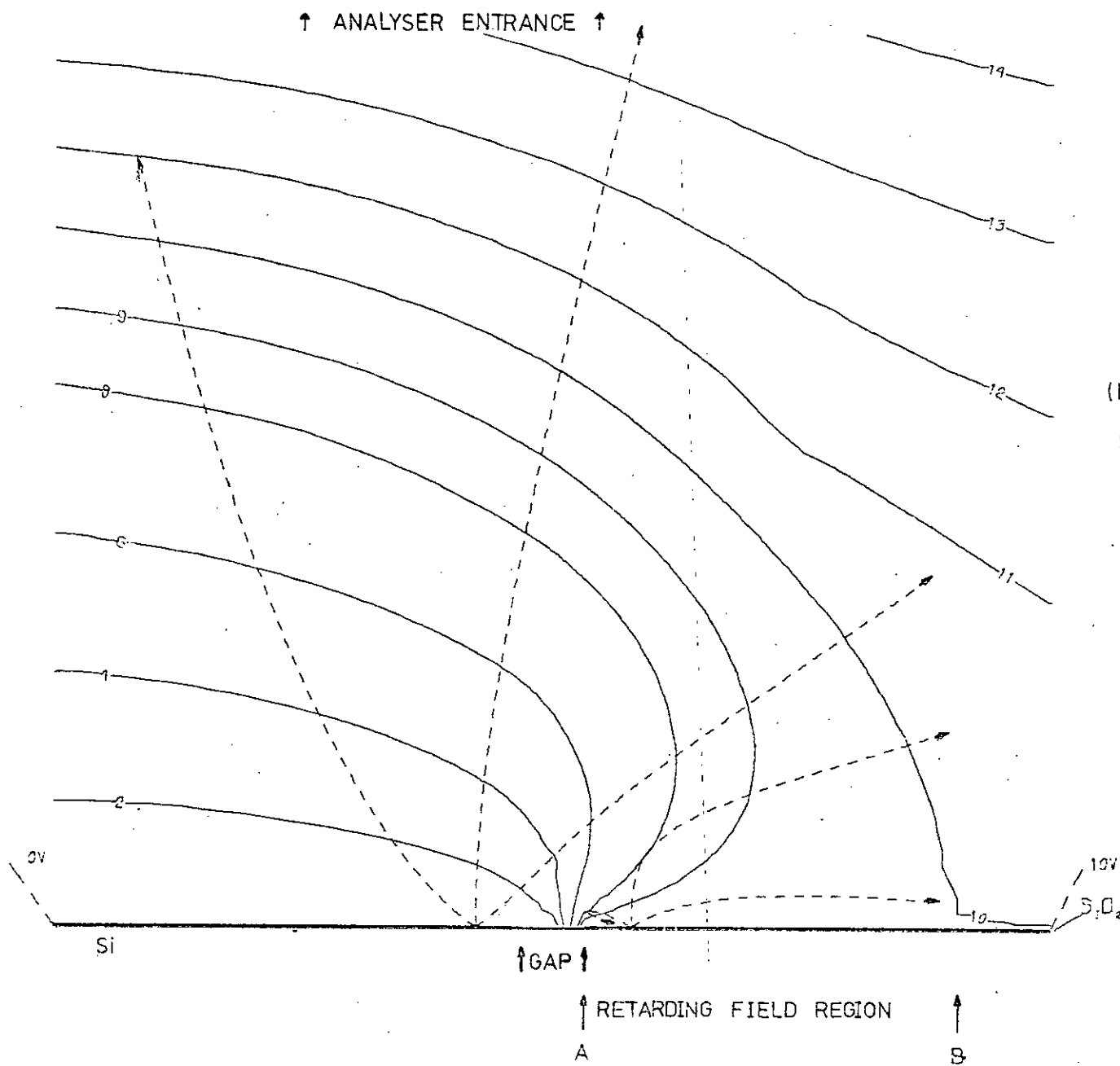
The device used in these experiments was approximately 350 μm square. This gave a surface field of the order of 5×10^4 V/m, with 10 volts applied between collector and emitter-base. The emitter and base were always *negative* with respect to the collector in these experiments.

All experimental results given were obtained with a gun voltage of 5 kV.

4.2.4 Study of Limitations

The results already given appear quite good, but further experimental work on other specimens showed that the accuracy of measurement was very much poorer for points very close to the *positive* side of a biased gap. This was in line with comments by O C Wells¹⁰² who stated that he had found it impossible to collect secondary electrons from the positive side of a back biased p-n junction.

Some understanding of this problem can be gained by considering the field distribution near a biased gap on the specimen surface as shown in Figure 4.2.8. The solid lines are computed equipotentials for the experimental specimen analyser arrangement and a 40 μm wide gap in a 1 μm thick Al film on 1 μm SiO_2 on an Si substrate. The left side of the gap is earthed, the right side is at +10 volts and the equipotentials have the values marked. From this diagram it can be seen that in the region A to B on the positive side of the gap there is a retarding electric field immediately above the specimen surface.



EQUIPOTENTIALS
NEAR SPECIMEN
SURFACE

(ELECTRON TRAJECTORIES
SHOWN DOTTED)

SCALE: - ————
90 μm

(ANALYSER ONLY)

FIGURE 4.2.8

The dotted lines show computed trajectories for electrons leaving the surface with an energy of 3 eV, at angles 60 degrees to left and right of and along the normal to the surface. These are shown for points 30 μm from either side of the gap.

On the positive side it can be seen that the effect of the electric field above the surface is to affect the trajectories of the emitted electrons so that some are deflected away from the analyser entrance and some may even return to the surface. This means that it becomes difficult to collect secondary electrons from a region very close to the positive side of a biased gap.

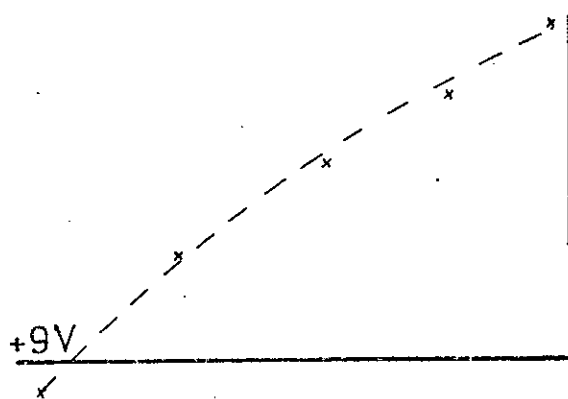
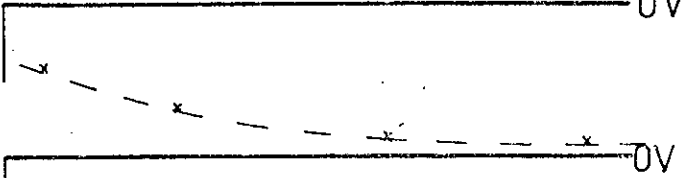
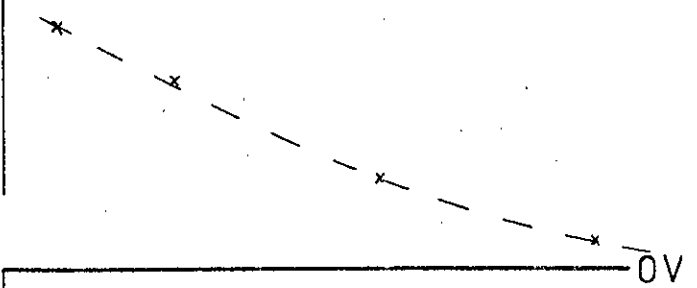
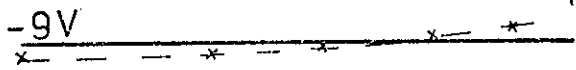
On the negative side of the gap the electrons will be accelerated by the field but some may also be deflected so as not to enter the analyser. The effect in this case will be considerably less than that on the positive side.

Figures 4.2.9(a) and (b) show experimental results which are very much as would be expected from the field configurations already considered. These show measured voltages (experimental points) and applied voltages (solid lines) for a specimen consisting of a 40 μm gap in an Al film on 1 μm SiO_2 on an Si substrate. The experimental setup was of the type in Figure 4.2.5. Figures 4.2.9(a) and (b) are for sweeps across the gap at two different positions along it, but both show that the error close to the positive side of the gap is very much greater than that on the negative side.

These effects of the fields close to a biased gap can be seen to be the major source of difficulty in measuring voltages on micro-circuits. The magnitude of this problem is seen by considering that a situation of 10 volts across a 10 μm gap would give a transverse field of the order of 10^6 V/m.

FIGURE 4.2.9(a)

ONE POSITION



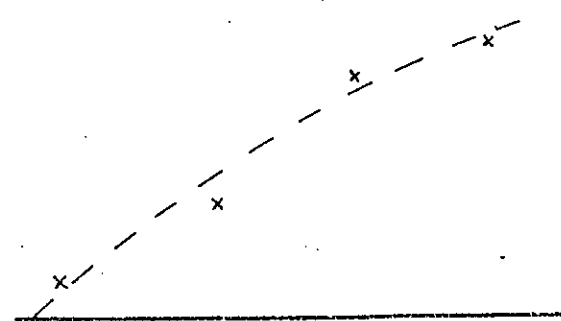
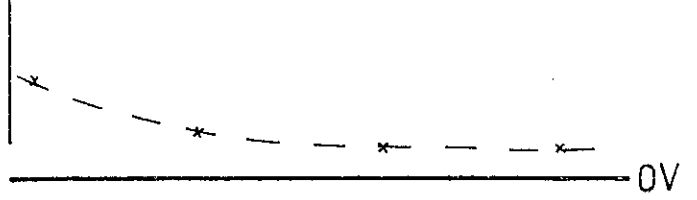
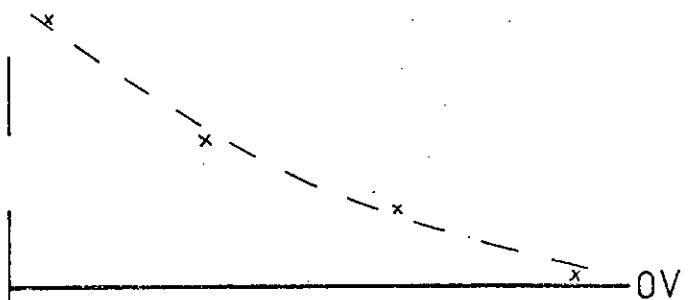
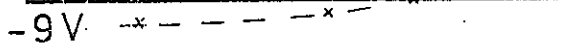
APPLIED VOLTAGES

MEASURED VOLTAGES

SWEEPS ACROSS GAP

FIGURE 4.2.9(b)

ANOTHER POSITION



The type of energy analyser already considered has been shown to give good results in many situations but to be unsatisfactory in situations with high transverse electric field components. If voltages on integrated circuits are to be measured with the required accuracy some other approach is necessary.

4.3 AN ELECTRON LENS AND ENERGY ANALYSER SYSTEM

4.3.1 Requirements

A system of voltage measurement utilising the shift in the peak of the secondary emission energy curve consists of two main processes involving the emitted electrons. These are conveyance of the electrons into the energy analyser and the determination of their energy.

Some of the problems associated with the first process have already been demonstrated. In general, electric field distributions near the specimen surface will affect the motion of electrons as they leave the surface. This means that the angular distribution of secondary electrons, at a distance from the surface, (of cosine form in the ideal case) will be affected by these fields, among other things. Thus the angular distribution as well as the relative energy of the electrons may vary with voltages applied to the specimen. The effect of this variation of the spatial distribution of emitted electrons with specimen potentials will depend on the characteristics of the analyser. The manner in which an analyser determines the electron energy varies but normally consists of a velocity selection process. Whether or not an electron will pass through the analyser will depend on the entry position and angle, as well as the electron velocity and the electric or magnetic fields in the analyser.

The form of this dependence is a function of the type of analyser.

From this the three main requirements which emerge are that the electrons leave the region above the specimen surface, that they are conveyed to the analyser with minimum variation in spatial distribution (as surface potential changes) and that the analyser has a characteristic which results in these variations having least possible effect.

4.3.2 Design

In order to reduce the effects of the electric fields near the surface on the emitted electrons it would seem desirable to have an accelerating field above the surface. A field of the correct magnitude would increase the proportion of electrons escaping from the region just above the surface, in the case where the local field was retarding in nature. The required field would have to be quite high, having at least the same order of magnitude at the specimen surface as the local fields. This means a high potential over a fairly short distance, if IC specimens are to be examined.

The accelerating field will tend to limit the spatial spread of the secondary electrons but it is necessary to convey the electrons into the analyser as well as controlling their distribution.

A consideration of these factors suggested the use of electron optical techniques using a type of electron lens. Desirable features of such a lens for this application are:

1. High field normal to specimen surface
2. Low disturbance of field at entrance to analyser
(ie exit of lens)
3. Low divergence or preferably convergence of overall lens

Resistive sheet and resistor mesh analogue models (2 dimensional) were used to investigate the design of a lens, to attempt to satisfy these contradictory requirements. A cross sectional diagram of the electrode arrangement of the lens developed is given in Figure 4.3.1. The first electrode (nearest to the specimen surface) was held at a high potential V_2 (+1kV) with respect to the specimen potential V_1 (0V). The second and third electrodes were held at potentials V_3 (+130V) and V_4 (+50V) respectively.

The first electrode provides the accelerating field required in order to overcome the effects of surface fields. The second two electrodes serve to create a field distribution with more desirable lens characteristics, to shield the analyser from the high field associated with the accelerating electrode and to reduce the electron velocities to allow energy analysis using straightforward types of analyser. This description of the operation of the lens is only approximate and more details will be given later.

In considering an analyser for use after the lens already described, desirable characteristics would be:

1. A band-pass characteristic
2. A fairly narrow energy passband
3. A low sensitivity to the angle at which an electron enters the analyser
4. A low sensitivity to the position of the point at which an electron enters the analyser.

Important practical points are the size and shape of the analyser since the space in the SEM specimen chamber is very restricted.

Although the curved plate analyser already constructed had limitations in terms of these desired characteristics, as will be shown more fully later, it was decided to use it in initial evaluation work. This was because it could be modified in shape to fit into the

specimen chamber and also because its use would allow some degree of comparison with previous results, obtained with this analyser alone.

Fig 4.3.2 shows an outline drawing of the lens and analyser arrangement. The primary electron beam passes through the analyser top plate, near the lens axis, as shown. This is necessary since it is required to have the first lens electrode close to the specimen surface in order to obtain a high accelerating field.

4.3.3 Construction and Installation

Details of the construction of the lens and its mounting onto the analyser are shown in Figures 4.3.3(a) and 4.3.3(b). The lens electrodes were made from thin brass and spaced as shown by using nylon screws and insulating spacers. The practical result of the construction was that very little insulator was exposed where it could produce charging problems. The mounting of the first lens electrode was arranged to interfere as little as possible with the electric field created by this electrode at the specimen surface. The electrodes were mounted on a tufnol former for initial alignment and construction of the lens. While the construction was not ideal it was considered to be the best possible without a considerable increase in fabrication complexity.

The necessity for the beam to pass through the top plate of the analyser in line with the lens axis produced some practical mounting problems in the SEM⁹. The analyser had to be mounted with its entrance parallel to the base of the specimen stage so that the collimator had to enter the cylindrical shield as shown in Figure 4.3.3(b) rather than as in Figure 4.2.1. This meant that the first lens electrode and therefore specimen position had to be a considerable distance from the final lens (65 mm). This working distance required was thus very much longer than that obtainable with the normal specimen stage (20 mm)

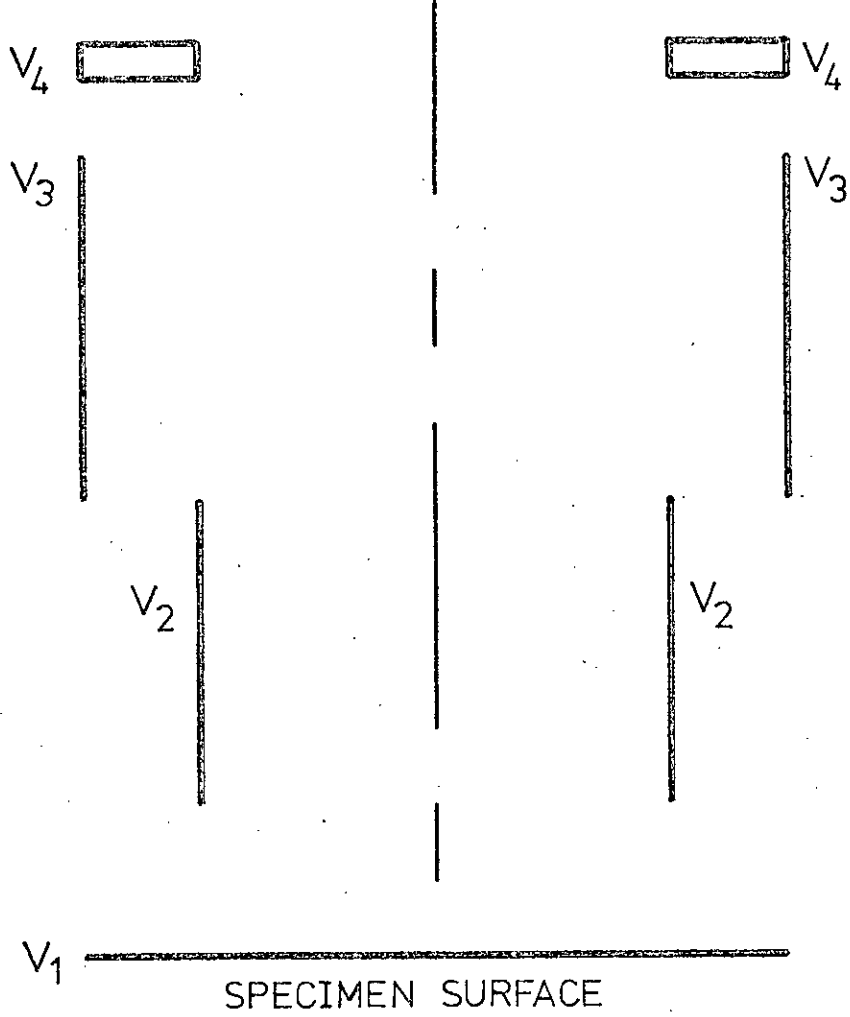


FIGURE 4.3.1
CROSS SECTION
OF LENS ELECTRODES

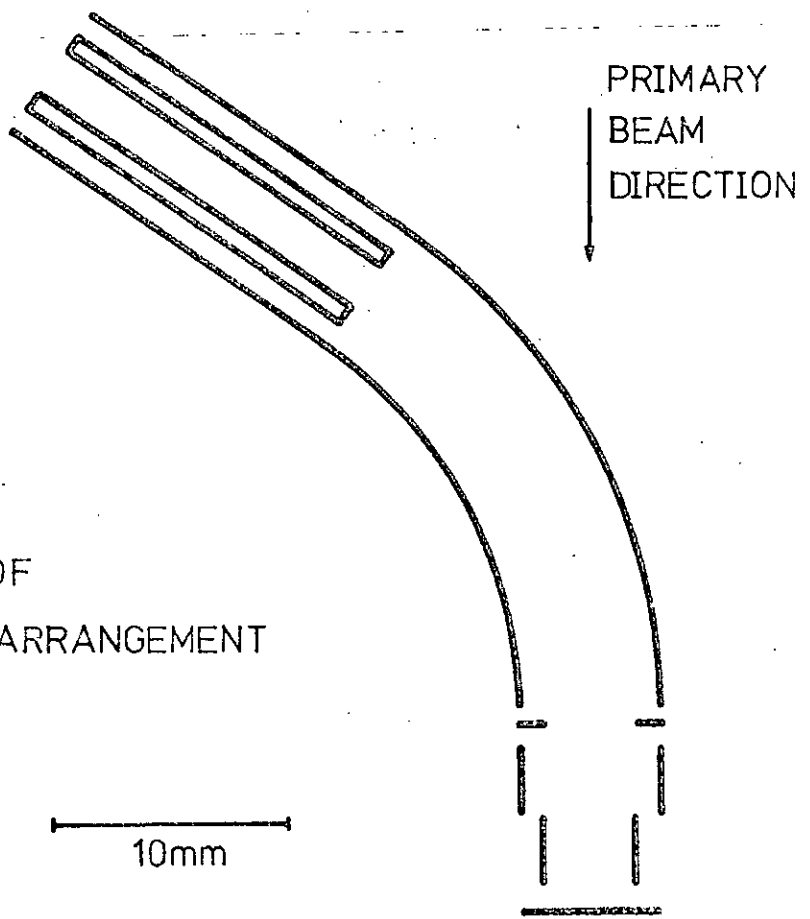


FIGURE 4.3.2
OUTLINE DRAWING OF
LENS & ANALYSER ARRANGEMENT

so this had to be modified as shown in Figure 4.3.4. This modified stage and specimen holder allowed only motion in the X,Y and Z directions without rotation or tilt of the specimen. The specimen surface was therefore always normal to the electron beam.

Figure 4.3.5 shows the lens and analyser mounted in the specimen stage of the SEM. It was found necessary to have a means of lining up the hole in the analyser top plate with the final aperture with the stage in place. This was accomplished by using the redundant specimen tilt and rotation controls and a simple mechanism to produce limited X and Y motion of the lens and analyser assembly. This was connected to the top of the cylindrical shield as shown. The accurate alignment of the whole system proved to be a problem requiring some patience. This problem could be overcome by using a more complex mechanism and more accurate construction. The present system performs well within the constraint of simple reversion to the normal use of the SEM.

Further problems associated with the long working distance required are the values of lens currents necessary to obtain this, the reduction in picture quality and the increase in astigmatism produced. The final lens control unit had to be interchanged with a condenser lens unit to give a low enough final lens current (0.3 A). Adjustment of the stigmator control allowed some reduction in the astigmatism. In fact the performance was really very good considering the very long working distance, several times the greatest normally used, which this system required.

4.3.4 Experimental Results

Initial experimental results were obtained using the setup of Figure 4.3.6. The specimen consisted of a thin (approx 1 μm) film of Al on 1 μm SiO_2 on an Si substrate with a gap approximately 30 μm

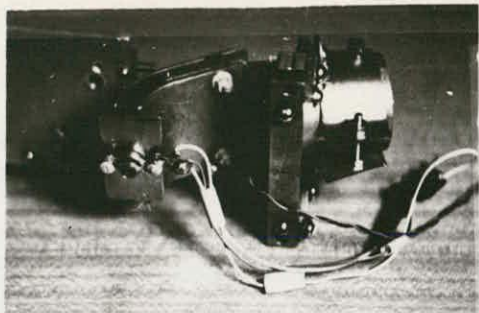


FIGURE 4.3.3(a)

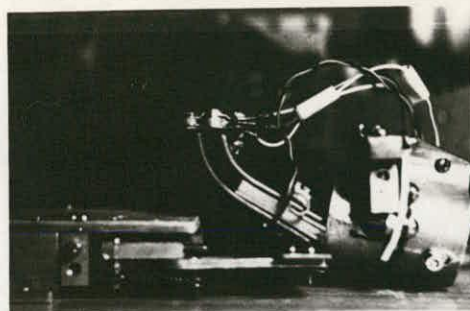


FIGURE 4.3.3 (b)

CONSTRUCTION OF LENS & MOUNTING ONTO ANALYSER

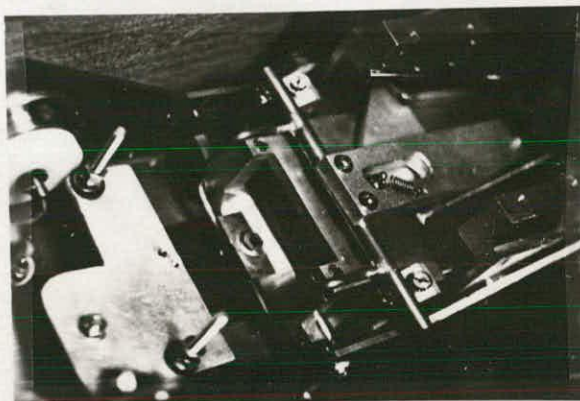


FIGURE 4.3.4

ALL
100mm

MODIFIED SPECIMEN STAGE

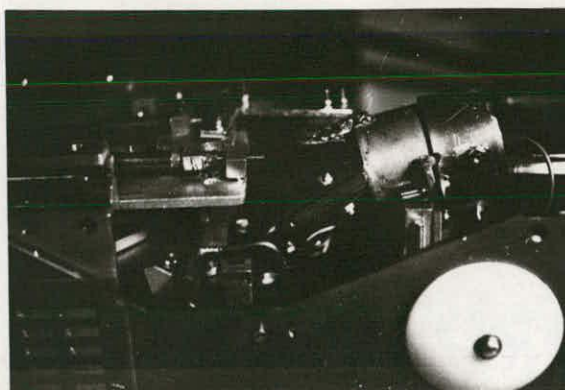


FIGURE 4.3.5

ALIGNMENT MECHANISM

wide in the centre of the film. Switch SW1 served to determine which side of the Al film was directly connected to the sweep voltage. V_{AB} was a switched set of nickel-cadmium cells which were not all of equal voltage although the total range was 0 to 12 volts with switchable polarity. Figures 4.3.7(a)-(e) show some typical secondary emission curves obtained (head amplifier output versus sweep voltage). In each case the X axis scale is 3 volts per division and 0.5 volts per division for the Y axis.

The beam was *kept* on strip A at a point approximately 15 μm from the edge of the gap and in each photograph V_{AB} varies from 0 to 12 volts, in discrete steps, with the polarity indicated. The figures are in three sets of two with the first one in each for the first lens electrode earthed and the second with the same electrode at +450 volts. Figures 4.3.7(a) and (b) show results for SW1 in position 1 and V_{AB} varying positively in each case, with V_1 0 and +450 volts respectively. In this case strip A is the *positive* side of the gap and Figure 4.3.7(b) shows the zero shift to be expected since SW1 is in position 1. Figures 4.3.7(c) and (d) show results for SW1 in position 2 and V_{AB} varying positively, with V_1 again 0 and +450 volts respectively. In this case strip A is again the *positive* side and Figure 4.3.7(d) shows the type of shift expected. Figures 4.3.7(e) and (f) are for identical conditions to the previous two but with V_{AB} varying negatively. In this case the latter figure is still an improvement over the former in terms of the shift. It should be noted in all these figures that the sweep voltage increases positively from *right* to *left* on the photographs due to the way the camera was mounted on the oscilloscope! The cases for the first electrode earthed would be expected to give a similar performance to the analyser without the lens. These results are in fact similar to Figs 4.2.4. Thus these results obtained show clearly the considerable improvement of this lens and analyser system over earlier methods particularly for points close to the gap. In fact for points close to the

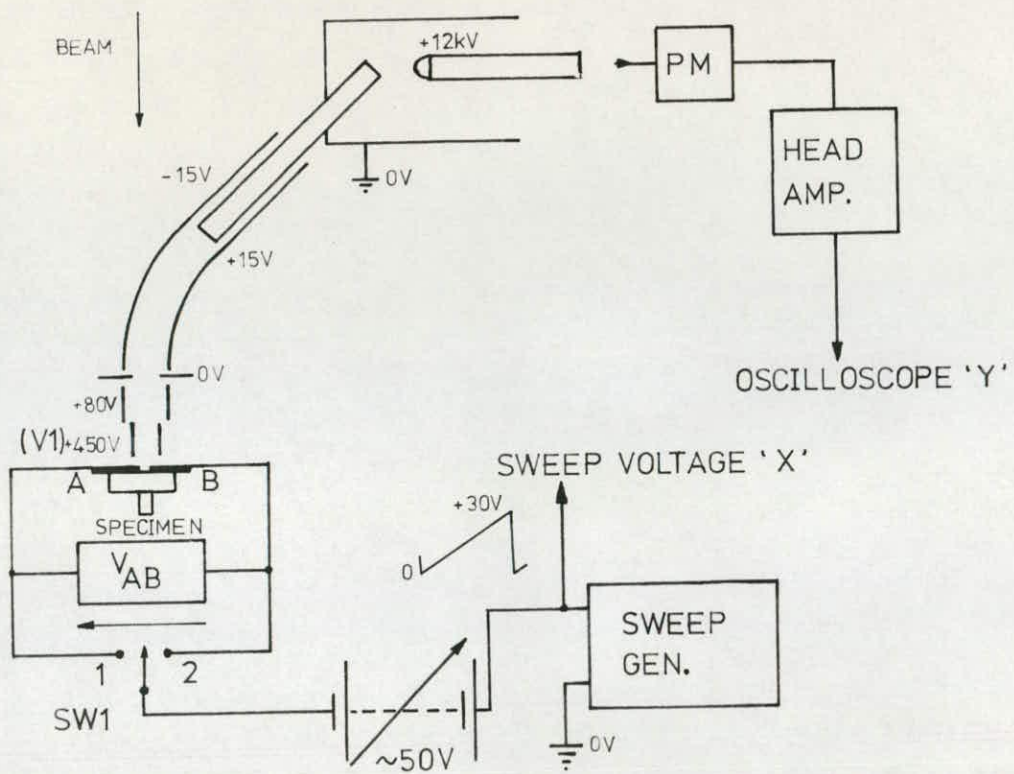


FIGURE 4.3.6 INITIAL EXPERIMENTAL SETUP

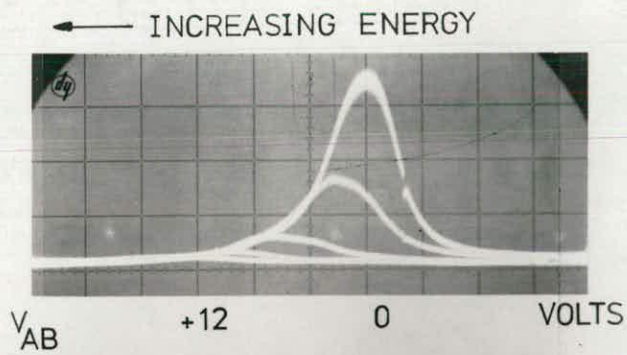


FIGURE 4.3.7(a)
SW1 IN POSITION '1'
V1=0V

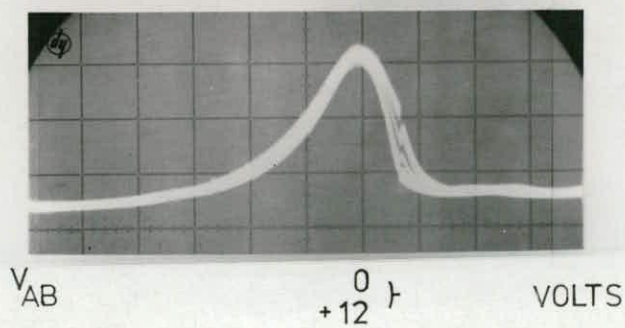
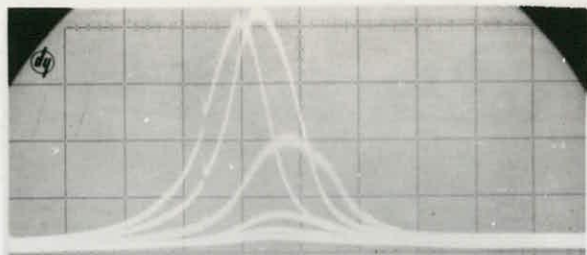


FIGURE 4.3.7(b)
SW1 IN POSITION '1'
V1=+450V

ALL X-3V/DIV. Y-0.5V/DIV.

← INCREASING ENERGY

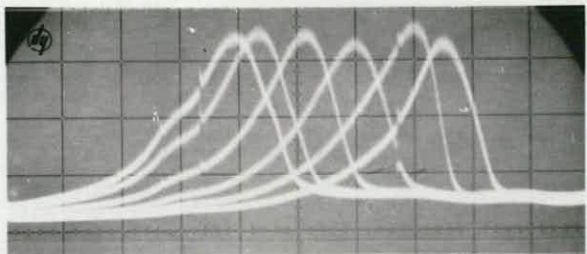


V_{AB} 0 +12 VOLTS

FIGURE 4.3.7(c)

SW1 IN POSITION '2'

$V1=0V$

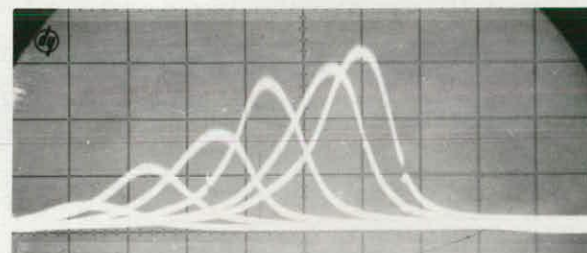


V_{AB} 0 +12 VOLTS

FIGURE 4.3.7(d)

SW1 IN POSITION '2'

$V1=+450V$

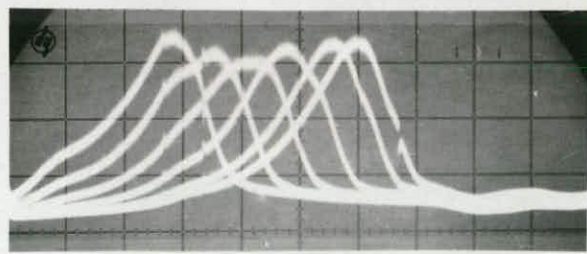


V_{AB} -12 0 VOLTS

FIGURE 4.3.7(e)

SW1 IN POSITION '2'

$V1=0V$



V_{AB} -12 0 VOLTS

FIGURE 4.3.7(f)

SW1 IN POSITION '2'

$V1=+450V$

ALL X-3V/DIV. Y-0.5V/DIV.

positive side of the gap the improvement is remarkable as shown by Figures 4.3.7(b) and (d).

These preliminary experiments indicated the order of the improvement over previous methods. In order to obtain the quantitative characteristics of this approach, the automated curve shift measuring system of Figure 4.2.5 was upgraded. The details of this system will be given later - the feature of importance here being the direct analogue and digital display of the secondary emission curve peak position, irrespective of the height of the curve.

The type of specimen chosen as a basis for further experiments was similar to that used in earlier work. A SEM photograph of such a sample is given in Figure 4.3.8. It was fabricated on a piece of silicon about 10 mm square on which a 1 μm thick SiO_2 film was thermally grown. A film of aluminium was evaporated onto the surface from a tungsten spiral with the gap produced by shadowing. These samples were simple to fabricate and were used since they give a controlled representation of the type of situation arising in IC specimens.

The first characteristic of the measuring system to be investigated was the relationship between the measured voltage and the voltage on the first electrode of the lens. Details of points for which the set of results given in Figures 4.3.10(a) and (b) were obtained, are shown in Figure 4.3.9. These points were not special in any way but their approximate position in relation to the lens axis and specimen gap is indicated in Figure 4.3.9, since these are relevant to a consideration of Figures 4.3.10(a) and (b). The orientation of the gap remained fixed (since no specimen rotation was available) but the actual position varied as noted on Figure 4.3.9.

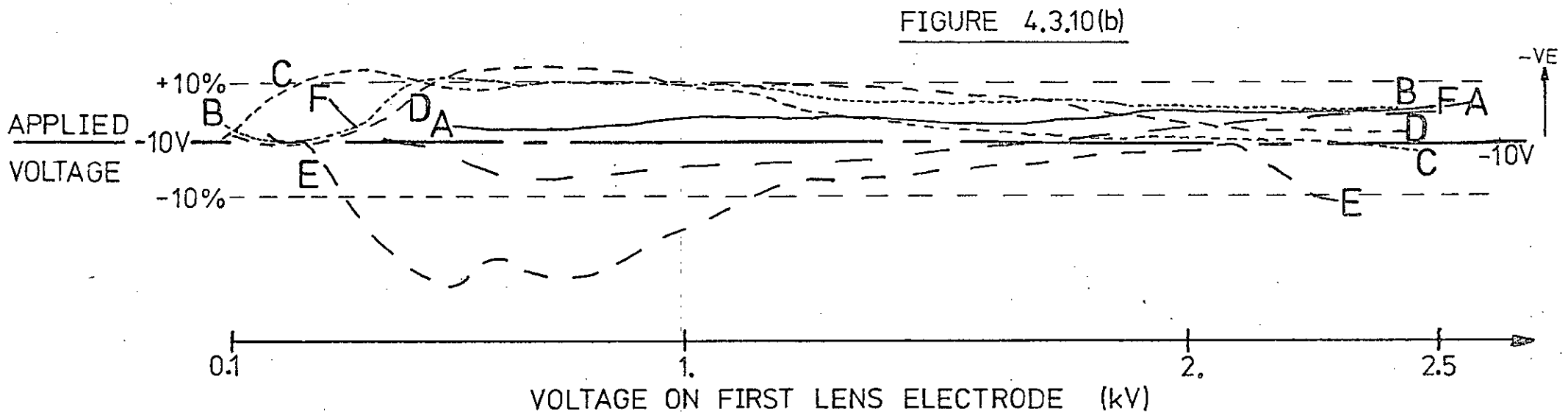
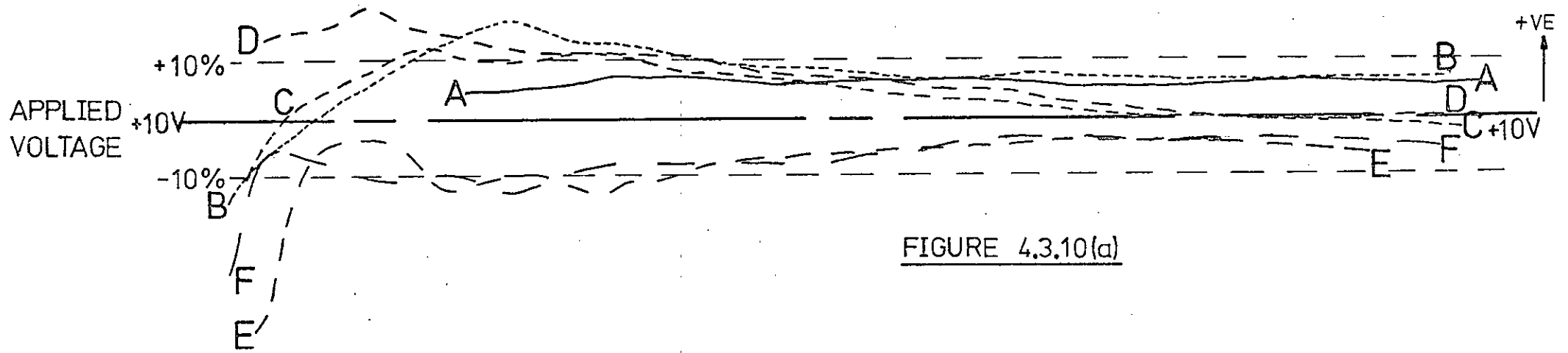
Figures 4.3.10(a) and (b) show the measured voltage for each of these points plotted against the voltage on the first lens electrode. The voltage on the specimen (across the gap) was either + or - 10 volts (as indicated) and the first electrode voltage was varied over the range 100 V to 2.5 kV. The curves were obtained on an X-Y plotter.

As might be expected the variations in the measured voltage at low values of first electrode voltage are considerable. The maximum error settles down to around 5% over a fairly wide range of voltages above about 1 kV. The curve shapes can be seen to vary with the position of the point of examination, relative to the edge of the gap and the axis of the lens. The error for points on one side of the gap (away from axis ie A, B, C, D) is generally opposite in sign to that for points on the other side (nearer axis ie, E, F). The results are fairly similar for positive and negative voltages, for the same point. For certain values of first electrode voltage the error for a particular point can be very small.

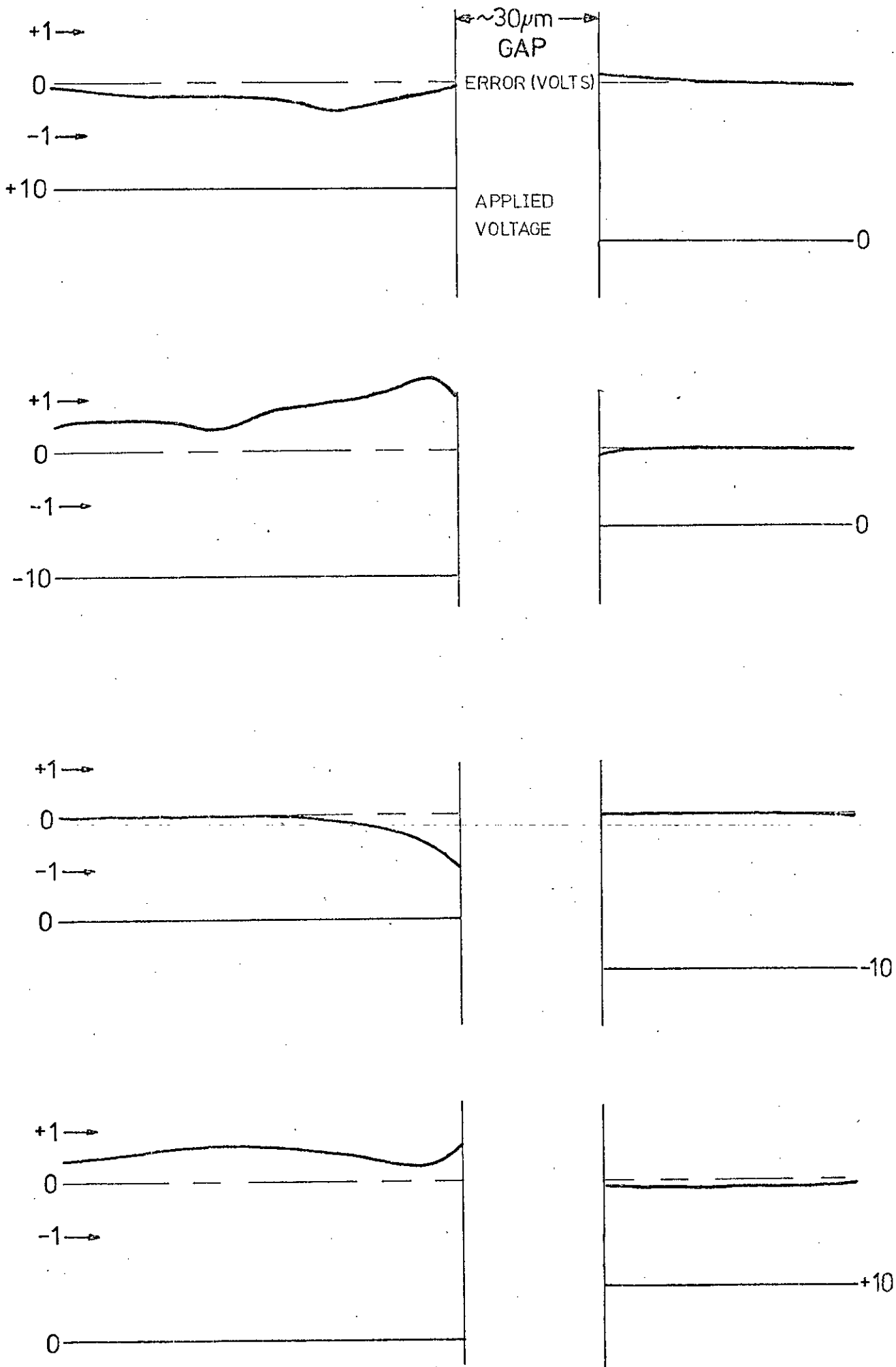
These investigations show that the potential on the first electrode of the lens is not a critical factor in the operation of this measuring system, provided it has a value between about 0.5 and 2 kV.

It was observed that varying the voltages on the second and third electrodes, about their usual values of +130 and +50 volts wrt the specimen, had very little effect on the overall characteristics of the system.

The results obtained by sweeping the electron beam across the approximately 30 μm wide gap of a test specimen are given in Figure 4.3.11. This shows a set of typical plots of error between measured and applied voltage, as the beam is moved across the gap, for the applied voltage distributions shown. The *exact* positions of the edges of the gap are



PLOTS OF MEASURED VOLTAGE Vs 1ST ELECTRODE VOLTAGE



(LENS \rightarrow 0.5kV)

FIGURE 4.3.11

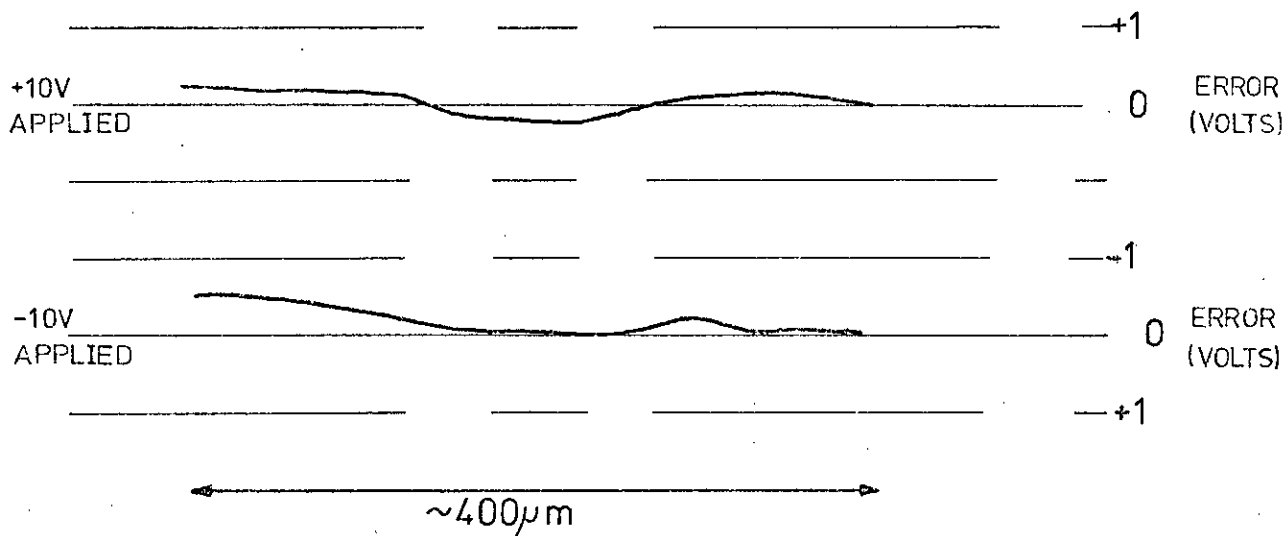
PLOTS OF ERROR BETWEEN APPLIED & MEASURED VOLTAGES (L TO GAP)

difficult to determine with great accuracy. A study of these plots shows that the error on one side of the gap (left) is always greater than the other and is worst for an electric field across the gap with direction right to left. This might indicate a relationship between the error and the field direction with respect to the position of the lens axis.

The actual values of the errors observed are generally fairly small except for very close to the gap. Even for this very difficult position the maximum error is not much above 10%. A comparison of the results in Figure 4.3.11 with those of Figures 4.2.9(a) and (b) shows clearly the very considerable improvement in performance of the present system over the earlier one. For points close to the positive side of the gap the improvement is especially marked.

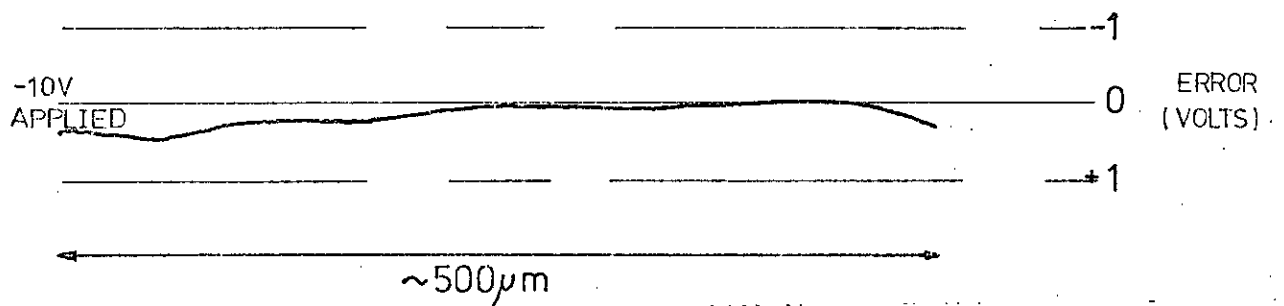
This good performance was found to hold for points along the gap edge over comparatively large distances and for different samples in different positions. This is difficult to demonstrate graphically but Figures 4.3.12(a)-(c) show typical plots of error between measured and applied voltages as the beam is moved along at a fixed distance from the gap edge. The samples were of the usual type. These plots show that the performance of the measuring system is not a critical function of the spatial position of the beam, even over distances as large as 1.5 mm.

An important characteristic of this measuring system is the excellent linearity of the relationship between measured and applied voltages. This is demonstrated by typical plots for two different samples as shown in Figures 4.3.13(a) and (b). These plots are seen to be single valued and linear for all points. In Figure 4.3.13(b) the plots are straight lines but with gradient close to but not exactly equal to 1.0. These correspond to situations in earlier



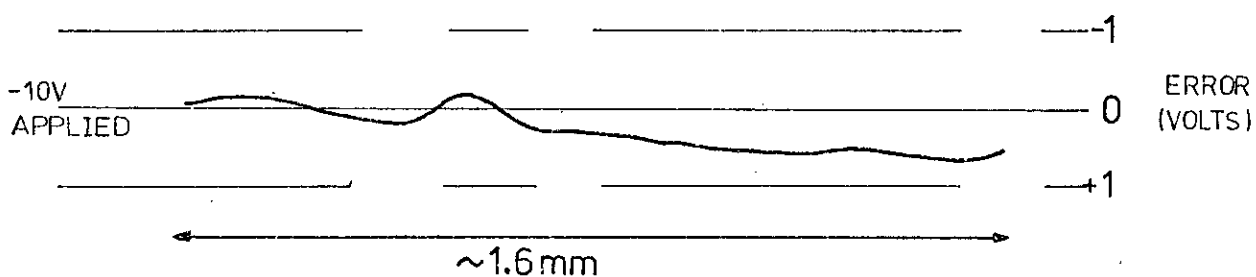
BEAM ALWAYS $\sim 8\mu$ m FROM EDGE OF $\sim 35\mu$ m GAP

FIGURE 4.3.I2(a)



BEAM ALWAYS $\sim 15\mu$ m FROM EDGE OF $\sim 35\mu$ m GAP

FIGURE 4.3.I2(b)



BEAM ALWAYS $\sim 80\mu$ m FROM EDGE OF $\sim 40\mu$ m GAP

FIGURE 4.3.I2(c)

(1st lens voltage 2kV in all cases)

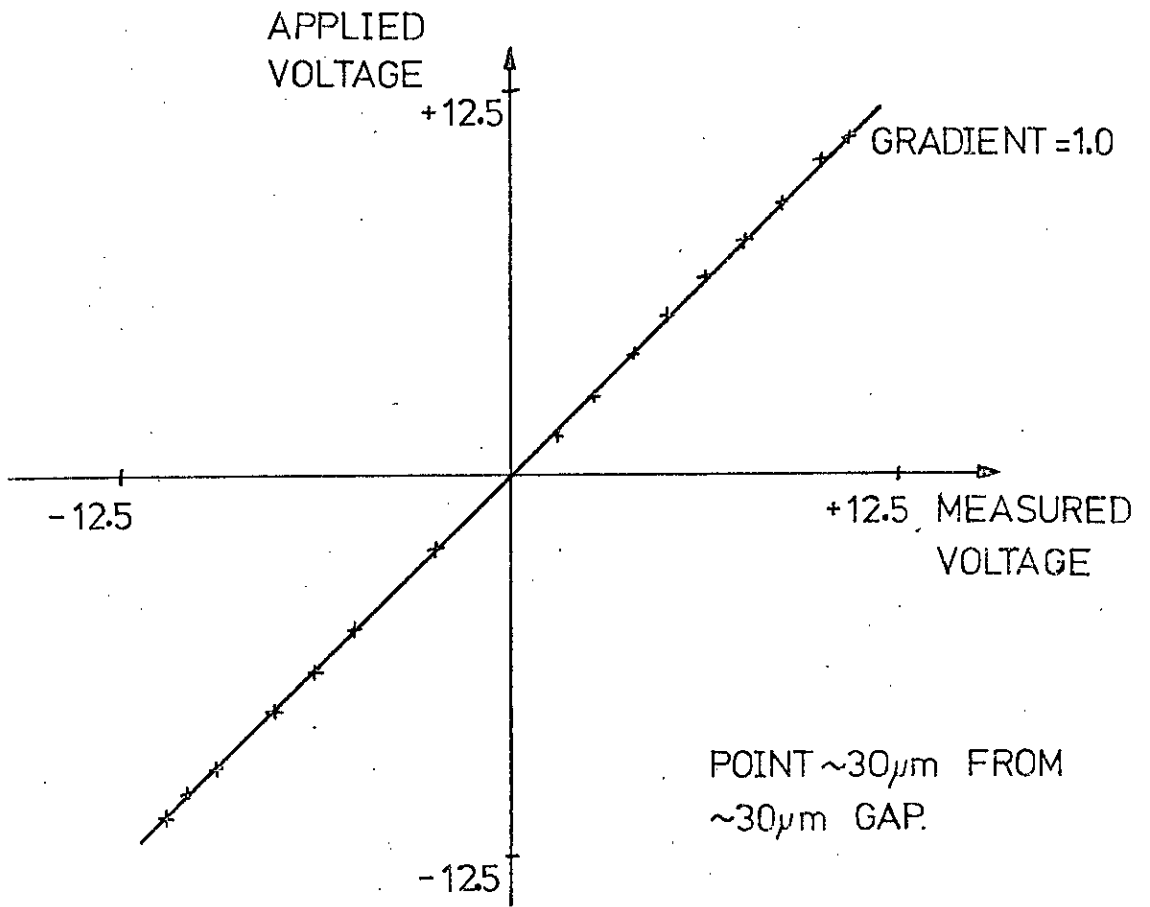


FIGURE 4.3.13(a)

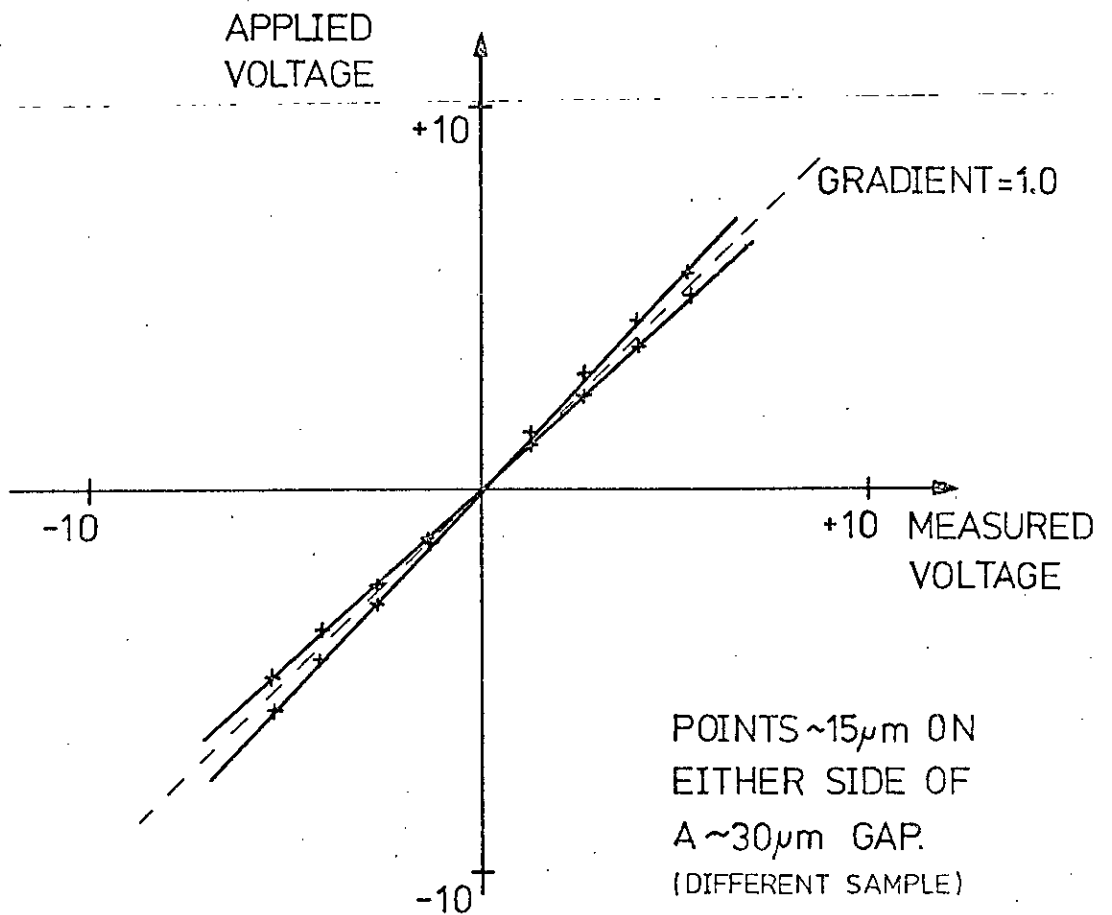


FIGURE 4.3.13(b)

figures when there was an error in the measured voltage. This was found to hold for all cases examined. Even when the measured voltage was not exactly equal to the applied voltage, the relationship between them was always substantially linear but with gradient slightly different from 1.0. This was true for both positive and negative applied voltages and over a range of at least 20 volts.

The results presented so far have all used the single gap type of Al on SiO₂ specimen described previously. In order to examine the performance of the system under very testing conditions the sample shown in Figure 4.3.14(a) was used. This device consisted of interdigitated aluminium fingers on a 1 μm SiO₂ layer on an Si substrate mounted on a T05 header. The fingers were 8 μm wide and the aluminium was around 1 μm thick. The device had three finger pairs and could be biased to produce a field between one strip and those on either side of it. (Similar sample to that shown in Figure 3.6.1). Figures 4.3.14(b) and (c) show typical shift of the secondary emission curve observed for various applied voltages with the beam on the centre of a finger. Figure 4.3.14(b) shows the response for a finger kept at constant potential with both positive and negative voltages applied to the other strips. The shift is very small, as expected. The expected almost linear shift is shown in Figure 4.3.14(c) for a finger with a variable voltage applied with respect to the other fingers. (The X scale of the traces is 3 V/div).

These figures demonstrate the very good performance of the system even with this type of sample which simulates the most difficult type of surface electric field conditions likely to occur in integrated circuits.



FIGURE 4.3.14(a)

INTERDIGITATED FINGER
SPECIMEN
(VIEWED WITH MEASURE-
MENT SYSTEM IN PLACE)

← 8 μ m

FINGER AT CONSTANT VOLTAGE

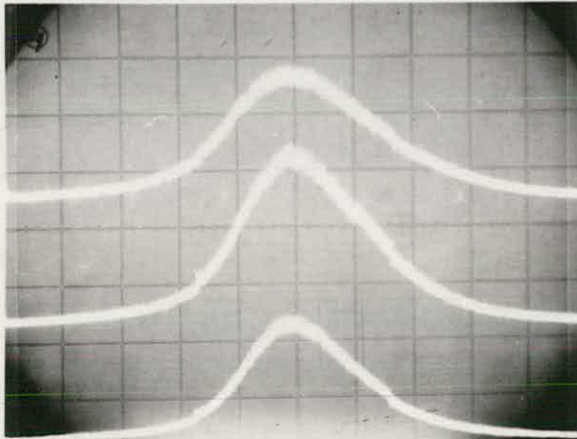


FIGURE 4.3.14(b)

OTHERS -10V

OTHERS 0V

OTHERS +10V

(W.R.T. THIS FINGER)

FINGER VOLTAGE VARIED

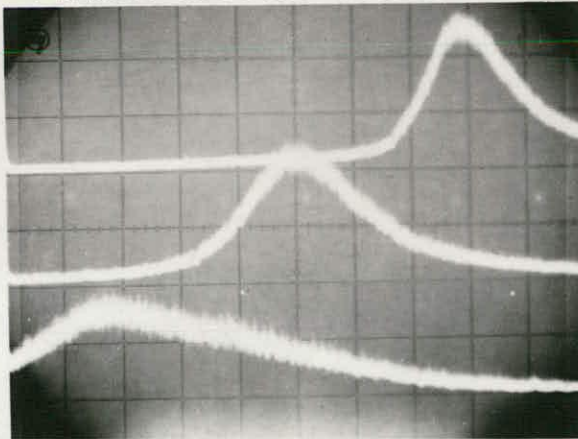


FIGURE 4.3.14(c)

-10V APPLIED

0V APPLIED

+10V APPLIED

(W.R.T. OTHERS FIXED)

BOTH X - 3V/DIV. Y - 0.5V/DIV.

It should be noted that Figure 4.3.14(a), showing the structure of the test specimen, was taken with the measurement system in place. This was photographed at an electron gun potential of 5 kV as this was the potential used for all experiments reported so far (except where stated otherwise). This shows that although the measurement system does degrade the resolution an adequate picture of the specimen surface can still be obtained. The resolution is really quite good considering the low gun voltage, very long working distance and presence of the lens and analyser.

Experiments were conducted to investigate the performance relative to contamination of the specimen. Typically less than 1% change in the measured voltage was noted over a 20 minute continuous observation of a point on an aluminium conductor with 5 kV beam voltage. This was the case even when beam induced contamination could be clearly seen on the specimen surface.

With the electron beam on the SiO_2 region in the gap a secondary emission curve shift with observation time was noted. This effect appeared to be very similar to the anomalous irradiation effect described by Wells¹⁰³.

4.3.5 Discussion of Results

The results which have been presented in the previous section show clearly the performance and characteristics of the voltage measuring system developed. These are:

1. Ability to give accurate, direct linear measurement of voltages, even in regions of high transverse field.
2. Relatively non-critical values of electron lens and analyser potentials and positioning of sample.
3. Low sensitivity to surface contamination effects.
4. Ability to view sample.

These characteristics have been demonstrated for samples which bear a very close resemblance to elements of monolithic IC devices. In fact use of these samples allowed controlled investigation of situations arising in integrated circuits, some of which were of the worst possible type which might occur in normal circuits.

The improvement in performance of this measuring system on others described previously, is shown by a comparison of the results. It is of interest to examine whether or not further improvements would be possible by redesign and what the magnitude of these would be. The experimental results include indications of some limitations which could possibly be reduced.

Further experimental study of system characteristics was limited by mechanical problems associated with the very simple mounting and motion components of this particular setup. Thus it was difficult to align the lens and analyser with the electron optical axis of the SEM and reproduce these positions for different specimens.

These further investigations of limitations and operating characteristics with a view to possible additional improvements indicate the need for a model of the system. This model would be required to give quantitative information about system operation and to be capable of predicting the performance of modifications. The next chapter will consider the development of methods to analyse and simulate the operation of the experimental system.

4.4 AN AUTOMATED MEASURING SYSTEM

4.4.1 Introduction

Previous sections have dealt mainly with the electron optical parts of the measuring system. The existence of electronic control and measurement equipment associated with these main components has already been mentioned. The following sections are intended to give a description of the operation of the overall setup and details of design.

4.4.2 Requirements and Design

The design aim of the system was to give a direct readout of voltages on a specimen, without requiring continual manual adjustment.

The method of operation of the voltage measuring approach has two main requirements:

1. Obtaining a secondary electron emission energy distribution curve,
2. Detecting and displaying the position (energy) of the peak (maximum) of this curve.

An energy distribution curve can be obtained by applying a sweep voltage to the specimen or analyser and displaying the output from the photomultiplier against this.

The amplitude of the peak of the secondary emission (SE) curve so obtained can vary for different points on the sample and different bias conditions (see Figures 4.2.4(a)-(e)). This variation can be considerable and although the electron lens reduces it a means of compensation is required to keep the amplitude relatively constant.

The peak of the SE curve can be found in different ways and the position of the peak measured by noting the sweep voltage at this point.

Figure 4.4.1 shows a block diagram of the overall system which was developed to meet these requirements. The system consisted of three main "blocks" of electronics (*sweep generation, amplitude control and peak detection*) in addition to the electron optics.

The hardware was largely digital for operational flexibility and since a future measuring system would probably be computer controlled. Integrated circuits were used extensively throughout the design. All logic circuitry was TTL with control and output signals TTL compatible.

4.4.3 Counter/Display and High Speed D/A Converter

The use of a counter and digital to analogue converter (DAC) was judged a better solution to the requirements of digital control and readout than the alternative combination of analogue sweep generator, sample and hold and analogue to digital converter.

A block diagram of the sweep generator is shown in Figure 4.4.1.

The main counter was a 3 digit BCD asynchronous unit with BCD to decimal decoders and NIXIE tube readout. The counter is capable of greater than 5 MHz clock rate.

Currently available commercial DAC's were unsuitable for this system due to inadequate output voltage range, low operating speed and high cost. The output voltage range required (30V) and the desirability of high operating speed meant that the conventional switched resistor network and summing amplifier approach to DAC design had to be rejected due to the limitations imposed by currently available operational amplifiers.

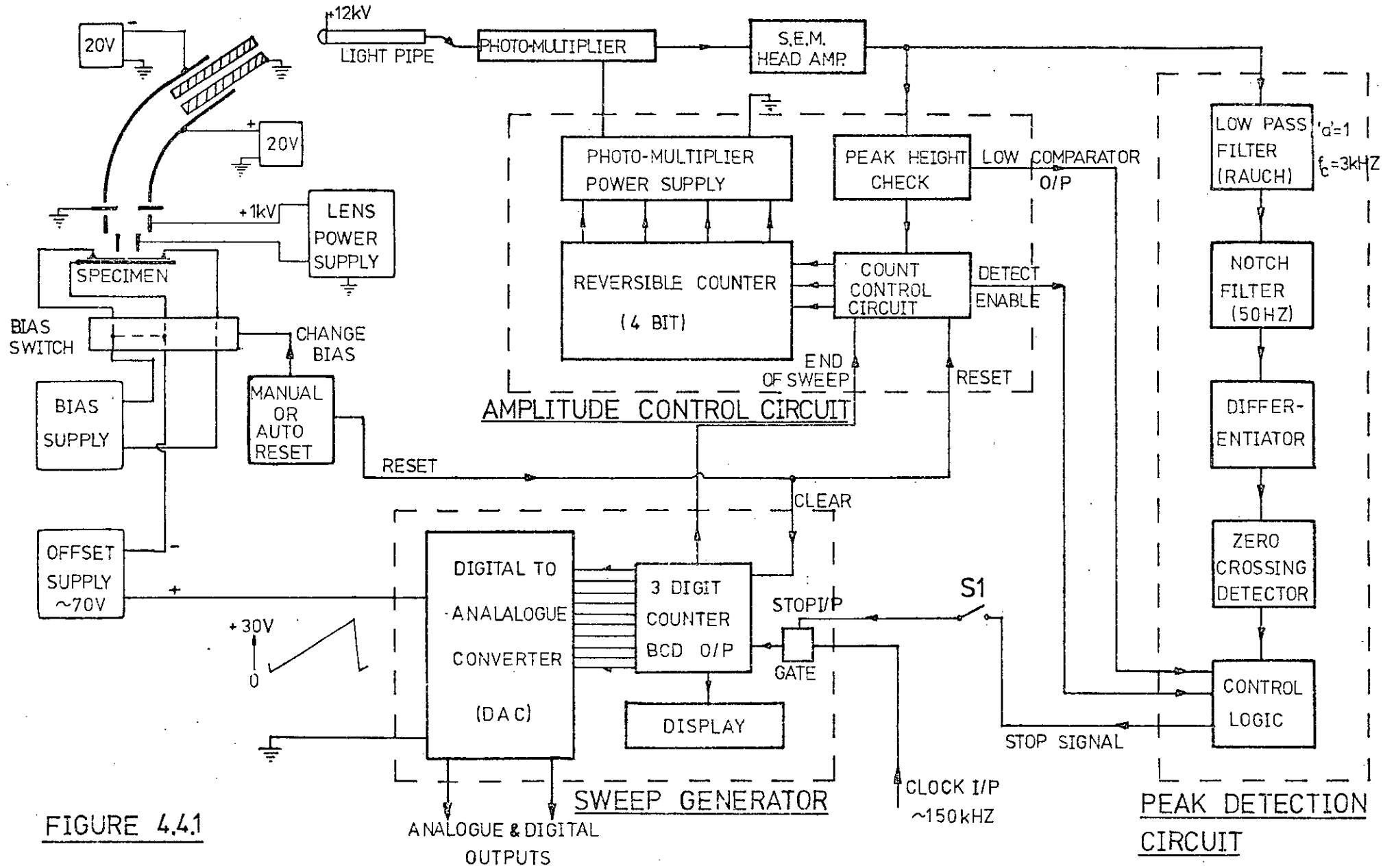


FIGURE 4.4.1

The design of DAC shown in Figure 4.4.2 was developed to fulfil system requirements. This was a 10 bit BCD unit and has some unusual design features necessary in order to obtain the required output range and speed. These include the use of separate ladder networks¹⁰⁴ for the first 8 and last 2 bits, complementary switching and special interface circuits. Separate switched ladder networks were required since high speed switching transistors do not have high collector emitter breakdown voltages. The complementary switching and special interface circuits were necessary to enable the ladder networks to be connected together to give the required output.

The performance of the DAC was found to be excellent. The settling time was 100 nS to $\frac{1}{2}$ LSB (least significant bit - 100 mV here), the linearity was better than 0.1% of full scale over 0 to 30V range and the total error at the upper end of the range was less than 0.1%. These even compare favourably with typical present day commercial device values of 5 μ s, 0.05% and 0.05% respectively. High accuracy was not the primary factor for this DAC but the performance was maintained over long periods with excellent reliability.

4.4.4 Amplitude Control Circuit

The problem of varying output signal from the photomultiplier has already been mentioned. The best means of compensating for this was considered to be varying the gain of the photomultiplier, as this will give best signal to noise performance.

A block diagram of the circuit developed to do this by varying the voltage applied to the photomultiplier dynode chain is included in Figure 4.4.1. The circuit operated to keep the head amplifier output voltage within preset limits set on two comparators at the input of the *peak height check* section. These sense whether or not the peak input voltage is above, below or in between the preset limits.

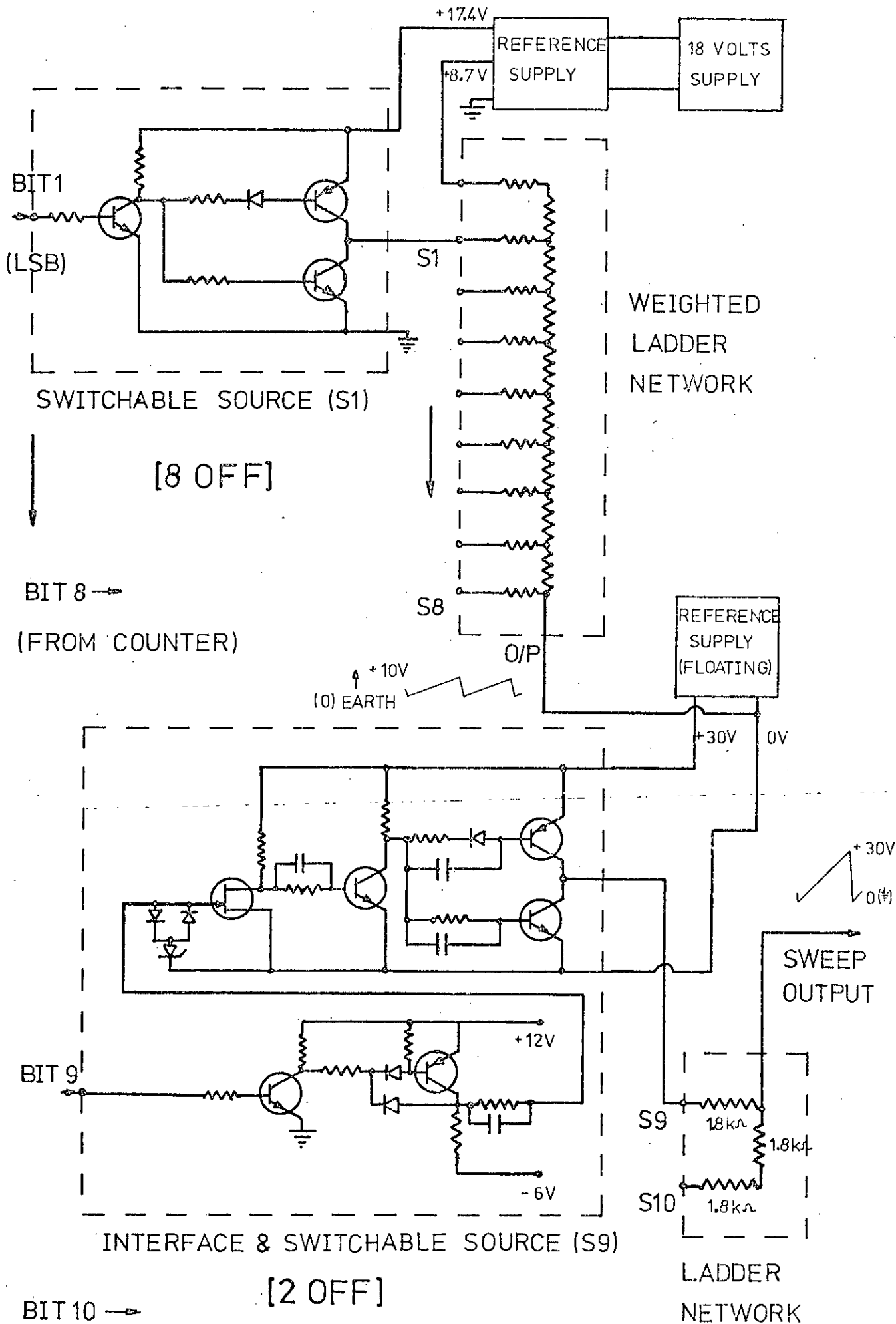


FIGURE 4.4.2

DIGITAL TO ANALOGUE CONVERTER

Depending on the outputs from these comparators the *count control circuit* instructs the *reversible counter* to count up one, down one or remain static at the end of the current sweep. The photomultiplier dynode voltage is varied in discrete steps by switching in or out resistors placed in the controlling bias chain of a commercial (Brandenburg) transistorised photomultiplier power supply. The switching is accomplished by reed relays, controlled by the counter, since the resistors are at EHT potential. The height check-circuit is inhibited during the next sweep to allow for reed relay contact bounce and transients in the EHT power supply (a 2 mS sweep period was more than adequate).

The sensitivity versus dynode chain voltage characteristic of the photomultiplier is logarithmic so the bias chain resistor values were chosen to give a gain range of 30 dB in 2 dB steps - about a dynode chain voltage of 500 V. This resulted in excellent performance with the peak level of the SE curve being easily kept within the preset range (typically 2-3 V wrt earth). This was found to be a very valuable part of the overall system.

4.4.5 Peak Detection Circuit

The block diagram of this section of the system, shown in Figure 4.4.1, indicates that mainly analogue circuitry was used. Approaches using digital techniques to allow complete flexibility did not give very good performance. This was mainly due to the fact that the signal to noise ratio at the head amplifier output can sometimes be in the 20 to 30 dB range.

The maximum noise reduction is obtained if bandpass filtering is carried out on the signal. This would result in phase shift over the passband producing apparent shift in the peak of the curve giving errors. Thus a *low pass* "Rauch" second order filter was designed

with a damping factor of unity and 3 dB cut off frequency of 3 kHz. This filter gives a phase shift which is approximately a linear function of frequency over the range of interest, which results in constant curve delay giving low error. A 50 Hz notch filter was also included to reduce the effects of mains pickup.

The remainder of the circuitry is straightforward with control information from the amplitude control circuit ensuring that the circuit only detects positive stationary points inside the preset amplitude window.

These circuits performed extremely well both with a simulation circuit to check accuracy and noise performance and also within the complete system.

4.4.6 Operation and Performance

The method of voltage measurement used in experiments described previously was as follows.

With the electron beam on the desired point on the specimen (with no bias applied), switch S1 (Figure 4.4.1) was opened. The sweep generator then ran in a continuous mode and the secondary emission curve (head amplifier output versus sweep) was displayed on an oscilloscope. The *offset voltage* supply (Figure 4.4.1) was adjusted so that the peak of the curve was inside the 30 V sweep window ie on the oscilloscope screen. With the amplitude control circuit off, the photomultiplier voltage was adjusted (if necessary) to give a reasonable signal. These adjustments were normally only required initially, for a new specimen and very occasionally thereafter. They would be unnecessary if a large sweep and amplitude control range were incorporated.

Bias is applied to the specimen and S1 closed. As the sweep generator sweeps, the amplitude control circuit checks the height of the curve peak during one sweep and changes the photomultiplier voltage (if necessary) during the next and checks again repeating until it is within the preset limits. When the peak is in the correct range the peak detection circuit is enabled to detect the peak during the next sweep and stop the sweep generator at this point giving a readout of the sweep voltage. The total measurement normally takes about 4 sweeps ie less than 10 mS at a 2 mS sweep period.

As the bias on the specimen is varied the difference between the readings on the display gives the required voltage measurement.

Faster operation of the system is possible but was not pursued since the performance of the present setup is more than adequate for manual observations.

The accuracy of the measuring electronics may be checked by varying the offset voltage supply and noting the change in the measured voltage. These changes should be equal since the offset voltage varies the position of the curve peak with respect to the generator sweep. Checking this always gave results with error not greater than 0.1 volt (least significant bit value for DAC). Most results were identical showing the excellent performance of the system.

The range of voltages which can be measured in an automatic mode is 25 volts just less than the sweep voltage range (30 V). Larger voltages can be measured simply by manually varying the offset voltage between measurements.

The operation of the system as described has been semi-automatic but the controls are all digital and linked in such a way that only a master command and data recording device need be added to allow completely automatic operation.

A consideration of the experimental results using this system and its mode of operation indicates its ability to meet the requirements already presented as desirable for a voltage measurement system for integrated circuits.

CHAPTER 5

METHODS FOR POTENTIAL DISTRIBUTION AND

ELECTRON TRAJECTORY CALCULATIONS

5.1 INTRODUCTION

The previous chapter has demonstrated the measured characteristics of the electron lens and energy analyser voltage measurement approach. It was noted that a model of the setup which would allow consideration of design changes with a view to still further improvement in performance would be a worthwhile development. A further study of limitations of the method will also be of value.

The aim of this chapter is to develop methods for quantitative analysis and study of the measurement approach.

5.2 GENERAL APPROACH

A qualitative description of the operation of the lens and analyser has been given in the previous chapter. In order to obtain a quantitative description it is necessary to be able to evaluate the trajectories of secondary electrons leaving the specimen surface and determine whether or not they pass through the lens and analyser and are collected. Determination of electron trajectories necessitates a knowledge of the electric field distributions in the regions of interest. The electric field distributions are normally found from potential distributions.

A consideration of the specimen, lens and analyser arrangement shows that analytical methods for obtaining the potential distributions are not suitable. Since analytic expressions for the electric fields are not available the evaluation of electron trajectories will not lend itself to an analytical approach. Thus numerical methods must be used in this analysis. The use of numerical methods for such a complex setup as the one to be studied requires the use of a digital computer in order to handle the very large number of calculations required. This means that for each step of the analysis a numerical method must be developed for solution and a computer program written to carry out the analysis.

Two main types of program are necessary to investigate the factors involved in the experimental system. These are:

1. Programs to describe the potential distribution in the regions of interest.
2. Programs to calculate electron trajectories in the desired regions and so to give the overall behaviour of the configuration under investigation.

In developing computer programs to model a physical situation a number of factors have to be considered. Perhaps the most important of these is how much the application of the program is restricted to the particular configuration it was written to model. That is, can the physical system be slightly modified without completely rewriting the program. Alternatively a very 'general' program is likely to be extremely time consuming to develop and expensive in terms of computer time to run.

The accuracy of the model is also an important consideration but it may have to be traded off against computing time.

The programs which were developed for this work are judged to be a good compromise between these various considerations.

5.3 POTENTIAL DISTRIBUTION IN LENS AND ANALYSER

5.3.1 Methods of Calculation

The method of numerical calculation is the normal one of using the potentials at points on a square mesh to represent those in the system. The main factor in this is the size of the mesh since a small size gives good accuracy but requires large storage (number of points). A compromise must be found.

Since for each set of potentials on the lens and analyser electrodes a different matrix is required to describe the potential distribution it is obviously important to choose as large a mesh size as possible to minimise storage requirements. Various other features were introduced to keep down the amount of stored data.

The meshes chosen are shown in Figure 5.3.1 and are the same size for both lens and analyser.

The electric field in the lens is of course axially symmetric whereas that in the analyser is a plane field (in the central region between the plates).

This means that the two dimensional mesh for the lens actually represents potentials in a radial plane. In fact the lens field will not be completely axially symmetric near the specimen and near the analyser entrance. It is very difficult to correct for this but the error it produces should be comparatively small in this case.

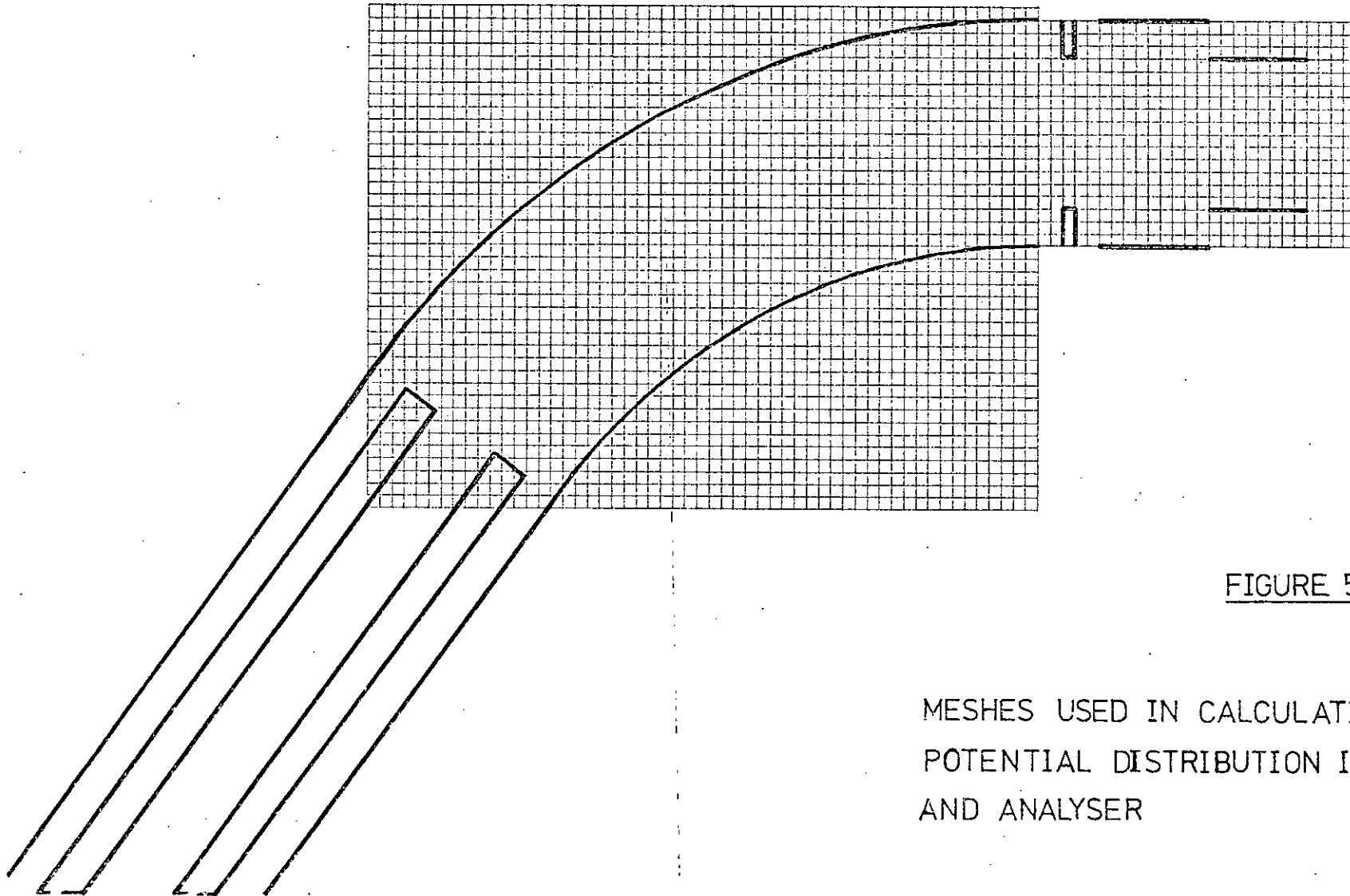


FIGURE 5.3.1

MESHES USED IN CALCULATION OF
POTENTIAL DISTRIBUTION IN LENS
AND ANALYSER

The method of calculation uses a finite difference equation for each node of the mesh. The form of equation will vary depending on the region in which the potentials have to be evaluated.

For a two dimensional Laplacian field (ie no enclosed charge) the finite difference equation for the potentials at a typical node as shown in Figure 5.3.2 is given by¹⁰⁵

$$V1 + V2 + V3 + V4 - 4V0 = 0 \quad \dots 5.3.1$$

For use in an iterative relaxation calculation this is best written as

$$RES = \frac{1}{4}(V1 + V2 + V3 + V4) - V0 \quad \dots 5.3.2$$

where RES is the *residual* at this step in the calculation.

There are many different approaches possible using this basic equation. The method of solution adopted was that of successive over-relaxation¹⁰⁶. This means that instead of altering the value of $V0$ by the value of RES it is altered by more than this at each step of the calculation ie a *convergence factor* is introduced. It was found that a good choice of this factor greatly reduced the number of relaxations to give a specified error. (The choice of an optimum convergence factor is dealt with in reference 105, p 122).

For an axially symmetric Laplacian field the finite difference equation for a typical node as in Figure 5.3.3 is given by^{107, 108}

$$V1 + V2(1 + h/(2R0)) + V3 + V4(1 - h/(2R0)) - 4V0 = 0 \quad \dots 5.3.3$$

This is the basic form required for the lens region. A convergence factor is also introduced in this case.

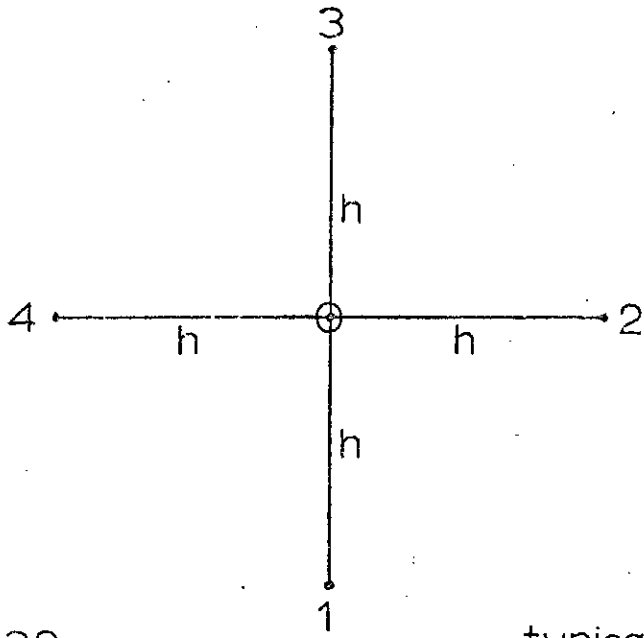
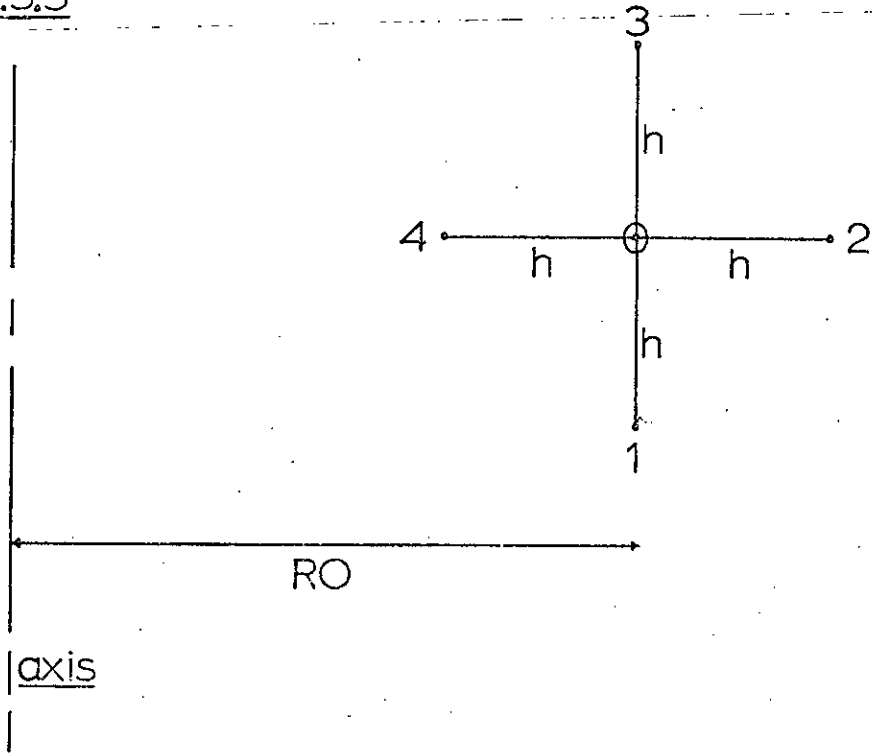


Fig.5.32

typical node

Fig.5.3.3



In the case of the analyser the fact that the plates are curved and the mesh is square means that near these a modified form of equation 5.3.1 must be used. This form for an asymmetrical star at a node as in Figure 5.3.4 is given by¹⁰⁹

$$V1/(1 + q) + V2/(p(1 + p)) + V3/(q(1 + q)) + V4/(1 + p) - V0(p + q)/(pq) = 0 \quad \dots 5.3.4$$

These are the basic equations required in the calculation of the potential distributions.

One of the primary considerations in any relaxation problem is the number of relaxation cycles to give a particular accuracy of solution. The factors involved fall into two main groups *truncation error* and *computational error*.

Truncation error is a function of the finite difference equation used to represent Laplace's equation since higher order terms are ignored in the derivation (as will be shown later). The validity of the approximation is a function of the mesh size.

The computational error will only be zero when the residuals for the equations at all nodes are zero. Since this can only be achieved after an infinite number of cycles a compromise must be reached.

5.3.2 Computer Program

A simplified flow diagram for the program to evaluate the potential distribution in the lens and analyser regions is shown in Figure 5.3.5. This consists of a main program (**VLNSANS**) and two main subprograms (**VAS** and **POTL**).

These programs make use of equations 5.3.1 (in **POTL**), 5.3.3 (in **VAS**) and 5.3.4 in the appropriate regions working through rows

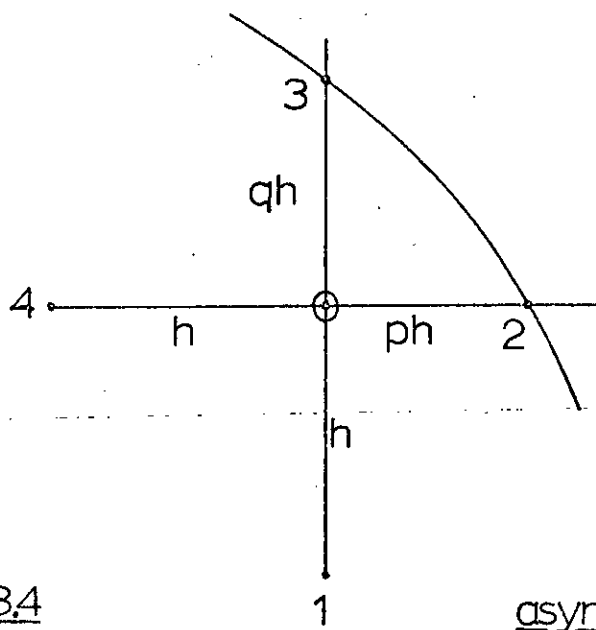
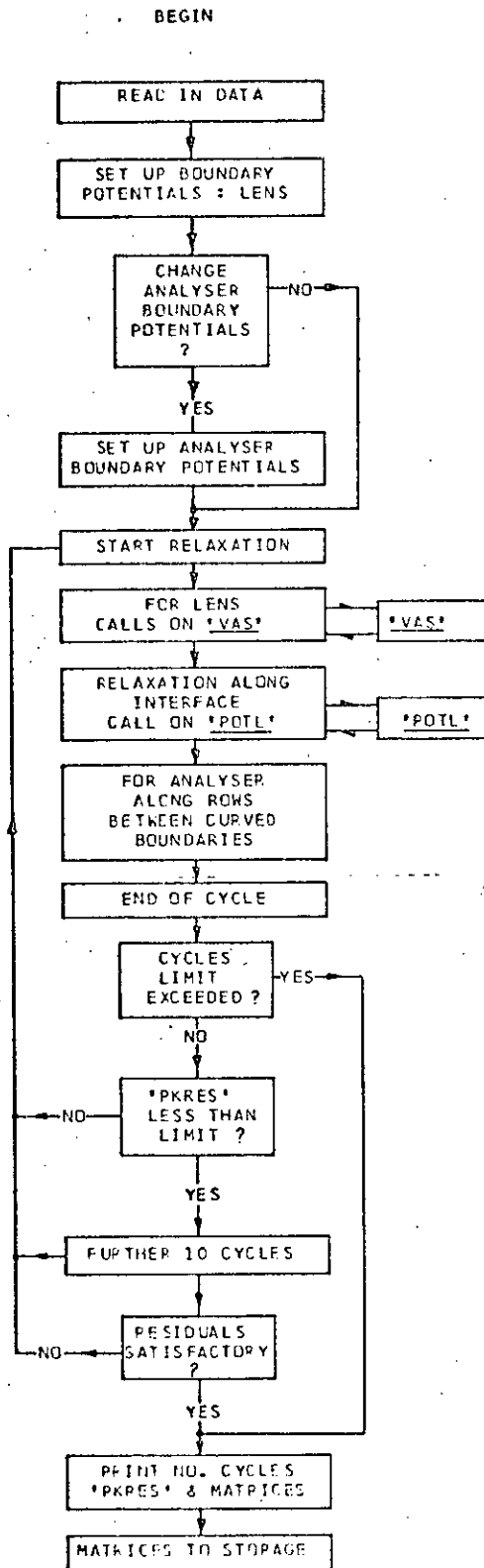


Fig. 5.34

asymmetrical star

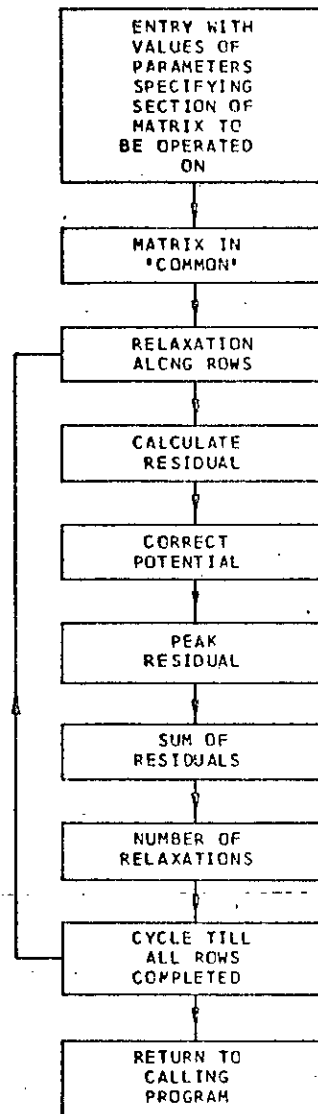
MAIN PROGRAM 'VLNSANS'

(179 FORTRAN STATEMENTS)



SUBROUTINE 'POTL'

(16 FORTRAN STATEMENTS)



SUBROUTINE 'VAS'

(39 FORTRAN STATEMENTS)

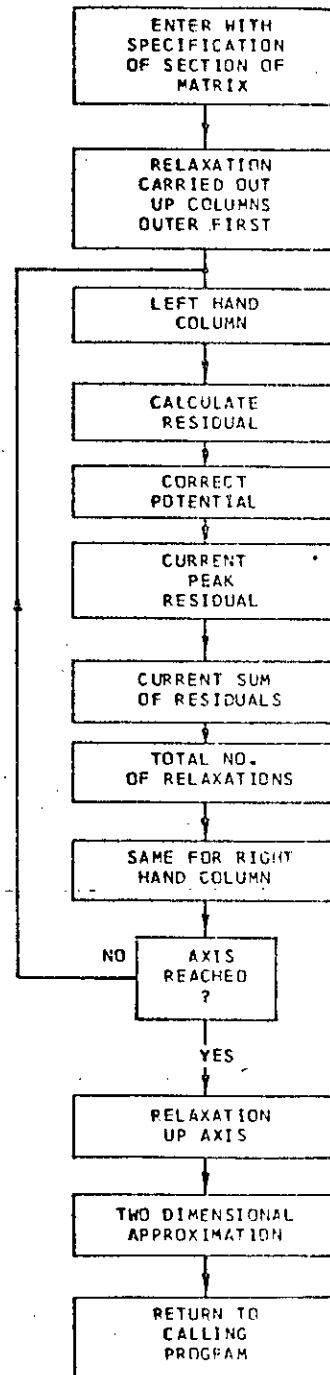


FIGURE 5.35

Computer Program Flow Diagram

and columns of the lens (27 x 19) and analyser (56 x 41) matrices shown in Figure 5.3.1.

It is of course essential to supply either boundary potential values or potential gradients in such a relaxation calculation. In all the programs potential values were specified. Only estimated values can be supplied in the case of gaps between electrodes however this has only limited effect on the values near the regions of main interest.

The section which deals with the analyser is much more complex than shown due to the complications of the curved plates which require a set of coefficients for use at each asymmetrical node boundary.

In Figure 5.3.5 in **VLNSANS** the checks used to determine the number of relaxation cycles required were

1. The maximum residual over each relaxation cycle was compared with a value specified in input data to the program.
2. When the residual was less than this a further 10 cycles were executed and the algebraic sum of residuals over these was compared with another value set up on input. The peak residual was normally set to be less than 0.01. No great advantage would be obtained by increasing the number of cycles for this type of numerical solution.

The calculation of the potentials for the lens is not straightforward since equation 5.3.4 includes the radius R_0 of node 0. The mesh appears coarse for this equation (see Figure 5.4.1). In fact a test program for a similarly dimensioned coaxial system gave results within 1% of theoretical values.

Figures 5.3.6(a)-(c) show computer drawn equipotentials using matrices of potentials produced by VLNSANS for lens voltages of 0.5, 1 and 2 KV. It can be seen that the forms of these are very much as would be expected - smooth with no singularities. This is an important check on the accuracy of the calculations.

5.4 POTENTIAL DISTRIBUTION NEAR SPECIMEN SURFACE

5.4.1 General Approach

Since secondary electrons leave the surface with a low energy (~5 eV) the mesh shown in Figure 5.4.1 is much too coarse to allow accurate evaluation of electron trajectories near the surface. This is because in the first few mesh spacings the electron energy is changed by at least 20 times its original energy. Thus in this region a much smaller mesh size must be used.

In order to minimise the total number of potential values to be stored it was decided to expand the lens matrix already produced, in the region of interest near the surface. A two or three stage expansion was used resulting in the optimum grid size for each region of interest. This is a very significant improvement over the approach of using a small mesh size for the whole lens region since it results in around 10^3 times reduction in the number of potential values to be stored.

It was also required to simulate the performance of the experimental system for IC type specimens. The types of physical device structures chosen for study are shown in Figure 5.4.2 which shows cross sections of these devices. They represent $1 \mu\text{m}$ of SiO_2 on an Si substrate with $1 \mu\text{m}$ thick aluminium on the top. The gaps had the widths shown and were considered to be long in relation to width. It is necessary to find the potentials above these integrated circuit type structures.

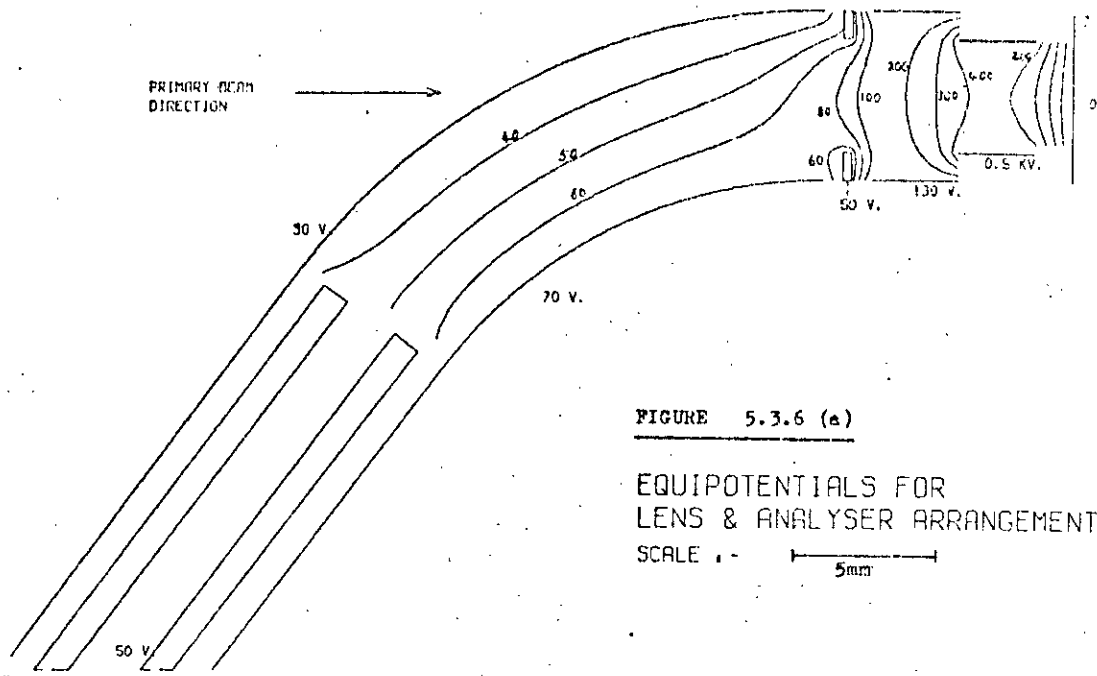


FIGURE 5.3.6 (a)

EQUIPOTENTIALS FOR LENS & ANALYSER ARRANGEMENT
SCALE 1 - 5mm

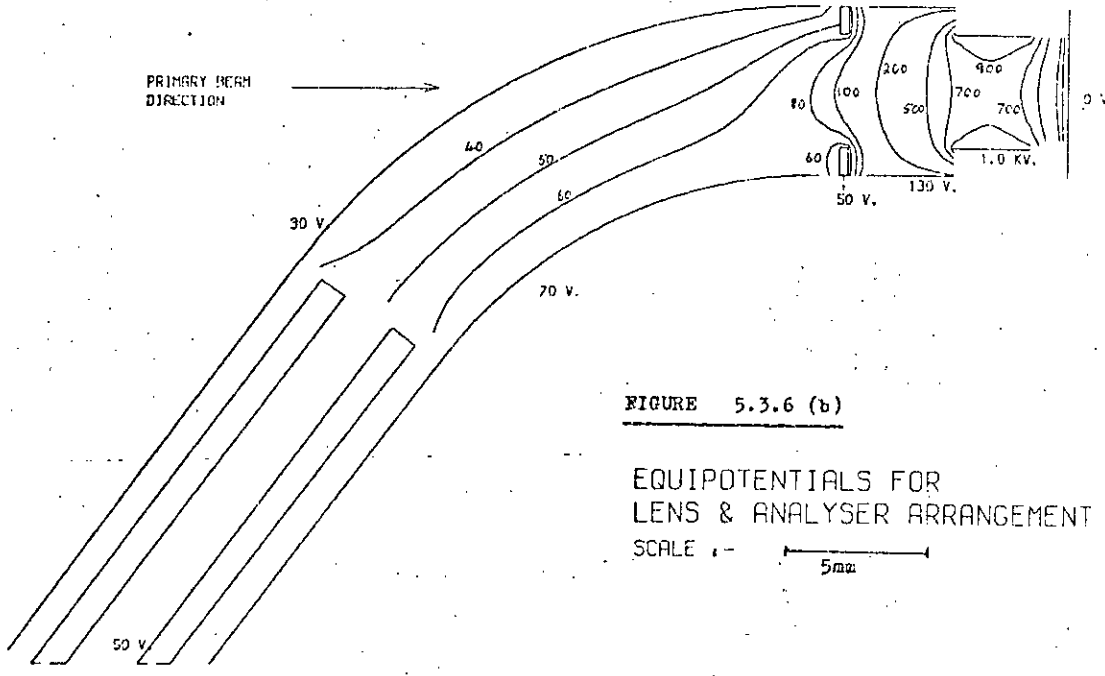


FIGURE 5.3.6 (b)

EQUIPOTENTIALS FOR LENS & ANALYSER ARRANGEMENT
SCALE 1 - 5mm

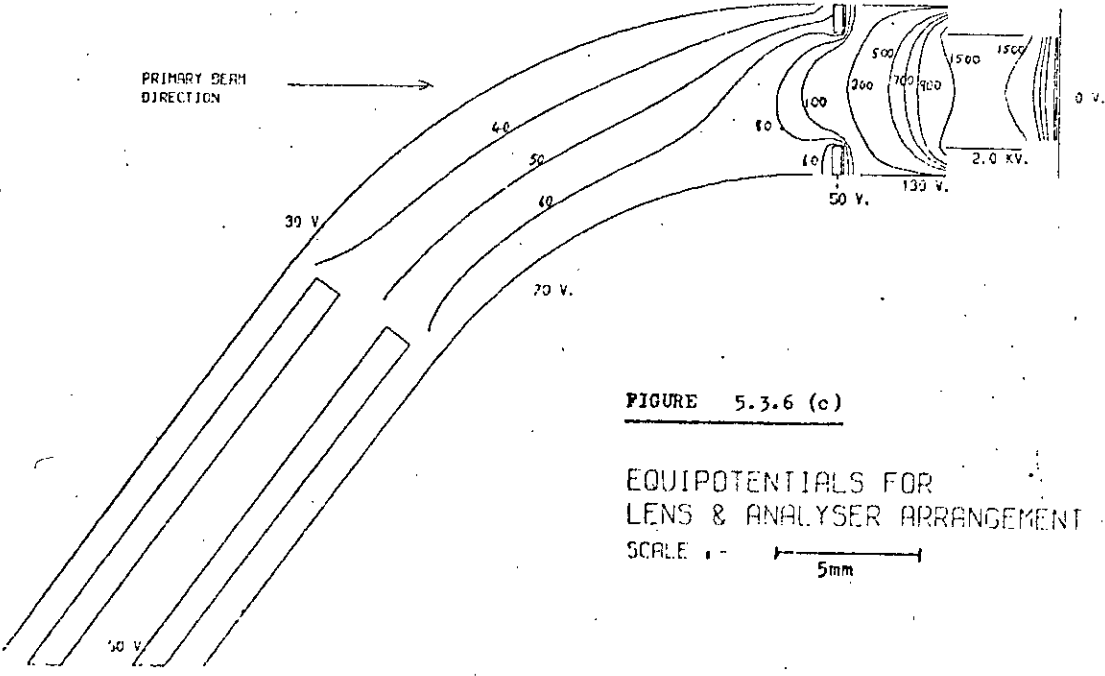


FIGURE 5.3.6 (c)

EQUIPOTENTIALS FOR LENS & ANALYSER ARRANGEMENT
SCALE 1 - 5mm

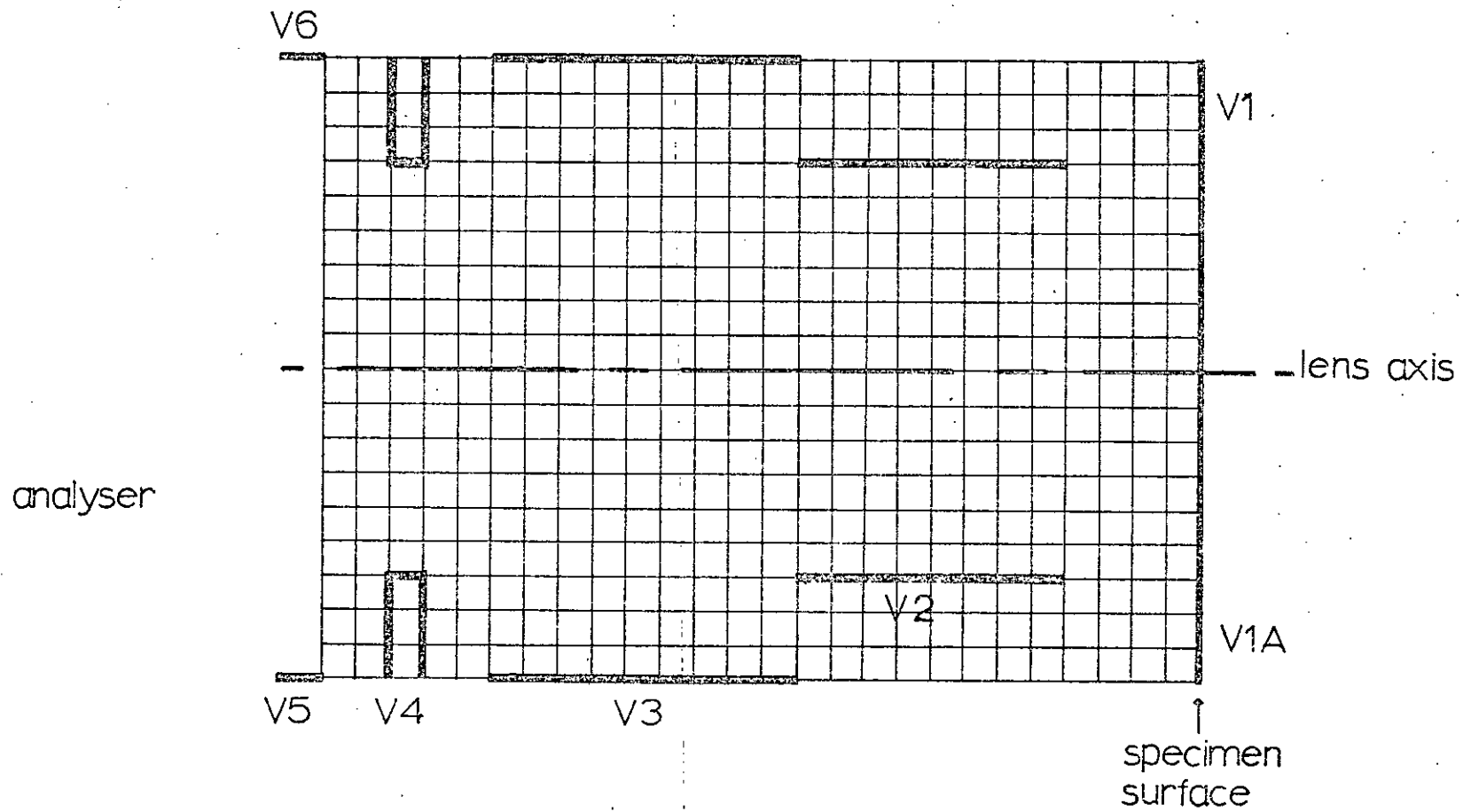


FIGURE 5.4.1

Detail of lens mesh

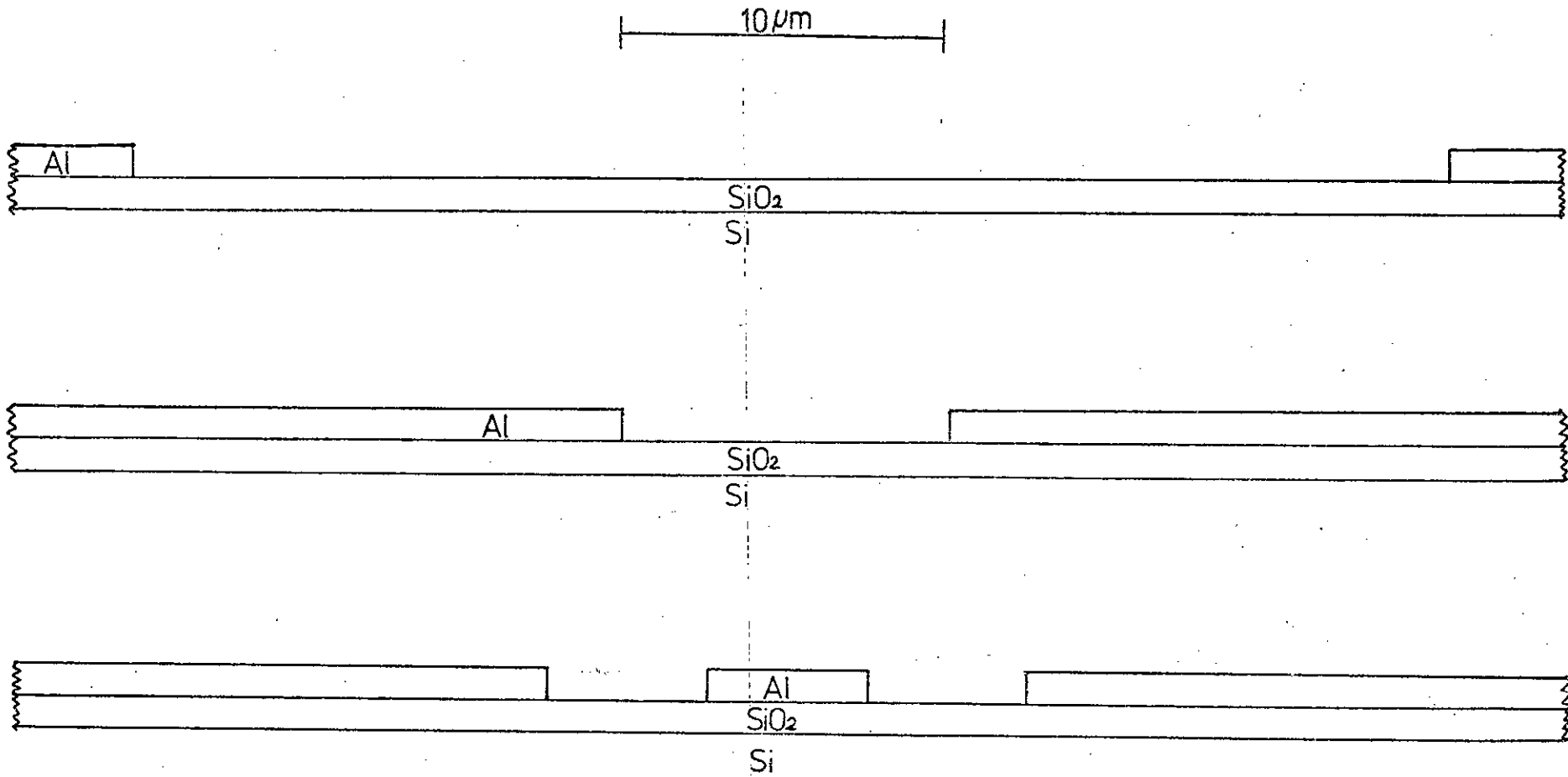


Fig. 5.4.2

Configurations Analysed

The method of expanding the original mesh is shown in Figure 5.4.3. The original lens mesh is shown dotted and the expansions are either X8, X32 or X8, X32, X128 giving two and three expanded matrices respectively. These matrices are located about the centre of the gap and are all 17 x 17 ie 16 meshes square.

5.4.2 Theory

In order to calculate the potentials near the surface it is necessary to consider the mesh boundary at the surface, here the top of the aluminium layer. To calculate the potentials in the gap region it is necessary to include the effect of the silicon and silicon dioxide. This requires the use of additional meshes in the gap region as shown in Figures 5.4.4(a) and (b). These cannot be square (as shown) since the thickness of the Al and SiO₂ is much smaller than the gap width. Also for ease of calculation the top of these matrices (VG, VG1, VG2) must coincide with the 'main' potential matrix at all times in the calculation. This results in a complex numerical solution.

None of the finite difference forms of Laplace's equation already mentioned are valid in this gap region of the specimen surface so a general form is derived below. This derivation is for a two dimensional field.

General difference form of Laplace's equation for unequal arms

Figure 5.4.5 shows a star about a node 0 with arms of the length shown and potentials VT, VR, VB, VL and V0.

From a Taylor's expansion of potentials about node 0 we have

$$VR = V_0 + HR \left(\frac{\partial V}{\partial x} \right) + \frac{HR^2}{2!} \left(\frac{\partial^2 V}{\partial x^2} \right) + \frac{HR^3}{3!} \left(\frac{\partial^3 V}{\partial x^3} \right) + \dots$$

$$VT = V_0 + HT \left(\frac{\partial V}{\partial y} \right) + \frac{HT^2}{2!} \left(\frac{\partial^2 V}{\partial y^2} \right) + \frac{HT^3}{3!} \left(\frac{\partial^3 V}{\partial y^3} \right) + \dots$$

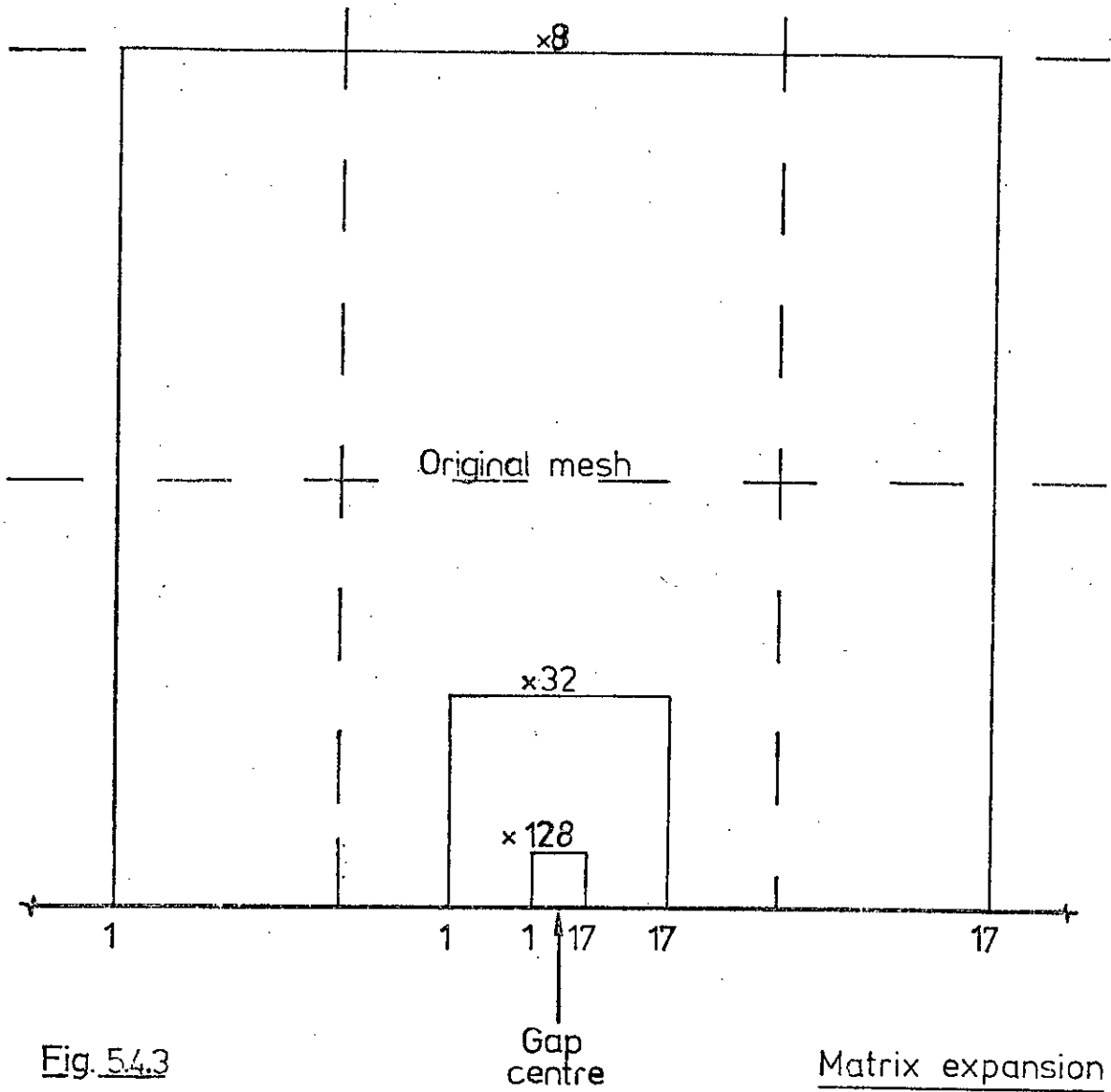


Fig. 5.4.3

Matrix expansion

Fig. 5.4.4(a)

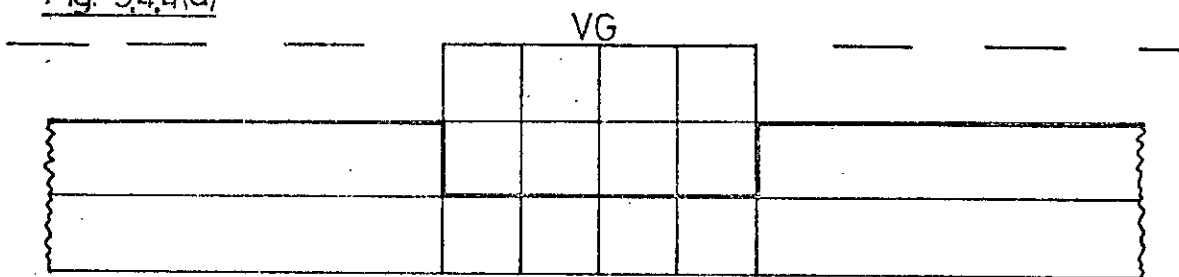
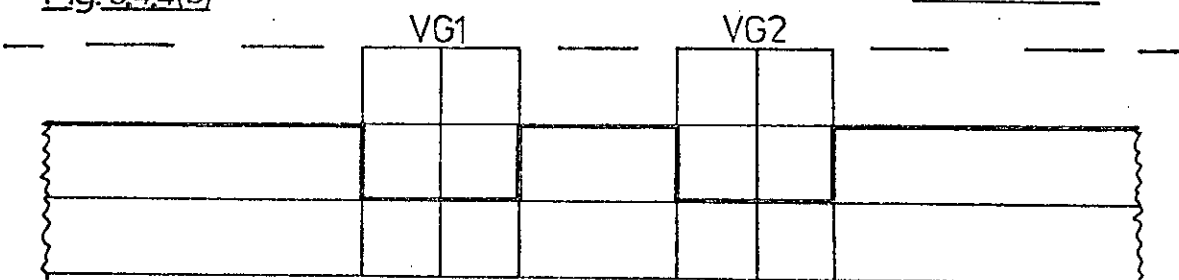


Fig. 5.4.4(b)

Not to scale



Additional meshes in gap region

and two similar equations for VL and VB but with negative odd power terms. All derivatives are evaluated at node 0.

Combining the four equations to eliminate odd power terms and ignoring terms in 'H'⁴ etc and above (valid if mesh is small enough) gives

$$\left(\frac{\partial^2 V}{\partial x^2}\right) = \frac{2(VR \times HL + VL \times HR - VO(HL + HR))}{HR \times HL(HR + HL)}$$

and

$$\left(\frac{\partial^2 V}{\partial y^2}\right) = \frac{2(VT \times HB + VB \times HT - VO(HT + HB))}{HT \times HB(HT + HB)}$$

If Laplace's equation is satisfied at node 0

$$\frac{\partial^2 V}{\partial x^2} + \frac{\partial^2 V}{\partial y^2} = 0$$

therefore

$$\begin{aligned} & \frac{VR}{HR(HR + HL)} + \frac{VL}{HL(HR + HL)} - \frac{VO}{HR \times HL} \\ & + \frac{VT}{HT(HT + HB)} + \frac{VB}{HB(HT + HB)} - \frac{VO}{HT \times HB} = 0 \quad \dots 5.4.1 \end{aligned}$$

If RES is the residual at point 0 we have

$$RES = VR \times CR + VL \times CL + VT \times CT + VB \times CB - VO \quad 5.4.2$$

where

$$CR = \frac{HT \times HB \times HL}{HDLR} ; CL = \frac{HT \times HB \times HR}{HDLR}$$

and

$$HDLR = (HR + HL)(HR \times HL + HT \times HB)$$

$$CT = \frac{HB \times HR \times HL}{HDTB} ; CB = \frac{HT \times HL \times HR}{HDTB}$$

and

$$HDTB = (HT + HB)(HR \times HL + HT \times HB)$$

(RES is the value which must be added to the VO of equation 5.4.2 to give a VO which satisfies equation 5.4.1)

Equation 5.4.2 can be seen to simplify to equations 5.3.2 and 5.3.4 for the appropriate arm lengths.

Interface between two dissimilar regions

Even equation 5.4.2 is not general enough for the case between two dissimilar regions as in Figure 5.4.6 (eg SiO_2 - air interface). Point 0 is on the boundary.

At point 0 in region 'a'

From equation 5.4.2

$$V_{Ra} \times C_R + V_{La} \times C_L + V_{Ta} \times C_T + V_{Ba} \times C_B - V_{0a} = 0 \quad \dots 5.4.3$$

At point 0 in region 'b'

$$V_{Rb} \times C_R + V_{Lb} \times C_L + V_{Tb} \times C_T + V_{Bb} \times C_B - V_{0b} = 0 \quad \dots 5.4.4$$

V_{Tb} and V_{Ba} have no physical meaning and are called fictitious potentials.

From continuity considerations at the boundary between the two regions.

Field strength tangential to boundary

The electric field strengths tangential to the boundary must be equal on the boundary
ie In finite difference form

$$V_{Ma} = V_{Mb} = V_M \quad \dots 5.4.5$$

where M denotes a general node on the boundary.

Component of flux normal to boundary

The normal flux density (D) on both sides of the boundary must be equal.

A finite difference approximation for the normal electric field gives

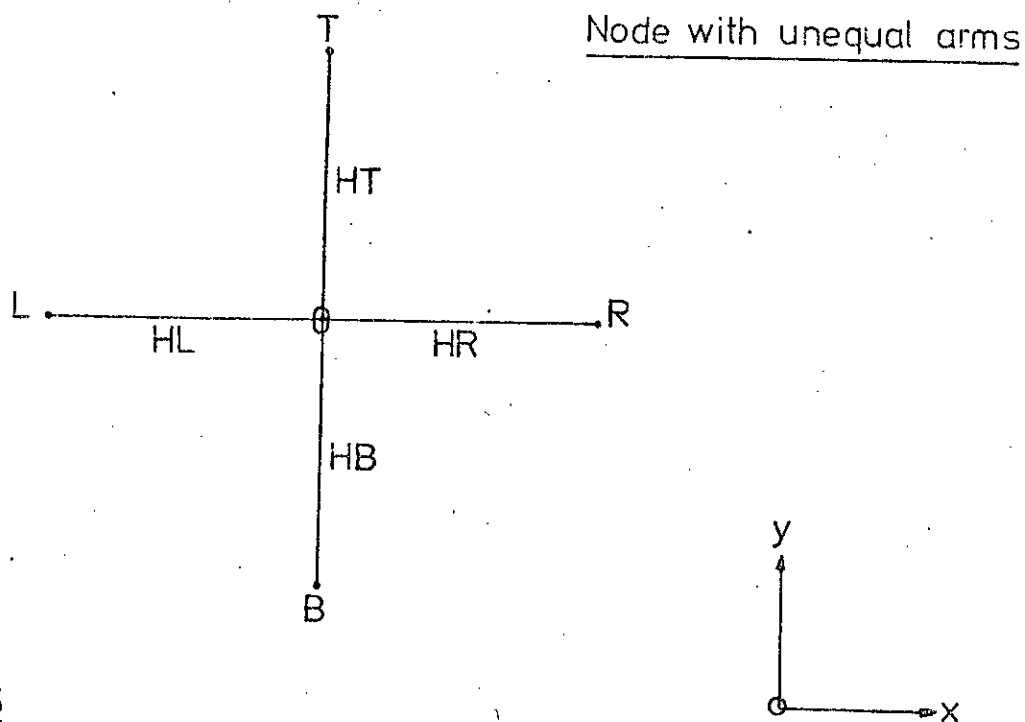


Fig.5.4.5

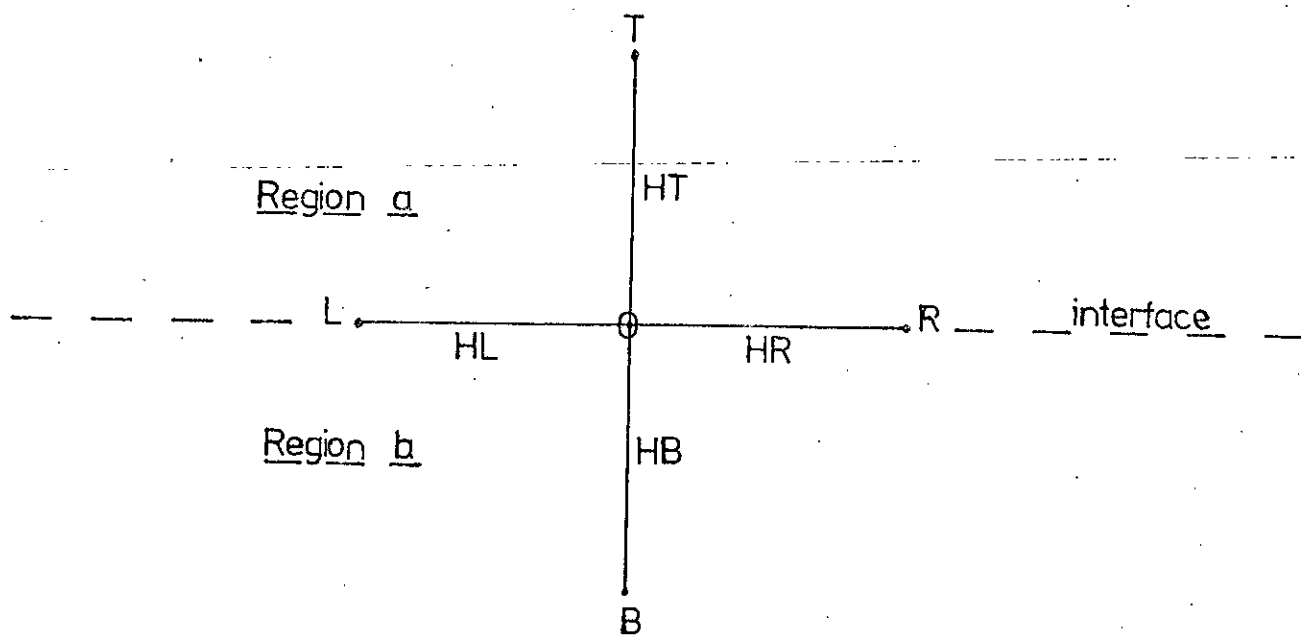


Fig.5.4.6

Interface between two dissimilar regions

$$EOa = \frac{VBa - VTa}{HT + HB}$$

$$EOb = \frac{VBb - VTb}{HT + HB}$$

Since $D = \epsilon E$ and $Da = Db$ (ϵ is permittivity)

$$\epsilon a(VBa - VTa) = \epsilon b(VBb - VTb) \quad \dots 5.4.6$$

Since $VTa = VT$ and $VBb = VB$ we have

$$VBa + S \times VTb = VT + S \times VB \quad \dots 5.4.7$$

where $S = \frac{\epsilon b}{\epsilon a}$

applying equation 5.4.5 to equations 5.4.3 and 5.4.4 and eliminating VBa and VTb between these and equation 5.4.7 gives

$$\begin{aligned} &CT(VR \times CR + VL \times CL + VT \times CT - V0) + \\ &S \times CB (VR \times CR + VL \times CL + VB \times CB - V0) \\ &+ (VT + S \times VB) \times CB \times CT = 0 \end{aligned}$$

Again if RES is the residual

$$\begin{aligned} RES = &VL \times CL + VR \times CR + VT \times \frac{CT(CT + CB)}{CT + S \times CB} \\ &+ VB \times \frac{S \times CB(CT + CB)}{CT + S \times CB} - V0 \quad \dots 5.4.8 \end{aligned}$$

This is a general finite difference form for the Laplace equation in two dimensions at a node on the boundary between two dissimilar regions and with unequal arms.

5.4.3 Computer Programs

Simplified flow diagrams for the programs developed are given in Figure 5.4.7. Two similar main programs were used for a one gap (EXPVS1G) and two gap sample (EXPVS2G) with two subroutines (VHM and VG)

FIGURE 5.4.7

Computer Program Flow Diagram

EXPVSIG & EXPVS2G

SUBROUTINE *VHM*

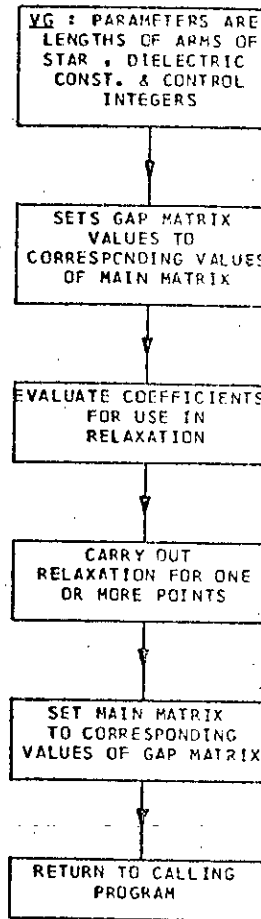
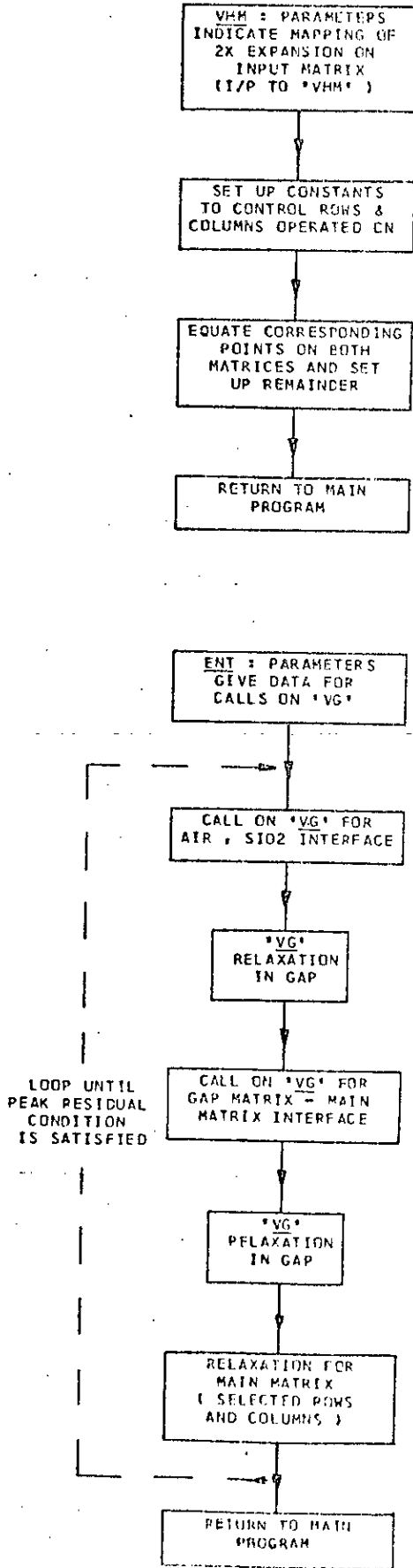
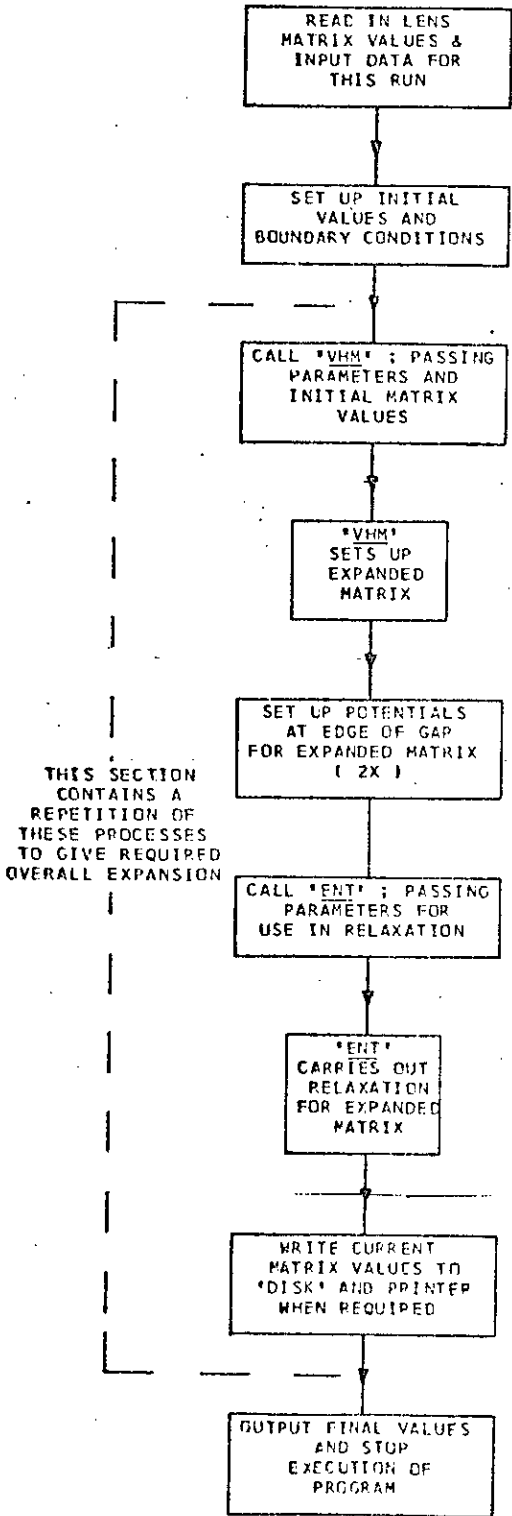
SUBROUTINE *VG*

MAIN PROGRAM

(68 FORTRAN STATEMENTS)

(27 FORTRAN STATEMENT

(77 FORTRAN STATEMENTS)



Apart from the potentials in the gap region a simple method was used to expand the original matrix. The mesh is expanded by a factor of two each time but points coinciding with the original mesh points are not altered in value during the relaxation cycle. This is done since for two dimensional relaxation and a small matrix, relaxation with only specified boundary potentials would give inaccurate results. This relaxation method will be valid near the flat specimen surface.

The details of the programs are considerably more complicated than suggested by the flow diagrams. This is due to the relaxation method mentioned above and also the inclusion of the effect of the gap (at a different scale) at each stage in the relaxation. This complicates the calling of the various routines since it is necessary to consider both the SiO_2 - air and gap and main matrix interfaces.

The approach adopted in these programs is an efficient method of obtaining the desired results without incurring large store and CPU time penalties.

Three examples of computer drawn equipotentials from matrices produced by EXPVS1G and EXPVS2G are shown in Figures 5.4.8(a)-(c). These show equipotentials near the surface for 1 kV on the first lens electrode for the three types of gaps shown in Figure 5.4.2, with 10 volts bias across the gap. These results appear reasonable. (Irregularities on the curves are a function of the equipotential plotting program).

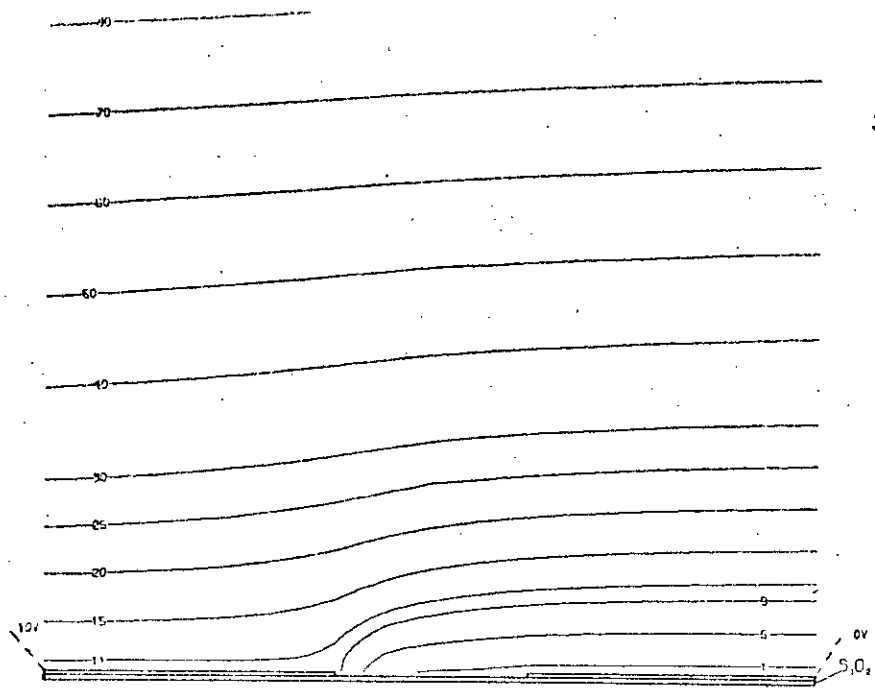


FIGURE 5.4.8 (a)
EQUIPOTENTIALS
NEAR SPECIMEN
SURFACE

SCALE: 20 μ m

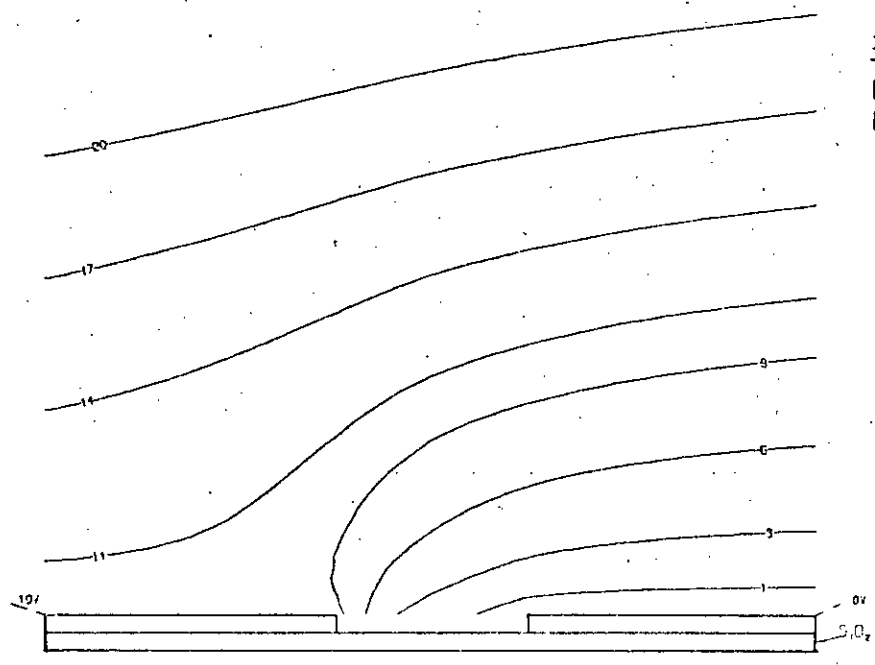


FIGURE 5.4.8 (b)
EQUIPOTENTIALS
NEAR SPECIMEN
SURFACE

SCALE: 5 μ m

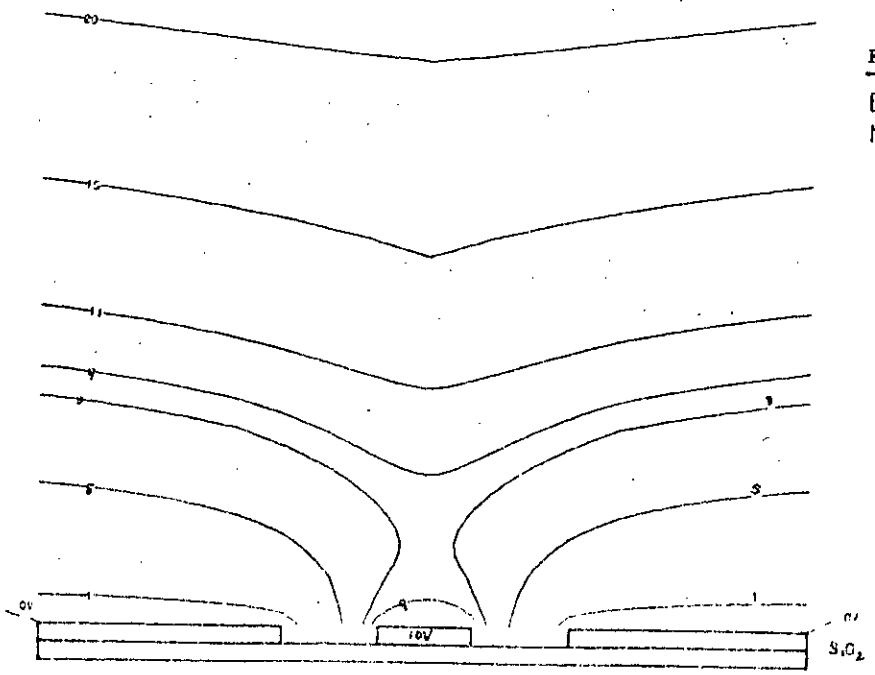


FIGURE 5.4.8 (c)
EQUIPOTENTIALS
NEAR SPECIMEN
SURFACE

SCALE: 6 μ m

5.5 CALCULATION OF ELECTRON TRAJECTORIES

5.5.1 Theory - Cartesian Co-ordinates

Consider the right handed system of Cartesian co-ordinates shown in Figure 5.5.1 with an electron at point P moving with a velocity \underline{V} (vector) in an electric field \underline{E} (at P).

Applying Newtons second law of motion gives

$$\frac{d(\underline{V})}{dt} = \frac{e}{m} \underline{E} \quad 5.5.1$$

where e is the electronic charge and m is the electron mass.

For this system of axes

$$\frac{d(V_x)}{dt} \underline{i} + \frac{d(V_y)}{dt} \underline{j} + \frac{d(V_z)}{dt} \underline{k} = \frac{e}{m} (E_x \underline{i} + E_y \underline{j} + E_z \underline{k})$$

where $V_x, V_y, V_z, E_x, E_y, E_z$ are components of \underline{V} and \underline{E} in the x, y and z directions. Since $V_x = \frac{dx}{dt}$ etc

$$\frac{d^2x}{dt^2} = \frac{e}{m} E_x$$

$$\frac{d^2y}{dt^2} = \frac{e}{m} E_y$$

... 5.5.2

$$\frac{d^2z}{dt^2} = \frac{e}{m} E_z$$

Since the electric field \underline{E} is non uniform E_x, E_y and E_z are functions of x, y and z .

In the cases of interest here it is not possible to find analytical expressions for \underline{E} in terms of x, y and z so that equations 5.5.2 must be solved by numerical methods. In all the situations of interest here the electric field, in regions in which a Cartesian co-ordinate system was used, had components in only two perpendicular directions.

(Near the specimen surface and in the analyser!)

Consider the equation,

$$\frac{d^2x}{dt^2} = \frac{e}{m} E_x$$

Integrating,

$$\frac{dx}{dt} = \frac{e}{m} \int E_x dt + C_1$$

approximating,

$$\frac{dx}{dt} = \frac{e}{m} E_x \Delta t + C_1$$

where Δt is a small time interval and C_1 is an integration constant.

Also,

$$\Delta x = \frac{1}{2} \frac{e}{m} E_x \Delta t^2 + C_1 \Delta t + C_2 \quad \dots 5.5.3$$

which will give the distance (Δx) moved in time Δt if E_x is considered constant over Δx . This will only be valid if $\frac{d(E_x)}{dx}$ is small or Δx is small. Equation 5.5.3 is of course one of the well known equations of motion since constants C_1 and C_2 are easily determined.

ie
$$\Delta x = V_x \Delta t + \frac{1}{2} \left(\frac{e}{m} E_x \right) \Delta t^2 \quad \dots 5.5.4$$

where V_x is velocity at time t and E_x is field at point x .

Thus it is necessary either to choose a very small fixed value of Δt and do a large number of calculations or to vary the value of Δt to suit each region of interest. The method chosen was to use an initial value of Δt and vary this only if the distance moved in the interval (Δx) was outside preset upper and lower limits. The same value of Δt was used for the other co-ordinate (ie y or z).

This is an efficient method of calculating the path since it provides a measure of optimisation over different regions of the path. The speed of the electron can vary by a ratio of greater than

30:1 over a typical path so that a fixed time interval would have to be that to give the required accuracy at the highest speed. Since the distance moved is dependent on the square of the time interval this would be very wasteful for much of the path. The present method reduces the total number of calculations considerably - greatly reducing computing time. Fuller details of the method used can be found from subroutine **TRAJ** described later.

5.5.2 Theory - Cylindrical Co-ordinates

Figure 5.5.2 shows the co-ordinate system used for evaluating electron paths in the lens region. Applying equation 5.5.1 to this system of axes;

$$\begin{aligned} (\ddot{r} - r\dot{\phi}^2) \underline{u}_r + \frac{1}{r} \frac{d}{dt} (r^2\dot{\phi}) \underline{u}_\phi + \ddot{z} \underline{k} \\ = \frac{e}{m} (E_r \underline{u}_r + E_\phi \underline{u}_\phi + E_z \underline{k}) \end{aligned} \quad \dots 5.5.5$$

where \underline{u}_r , \underline{u}_ϕ and \underline{k} are unit vectors in the appropriate directions and $\dot{}$ and $\ddot{}$ mean first and second derivatives with respect to time (t).

In the lens region the electric field is axially symmetric ie there is no E_ϕ component.

Thus from Equation 5.5.5 we have;

$$\frac{1}{r} \frac{d}{dt} (r^2\dot{\phi}) = \frac{e}{m} E_\phi = 0$$

$$\therefore r^2\dot{\phi} = K, \text{ where } K \text{ is a constant. (finite } r)$$

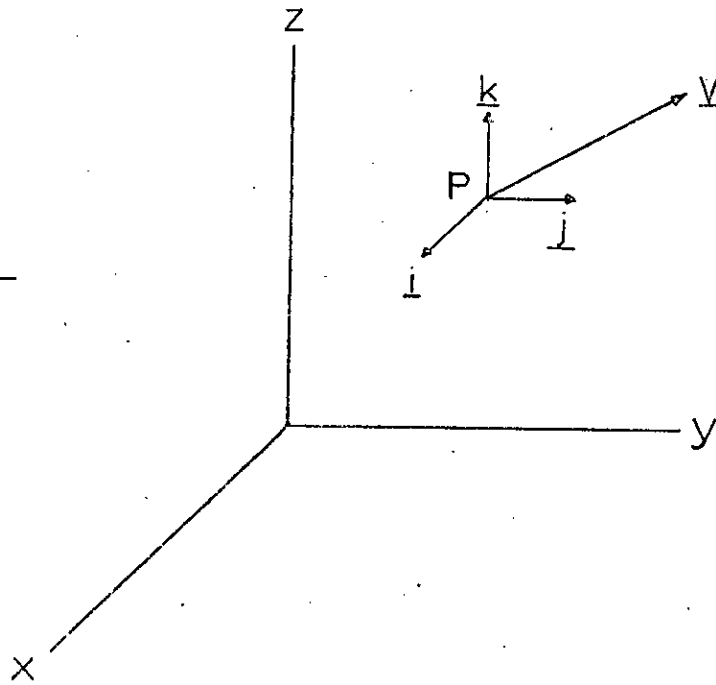
$$\therefore \dot{\phi} = K/r^2 \quad \dots 5.5.6$$

$$\therefore \ddot{r} = \frac{e}{m} E_r + \frac{K^2}{r^3} \quad \dots 5.5.7$$

$$\text{and} \quad \ddot{z} = \frac{e}{m} E_z \quad \dots 5.5.8$$

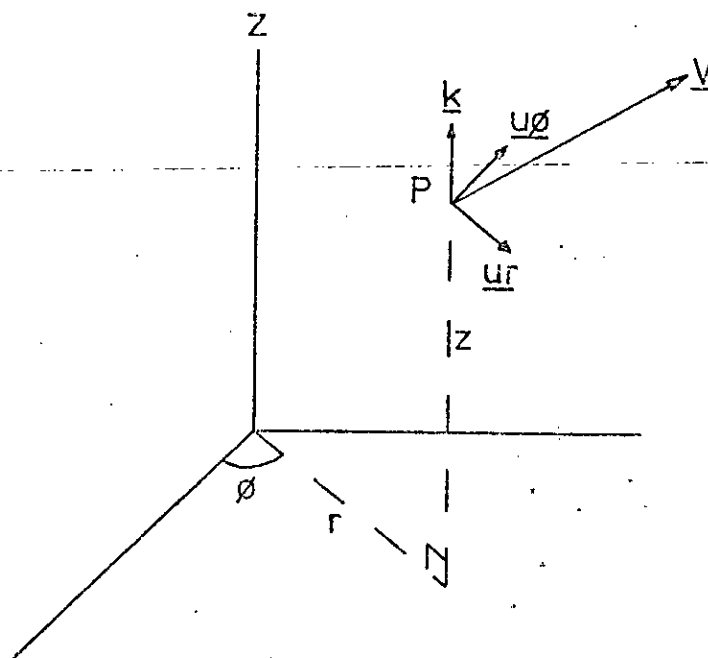
Again these differential equations can only be solved by numerical methods for the cases of interest here. Approximating the solution of Equation 5.5.7, as before, gives

Fig. 5.5.1



Right handed cartesian coordinates.

Fig. 5.5.2



Cylindrical coordinates.

$$\Delta r = \dot{r} \Delta t + \frac{1}{2} \left(\frac{e}{m} E_r + \frac{K^2}{r^3} \right) \Delta t^2 \quad \dots 5.5.9$$

The approximation will only be valid if Δt is very small, if Δr works out to be a small fraction of r and E_r does not vary significantly over the interval r to $r + \Delta r$.

This last consideration can be satisfied by using the time interval optimising procedure already described. Some investigation of the other validity criteria is necessary.

Basically equation 5.5.9 can be used over an interval Δr if the acceleration term does not vary "greatly" over this interval.

$$\text{Acceleration term (AT)} = \left(\frac{e}{m} E_r + \frac{K^2}{r^3} \right)$$

$\frac{d}{dr} (\text{AT}) = -\frac{3K^2}{r^4}$, assuming E_r does not vary significantly (already accounted for).

$$\therefore \Delta(\text{AT}) = -\frac{3K^2}{r^4} \Delta r$$

Considering relative change

$$\begin{aligned} \frac{\Delta(\text{AT})}{\text{AT}} &= \frac{-3K^2/r^4}{\left(\frac{e}{m} E_r + \frac{K^2}{r^3} \right)} \Delta r \\ &= \frac{-3K^2}{r^3 \left(\frac{e}{m} E_r + \frac{K^2}{r^3} \right)} \cdot \frac{\Delta r}{r} \end{aligned}$$

For change in acceleration term over interval Δr to be no greater than say 5%

$$\Delta r \leq \left| \frac{\left(\frac{e}{m} E_r + \frac{K^2}{r^3} \right) r}{60 \left(\frac{K^2}{r^3} \right)} \right|$$

ie

$$\Delta r \leq \left| \frac{r}{60} \left(\frac{\frac{e}{m} E_r}{K^2/r^3} + 1 \right) \right| \quad \dots 5.5.10$$

This gives an upper limit for the change in r to be allowed in any step in which equation 5.5.9 is used. From equation 5.5.10 it can be seen that the allowable change in r depends on the current value of r and also the value of the electric field. If r is large the limit will be unimportant in practice. If r is very small the limit can become too small to use this method of evaluation so that it is difficult to accurately compute electron paths which are very close to the lens axis.

Since the electric field is axially symmetric the value of K is found using equation 5.5.6 and the initial radial velocity ($\dot{\phi}$) and radius (r) of the electron entering this region. This equation also allows the calculation of $\dot{\phi}$ as the electron moves through the region.

Equation 5.5.8 is used in the way already described for the Cartesian co-ordinate system. These various equations form the basis of subroutine TRAX (to be described later) which optimises time interval Δt as does TRAJ but with an overall check that the limit of equation 5.5.10 is satisfied.

5.5.3 Calculation of Electric Field

All the equations derived for use in calculating electron trajectories require values of the electric field components in appropriate directions for many points along the path. The available data are matrices of potentials representing points on a square mesh grid obtained from previous calculations.

The basic relationship is

$$\underline{E} = -\nabla V.$$

Considering Figure 5.5.3 a simple approximation to the components of the electric field at P would be

$$E_x = \frac{(VC - VB) + (VD - VA)}{2h} \quad \dots 5.5.11$$

and

$$E_y = \frac{(VB - VA) + (VC - VD)}{2h}$$

These equations will only describe the electric field with sufficient accuracy if it does not vary much over the region immediately surrounding P. This condition can always be satisfied if h is made very small in regions where the electric field varies rapidly with distance. The penalties of a small grid size have already been mentioned.

An alternative approach using a coarser mesh than required by equations 5.5.11 and employing an interpolation procedure was adopted. Consider the points A, B, C and D on the row marked 1 in Figure 5.5.4(a). Using Bessel's interpolation with second differences¹¹⁰ we have,

$$V_p' = VB + n(VC - VB) + \frac{n(n-1)}{4} ((VD-VC) - (VB - VA)) \quad \dots 5.5.12$$

If this is carried out for rows 2, 3 and 4 and then the values of V_p' at the four points obtained are used in a similar way vertically ('m' instead of 'n') a value for the potential P can be found.

This was repeated for the points R, S, T, U and V in Figure 5.5.4(b) (same mesh and same points). The electric field components at P were evaluated from these values by

$$E_x = \frac{(VR - VS) + (VP - VT) + (VV - VU)}{3XD}$$

and

$$E_y = \frac{1}{4}((VV - VR) + (VU - VS))/YD \quad \dots 5.5.13$$

The values of YD and XD (Figure 5.5.4(b)) were chosen in relation to the maximum values of X and Y step distances allowed in the path calculating routines. Only X values above P were chosen in the electric field evaluation since the electrons were moving, in general, in the positive X direction.

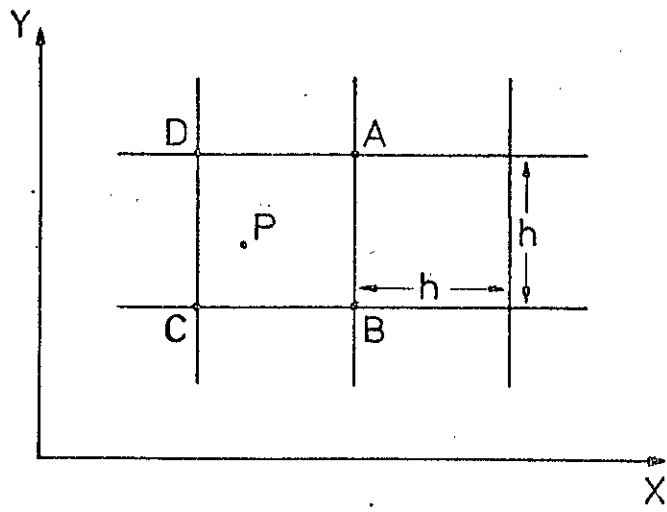


FIGURE 5.5.3

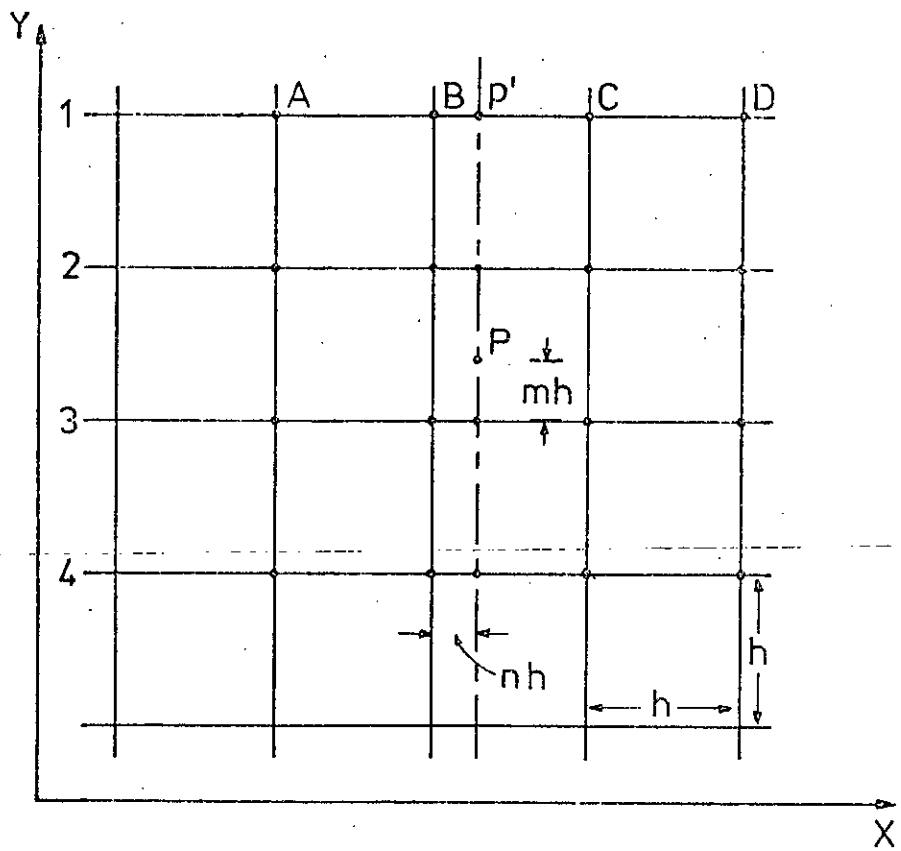


FIGURE 5.5.4(a)

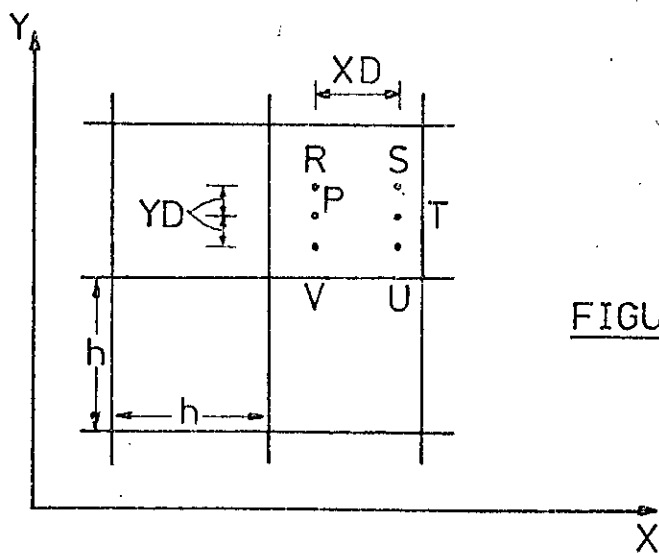


FIGURE 5.5.4(b)

This method is used in subroutine **VCAL** and a similar approach but using only linear interpolation in the X direction, for use near the specimen surface, is used, in **VC** (both to be described later).

5.5.4 Simulation Programs

In order to simulate the experimental system it is necessary to compute electron paths for secondary electrons emitted with different energies and over a range of angles from the specimen surface. The numbers of these electrons which reach and pass through the energy analyser have to be evaluated considering the cosine distribution of emitted secondaries and the sweep voltage of the specimen with respect to the analyser. This will allow a secondary emission curve to be built up of the relative number of secondaries versus the sweep voltage applied to the specimen. This can be compared with that from experiment.

Simplified flow diagrams for the main program (**SIMRNI**) and associated subroutines are given in Figures 5.5.5 to 5.5.10.

This simulation program (**SIMRNI** - Fig 5.5.5) takes the matrices of potentials obtained previously and computes the trajectory of an electron starting from a given point on the specimen surface. The computation is carried out in three main sections.

First the region close to the specimen surface where the electric field is assumed to have components in only two perpendicular directions. This is controlled by subroutine **TRNS** (Figure 5.5.6) and uses the expanded matrices considered already. The coordinates of the electron are initially referred to the point of emission and scale factors have to be introduced during the calculation since each of the expanded matrices has a different mesh size. This subroutine makes use of **TRAJ** (Figure 5.5.8(a)) which deals with the incremental evaluation of the path of the electron optimising the time intervals used, as shown. The velocity components and coordinates at the end of this region are transformed to a cylindrical coordinate system

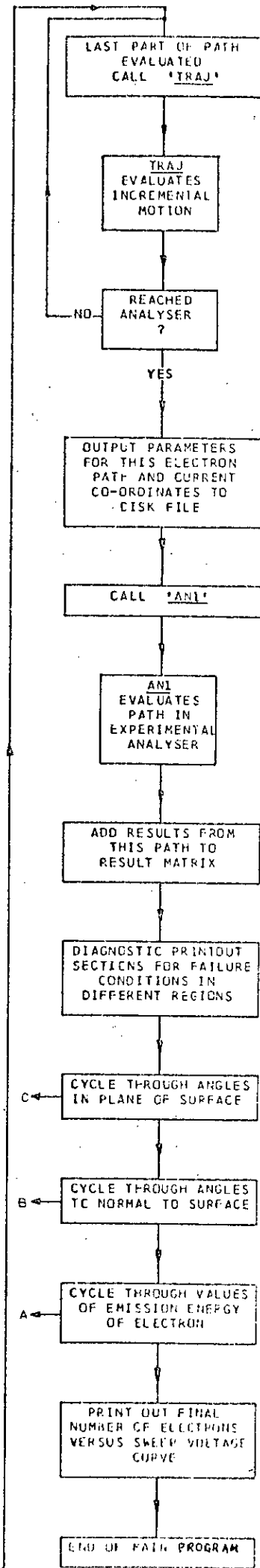
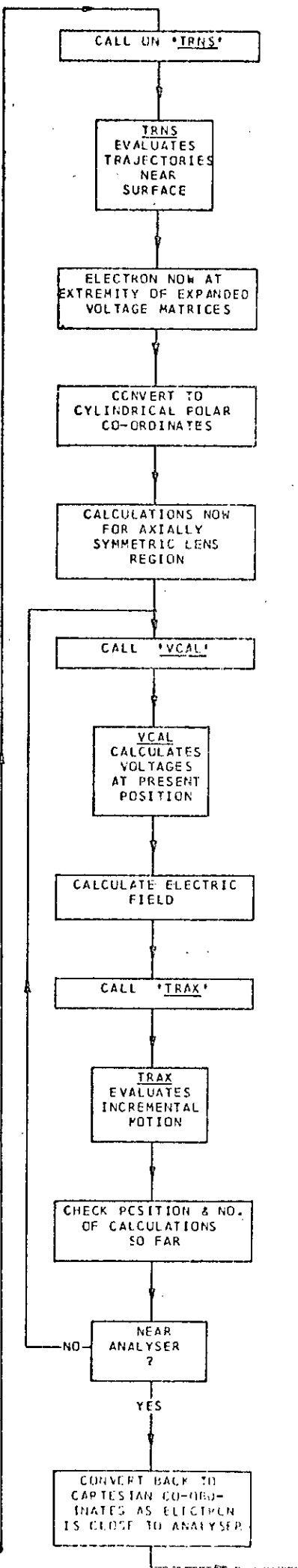
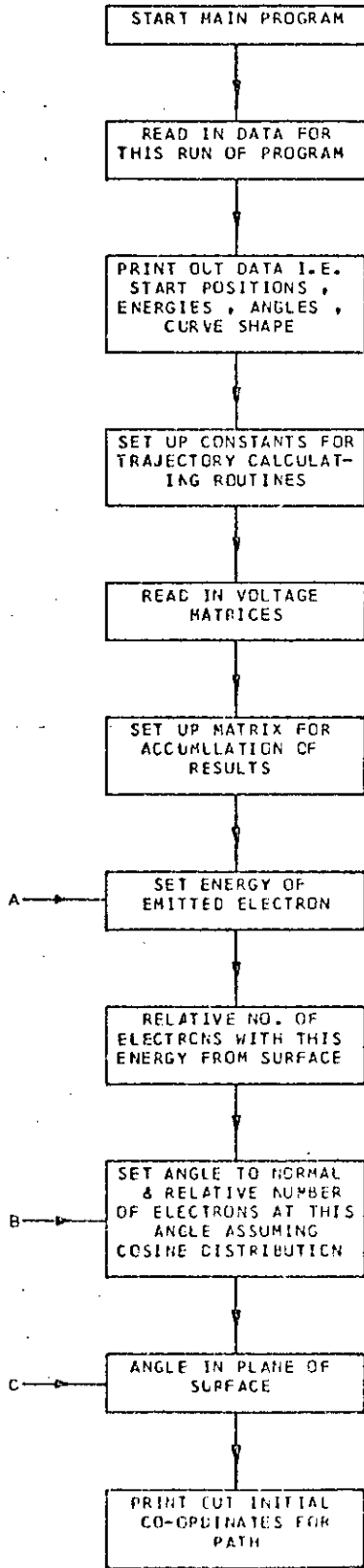
FIGURE 5.5.5

Flow Diagram

SIMRNI

MAIN PROGRAM

(213 FORTRAN STATEMENTS)



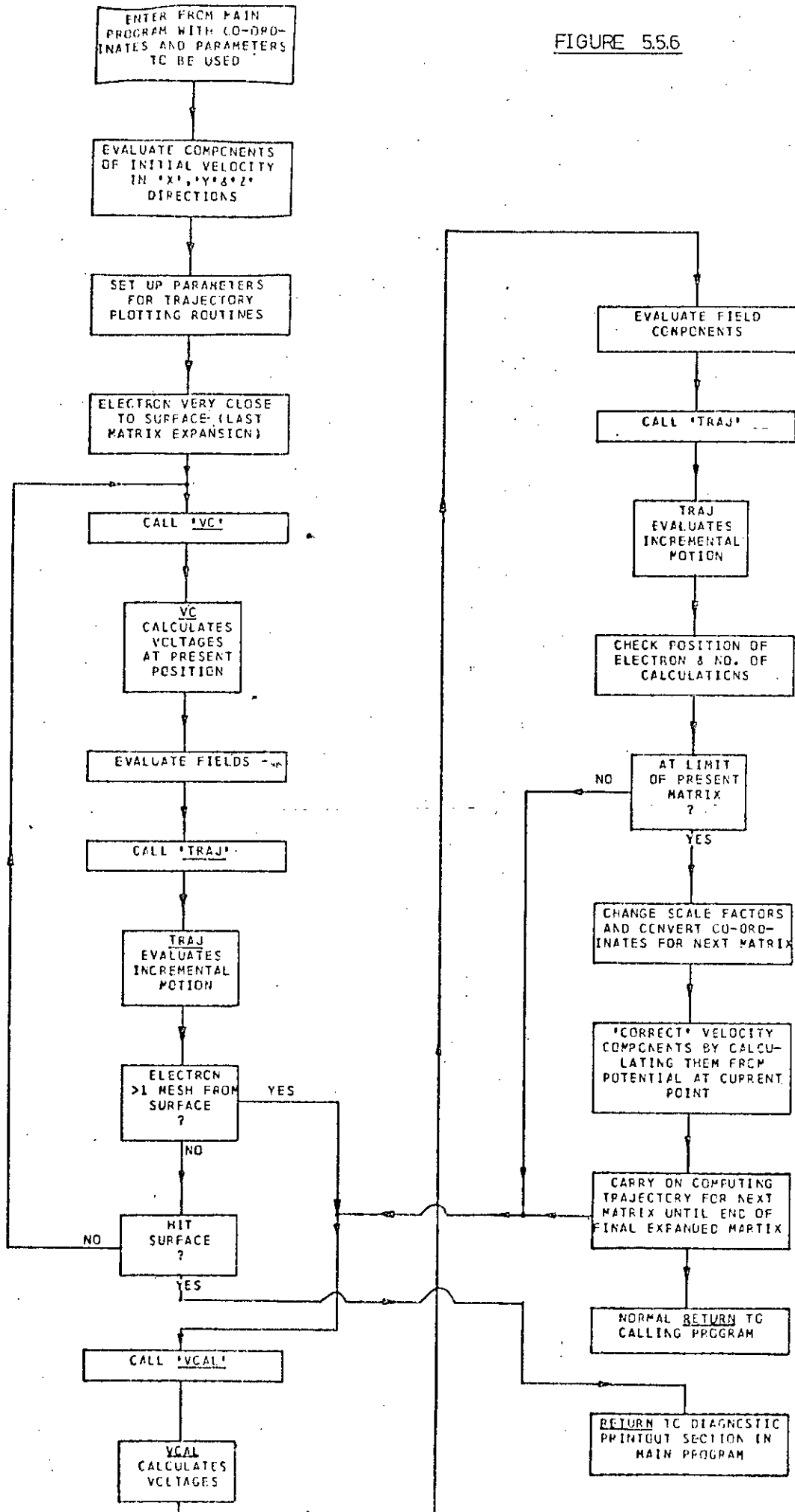
referred to the lens axis.

The next main section is the motion of the electron through the lens and is controlled by the main program (**SIMRNI**). The electric field in this region is axially symmetric so that subroutine **TRAX** (Figure 5.5.8(b)) is used in calculating the incremental elements of the path. This is similar to **TRAJ** in its optimisation but includes an extra factor as mentioned in section 5.5.2. As the electron nears the lens exit the coordinate system is converted back to Cartesian and the coordinates and angles of motion of the electron at the exit are deposited on a data file for use in other programs (for different types of analyser).

The last region is the energy analyser. At this point the main program may call the subroutine **ANI** (Figure 5.5.7). This calculates the behaviour of the electron in the experimental analyser. The flow diagram shows the involved decision making to simulate the effect of "sweeping" the electron energy at the input to the analyser. This is equivalent to "sweeping" the potential of the whole specimen with respect to the analyser. The values of the sweep voltage for which the electron passes through the analyser are recorded.

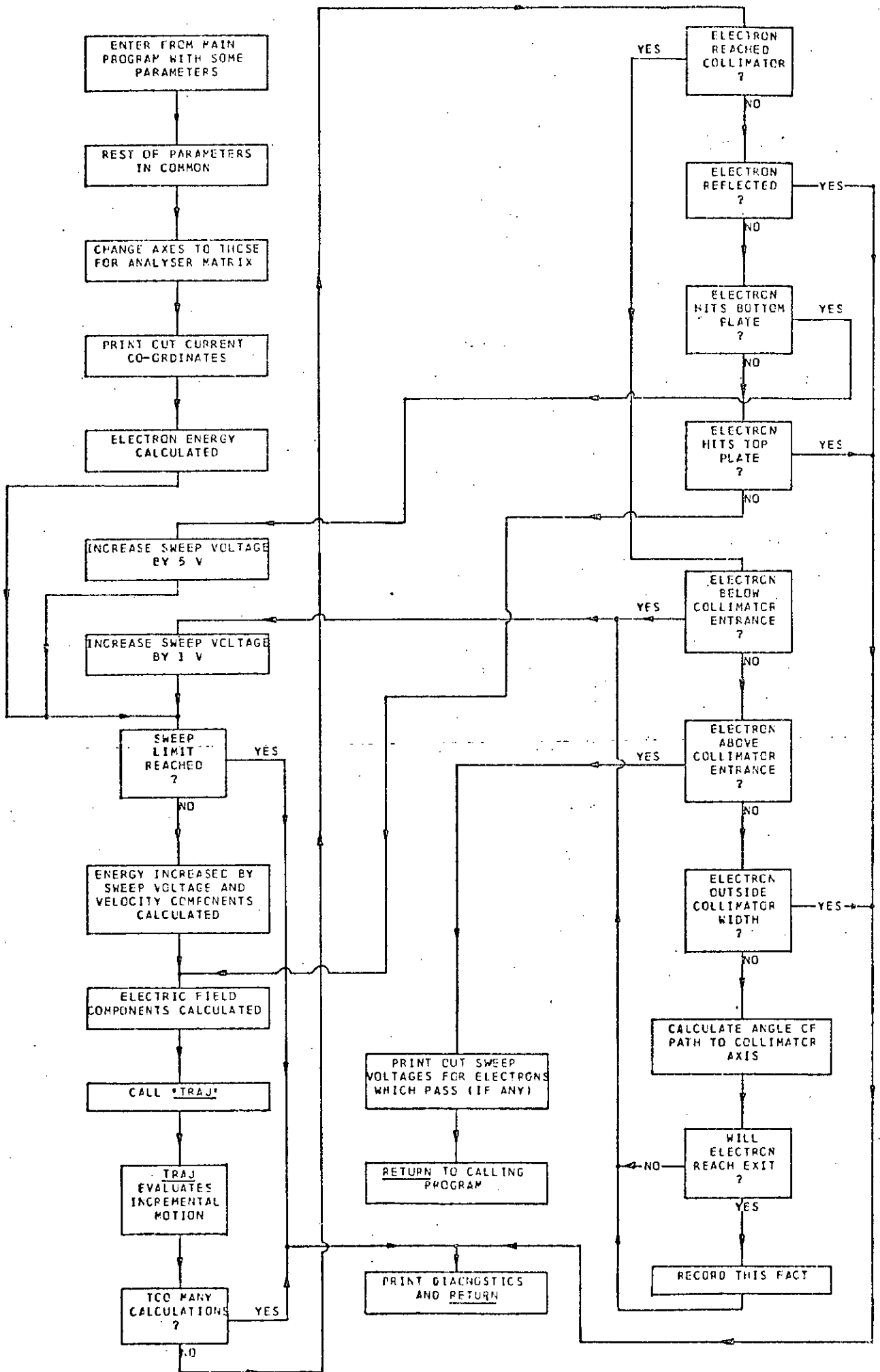
The whole process is repeated a specified number of times for electrons emitted from the same point on the surface with different energies and angles of emission to simulate the complete secondary emission from a point (around 270 electrons used). The final results are a record of those electrons which reach and pass through the analyser and a summary of the relative number of electrons versus energy, as would be obtained experimentally.

FIGURE 5.56



Computer Program Flow Diagram

(100 FORTRAN STATEMENTS)



The subroutines **VCAL** and **VC** (Figures 5.5.9(a) and (b)) are used by many of the other subroutines to evaluate the potential at a point inside one of the potential matrices.

The subroutine **AN** (Figure 5.5.10) may be called in place of **ANI**. This simulates an idealised bandpass energy analyser the characteristics of which will be described in the next chapter. It is incorporated to allow further investigation of the limitations of the system.

Another main program **SIMRN2** (not shown) allowed the lens exit coordinates to be used as input for other analysers without the wasteful rerunning of **SIMRN1**.

These simulation programs were intended to be as fully automatic in operation as possible since their aim is to predict electron trajectories which can take very different forms even when the electrons are emitted from the same point. This results in a large number of checking and control functions being required to ensure that the programs can adequately deal with this. These are not all shown in the appropriate flow diagrams for reasons of space and clarity.

The final programs can deal with most cases which occur and print out diagnostics for those electrons which go out of the operating range. The number of cases when the programs "failed" in some way was very small and normally corresponded to physical situations where the electron would never reach the analyser anyway.

Figures 5.5.11(a) and (b) show typical results for a run of **SIMRN1** for experimental and idealised analyser respectively. They are both for a gap of the bottom type in Figure 5.4.2 with the beam on the middle of the centre A1 strip and this strip at the potentials shown on the figures with respect to the other two strips.

SUBROUTINE TRAJ

(30 FORTRAN STATEMENTS)

FIGURE 5.5.8(a)

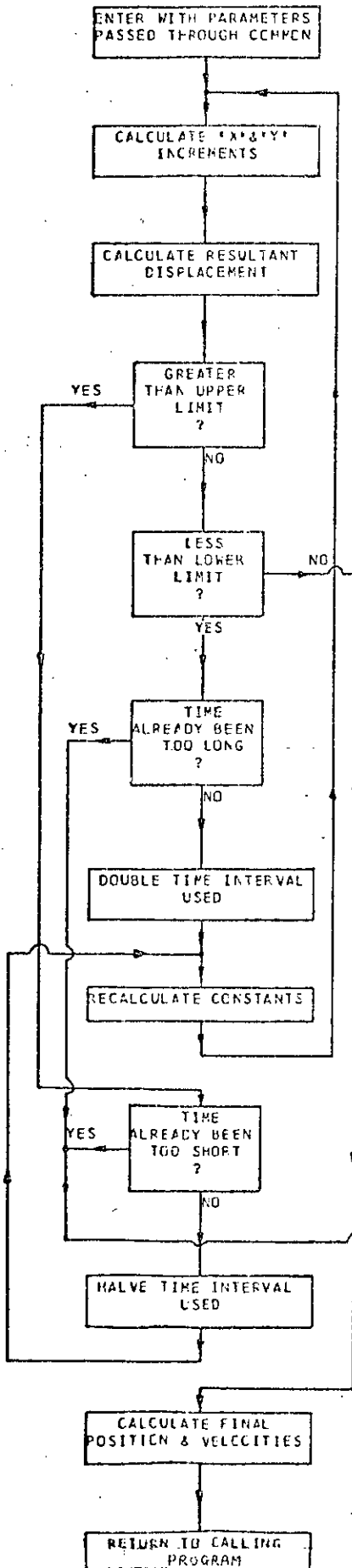


FIGURE 5.5.8(b)

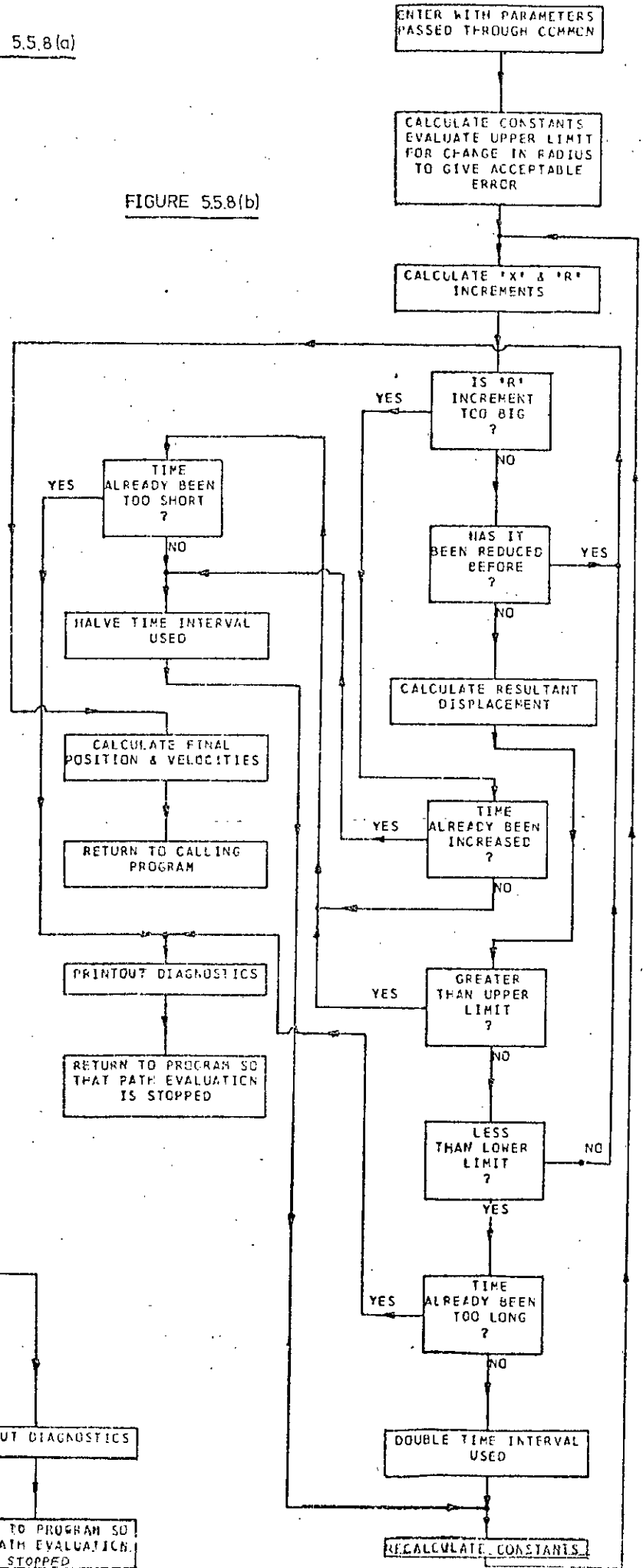
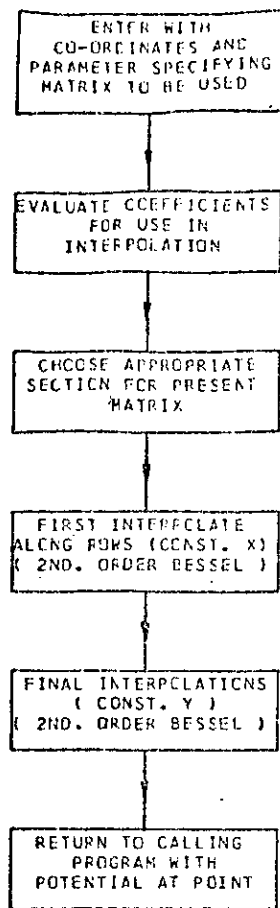


FIGURE 5.5.9(d)



SUBROUTINE VCAL

(31 FORTRAN STATEMENTS)

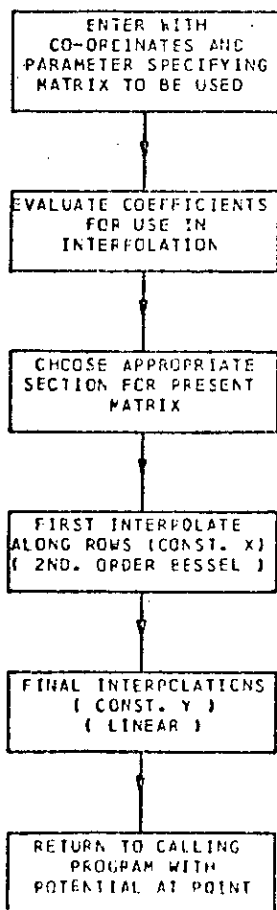


FIGURE 5.5.9(b)

(37 FORTRAN STATEMENTS)

Computer Program Flow Diagrams

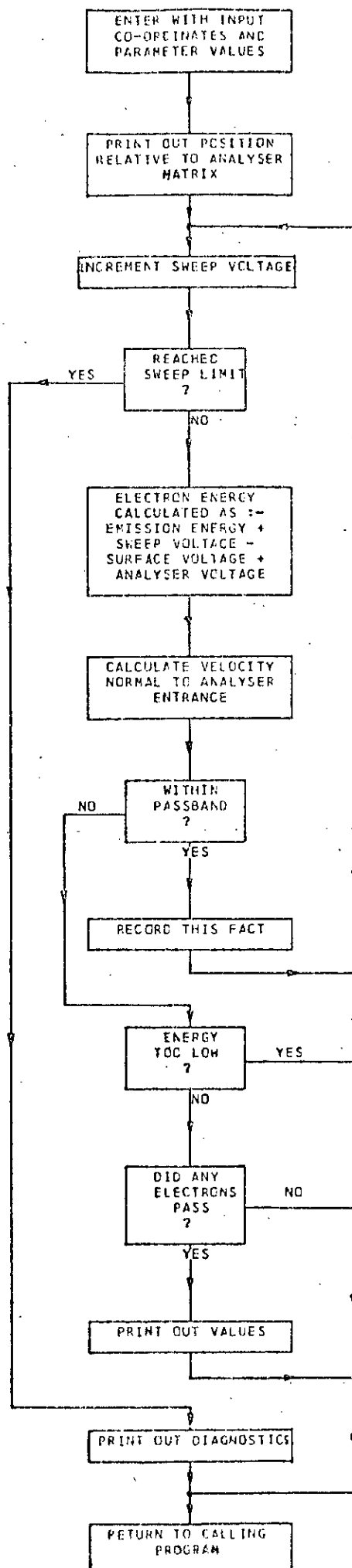


FIGURE 5.5.11(a)

Results from SIMRN1 for experimental analyser

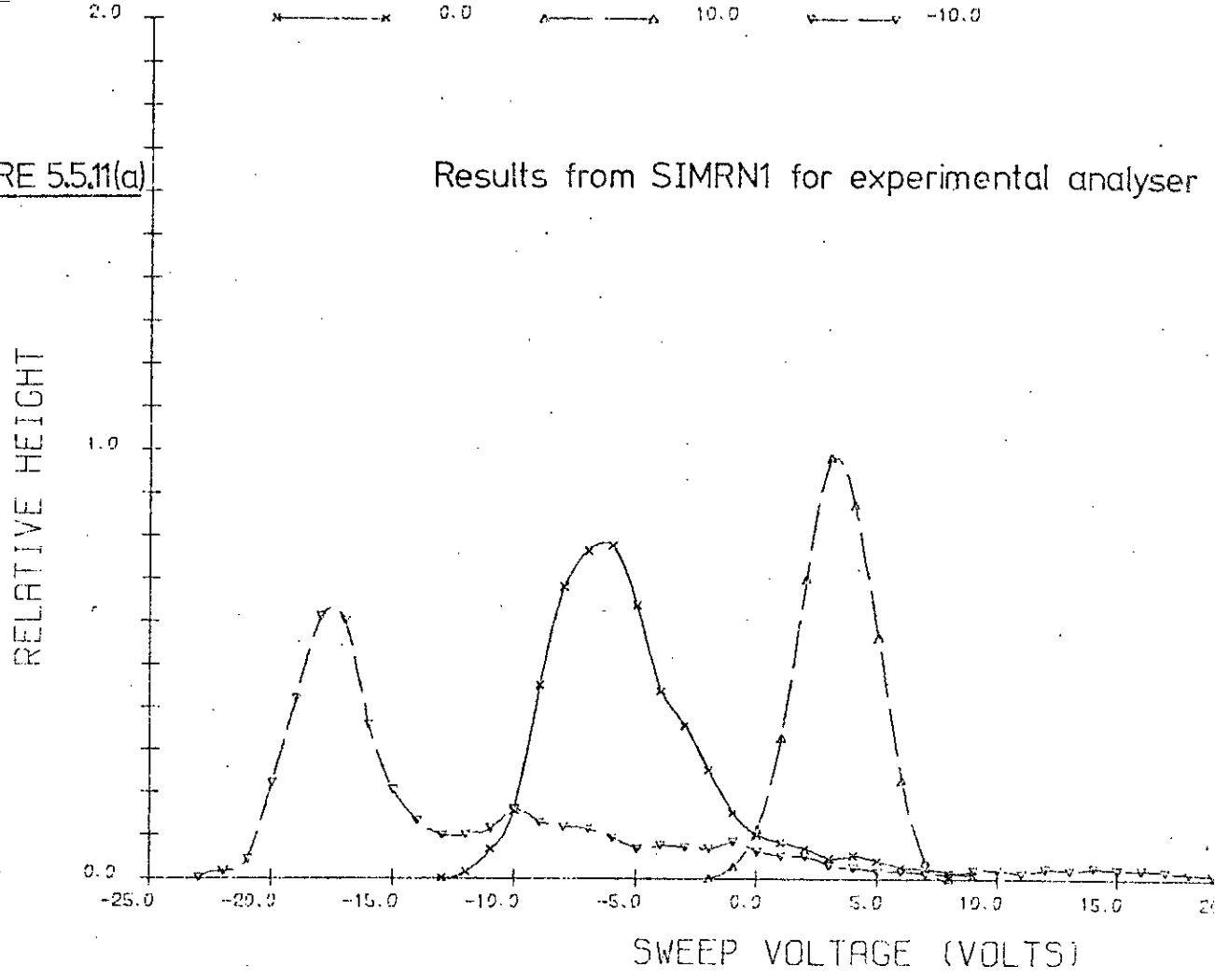
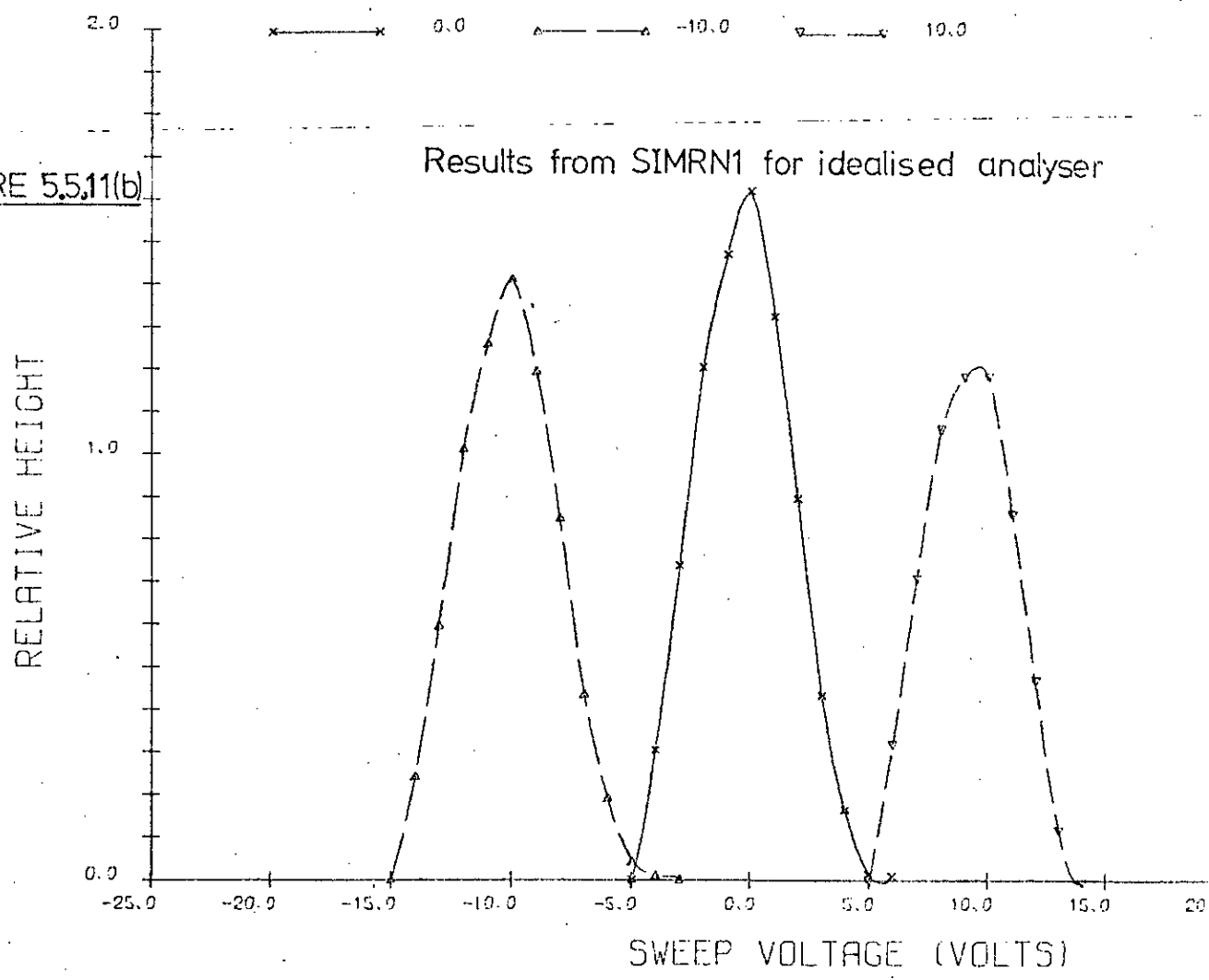


FIGURE 5.5.11(b)

Results from SIMRN1 for idealised analyser



5.6 EFFICIENCY, ACCURACY AND SCOPE OF PROGRAMS

5.6.1 Efficiency

All programs were written in Fortran IV¹¹¹ and are IBM Fortran G/H¹¹² compatible. All variables were single precision.

The programs were run on both an ICL 4-75 and an IBM 370/155 at Edinburgh Regional Computing Centre. Some of the development work was done on an interactive time sharing system on the ICL 4-75. This was particularly valuable in the development of the trajectory calculating programs.

The programs were written with a view to obtaining good operating efficiency and therefore speed. The IBM Fortran H compiler with full optimisation of object code was used as much as possible to give best execution speeds. The operation of the programs to simulate the system with a typical set of electrode voltages was as follows.

VLNSANS was run with input data the electrode voltages and output matrices of potentials were stored on a disk file. The run time was around 10 seconds and region size required 72K bytes. (Peak residual 0.01).

EXPVS1G or EXPVS2G was run using these matrices as input, expanding the lens matrix and adding expansions to disk file. The run time was around 5 seconds and region size 60 K bytes for the same peak residual value.

SIMRN1 used these potential matrices and required input data specifying point on specimen, number of paths etc to be used. Intermediate (lens exit coordinates) output was stored on a disk file and results were printed and punched. The run time was variable for this depending on the electron trajectories but was less than

150 seconds with a region size of 84 K bytes. (This was for 275 electron paths, for 3 expansion matrices with all electrons travelling right through to the experimental analyser).

The voltage matrices stored on disk required a maximum storage space for one specimen-lens-analyser configuration of 26 K bytes.

Thus the method of analysis used can be seen to be efficient, requiring only modest computing time and core space and minimising storage requirements for the matrices used.

5.6.2 Accuracy

This is very difficult to determine since the complexity of the analysis is such that manual checking is almost impossible.

The accuracy of the potential distribution calculating programs has already been considered and can be improved by specifying smaller peak residual limits. The accuracy of these programs is considered to be adequate for this analysis.

The trajectory calculating programs present quite a different problem. The accuracy of each section has to be checked by empirical methods as the program development proceeds. The results can be checked for consistency with general predictions from theory and for anomalous behaviour as control parameters vary.

The final test is comparison between experimental and predicted results since this provides an overall check on the accuracy of the model ie its ability to represent the physical situation.

This agreement was found to be quite good as will be shown more fully in the next chapter.

5.6.3 Scope

The programs which have already been described were the main ones which were used in the analysis. A number of others were developed to perform special functions in the general study. Some of these made use of the subroutines already described to evaluate

such things as lens and analyser characteristics, as will be shown in the next chapter.

The value of developing flexible yet efficient programs was noted at the beginning of this chapter. The programs which have been developed are quite flexible as originally intended. They have been separated as much as possible into control sections and subroutines. The control sections are particular to a specific physical situation but can be modified easily to cope with a variety of configurations.

The methods of potential distribution and electron trajectory calculations presented in this chapter represent a good approach to analysing the behaviour of electrons in a non-uniform electrostatic field.

CHAPTER 6

COMPUTER AIDED ANALYSIS, DESIGN AND SIMULATION

6.1 INTRODUCTION

This chapter describes work which made use of the methods of calculation and computer programs described in the previous chapter. It contains an analysis of the operation of the experimental measuring system and a further consideration of the design criteria with the aim of possibly improving the performance. Results from a computer aided simulation study of the experimental setup are presented which give an explanation of some of the points noted from the measurements given in chapter 4. The limitations of this particular type of electron lens and energy analyser approach to voltage measurement are assessed by means of simulation studies carried out for the case of an "idealised" energy analyser.

6.2 CHARACTERISTICS OF THE ELECTRON LENS AND ENERGY ANALYSER

6.2.1 Electron Lens Characteristics

The electron lens is electrostatic with three electrodes and possesses axial symmetry as described in chapter 4.

The normal approach to obtaining the characteristics of an electron lens is to assume that the electrons are paraxial and to evaluate principal plane position and focal length as in geometrical light optics. The effects of aberrations would then be considered. While of some interest this approach does not yield satisfactory results in the present application since the electron paths may be relatively far from the axis (ie not paraxial) in this case.

Thus use must be made of the computer programs already developed to obtain the relevant characteristics of this lens.

The equipotentials for the lens, analyser and specimen arrangement have been shown in Figures 5.3.6(a)-(c) for a plane specimen 1.3 mm from the first electrode. The specimen and analyser must be included in this study since their positions and potentials affect the field distribution and hence lens behaviour to a certain extent.

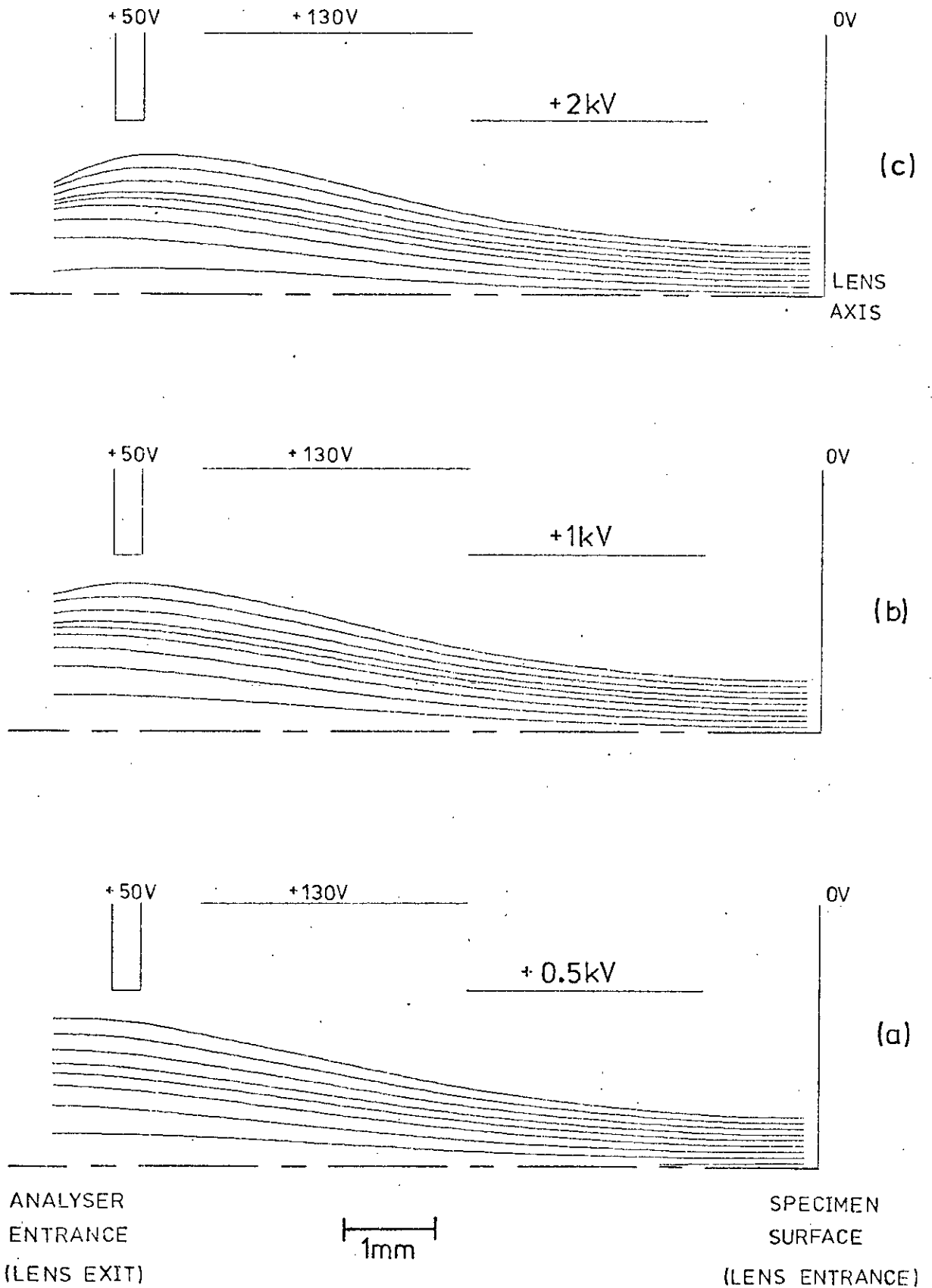
Computer produced plots of electron trajectories in the lens are given in Figure 6.2.1(a)-(c). These show the motion of electrons which leave the specimen surface at right angles with 5 eV energy for 0.5, 1 and 2 kV on the first lens electrode. Only one half of the lens is shown since it possesses symmetry about the axis.

As already observed experimentally the potentials on the other two lens electrodes did not greatly affect the lens characteristics. This was true for values within a reasonable range of the voltages used for these plots which were +130 V and +50 V with respect to the specimen surface for the second and third lens electrodes.

The plots in Figures 6.2.1(a)-(c) do not give a complete description of the lens characteristics since these are difficult to present in two dimensional form but they do indicate the factors which are important in this situation. The lens is seen to be *divergent* for electrons leaving the specimen surface and reaching the analyser entrance. The divergence can be seen to be dependent on the first electrode voltage and the position of the electron at the lens entrance (above the specimen surface). Divergence is defined *here* to be the rate of change in the exit position of the electron with respect to the input position.

FIGURE 6.2.1

ELECTRON TRAJECTORIES IN LENS



Figures 6.2.1(a)-(c) show that the divergence varies with the distance of the electron from the lens axis at the input. Approximate minimum and maximum values are 2 and 3 for 500 V, 1 and 10 for 1 kV and 0.5 and 8 for 2 kV. In general the maximum values are obtained for close to the lens axis at the input. The electrons at the exit are seen to be almost parallel to the axis for the 500 V case becoming less parallel as the voltage is raised, especially at a distance from the axis. Even when the divergence as defined above is low the electrons at the exit are always more than twice the distance from the axis that they were at the input.

These then are the general characteristics of this electron lens configuration.

6.2.2 Energy Analyser Characteristics

The experimental energy analyser was of cylindrical parallel plate electrostatic type with a collimator as described in chapter 4. The sector angle of the particular version used with the electron lens was approximately 55 degrees as shown diagrammatically in the previous chapter.

Equipotentials for this analyser have already been given in Figures 5.3.6(a)-(c).

The pass energy characteristics for this analyser can be found using the computer programs of chapter 5 but it is difficult to present these clearly in two dimensions. The parameters involved are the energy of the electron, its position at the analyser entrance and its angle of entry. Since the collimator entrance is wide in relation to its depth and the analyser gives no energy selection in this plane (ie normal to the paper in Figure 5.3.1) the position and angle in this plane are not considered here. Thus the electrons are assumed to be in the plane of the paper in the equipotential plots

of Figures 5.3.6(a)-(c) and the variables in this case are the position across the entrance and angle to the normal at this point.

Three dimensional computer plots of the energy which an electron at the entry position and angle shown must have to pass through the analyser are given in Figures 6.2.2(a)-(d). The upper limit of the pass energy is shown by a solid line and the lower by a dotted line. These were evaluated for points corresponding to those values marked on the axis and the additional vertical lines are drawn to emphasise the discrete planes of constant angle which are represented. The differing widths of the vertical planes result from the fact that electrons with certain combinations of entry angle and position will not be able to pass through the analyser whatever their energy.

These figures are each for 70 V on the lower plate (left hand end of longest axis in figures) 50 V on the collimator and 30 V on the upper plate (right hand end). In Figure 6.2.2(a) the results given are for a theoretical linear field at the analyser entrance with no fringing field and no lens. Figures 6.2.2(b)-(d) are for the experimental setup with 0.5, 1 and 2 kV on the first lens electrode respectively. In each figure the vertical (energy) scale is the potential of the point of original emission of the electron with respect to 0 V for a 1 eV electron.

These figures show that the width of the energy passband can vary with the potential on the lens first electrode and the position and angle of the electron at the entrance but is typically about 4 eV. The energy of the mean of the passband varies considerably with both position and entry angle to the analyser. These results also show that the shape of the characteristic varies with the potential on the lens first electrode. The pass energy versus entry position and angle characteristic can be seen to have a complex shape with in general

FIGURE 6.2.2(a)

No Lens, Uniform Field.

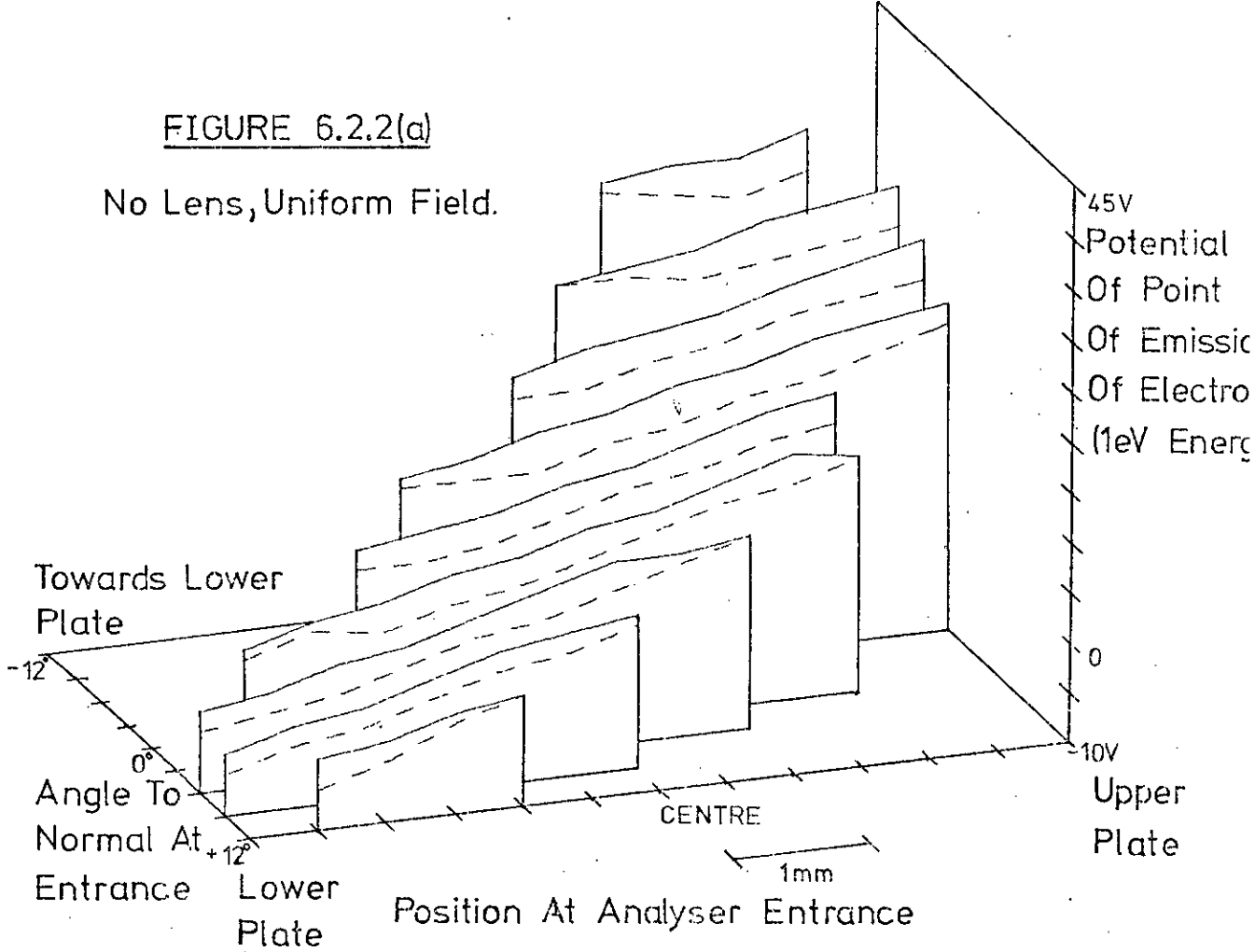


FIGURE 6.2.2(b)

Lens Voltage 0.5kV

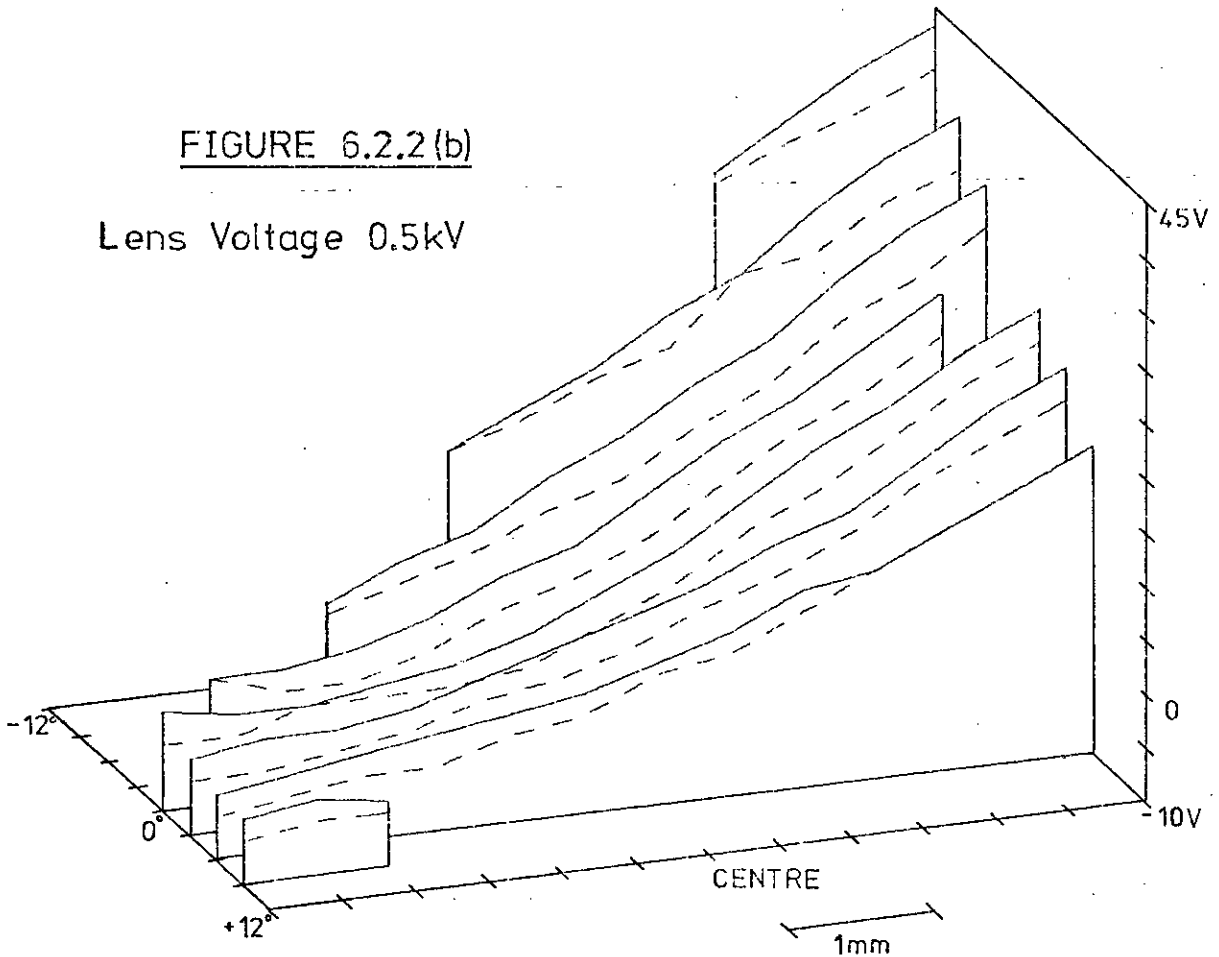


FIGURE 6.2.2(c)

Lens Voltage 1kV

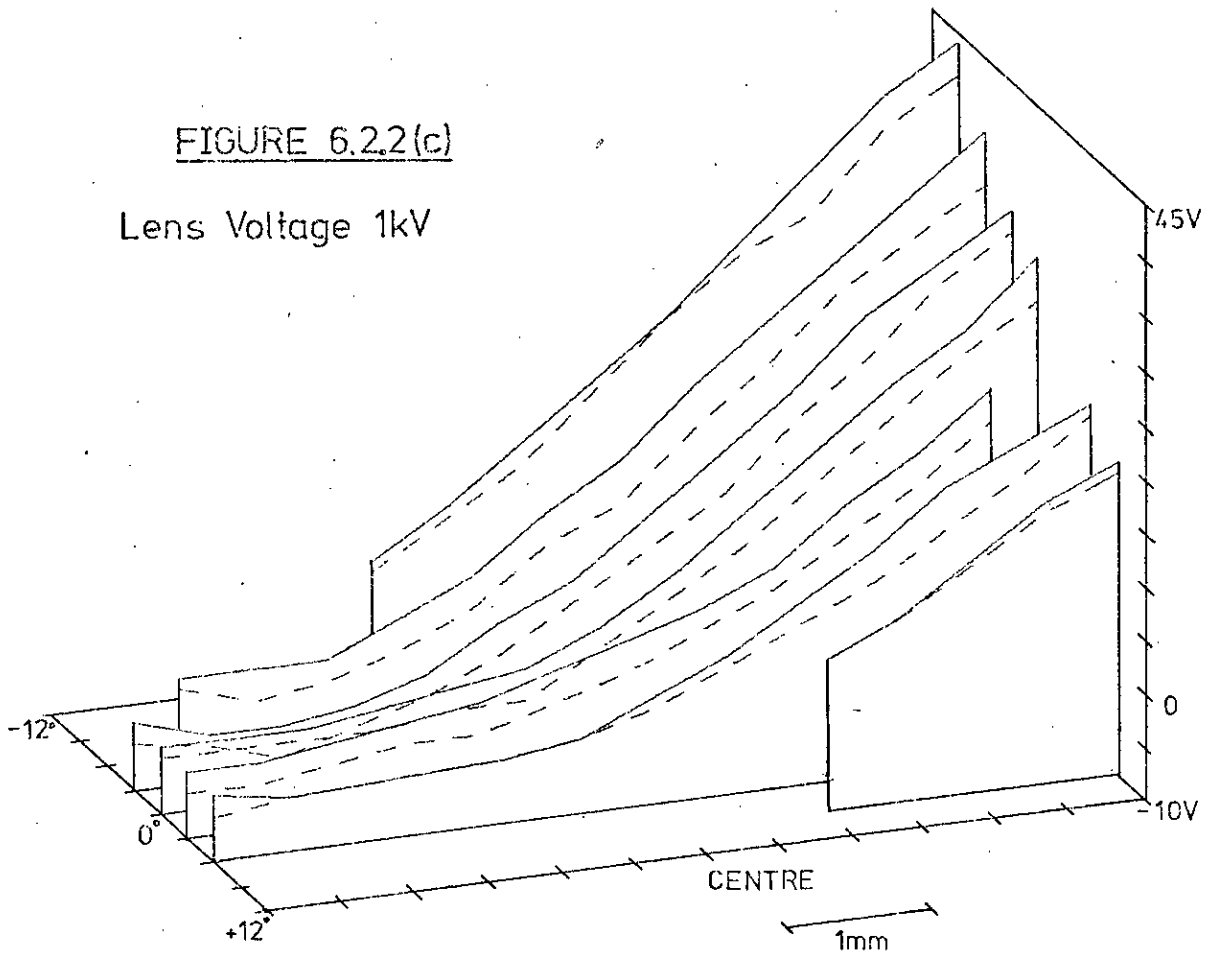
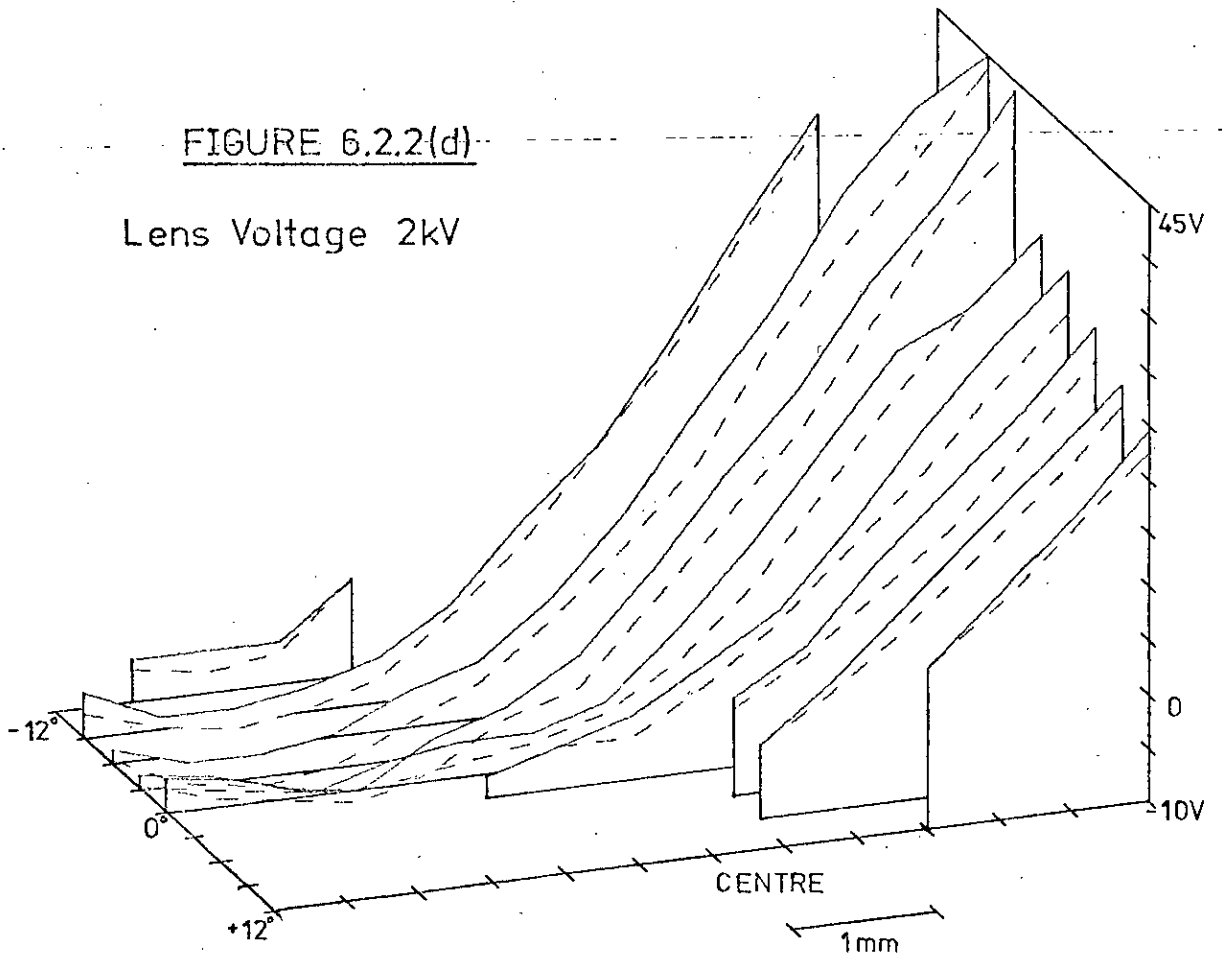


FIGURE 6.2.2(d)

Lens Voltage 2kV



ANALYSER CHARACTERISTICS

a slope across the entrance and a slope with entry angle. The slope from left to right across the entrance is least for the linear field case and highest for 2 kV on the lens electrode. The slope relative to entry angle (front to back) varies less between the figures but is still considerable. The characteristics are particularly steep for Figure 6.2.2(d) since the high voltage on the first lens electrode greatly affects the field in the analyser as shown in Figure 5.3.6(c).

These results indicate the characteristics of the energy analyser which are important in the present mode of usage.

6.3 ANALYSIS OF OPERATION OF THE SYSTEM

6.3.1 Introduction

The computer programs already described and the lens and analyser characteristics given in the previous section allow a more detailed analysis of the operation of the experimental measuring system than that given in chapter 4.

For the purposes of this analysis the system can be considered in three parts corresponding to the three main regions through which an emitted secondary electron must pass before it reaches the collector. These are:

1. The region immediately above the specimen surface
2. The electron lens
3. The energy analyser.

These may now be examined in turn.

6.3.2 The Region Above the Specimen Surface

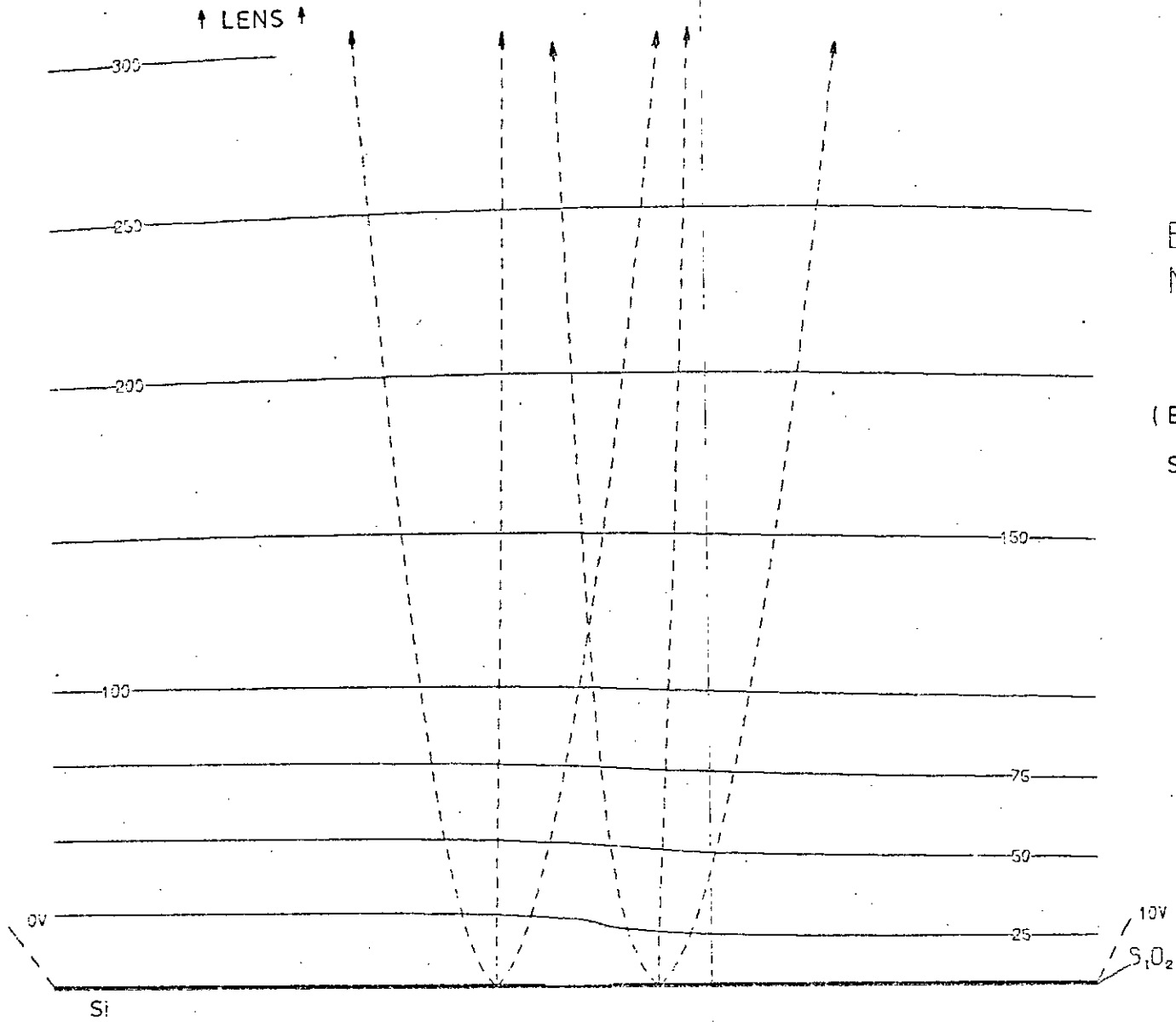
This is the region in which the emitted electrons are travelling very slowly and in which their direction of motion is very considerably affected by the electric field distribution. Its extent is difficult

to define but can be considered to be within a few hundred μm from the surface for IC type specimens.

The electric fields in this area are determined by the conductor configuration on the specimen surface and voltages applied between these conductors. They are also affected by potentials on electrodes etc at some distance from the surface (mm). Since the secondary electrons are emitted with such low energies (~ 5 eV) the field distribution very close to the specimen surface determines whether they will be reflected back towards the surface or travel along their original path with little deviation (extreme cases!) as noted in section 4.2.4. Thus if the field distribution is "unfavourable" the electrons will never travel a significant distance from the surface in a direction in which they can easily be collected.

The favourable effect of the potential on the first lens electrode on the field distribution above the surface is demonstrated in Figure 6.3.1 which should be compared with Figure 4.2.8. Figure 6.3.1 show computed electron trajectories, to the same scale, for the same energy and angles as Figure 4.2.8 but with the electron lens between the specimen and analyser with 1 kV on the first lens electrode (positioned 1.3 mm above the specimen surface). The "improvement" in the electron trajectories which the presence of the lens brings is seen to be very marked. The higher the field (normal to the specimen surface) due to this electrode the more closely the electrons tend to leave the *region above the surface* in an almost *normal* beam with very few electrons being reflected back to the surface even for very unfavourable surface potential distributions.

Although the spread of the electrons in the region just above the surface is reduced by applying a high positive potential to the first lens electrode there are still differences in the spatial and



EQUIPOTENTIALS
NEAR SPECIMEN
SURFACE

(ELECTRON TRAJECTORIES
SHOWN DOTTED, ALL 3eV)

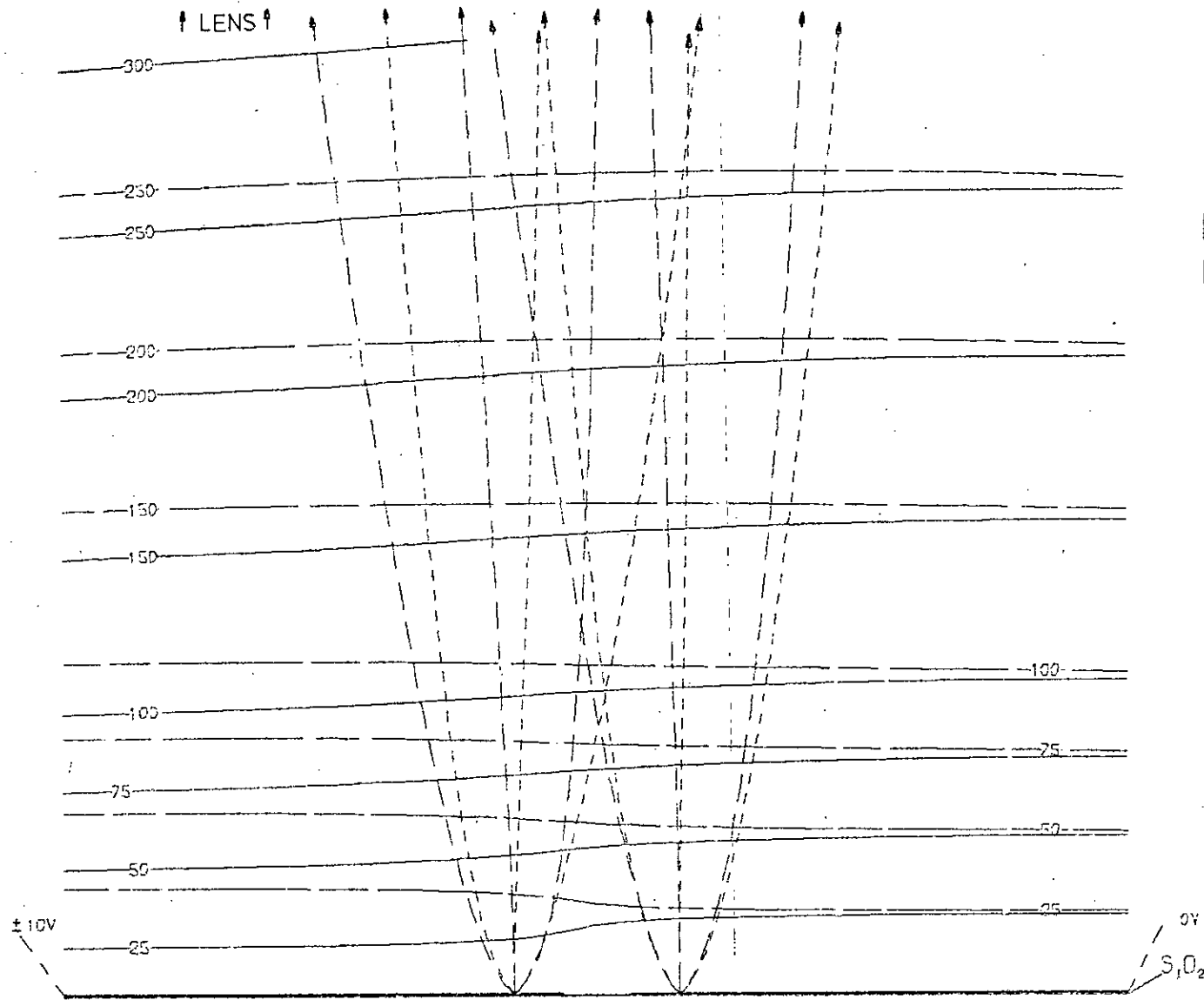
SCALE: - |-----|
80μm

(1ST LENS ELECTRODE VOLTAGE 1kV)

FIGURE 6.3.1

angular distributions of these electrons for varying potential distributions on the specimen surface. The computed equipotential and trajectory plots shown in Figure 6.3.2 demonstrate this fact. These are obtained for conditions identical to those relating to Figure 6.3.1 except that the right hand strip is now at 0 V and the left hand strip is at + or - 10 V. The solid equipotentials are for +10 V on the left strip and the chain dotted ones are for -10 V on the strip. The short dashes represent the trajectories for the left strip at -10 V, and the long dashes represent those for +10 V on this strip. The differences in the distribution (at the top of the diagram) for electrons leaving the surface at the same point and angle are seen to be quite marked. Those trajectories for +10 V on the left hand strip are seen to be to the left of the corresponding ones for -10 V applied. The mean deviation of the angle of motion of the electrons from the normal to the surface would seem to be related to the large scale "tilt" of the equipotentials above the surface. This is illustrated by a comparison of Figures 6.3.1 and 6.3.2 which shows the shorter dashed trajectories to be very closely similar for both figures, even though the surface voltages are different, since the equipotentials are almost identical in shape. In general the differences in the distribution of the electrons are a function of the field configuration above the surface and the electron emission energy.

Thus in the region above the specimen surface the factors which are under direct control are the voltage on the first lens electrode and its position relative to the specimen. Varying either or both of these factors to give a high accelerating field above the surface ensures that a very high percentage of all the emitted secondaries leave the surface and are approximately normal to it after a short distance.



EQUIPOTENTIALS
NEAR SPECIMEN
SURFACE

SOLID +10V ON LEFT STRIP
CHAIN -10V " " "

SCALE: ————
80μm

TRAJECTORIES ALL 3eV :-
————— +10V ON LEFT STRIP
- - - - - -10V " " "

(LENS 1kV)

FIGURE 6.3.2

These considerations given above refer directly to the case of a flat specimen with a smooth surface. In fact these conditions will be largely satisfied (in relative scale) by many IC specimens.

6.3.3 Electron Lens

Those electrons which successfully leave the specimen surface and pass through the region immediately above it now have to pass through the electron lens.

The characteristic of this lens has been shown to be a function of the voltages on the lens electrodes (mainly the first electrode voltage) and the entry position and angle of the electron (Figure 6.2.1). The fact that, as has been already shown, the lens is in general divergent means that differences in the spatial and angular distributions of the electrons at the entrance will be increased at the lens exit. Thus the spread in the electron distribution at the top of Figure 6.3.1 (for a single point of emission) will be increased by the lens so that at the exit the "beam" of electrons will be quite broad.

As has been already noted the lens first electrode potential can be varied so that the electrons converge as they leave the lens, for certain entry positions and angles. In general as the potential on this electrode is increased positively the electrons are more convergent at the lens exit. This means that the spread of the electrons at the exit can sometimes be reduced but this is normally achieved at the expense of increasing differences in the angular distribution of the electrons. As will be shown later, the electron motion would ideally be parallel to the lens axis at the exit.

Another consequence of the lens being divergent is that only electrons emitted from a region on the specimen surface near the axis of the lens (within about 0.7 mm radius) will pass through. This is of course not a major problem since the specimen can easily

be moved mechanically, as would normally be necessary during observation in the SEM in any case.

The main variable factor determining the behaviour of the electrons in the lens region is again seen to be the potential on the first lens electrode.

6.3.4 Energy Analyser

Those electrons which pass through the lens then enter the energy analyser where it is desired to determine their energy. This is done by sweeping the potential of the whole of the specimen with respect to the fixed analyser voltages and so varying the velocities with which the electrons reach the analyser. Those electrons which have the correct velocity to reach and pass through the collimator of the analyser are collected and give an output signal. This signal displayed against the sweep voltage gives the desired energy distribution curve of the emitted electrons.

This analyser has a *bandpass* characteristic which has already been shown to be a function of the entry position and angle of the electron (Figures 6.2.2(a)-(d)). This means that electrons emitted from the specimen with the same energy but which arrive at the analyser with different positions or angles will have different chances of passing through and being collected. Thus differences in the spatial and angular distribution of electrons at the analyser entrance may result in indications of differences in energy which do not exist. That is errors in "measured voltage" may occur due to the differing analyser entry positions for electrons emitted from the same point on the specimen under different specimen bias conditions.

Section 6.2.2 has already demonstrated that the sensitivity of the analyser characteristic to the position and angle of the electrons is largely a function of the potential on the first lens

electrode since this has a major effect on the field distribution at the analyser entrance. The width of the analyser energy passband also affects the energy selection process for those electrons which reach the entrance.

From this consideration of the operation of each part of the setup it can be seen that the requirements for each region in many respects conflict necessitating a compromise. The factor which has a great effect on the behaviour of the electrons in all the regions is the potential on the first lens electrode. Considerations for the region above the specimen surface would demand a high value. The lens characteristics indicate an intermediate value to produce the most favourable spatial and angular distributions of the electrons at the exit. The analyser analysis has just shown the need for as low a value as possible to reduce the sensitivity of the characteristic to the entry position and angle of the electrons. Thus a compromise intermediate value would be expected to give the best results. This is completely in agreement with the conclusions reached from experimental work.

This analysis has indicated the main factors involved in the operation of the measuring system. The major error mechanism has been shown to be the effects of the different positions and angles of electrons in the analyser for conditions of "bias" and "no bias" on the specimen. In view of this it was decided to further investigate the design of, and possibly redesign, the electron lens and energy analyser components with a view to obtaining further improvements in the performance of the measuring system.

6.4 DESIGN STUDIES FOR LENS AND ANALYSER

6.4.1 Electron Lens Design

The desirable features of a lens for the present application have already been noted in section 4.3.2. The type of lens required is similar to the *immersion objective*¹¹³ or *cathode lens*¹¹⁴. The references given indicate that for these types of lenses the requirements of *low divergence* and *high accelerating field* are incompatible. The requirements in this case are even more exacting than for the normal type of immersion objective or cathode lens since it is desired to retard the electrons after they have been accelerated away from the surface. This is necessary both to give *low disturbance of analyser fields* and also to facilitate energy analysis by a simple type of analyser. The lens design is of course dependent to a certain extent on the type of analyser to be used but the general assumption can be made that the energy analysis process will be simpler to carry out at electron energies lower than a few hundred eV (For the SEM physical layout!).

The approximate form of the potential distribution along the lens axis which is required for this application is shown in Figure 6.4.1. A high rate of rise of potential near the specimen (right) is required and the potential must be low at the lens exit (left). A maximum must occur at some point in between. This type of characteristic is necessary to fulfil the requirement for a high accelerating field near the surface and low field disturbance at the analyser.

If only electrons close to and almost parallel to the z axis of a lens with an axially symmetric field are considered (ie paraxial electrons) the paraxial ray equation can be given as¹¹⁵:

$$\frac{d^2 r}{dz^2} + \left(\frac{V'(z)}{2V(z)} \right) \frac{dr}{dz} + \left(\frac{V''(z)}{4V(z)} \right) r = 0 \quad \dots 6.4.1$$

Where r is the distance of the electron from the axis and $V(z)$, $V'(z)$ and $V''(z)$ are the potentials and derivatives with respect to z along the z -axis. This equation requires numerical methods of solution in the cases under consideration here.

The solid curve in Figure 6.4.2(a) shows an electron trajectory evaluated using equation 6.4.1 for appropriate initial conditions and the potential distribution along the lens axis shown by the broken curve. This potential distribution would give a highly desirable accelerating field near the surface of 1.5 kV/mm and a low field disturbance at the lens exit. The electron path is however more than ten times further from the axis at the exit than it was at the specimen surface. The potential distribution shown in Figure 6.4.2(b) would give a divergence very much lower than the previous one as indicated by the trajectory given. The accelerating field near the surface in this case is much smaller, only 0.25 kV/mm. The potential distribution shown in Figure 6.4.2(c) is one obtained for the existing lens design with 1 kV on the first lens electrode and 130 V and 50 V on the others, as usual. The accelerating field is around 0.5 kV/mm and the electron trajectory shows the displacement from the axis at the exit to be about three times that at the surface. These results illustrate the general requirement that the second derivative of the voltage near the specimen must be positive to give the lowest possible divergence for the lens. This implies a low accelerating field at the specimen surface (as in Figure 6.4.2(b)).

Thus even considering only paraxial electrons and axial voltage distributions which may or may not be physically realisable the requirements of high accelerating field and low overall divergence can

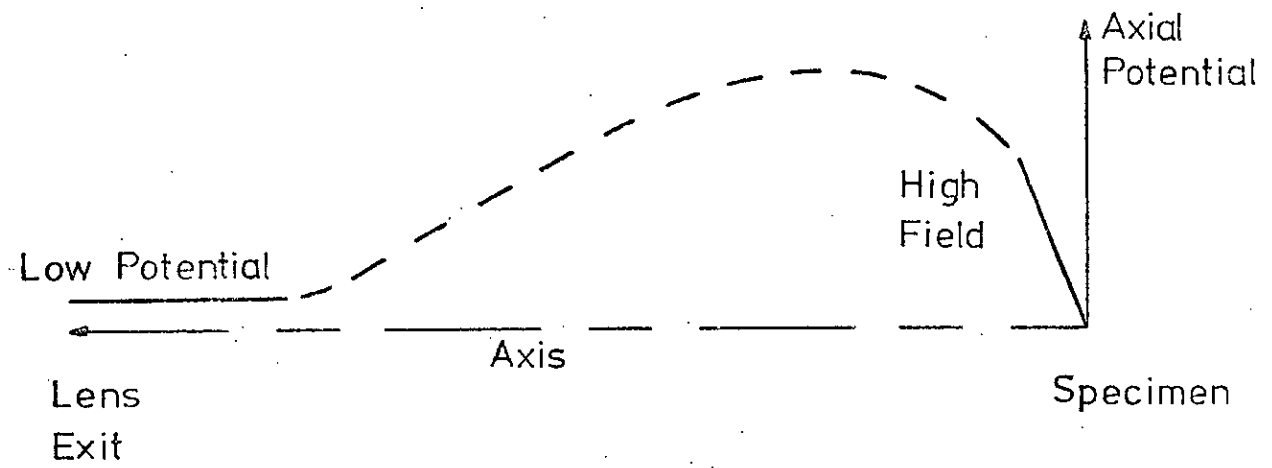
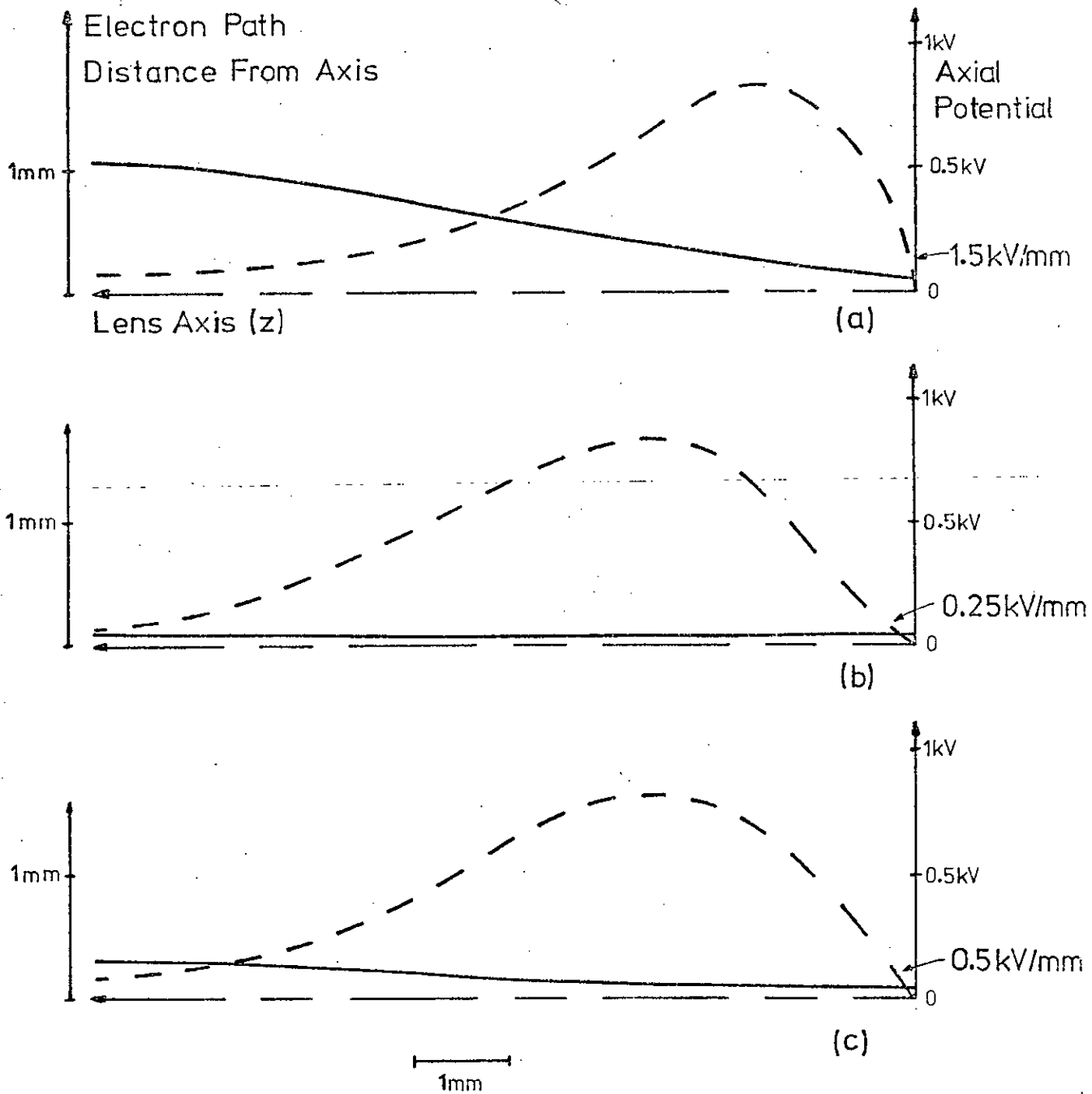


FIGURE 6.4.1 REQUIRED POTENTIAL DISTRIBUTION ALONG AXIS



FIGURES 6.4.2

PARAXIAL ELECTRON TRAJECTORIES

be seen to be contradictory necessitating a compromise.

Further consideration of the compromise necessary in the design of the lens was carried out by using the computer programs described previously to analyse the performance for modifications of the electrode shapes and positions. It was found that although it was possible to produce a lens which was more convergent at the exit, reducing the displacement from the axis by a factor of 2, the angular differences between the electron paths was much greater. This meant that there would be no overall improvement in the performance of the lens and analyser combination.

The conclusion from this work was that the original design of the lens had resulted in near optimum performance for this component within the framework of the requirements and constraints of this particular application. In view of this the lens design was not modified in any way.

6.4.2 Energy Analyser Design

The close relationship between the designs of the lens and analyser has already been noted. In fact the analyser design has a great effect on the arrangement of the rest of the system.

The design criteria for the energy analyser were given in section 4.3.2. A *bandpass* characteristic is highly desirable but not absolutely essential since a low pass energy filter could be used. But in practice only high and band pass types are readily available. The requirement of a fairly *narrow energy passband* is one of the reasons why it is desirable to keep the energy of the electrons to be analysed low, as mentioned in the previous section. This can be understood by assuming that the passband width is a fixed fraction of the centre energy of the passband, which will be approximately true for most analysers. Thus the higher the pass energy the wider the actual passband. This assumes an analyser of fixed geometry with only

the potentials applied to it varied. The requirements of *low sensitivity to the position and angle* of the electron at the entrance are statements of the features of an ideal analyser which would only indicate the absolute emission energy of the electron. This obviously cannot be completely achieved in practice.

It is in these last respects that the performance of the type of curved plate analyser used is least satisfactory as shown in section 6.2.2. Even for the best case, with no disturbing field (Figure 6.2.2(a)), the sensitivity to input position for electrons normal to the entrance near the centre is around 0.05 V/10 μm . This is to be expected since there is a potential gradient between the plates of the analyser and the velocity of the electron at the entrance depends on the difference between the specimen potential and the potential at the current position. In a practical case the field disturbance of the lens system will result in a sensitivity to position several times (up to 4 - Figure 6.2.2(d)) worse than that already given. Thus a difference in input position of only 50 μm could give up to 1 volt error for electrons of the same emission energy. The best case sensitivity to differences in angle to the axis for electrons at the analyser entrance is of the order of 1 V/degree near the centre. This will also be worse with the lens in place and will produce additional errors. In fact it is these characteristics of the energy analyser which are the principal sources of error in the experimental measuring system.

The problem of design modifications to the energy analyser is much less straight forward to solve than that of lens modifications. It is difficult to design an analyser having the desired characteristics.

Obviously a different type of analyser is required since the problems with the present component are due to its basic operation rather than the particular realisation.

Analysers of the cylindrical mirror or concentric hemisphere type were considered. Both these types will suffer from similar difficulties to those of the parallel plate type with regard to their sensitivity to the angle and position of the electrons at the entrance.

At this point the physical constraints in the microscope specimen chamber must be mentioned since these very much affect the design of a suitable analyser. The analyser must be small to fit into the available space and must be close to the electron lens which means that the primary beam must pass through it. It is also preferable that the electrons passing through the analyser can be collected using a scintillator-photomultiplier setup for best signal to noise performance. These constraints make the problems more difficult to solve since otherwise the electrons could be focussed into a narrower beam over a longer distance allowing some of the conventional types of analyser to be used successfully.

The ideal analyser in the present application would be a retarding field combination with a band pass characteristic. This would allow a wide area of acceptance with lowered sensitivity to input position and angle. The design of a suitable component within the physical constraints of the present system is by no means a simple task!

The analysers considered so far have all been electrostatic. Magnetic or combined types were not studied in great detail due to the obvious physical difficulties of installation and operation in the SEM specimen chamber.

These design studies have shown that although the analyser operates fairly successfully in the present system, it is the component which most limits the further development of the system.

6.5 SIMULATION OF SYSTEM

6.5.1 Introduction

The computer aided studies of the characteristics of the lens and analyser and the operation of the system have yielded much useful information about the behaviour of the measuring system. The characteristics of each of the components and their interaction are so complex that a fuller understanding can only be obtained by considering the whole process from electron emission to collection. The simulation programs developed and described in the previous chapter were intended to predict the performance of the complete system in a quantitative manner. This was to allow more detailed study of the experimental system. Also since the previous section has shown that the curved plate type of analyser is not ideal for this application the simulation programs were intended to enable the capabilities of the system, if an "idealised" analyser was used, to be investigated. This allows a study of the limitations of the lens and energy analyser type of approach to voltage measurement in the SEM to be carried out.

6.5.2 General Approach

Cross sections of the three types of samples chosen for modelling have already been given in Figure 5.4.2. These consist of 1 μm thick Al on 1 μm SiO_2 on an Si substrate. The one with a 40 μm wide gap was chosen to be similar to ones used in experiments as described in chapter 4. The 10 μm gap is to allow examination of performance with higher tangential fields and the sample with two 5 μm gaps to simulate a very exacting situation. Equipotential plots for the

region above the surface have been given in Figures 5.4.8(a)-(c). Figures 6.5.0(a)-(c) show equipotentials for the same gaps under identical conditions but with the corresponding strips negative rather than positive. These again indicate the favourable effect of the high positive potential on the first lens electrode.

The distribution function of the secondary electrons emitted from the aluminium surface has to be incorporated into the simulation programs. As already noted in chapter 2 there is not a great deal of data available on measured energy and angular distributions. The actual number of electrons versus energy distribution and number of electrons versus angle distribution are continuous but must be approximated by discrete distributions in this analysis.

The distributions were approximated by evaluating the paths of a large number of electrons emitted with different energies at different angles to the surface and associating with each electron a weighting which was a function of the energy and angle of emission. These angles were to the surface normal (usually 5 angles) and around half the hemisphere (usually 11 angles). Only half the hemisphere of emission was used since there was normally symmetry with respect to the specimen gap and the analyser entrance. The weighting function dependent on the angle of emission was of course a cosine one (see section 2.5). Many results were obtained for electrons emitted with energies of 1-5 eV assuming the energy weighting function shown in Figure 6.5.1(a). This resulted in contributions from up to 275 electrons producing the final *secondary emission curve*. Figure 6.5.1 (b) shows the curve which would be produced if all these electrons reached an analyser with a 5 V passband. This represents the analyser output in relative units against a sweep voltage applied to the specimen.

FIGURE 6.5.0 (a)

EQUIPOTENTIALS
NEAR SPECIMEN
SURFACE

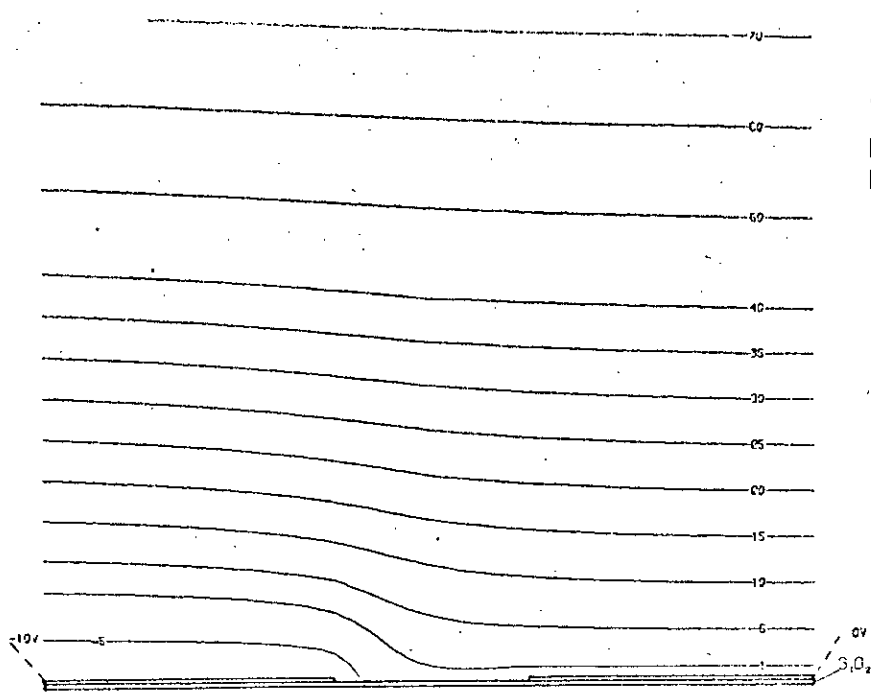


FIGURE 6.5.0 (b)

EQUIPOTENTIALS
NEAR SPECIMEN
SURFACE

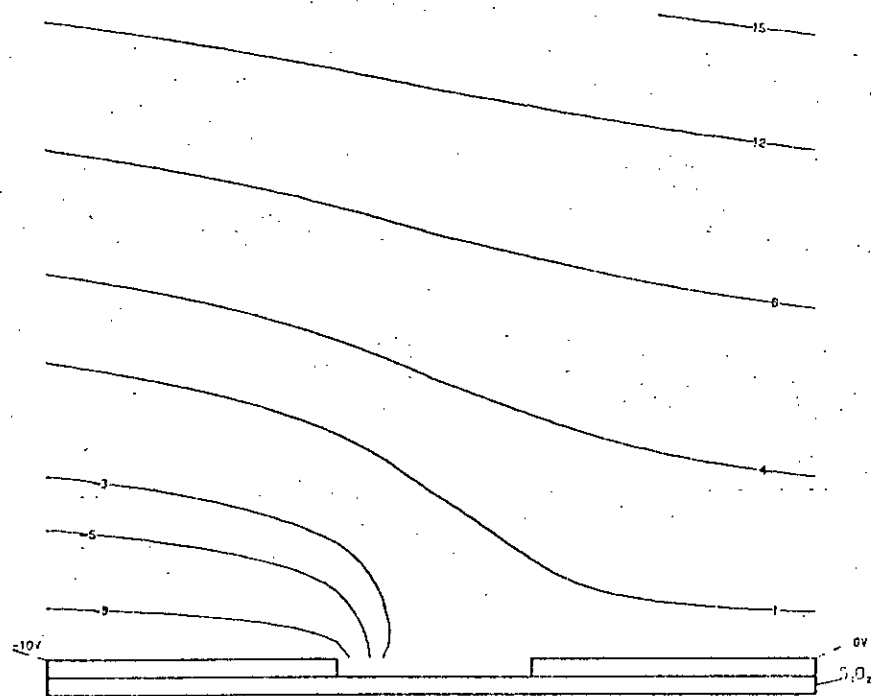
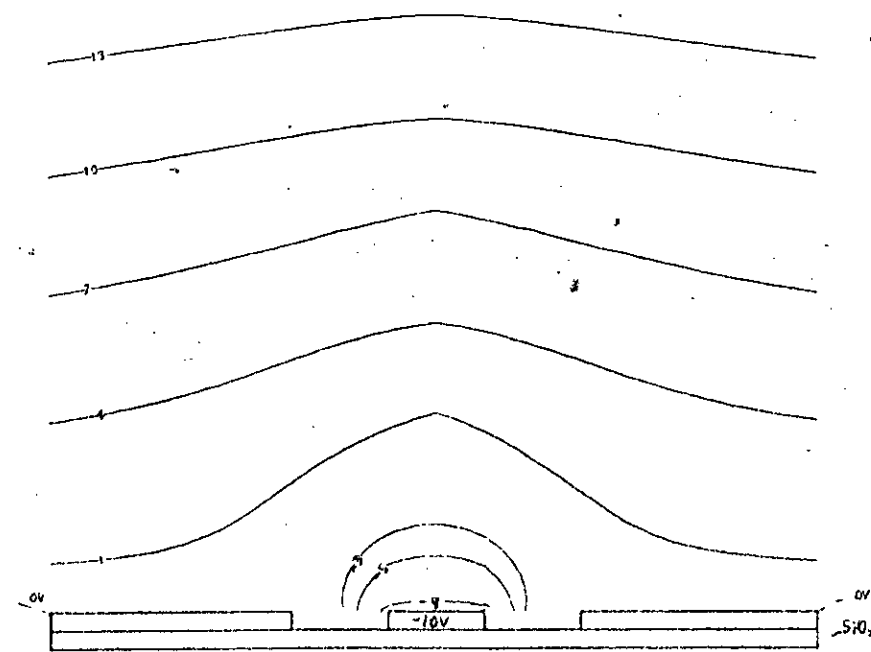


FIGURE 6.5.0 (c)

EQUIPOTENTIALS
NEAR SPECIMEN
SURFACE



The use of 1-10 eV electrons and the energy weighting function shown in Figure 6.5.1(c) would produce the analyser output given in Figure 6.5.1(d). This approximation corresponds to the peak on the emission curve occurring at a lower energy and uses more points thus requiring double the computing time. It was used later in the simulation work to check if the predicted results were altered. This was not found to be the case.

6.5.3 Results from Simulation of the Experimental System

The positions and orientations of the gaps of the specimens for which results were obtained are shown in Figure 6.5.2 in relation to the lens axis and the analyser entrance. In the cases marked A, B and C the gap was parallel to the analyser plates at the entrance and for those marked D, E and F it was at right angles to this. The points examined were either along the normal to the plates through the lens axis or a line parallel to the plates through the axis.

Some examples of the type of secondary emission curve produced by the simulation programs (SIMRNI) have already been given in Figure 5.5.11(a). These were for a double gap sample in position A (Figure 6.5.2) with the beam on the centre strip. Figure 6.5.3 shows more examples of curves obtained for a 10 μm wide gap also in position A with the electron beam 1 μm from the gap edge on the side nearer the lens axis. The figures marked on the key to the curves at the top of the diagram are the potentials of the strip nearer the axis with the other strip kept at 0 V.

The results from the secondary emission curves produced by the simulation programs for the three types of specimen and a number of different conditions are summarised in Tables 6.5.1-6.5.10.

FIGURE 6.5.1(a)

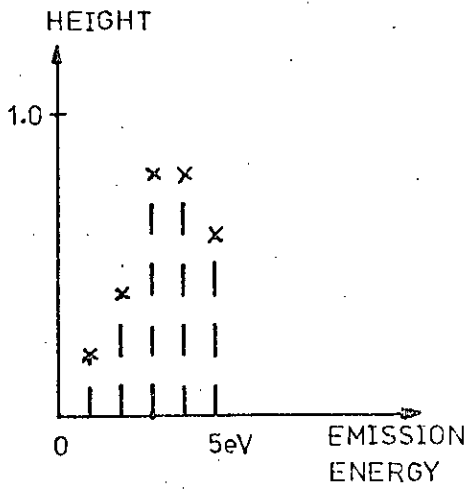
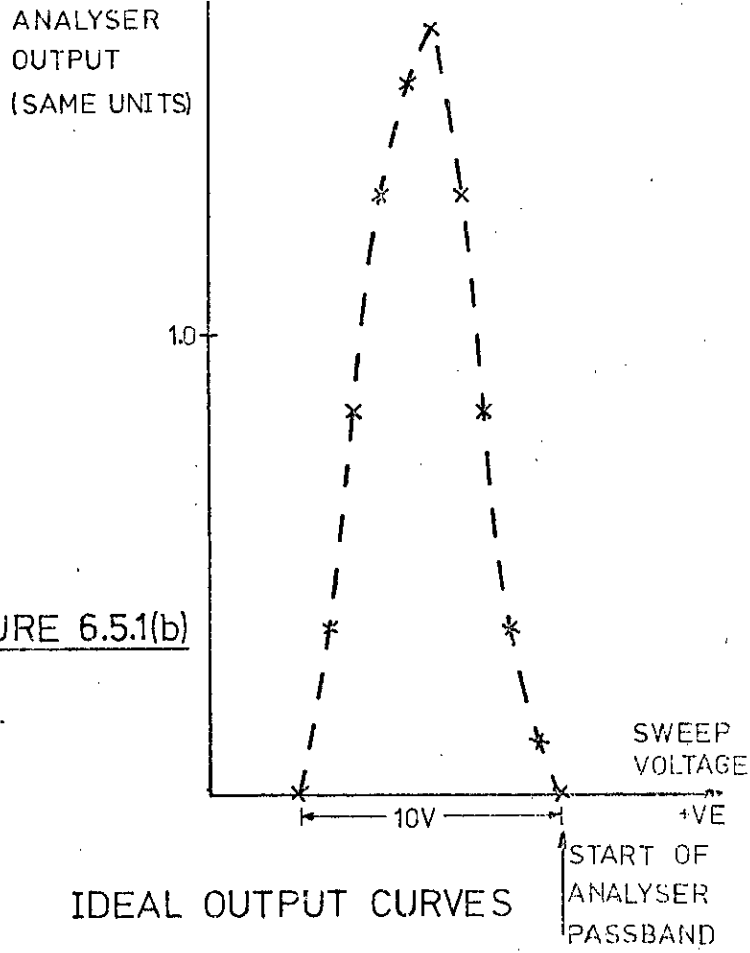
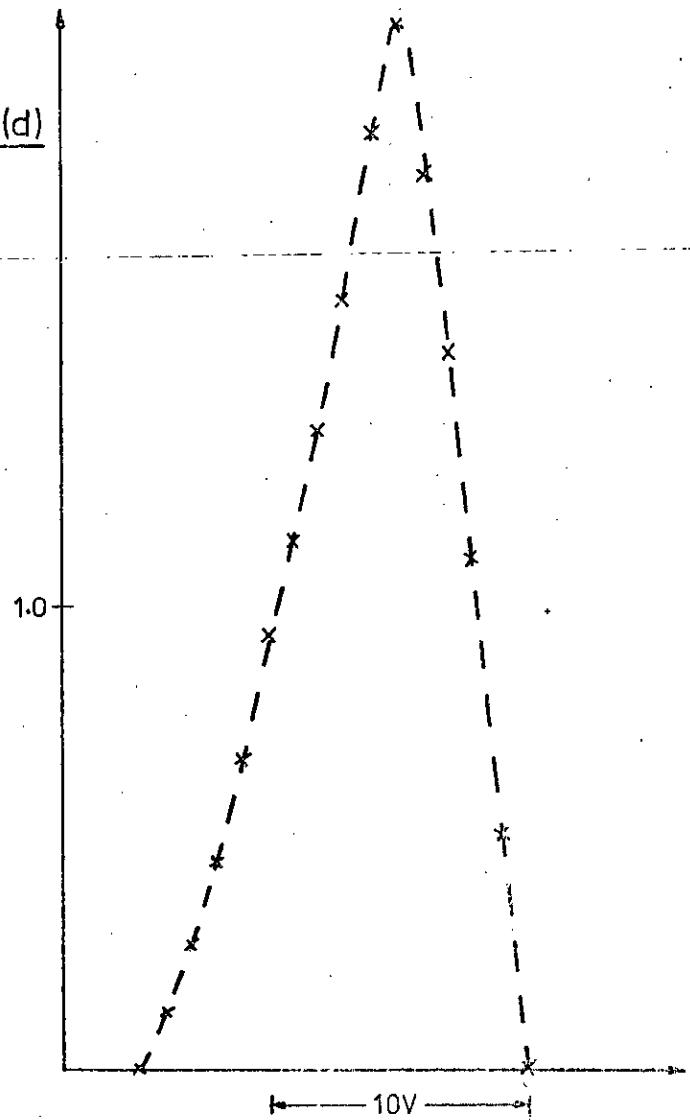


FIGURE 6.5.1(b)



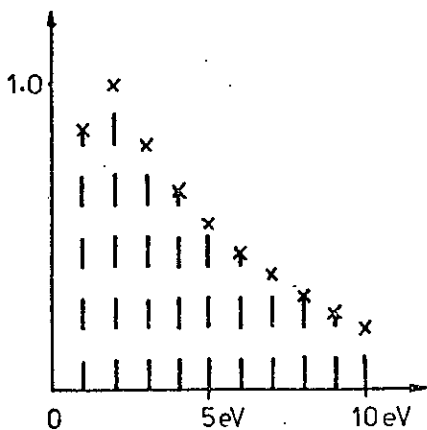
IDEAL OUTPUT CURVES

FIGURE 6.5.1(d)



ENERGY
WEIGHTING
FUNCTIONS

FIGURE 6.5.1(c)



TOP VIEW

(Primary beam direction, from inside analyser)

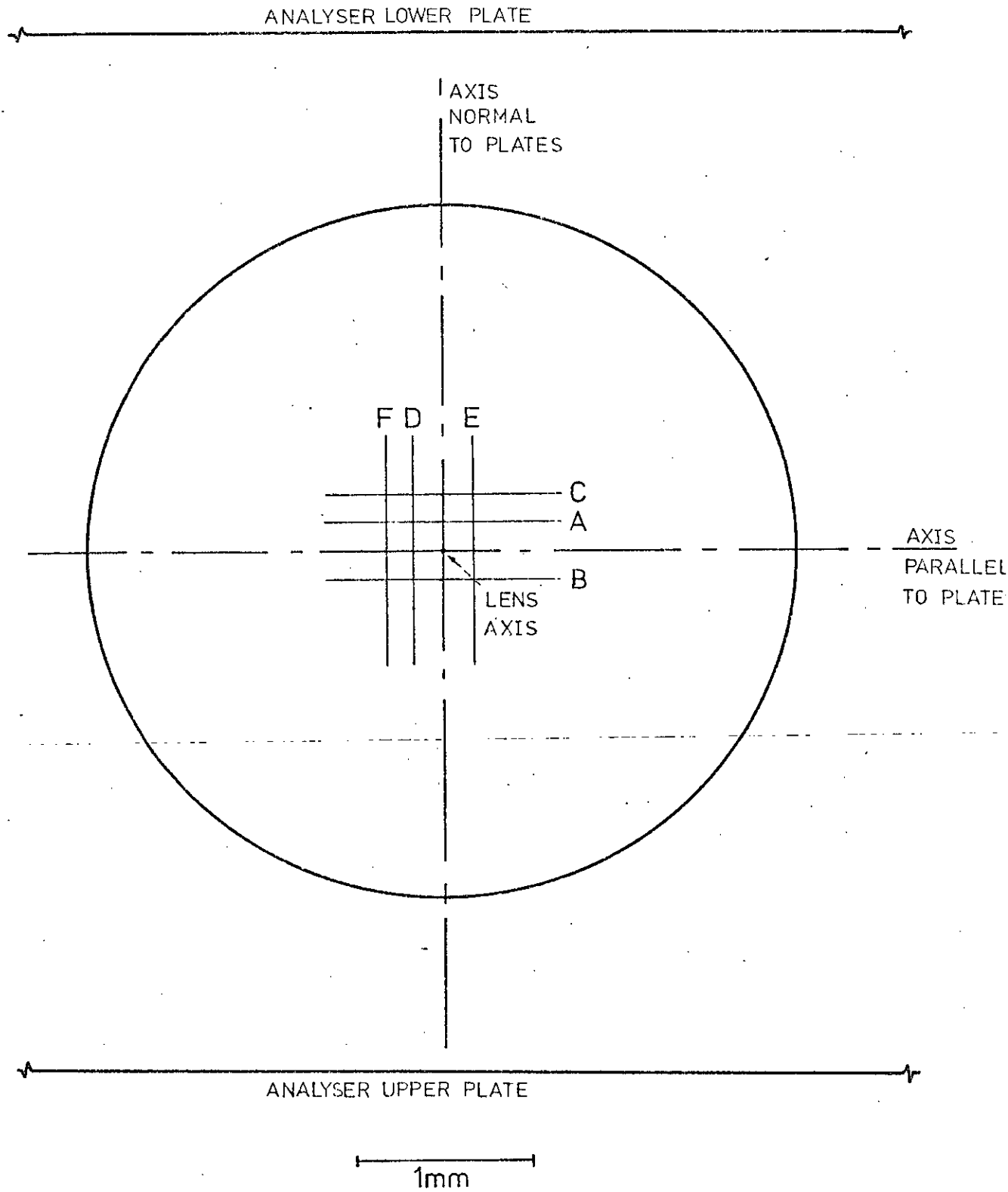
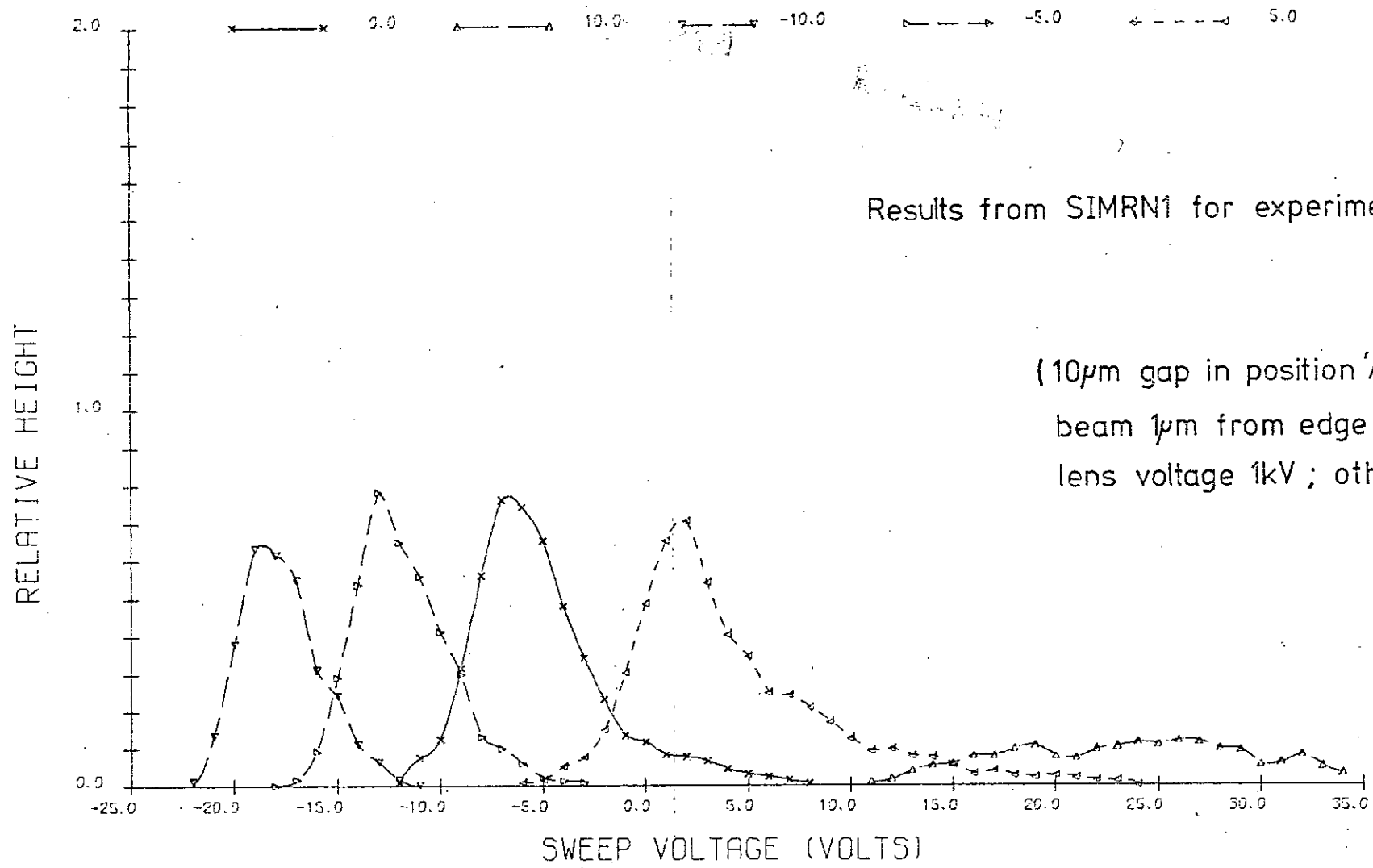


FIGURE 6.5.2

SHOWING GAP ORIENTATIONS AND POSITIONS



Results from SIMRN1 for experimental analyser

(10µm gap in position 'A' - FIG. 6.5.2
 beam 1µm from edge nearer axis
 lens voltage 1kV ; other strip 0V)

FIGURE 6.5.3

First lens electrode voltage 1 kV
 40 μm gap in position A (Fig 6.5.2)

VOLTAGE APPLIED TO STRIP	INDICATED CURVE PEAK POSITION (V)				VOLTAGE APPLIED TO STRIP
	at 30 μm FROM GAP	at 1 μm FROM GAP	at 1 μm FROM GAP	at 30 μm FROM GAP	
0	-6	-6	-6	-6	0
-10		-14	-5		0
+10	+3	+1	-8		0
0		-4	+17	+7	+10
0		-8	-18	-18	-10
Side <i>farther</i> from axis			Side <i>nearer</i> to axis		

TABLE 6.5.1

First lens electrode voltage 1 kV
 40 μm gap in position B (Fig 6.5.2)

VOLTAGE APPLIED TO STRIP	INDICATED CURVE PEAK POSITION (V)		VOLTAGE APPLIED TO STRIP
	at 1 μm FROM GAP	at 1 μm FROM GAP	
0	-6	-6	0
-10	****		0
+10	+6		0
0		+29	+10
0		-15	-10
Side <i>nearer</i> to axis		Side <i>farther</i> from axis	

TABLE 6.5.2

First lens electrode voltage 1 kV
 40 μm gap in position D (Fig 6.5.2)

VOLTAGE APPLIED TO STRIP	INDICATED CURVE PEAK POSITION (V)		VOLTAGE APPLIED TO STRIP
	at 30 μm FROM GAP	at 30 μm FROM GAP	
0	+2	+2	0
-10			0
+10	+12		0
0		+12	+10
0		-8	-10
Side <i>farther</i> from axis		Side <i>nearer</i> to axis	

TABLE 6.5.3

First lens electrode voltage 1 kV
 40 μm gap in position E (Fig 6.5.2)

VOLTAGE APPLIED TO STRIP	INDICATED CURVE PEAK POSITION (V)		VOLTAGE APPLIED TO STRIP
	at 1 μm FROM GAP	at 1 μm FROM GAP	
0	+2	+2	0
-10	-9		0
+10	+15		0
0		+11	+10
0		-6	-10
Side <i>nearer</i> to axis		Side <i>farther</i> from axis	

TABLE 6.5.4

First lens electrode voltage 1 kV

40 μm gap in position C (Fig 6.5.2)

VOLTAGE APPLIED TO STRIP	INDICATED CURVE PEAK POSITION(V)		VOLTAGE APPLIED TO STRIP
	at 30 μm FROM GAP	at 30 μm FROM GAP	
0	-6		0
-10			0
+10	+3		0
Side <i>farther</i> from axis			Side <i>nearer</i> to axis

TABLE 6.5.5

First lens electrode voltage 1 kV

40 μm gap in position F (Fig 6.5.2)

VOLTAGE APPLIED TO STRIP	INDICATED CURVE PEAK POSITION (V)			VOLTAGE APPLIED TO STRIP
	at 30 μm FROM GAP	at 1 μm FROM GAP		
0	+2	+2		0
-10	-8			0
+10	+12	+14		0
Side <i>farther</i> from axis			Side <i>nearer</i> to axis	

TABLE 6.5.6

First lens electrode voltage 1 kV

10 μm gap in position A (Fig 6.5.2)


VOLTAGE APPLIED TO STRIP	INDICATED CURVE PEAK POSITION (V)				VOLTAGE APPLIED TO STRIP
	at 7.5 μm FROM GAP	at 1 μm FROM GAP	at 1 μm FROM GAP	at 7.5 μm FROM GAP	
0		-6	-6	-6	0
-10		-13	-2		0
+10		*****	-8		0
0		-3	+25	+8	+10
0		-9	-18	-18	-10
0			+2		+5
0			-12		-5
Side <i>farther</i> from axis			Side <i>nearer</i> to axis		

TABLE 6.5.7

First lens electrode voltage 1 kV

10 μm gap in position D (Fig 6.5.2)

VOLTAGE APPLIED TO STRIP	INDICATED CURVE PEAK POSITION (V)		VOLTAGE APPLIED TO STRIP
		at 7.5 μm FROM GAP	
0		+2	0
-10			0
+10			0
0		+14	+10
0		-9	-10
Side <i>farther</i> from axis		Side <i>nearer</i> to axis	

TABLE 6.5.8

1st lens electrode voltage 0.5 kV

40 μm gap in position A (Fig 6.5.2)

VOLTAGE APPLIED TO STRIP	INDICATED CURVE PEAK POSITION (V)		VOLTAGE APPLIED TO STRIP
	at 1 μm FROM GAP	at 1 μm FROM GAP	
0	-1	-1	0
-10	-9		0
+10	****		0
0		+26	+10
0		-12	-10
Side <i>farther</i> from axis		Side <i>nearer</i> to axis	

TABLE 6.5.9

First lens electrode voltage 1 kV

2 x 5 μm gaps in position A (Fig 6.5.2)
Beam on centre strip

VOLTAGE APPLIED TO STRIP	INDICATED CURVE PEAK POSITION (V)		VOLTAGE APPLIED TO STRIP
	at 2.5 μm FROM GAP		
0	-6		0
-10	-16		0
+10	+4		0
Centre strip		Other two strips	

TABLE 6.5.10

These give the *sweep voltage* at which the peak of the curve occurred for the particular specimen and applied potentials noted. These tables have some blanks in them since simulation programs were only run for a limited number of conditions, partly because of restrictions on computing expenditure. Those entries marked with asterisks were cases where a secondary emission curve was not obtained since hardly any electrons passed through the analyser.

Not a great deal of work was done on the effects of using different accelerator voltages since the results obtained for varying position were of greater interest in this study. Those simulations which were carried out show that there is no great difference between 500 V and 1 kV, for the samples used in the tables shown (6.5.1 and 6.5.9). It was found that for equivalent conditions 2 kV on the first lens electrode yielded a very poor secondary emission curve.

Tables 6.5.1 to 6.5.6 show a number of results for a 40 μm gap similar to the type used in the experiments described earlier. A consideration of these results shows that the position of the peak of the curve appears to depend on the distance of the point under examination from the gap and the position and orientation of the gap with respect to the lens axis as well as the potential at the point.

The results given in the top line of each of these tables show that with no bias across the gap the curve peak position is a function only of the various lens electrode voltages and the position of the point with respect to the analyser entrance (ie positions A, B and C are different from D, E and F - Fig 6.5.2).

If the potential of a point is measured by noting the difference in the curve peak positions between bias and no bias conditions (the method used experimentally), then the error will be the difference between the expected and actual values. In the tables the expected value is the applied voltage given in either the leftmost or rightmost columns and the actual value is found by taking the curve peak position in the required column and subtracting the figure in the topmost row of this column. Tables 6.5.1-6.5.6 show that this error increases as the point under examination is brought closer to the gap edge. The errors for the positive side of a biased gap can also be seen to be greater in general, than those for the negative side for points at the same distance from the gap edge. These results are very much in line with observations from experiment.

A comparison of the results in Tables 6.5.1, 6.5.2 and 6.5.5 with those in Tables 6.5.3, 6.5.4 and 6.5.6 shows clearly the dependence of the error on the orientation of the gap with respect to the analyser entrance. When the gap is parallel to the analyser entrance (positions A, B and C) variations in arrival positions of the electrons at the analyser produce greater errors than when the gap is at right angles to the entrance (positions D, E and F). This is because in the latter case the effects of the field across the gap on the electrons are less serious since the analyser is less sensitive to the entry position of the electrons in the plane parallel to the plates. In order to compare these errors with those measured experimentally it is necessary to know the orientation of the gap in the experimental setup. In most cases the gap had an orientation which lay between the extreme positions, giving results nearer to the excellent predicted performance shown in Table 6.5.3.

Tables 6.5.7 and 6.5.8 show results obtained for a similar sample but with a 10 μm rather than a 40 μm gap. These indicate that the errors are in general slightly greater for a narrower gap but that the approach is still useable, particularly for a gap in position D.

Results for a double 5 μm gap with a centre 5 μm aluminium strip are given in Table 6.5.10. These results can be seen to be excellent even with the gap in position A. It has already been noted that the field conditions above this type of gap are particularly unfavourable - the reason it was chosen for study. These results indicate that the system would work well even in this situation. This agrees with results obtained in chapter 4 for a similar but less exacting arrangement.

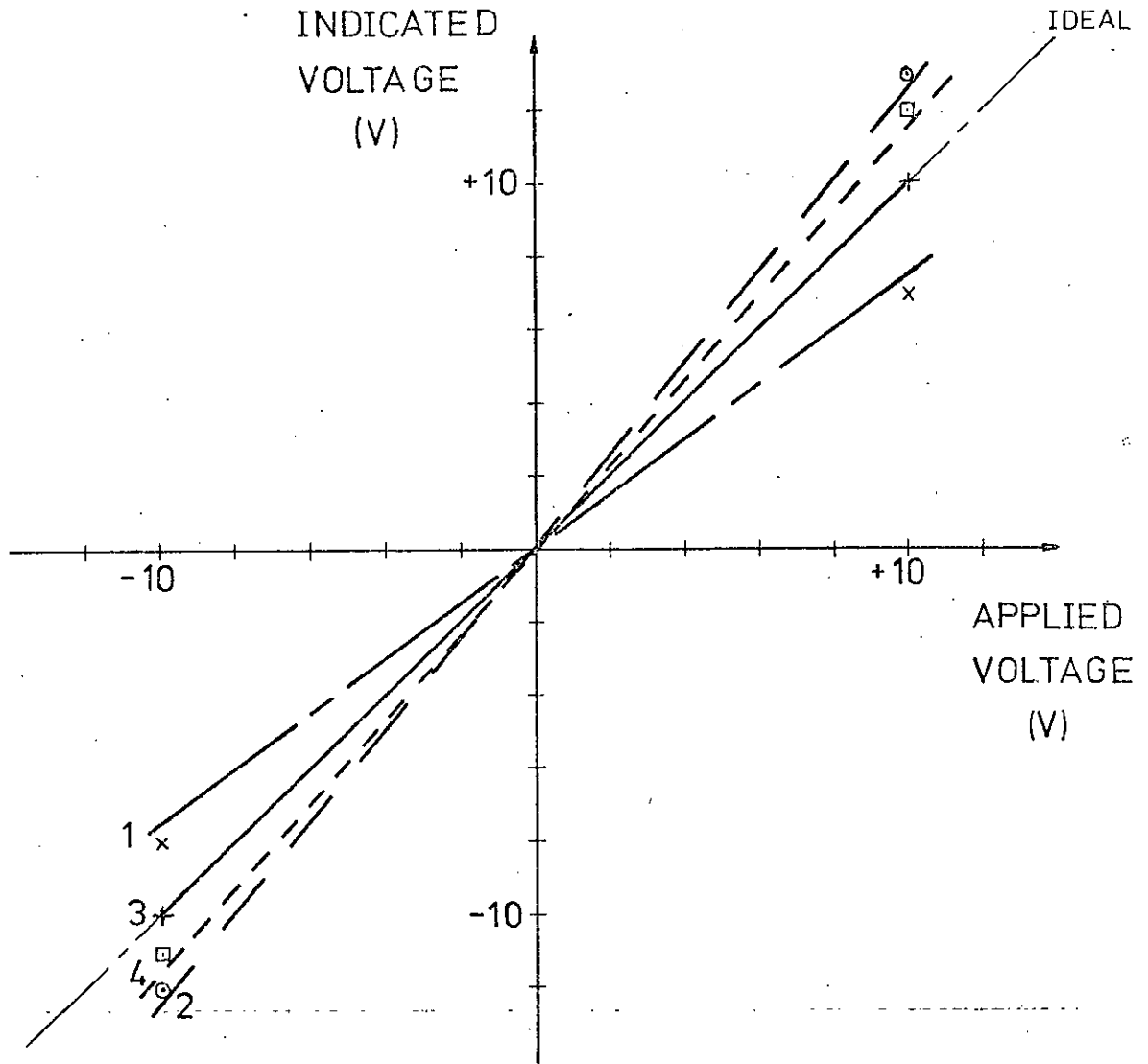
A consideration of the results in Tables 6.5.1, 6.5.7, 6.5.9 and 6.5.10, for a gap in positions A and C, indicates that a bias condition which would produce a net tangential force on the electrons above the surface directed *towards* the lens axis gives a *positive* error, whereas a net force acting *away* from the axis gives a *negative* error. This appears reasonable since a net tangential force directed towards the lens axis will, for these specimen positions, result in the electrons arriving at the analyser entrance nearer to the upper plate than would be the case for no net tangential force (ie no bias). From the analyser characteristics (Figure 6.2.2(c)) this will result in a higher sweep voltage being necessary to ensure passage of the electrons through the analyser thus giving a positive shift in the secondary emission curve position. A net tangential field above the surface in the opposite direction will have exactly the opposite effect resulting in a negative shift in the curve position.

Less data is available for a gap in position B (Table 6.5.2) but similar effects are observed, modified slightly by the fact that the analyser pass characteristic normally has a steeper slope for electrons which arrive very close to the upper plate.

The results given in these various tables confirm earlier deductions that the main error producing mechanism in the experimental setup is the effect of the net tangential field above the specimen surface on the arrival position of the electrons at the analyser entrance. A very good indication of this is the fact that for constant bias the errors for either side of the gap have the same sign and are approximately equal in magnitude. This implies that the field of importance is that a short distance above the specimen surface. This is further substantiated by the results given in Table 6.5.10 where a symmetrically biased gap (ie with low net tangential field) gives small errors even though the field distribution very close to the surface is highly non-uniform. For points very close to the positive side of biased gaps the effects of the very local fields have to be considered. A very good indication of the effects of analyser entry positions is obtained by considering the improvement in results noted for the gaps in positions D, E and F since the arrival position is less critical in these cases although the angle of entry is still important.

Some of the results from the tables are given in graphical form in Figure 6.5.4. The computed results, to a first approximation, appear to lie on straight lines through the origin with gradients in the region of unity. A generalisation can be made that the lines for points away from the lens axis have a slope greater than unity whereas points on the side nearer the axis have a slope of less than unity.

FIGURE 6.5.4



- 1 * - * 40 μ m GAP in position 'A' (Fig.6.5.2) ,
Point 1 μ m from edge , Side farther from axis .
- 2 ○ - ○ 40 μ m GAP in position 'A' (Fig.6.5.2) ,
Point 30 μ m from edge , Side nearer to axis .
- 3 + - + 40 μ m GAP in position 'D' (Fig.6.5.2) ,
Point 30 μ m from edge , Side nearer to axis .
- 4 □ - □ 10 μ m GAP in position 'D' (Fig.6.5.2) ,
Point 7.5 μ m from edge , Side nearer to axis .

These results are similar to experimental ones given in Figures 4.3.13(a) and (b), allowing for the orientations of the gaps. A reasonable explanation for these results can be deduced from Figure 6.5.5 which shows a typical analyser pass energy characteristic plotted against position of entry. The *average* entry position at the analyser of electrons emitted from a point on the specimen surface will vary on either side of the no bias position depending on the direction of the net field across the gap. The shift in the average position will be small giving a fairly low error due to the slope of the characteristic (the distances shown in Figure 6.5.5 are exaggerated for clarity). Thus the analyser pass characteristic can be approximated, near the point of entry corresponding to no bias, by a straight line through this point. The gradient of this line and so the magnitude of the error will be a function of the position of the point on the specimen under examination relative to the system axes since this determines the portion of the analyser characteristic which is of interest. The magnitude of the shift in entry position is assumed to be the same for positive and negative applied voltages, which will be true unless the point is very close to the gap edge (when straight lines as in Figure 6.5.4 would not be obtained in any case). Thus the gradient of the straight line, as in Figure 6.5.5 is a function of the slope of the analyser pass characteristic in the region of interest as well as the shift in average entry position produced by the surface field. These considerations give an approximate explanation of the errors observed during experimental work.

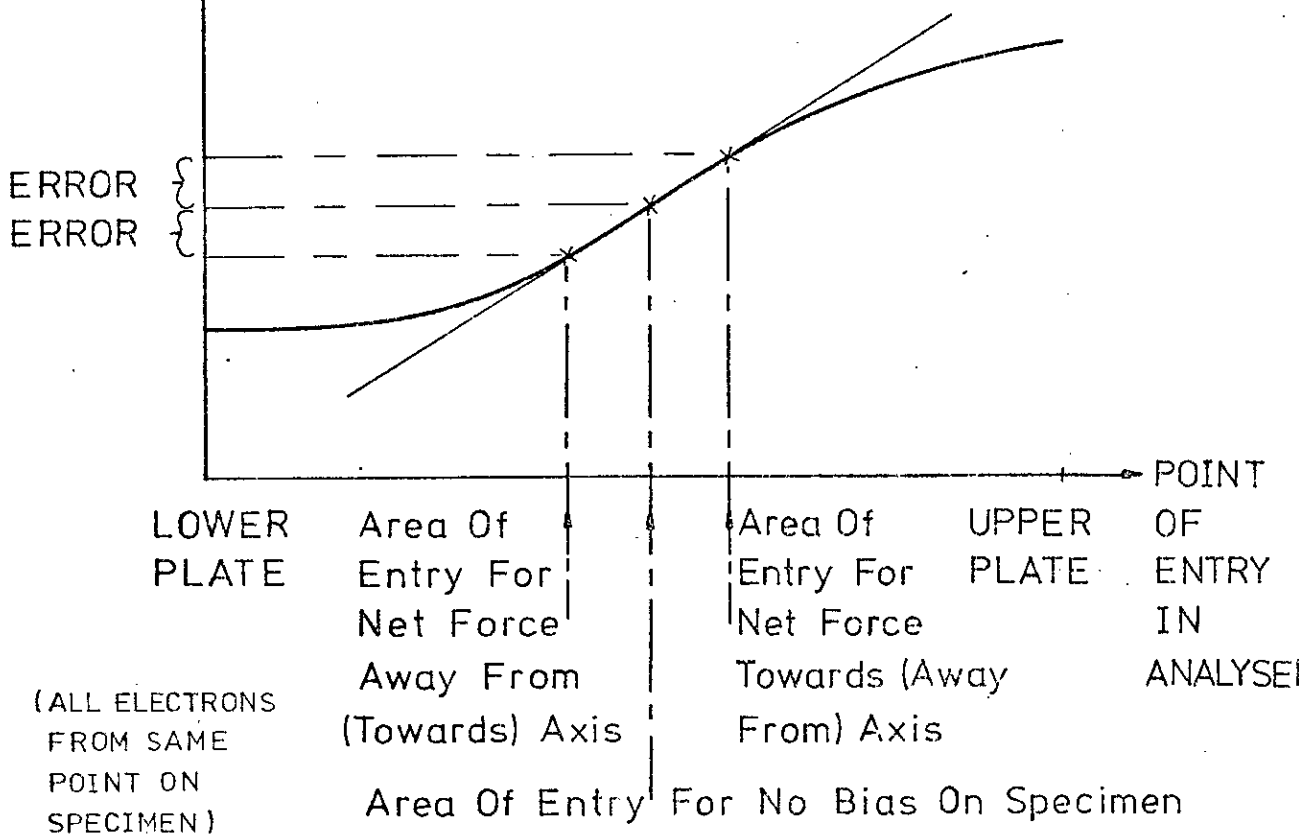
In the discussions presented so far the errors mentioned have been based on the concept of measuring voltages by noting the shift of the curve peak with respect to the peak position with no voltage (bias) applied to the specimen for electrons from the same point.

An examination of the results given in the various tables reveals that in all cases taking the difference between the curve peak positions for corresponding points on both sides of the gap with constant bias applied, gives a much better indication of the potential difference across the gap than referring each separately to the no bias condition. This can again be explained in terms of the average arrival position of the electrons at the analyser. Figure 6.5.6 shows a typical analyser pass characteristic with observed average arrival positions for 3 eV electrons. The arrival positions for electrons from both sides of the biased gap can be seen to be closer together than they each are from the arrival position for no bias. This is because the electrons from both sides of the gap are similarly affected by the tangential field which does not exist to affect the electrons in the unbiased case. Thus the error introduced by the different arrival positions is smaller between the electrons from either side of the gap. This indicates that improved accuracy can be obtained by measuring potentials for conditions of constant bias. This could prove useful in practical cases of voltage measurement on integrated circuits.

These results produced by the simulation programs show great similarities to those obtained experimentally and give a further understanding of these. The specimens used in these studies being idealised in shape and requiring the field determining methods already described would tend to give more exacting situations than those likely in practice. This is probably the reason why some of the predicted results (for points very close to the gap) are poorer than those obtained in practice.

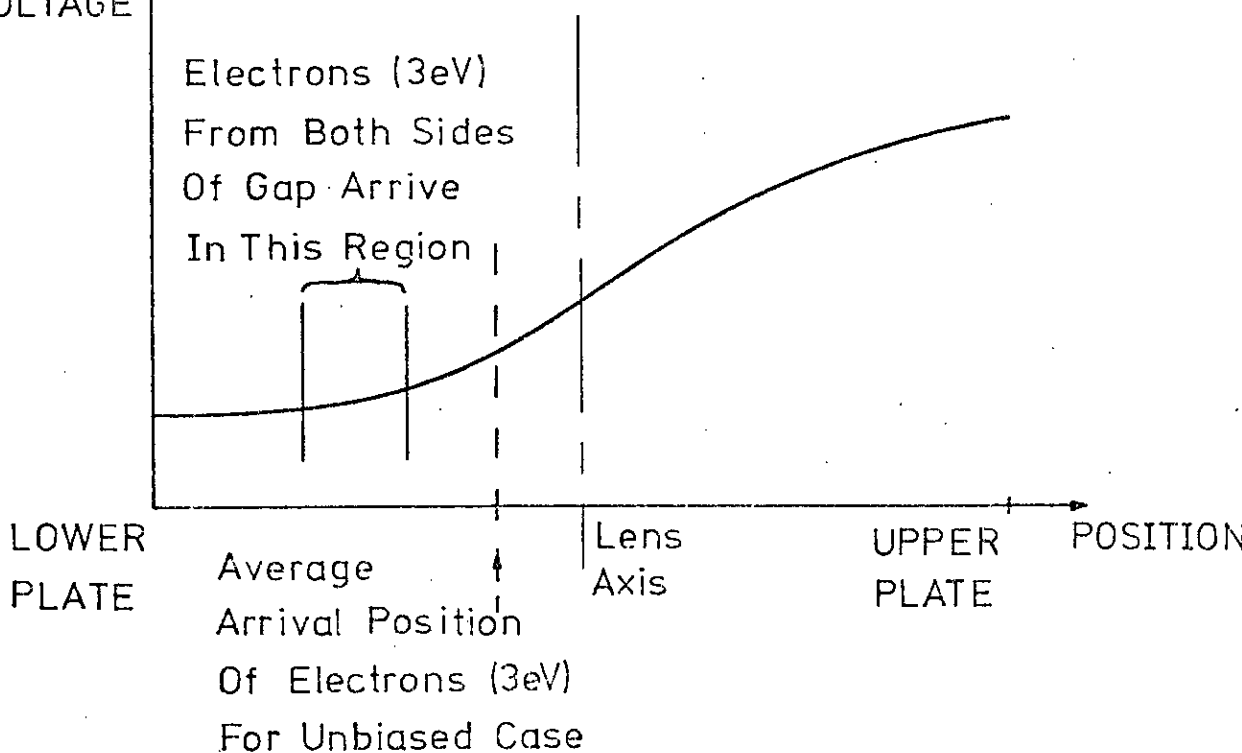
SWEEP
VOLTAGE

FIGURE 6.5.5



SWEEP
VOLTAGE

FIGURE 6.5.6



The considerations of those errors which have been observed have pointed to the importance of the characteristics of the energy analyser. With a view to considering the performance of the specimen and electron lens part of the system it was decided to carry out simulations assuming the use of an "idealised" energy analyser.

6.5.4 Results from Simulation of a System with an "Idealised" Analyser

The analyser model included in this study has a band-pass characteristic and is "idealised" in that it has only one pass criterion. This is the condition that the component of the electron velocity normal to the lens exit is within a fixed range (equivalent to a range in kinetic energy of 5 eV starting at 100 eV). That is whether or not the electron passes through the analyser is a function only of the emission energy, the arrival angle, the potential of the point on the specimen surface and the value of the sweep voltage.

Examples of the type of secondary emission curve produced by the simulation programs for an idealised analyser have already been given in Figure 5.5.11(b). Figure 6.5.7 shows more examples of curves obtained for the same sample (10 μm gap) and identical conditions to those giving Figure 6.5.3. A comparison of the curves in Figures 5.5.11(b) and 6.5.7 with the corresponding ones for the experimental analyser ie Figures 5.5.11(a) and 6.5.3, shows clearly the improvement in performance of the idealised analyser system. This is particularly noticeable from Figures 6.5.3 and 6.5.7 where the improvement is dramatic for the point very close to the positive edge of the gap. The shapes of the secondary emission curves in Figures 5.5.11(b) and 6.5.7 are close to those of Figure 6.5.1(b) as might be expected.

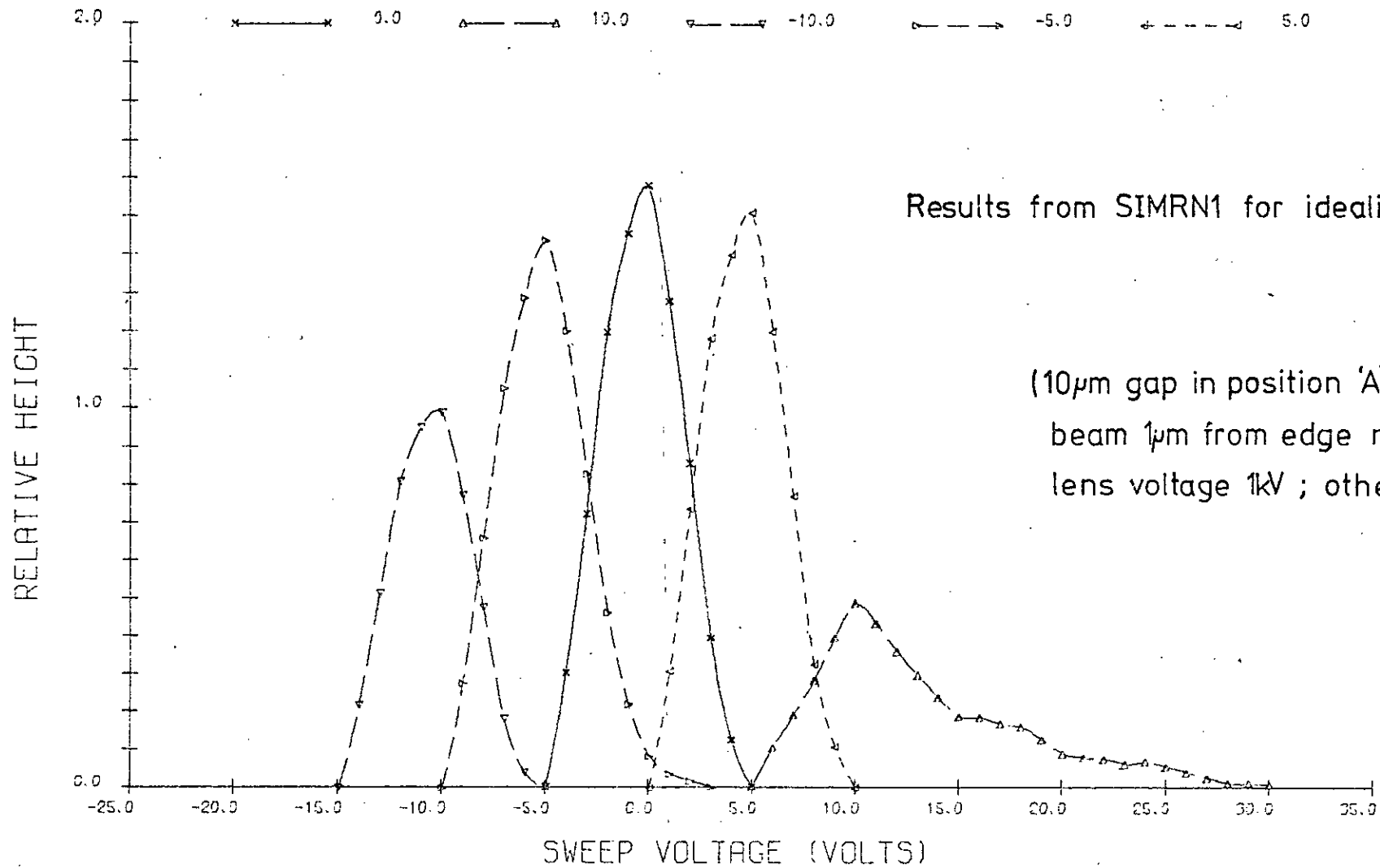


FIGURE 6.5.7

Simulation studies were carried out for this arrangement for all the cases already noted in Tables 6.5.1 to 6.5.10 for the experimental system. The corresponding tables of results are not listed here since there were *only* 3 cases out of all 53 where *any* error was observed. These are noted in Table 6.5.11 from which the errors can be seen to be 1V twice and 2V once. These represent two cases where the point under examination is very close (1 μm) to the edge of the gap on the positive side and farthest from the lens axis (so that not all emitted electrons pass through the lens) and one case where the surface field is very unfavourable (case 3) and not all electrons leave the region above the surface.

These results show very clearly the excellent performance of the electron lens arrangement and the value of this secondary emission curve shift approach to voltage measurement in the SEM. They also verify the conclusion reached earlier that it is the characteristics of the type of energy analyser used which limit the performance of the measuring system.

6.5.5 Consideration of Limitations

The computer aided analysis and simulation studies already presented have given a clearer understanding of the operation of the measuring system and identified its limitations in both a qualitative and quantitative manner.

Although the interaction between the various components of the system has been shown to be important, it is instructive to consider the limitations primarily associated with the two major components.

One of the purposes of the simulation studies using the "idealised" analyser was to investigate limitations of performance which might be associated with the electron lens. The results of these indicate

Cases giving any error with 'idealised analyser'.

First lens electrode voltage all 1 kV.

Case 1

40 μm gap in position 'A' (Fig 6.5.2).

Beam at 1 μm from edge of gap *away* from lens axis

+10 V applied to this side of gap, Error +1 V

+ 0 V applied to other side of gap, Error 0 V

Case 2

40 μm gap in position 'B' (Fig 6.5.2)

Beam at 1 μm from edge of gap *away* from lens axis

+10 V applied to this side of gap, Error +2 V

0 V applied to other side of gap, Error 0 V

Case 3

2 x 5 μm gaps in position 'A' (Fig 6.5.2)

Beam in centre of centre strip ie 2.5 μm from edge

+10 V applied to centre strip, Error -1 V

0 V applied to other strips

TABLE 6.5.11

that the positioning of the specimen with respect to the lens axis at the entrance is not critical but that a region within about 0.5 mm of the axis will give best results. The main conclusion of these studies is that the lens fulfils its design aim of conveying most of the emitted electrons to the analyser for all practical cases. The *only* case where most of the electrons did not leave the region above the specimen surface was one with a very unfavourable retarding field distribution representing the worst type of situation likely to be experienced. Even in this exceptional case the maximum final error was only 10% confirming the experimental fact that good results were obtainable for this type of specimen. The performance of the lens can be seen to be excellent overcoming many of the problems which are associated with voltage measurement in the SEM for integrated circuit type specimens.

The results of the simulations for the actual experimental system indicate the limitations introduced by the type of analyser used. These limitations are most noticeable for a particular gap orientation and points very close to the positive side of a biased gap. For most cases of practical interest the results are adequate as has already been demonstrated experimentally. Errors have been shown to be reduced if potential differences between points close together but at different potentials are used, rather than those taken with respect to unbiased conditions.

The general conclusion from these various results is that the limitations of the actual experimental system, while capable of elimination with a very different type of analyser, do not preclude its successful use in measuring voltages. In fact in most practical circuits conditions are much more favourable than for those examples used in

simulation studies. This is because in most situations it is of little value to measure the voltages $1\ \mu\text{m}$ from the edge of an abrupt gap since only the potentials on conductors (which may have a wide range of widths) are required. The results have also demonstrated the system operation in such a way as to give useful pointers to obtaining the best possible performance when measuring voltages on integrated circuit metallisation in the SEM.

CHAPTER 7

CONCLUSIONS

The summary of current applications of the SEM to integrated circuits given in chapter 3 has shown its special capabilities in electron beam fabrication and basic device and material studies. In the areas of routine testing and failure analysis of integrated circuits current applications have been shown to be of a mainly qualitative nature.

A consideration of the manufacturing process for integrated circuits has indicated the importance of device testing if good reliability of the final product is to be achieved. The quality of the aluminium metallisation on integrated circuits is a crucial factor in device reliability and the SEM has been shown to play a valuable role in inspecting this. The conventional method of *routine testing* of the fabricated circuits is seen to allow only measurements of the overall circuit functions since external connections are only available at the input and output terminals of the complete device. If an examination of operating conditions "inside" the circuit is desired, as in *failure analysis*, the conventional method is to use a mechanical probe. The current trend towards *large scale integration* has been shown to increase the severity of the problems of electrical contact, positioning and surface damage associated with such mechanical methods. A consideration of these and other factors suggests the need for some other method of measuring the voltages on integrated circuit metallisation. The use of the *voltage contrast* mechanism in the SEM appears to offer an attractive approach to solving this problem.

A survey of approaches to voltage contrast in the SEM has indicated the problems associated with the use of this technique for the present type of application. It has been shown that methods using the conventional collector system or a modified electron collection arrangement do not appear to be satisfactory for integrated circuit type specimens. The use of *Auger* electrons rather than low energy secondary electrons offers attractive advantages but was rejected due to the vacuum, surface cleanliness and electrical noise problems involved. The conclusion from this survey is that none of the approaches studied meet the requirements of the desired measuring system. A method using an electron *energy analyser* was chosen for further study since it seemed to offer the best possibilities of improvement.

The use of this type of energy analyser alone has been shown to give good results for certain samples and voltage distributions but to give very poor results for points close to the positive edge of a biased gap. Considerations of electric field plots have indicated that these effects are due to the fields immediately above the specimen surface. An examination of the requirements of this type of arrangement has shown the need for a field distribution above the specimen which will ensure that most electrons leave the surface region and are conveyed to the energy analyser. The design of an *electron lens* which largely fulfils these requirements has been presented. The experimental results obtained using the electron lens and energy analyser system have shown the *very considerable* improvement in performance over the previous method. These measurements have been made on aluminium on silicon dioxide specimens with similar structures and dimensions to those found in silicon integrated circuits. They have indicated the suitability

of this approach for the desired application of measuring voltages on integrated circuits. The electronic circuitry which has been described at the end of chapter 4 allows the lens and analyser method of voltage measurement to be used in a direct and almost completely automatic manner, giving both analogue and digital outputs.

The methods for potential distribution and electron trajectory calculations which have been developed in chapter 5 constitute an efficient method of analysing the operation of the electron lens and energy analyser system. In fact they represent a valuable solution to the problem of determining electron trajectories in a non-linear electrostatic field.

Computer aided analysis and design studies have shown that the characteristics of the electron lens are the best that could be achieved given the physical and other constraints applicable to the measuring system. The characteristics of the energy analyser have been shown to be rather poor in relation to the requirements of this setup. The size and shape of this particular analyser are very convenient for this application and no suitable alternative has been found. Results of computer simulation studies have shown good agreement with experimental results and have indicated clearly the factors which affect the performance of this measuring system giving a full understanding of its operation. Simulation studies carried out for a system with an "idealised" analyser replacing the experimental one have shown that it is the characteristics of this component which limit the performance of the experimental system. They also have shown that the use of the electron lens is indeed an excellent solution to the problems associated with voltage measurement in the SEM, even for extremely difficult types of specimens.

The voltage measuring system which has been developed in this work has been fully characterised and has been shown to be very suitable for use on integrated circuit type specimens. Used in conjunction with the circuitry described in chapter 4 it is virtually automatic in operation and lends itself easily to computer control. As already noted it is direct reading and involves no complicated interpretation of results which means that it could be used by personnel with little knowledge of the SEM. The fact that the circuit under examination can be viewed between voltage measurements is also a useful feature of this approach.

The use of this measuring system on integrated circuits at the final stage of testing in the production process would allow an examination of working conditions of individual devices in the complete circuits. As noted earlier this would enable those areas of the circuit where devices may be operating too near design limits to be identified and appropriate action taken. This information is not readily available from the normal electrical functional tests carried out on these circuits since these only check whether or not the whole device performs within its specifications at the time of manufacture. These checks for potential device failure areas would probably not be carried out on a 100% basis (except perhaps for military type devices) since the pump down time of the conventional SEM would introduce intolerable time delays in the testing procedure. (A specialised instrument with an airlock mechanism could be developed to reduce this pumping time but it would still be relatively slow and expensive). These tests could be carried out on a batch sampling basis to keep checks on the basic processing of the devices. This testing could be simplified if comparison was made between the device under test and recorded results for a known "good" device.

The automated system using the electron lens and energy analyser would be suitable for use in this way.

In most present day integrated circuit manufacturing the chip layout and masks for a new device are produced by computer aided design. The first devices which are produced from these masks may or may not work. These devices must be checked to determine their performance or if they are not functional the reasons for this must be identified. As already noted mechanical probes have severe disadvantages and the voltage measuring system using the SEM would be very valuable in this application. The points mentioned above about checking individual device operating conditions would also apply here since it is desired to obtain information which could be used to improve the design.

The voltage measuring system would be useful in a similar way for investigating devices which have failed to pass production tests or failed in service. The ability to measure voltages on various parts of the circuits enables the area where failure has occurred to be identified. This could be useful for aluminium steps where it is difficult to tell visually whether or not the layer is continuous. When the region with the fault has been identified the SEM can be used in its other modes of operation (eg conductive, X ray) to give further information, if the reason for the defect is not immediately obvious.

The facilities offered by this means of voltage measurement in the SEM would be valuable in research work on new types of integrated circuits. Work on new devices has continued at a fast pace in recent years and no doubt will continue to do so. In view of the almost universal trend to smaller individual devices giving higher

packing densities on larger chips the need for non mechanical methods of voltage measurement inside these circuits will be more pressing. The voltage measuring system developed in this work is a significant contribution to meeting this need.

In view of these applications of the SEM to integrated circuit testing there is much opportunity for further research along this line. The practical mechanical arrangements for mounting integrated circuits in the SEM together with optimal test procedures for use with this instrument would be worthy of study. It has already been noted that the performance of the measuring system could possibly be improved upon by the use of another type of energy analyser. Further work along the lines set out in chapter 6 might be valuable, although the computer simulations have indicated that the resultant improvement would not be substantial.

There seems little doubt that as integrated circuit technology becomes more sophisticated the SEM will become an indispensable part of the manufacturing and testing processes for these devices. The present work has sought to demonstrate ways in which this development might proceed.

REFERENCES

NB: References given as IITRI SEM' "year" are to:

Scanning Electron Microscopy/"year"

Proceedings of the annual scanning electron microscope
symposium, Editor O Johari

IIT Research Institute, Chicago, Illinois

1. VON ARDENNE, M,Z Phys, 1938, 109, p 553.
2. The Cambridge Instrument Company, Scanning Electron Microscope.
3. THORNTON, P R: 'Scanning electron microscopy', Chapman and Hall, London, 1968.
4. HAWKES, P W: 'Electron optics and electron microscopy', Taylor and Francis, London, 1972.
5. HEARLE, J W S, SPARROW, J T, and CROSS, P M: 'The use of the scanning electron microscope', Pergamon Press, 1972.
6. NIXON, W C: 'Introduction to scanning electron microscopy', IITRI SEM' 69, pp 1-9.
7. PEASE, R F W: 'Fundamentals of scanning electron microscopy', IITRI SEM'71, pp 9-16.
8. WELLS, O C: 'Bibliography on the scanning electron microscope', IITRI SEM'72, pp 375-442.
9. Cambridge Instrument Company, 'Stereoscan 2A'; Electrical Engineering Department, University of Edinburgh.
10. EVERHART, T E, and THORNLEY, R F: 'Wide-band detector for micro-microampere low-energy electron currents', J Appl Phys, 1960, 31, pp 1483-1490.
11. BROERS, A N: 'Some experimental and estimated characteristics of the lanthanum hexaboride rod cathode electron gun', J Sci Instr, 1969, 2, pp 273-276.

12. CREWE, A V, EGGENBERGER, D N, WALL, J, and WELTER, L M:
'Electron gun using a field emission source', Rev Sci Instr,
1968, 39, pp 576-583.
13. BROERS, A N: 'Factors affecting resolution in the SEM', IITRI
SEM'70, pp 1-8.
14. COSSLETT, V E, and THOMAS, R N: 'Multiple scattering of
electrons 5-30 kV in evaporated metal films: total distribu-
tions and angular distribution', Brit J Appl Phys, 1964, 15,
pp 883-907.
15. COSSLETT, V E: 'The diffusion depth for electrons in solid
targets', Brit J Appl Phys, 1964, 15, pp 107-109.
16. COSSLETT, V E, and THOMAS, R N: 'Multiple scattering of
electrons 5-30 kV in evaporated metal films: range and
energy relations', Brit J Appl Phys, 1964, 15, pp 1283-1300.
17. KANTER, H: 'Electron scattering by thin foils for energies
below 10 KeV', Phys Rev, 1961, 121, pp 461-471.
18. EVERHART, T E: 'Simple theory concerning the reflection of
electrons from solids', J Appl Phys, 1960, 31, pp 1483-1490.
19. ARCHARD, G D: 'Back scattering of electrons', J Appl Phys
1961, 32, pp 1505-1509.
20. COSSLETT, V E, and THOMAS, R N: 'Multiple scattering of
electrons 5-30 kV in evaporated metal films: back-scattering
and absorption', Brit J Appl Phys, 1965, 16, pp 779-796.
21. KOLLATH, R, Ann Physik, 1947, 1, p 357.
22. BRUINING, H: 'Physics and applications of the secondary
emission process', Pergamon Press, London, 1954.
23. JONKER, J L H, Philips Research Rept, 1957, 12, p 249.

24. KANTER, H: 'Energy dissipation and secondary emission in solids', Phys Rev, 1961, 121, pp 677-681.
25. KANTER, H: 'Contribution of backscattered electrons to secondary electron formation', Phys Rev, 1961, 121, pp 681-684.
26. HACHENBERG, O, and BRAUER, W: 'Secondary electron emission from solids', Advances in Electronics and Elect Phys, 1959, 11, pp 413-499.
27. McMULLAN, D: 'An improved scanning electron microscope for opaque specimens', Proc Instn Elect Engrs, 1953, 100, pp 245-259.
28. EVERHART, T E, WELLS, O C, and OATELY, C W: 'Factors affecting contrast and resolution in the scanning electron microscope', J Electron Control, 1959, 7, p 97.
29. CLARKE, D R: 'Review: image contrast in the SEM', J Materials Sci, 1970, 5, pp 689-708.
30. GRIFFITHS, B W, and VENABLES, J W: 'Scanning electron microscopy at liquid helium temperatures', IITRI SEM'72, pp 9-16.
31. WARNER, R M, and FORDEM WALT, J N (Editors): 'Integrated circuits design principles and fabrication', Motorola series in Solid State Electronics, McGraw Hill, 1965.
32. HIBBERD, R G: 'Integrated circuits a basic course for engineers and technicians', TI Electronics Series, McGraw Hill, 1969.
33. WORKMAN, W: 'Failures of integrated circuits and their relationship to reliability', Microelectronics and Reliability, 1968, 7, pp 257-264.
34. SAITOU, N, MORISHITA, H, NONOGAKI, S, ITOH, H, and MAEKAWA, A: 'Mask fabrication with submicron linewidth by electron beam', Japan J Appl Phys, 1971, 10, pp 1486-1487.

35. LARKIN, M W, and MATTA, R K: 'The electron beam fabrication of small geometry transistors', Solid-State Electronics (GB), 1967, 10, pp 491-496.
36. O'KEEFFE , T W, and HANDY, R M: 'Fabrication of planar silicon transistors without photoresist', Solid-State Electronics, 1967, 11, pp 261-266.
37. CHANG, T H P: 'Device fabrication using a scanning electron beam system', IITRI SEM'71, pp 417-424.
38. MILLER, R T: 'Electron beam fabrication', Solid State Technology, July 1973, pp 25-29.
39. WELLS, O C, EVERHART, T E, and MATTA, R K: 'Automatic positioning of device electrodes using the scanning electron microscope', IEEE Trans Electron Devices, 1965, ED-12, pp 556-563.
40. BLACK, J R: 'Electromigration - a brief survey and some recent results', IEEE Trans Electron Devices, 1969, ED-16, pp 338-347.
41. BERENBAUM, L, and ROSENBERG, R: 'Surface topology changes during electromigration in metallic thin film stripes', Thin Solid Films, 1969, 4, pp 187-204.
42. SPITZER, S M, and SCHWARTZ, S: 'A brief review of the state of the art and some recent results on electromigration in integrated circuit metallization', J Electrochem Soc, 1969, 116, pp 1368-1372.
43. DEVANEY, J R: 'Investigation of current induced mass transport in thin metal conducting stripes', IITRI SEM'70, pp 417-424.
44. MUNAKATA, C and WATANABE, H: 'Measurement of resistance by means of an electron beam - III', Japan J Appl Phys, 1969, 8, pp 1307-1309.
45. MACDONALD, N C, and EVERHART, T E: 'Direct measurement of the depletion layer width variation vs applied bias for a p-n junction', Appl Phys Letters, 1965, 7, pp 267-269.

46. MUNAKATA, C: 'An electron beam method of measuring resistivity distribution in semiconductors', Japan J Appl Phys, 1967, 6, pp 963-971.
47. HIGUCHI, H and TAMURA, H: 'Measurement of the lifetime of minority carriers in semiconductors with a scanning electron microscope', Japan J Appl Phys, 1965, 4, pp 316-317.
48. BRESSE, J F: 'Electron beam induced current in silicon planar p-n junctions: physical model of carrier generation. Determination of some physical parameters in silicon', IITRI SEM'72, pp 105-111.
49. OATLEY, C W, and EVERHART, T E: 'The examination of p-n junctions with the scanning electron microscope', J Electronics, 1957, 2, pp 568-570.
50. WILSON, P R: 'Measurements on the depletion layer properties of planar diodes', Solid-State Electronics, 1969, 12, pp 539-547.
51. MACDONALD, N C, and EVERHART, T E: 'Scanning electron microscope investigation of planar diffused p-n junction profiles near the edge of a diffusion mask', J Appl Phys, 1967, 38, pp 3685-3692.
52. EVERHART, T E, WELLS, O C, and MATTA, R K: 'A novel method of semiconductor device measurements', Proc IEEE, 1964, 52, pp 1642-1647.
53. GREEN, D and NATHANSON, H C: 'Observation of inversion layers under insulated-gate electrodes using a scanning electron microscope', Proc IEEE, 1965, 53, pp 183-184.
54. HIGUCHI, H, and MAKI, M: 'Observations of channels of MOS field effect transistors using a scanning electron microscope', Japan J Appl Phys, 1965, 4, pp 1021-1022.

55. SULWAY, D V, HUGHES, K A, THORNTON, P R, and EVANS, W A:
'Direct observation of MOS transistor pinch-off by scanning electron microscopy', Appl Phys Letters, 1966, 8, pp 296-298.
56. NEVE, N F B, SULWAY, D V, HUGHES, K A, and THORNTON, P R:
'The scanning electron microscope as a means of investigating second breakdown and similar phenomena', IEEE Trans Electron Devices, 1966, ED-13, pp 639-642.
57. ROBINSON, G Y: 'Scanning electron microscopy study of the avalanche multiplication factor', Proc IEEE, 1969, 57, pp 2169-2170.
58. LAST, J D, and LUCAS, D W: 'Scanning electron microscopy studies on switching lateral transistors in integrated circuits', Solid-State Electronics, 1971, 14, pp 481-486.
59. DAVIES, I G, HUGHES, K A, SULWAY, D V, and THORNTON, P R:
'The direct observation of electrical leakage paths due to crystal defects by use of the scanning electron microscope', Solid-State Electronics, 1966, 9, pp 275-279.
60. GRATZE, S C, and THOMAS, R T: 'Observations on epitaxial gallium arsenide varactor diodes using the scanning electron microscope', Microelectronics and Reliability, 1970, 9, p 71.
61. GOPINATH, A, SANGER, C C, PARACCHINI, C and JONES, G A C:
'Quantitative voltage and temperature distribution studies in GaAs transverse Gunn diodes using an SEM', IITRI SEM'71, pp 457-464.
62. BUNTON, G V: 'Observations on silicon carbide devices using the scanning electron microscope', Solid-State Electronics, 1969, 12, pp 977-979.

63. THORNTON, P R, HUGHES, K A, SULWAY, D V; and WAYTE, R C:
'Quantitative measurements by scanning electron microscopy -
1, the use of conductivity maps', Microelectronics and Reliability,
1966, 5, pp 291-298.
64. FLUTIE, R E: 'A method for sequential etching of passivation
for the SEM inspection of subsurface metallic layers', IITRI
SEM'72, pp 185-192.
65. CLINE, J E, MORRIS, J M, and SCHWARTZ, S: 'Scanning electron
mirror microscopy and scanning electron microscopy of integrated
circuits', IEEE Trans Electron Devices, 1969, ED-16, pp 371-375.
66. OGILVIE, R E, SCHIPPERT, M A, MOLL, S H, and KOFFMAN, D M:
'Scanning electron mirror microscopy', IITRI SEM'69, pp 425-430.
67. COX, S B: 'Applications of scanning electron mirror microscopy
to electronics', IITRI SEM'71, pp 433-440.
68. EVERHART, T E, WELLS, O C, and MATTA, R K: 'Evaluation of pas-
sivated integrated circuits using the scanning electron micro-
scope', J Electrochem Soc, 1964, Vol 111 (2), pp 929-936.
69. THORNHILL, T W, and MACKINTOSH, I M: 'Application of the scanning
electron microscope to semiconductor device structures',
Microelectronics and Reliability, 1965, 4, pp 97-100.
70. PLOWS, G S, and NIXON, W C: 'Operational testing of LSI arrays
by stroboscopic scanning electron microscopy', Microelectronics
and Reliability, 1971, 10, pp 317-323.
71. ROBINSON, G Y: 'Stroboscopic electron microscopy at gigahertz
frequencies', J Appl Phys, 1971, 42, pp 251-255.
72. THORNTON, P R, HUGHES, K A, KYAW, H, MILLWARD, C, and SULWAY, D V:
'Failure analysis of microcircuitry by scanning electron
microscopy', Microelectronics and Reliability, 1967, 6, pp 9-16.

73. SULWAY, D V, THORNTON, P R, and TURNER, M J: 'Direct observations of electrical faults in planar transistors made in epitaxially grown silicon', *Solid-State Electronics*, 1968, 11, pp 567-568.
74. COX, R H, CROSTHWAIT, D L, and DOBROTT, R D: 'The application of the scanning electron microscope to the development of high reliability semiconductor products', *IEEE Trans Electron Devices*, 1969, ED-16, pp 376-380.
75. THORNTON, P R, SULWAY, D V, and SHAW, D A: 'Scanning electron microscopy in device diagnostics and reliability physics', *IEEE Trans Electron Devices*, 1969, ED-16, pp 360-371.
76. THORNTON, P R, DAVIES, I G, SHAW, D A, SULWAY, D V, and WAYTE, R C: 'Device failure analysis by scanning electron microscopy', *Microelectronics and Reliability*, 1969, 8, pp 33-53.
77. GREEN, D, SANDOR, J E, O'KEEFFEE, T W, and MATTA, R K: 'Reversible changes in transistor characteristics caused by scanning electron microscope examination', *Appl Phys Letters*, 1965, 6, pp 3-4.
78. SZEDON, J R, and SANDOR, J E: 'The effect of low-energy electron irradiation of metal-oxide-semiconductor structures', *Appl Phys Letters*, 1965, 6, pp 181-182.
79. SPETH, A J, and FANG, F F: 'Effects of low-energy electron irradiation on Si-insulated gate FETs', *Appl Phys Letters*, 1965, 7, pp 145-146.
80. MACDONALD, N C, and EVERHART, T E: 'Selective electron-beam irradiation of metal-oxide-semiconductor structures', *J Appl Phys*, 1968, 39, pp 2433-2447.

81. MACDONALD, N C: 'Quantitative scanning electron microscopy: solid state applications', IITRI SEM'69, pp 431-437.
82. EVERHART, T E: 'Reflections on scanning electron microscopy', IITRI SEM'68, pp 1-12.
83. OATELY, C W: 'Isolation of potential contrast in the scanning electron microscope', J Sci Instrum (J Phys E), 1969, 2, pp 742-744.
84. GAFFNEY, D P: 'Time varying potential difference observations with the SEM', IITRI SEM'70, pp 433-440.
85. DRIVER, M C: 'A spherically symmetrical detector for the scanning electron microscope', IITRI SEM'69, pp 403-413.
86. GOPINATH, A, and SANGER, C C: 'A method of isolating voltage contrast in the scanning electron microscope', J Phys E: Sci Instrum, 1971, 4, pp 610-611.
87. GOPINATH, A, SANGER, C C, PARACCHINI, C, and JONES, G A C: 'Quantitative voltage and temperature distribution studies in GaAs transverse Gunn diodes using an SEM', IITRI SEM'71, pp 457-464.
88. FLEMMING, J P, and WARD, E W: 'Improved technique for voltage measurement in the scanning electron microscope', Electronics Letters, 1969, 5, pp 435-436.
89. FLEMMING, J P, and WARD, E W: 'Improved technique for voltage measurement using the scanning electron microscope', Electronics Letters, 1970, 6, pp 7-9.
90. FLEMMING, J P, and WARD, E W: 'A technique for accurate measurement and display of applied potential distributions using the scanning electron microscope', IITRI SEM'70, pp 465-472.
91. BANBURY, J R, and NIXON, W C: 'A high contrast detector for the scanning electron microscope', J Sci Instrum (J Phys E), 1969, 2, pp 1055-1059.

92. BANBURY, J R, and NIXON, W C: 'Voltage measurement in the scanning electron microscope', IITRI SEM'70, pp 473-480.
93. YAKOWITZ, H, BALLANTYNE, J P, MUNRO, E, and NIXON, W C: 'The cylindrical secondary electron detector as a voltage measuring device in the scanning electron microscope', IITRI SEM'72, pp 34-39.
94. WELLS, O C, and BREMER, C G: 'Voltage measurement in the scanning electron microscope', J Sci Instrum (J Phys E), 1968, 1, pp 902-906.
95. WELLS, O C, and BREMER, C G: 'Method for measuring voltages in the scanning electron microscope', IITRI SEM'69, pp 397-401.
96. WELLS, O C, and BREMER, C G: 'Improved energy analyser for scanning electron microscope', J Sci Instrum (J Phys E), 1969, 2, pp 1120-1121.
97. MACDONALD, N C: 'Potential mapping using Auger electron spectroscopy', IITRI SEM'70, pp 481-487.
98. MACDONALD, N C: 'Auger electron spectroscopy in scanning electron microscopy' Potential-Measurements, Appl Phys Letters, 1970, 16, No 2, pp 76-80.
99. WALDROP, J R, and MARCUS, H L: 'Auger electron spectroscopy in the scanning electron microscope', Journal of Testing and Evaluation (ASTM), May 1973, pp 194-201.
100. MACDONALD, N C: 'Auger electron spectroscopy for scanning electron microscopy', IITRI SEM'71, pp 89-96.
101. HATZAKIS, M: 'A new method of forming scintillators for electron collectors', Rev Sci Instrum, 1970, 41, p 128.
102. WELLS, O C, Comment in IITRI SEM'70 pp 486-487.

103. WELLS, O C: 'An irradiation effect in thermally grown SiO_2 ', Appl Phys Letters, 1969, 14, pp 5-6.
104. AARON, M R, and MITRA, S K: 'Synthesis of restive digital-to-analogue conversion ladders for arbitrary codes with fixed positive weights', IEEE Trans on Electronics Computers, 1967, EC-16, pp 277-281.
105. VITKOVITCH, D (Editor): 'Field analysis: experimental and computational methods', Van Nostrand, London, 1966.
106. Reference 105; pp 118-125.
107. Reference 105; p 150.
108. SHAW, F S: 'Introduction to relaxation methods', Dover, New York, 1953.
109. Reference 105; pp 143-148.
110. COMRIE, L J: 'CHAMBERS four figure methematical tables', CHAMBERS, 1966, p 49.
111. IBM Manual GC28-6515, 'Fortran IV language'.
112. IBM Manual GC28-6817, 'Fortran IV (G and H) programmers guide'.
113. GRIVET, P: 'Electron optics', Pergamon Press, London, 1965, pp 317-319.
114. PASZKOWSKI, B: 'Electron optics', Iliffe Books, London, 1968, pp 194-199.
115. Reference 114; p 123.

DECLARATION

I hereby declare that this thesis has been composed entirely by me and that the work described in it is my own.